



THE HONG KONG
POLYTECHNIC UNIVERSITY

香港理工大學

Pao Yue-kong Library

包玉剛圖書館

Copyright Undertaking

This thesis is protected by copyright, with all rights reserved.

By reading and using the thesis, the reader understands and agrees to the following terms:

1. The reader will abide by the rules and legal ordinances governing copyright regarding the use of the thesis.
2. The reader will use the thesis for the purpose of research or private study only and not for distribution or further reproduction or any other purpose.
3. The reader agrees to indemnify and hold the University harmless from and against any loss, damage, cost, liability or expenses arising from copyright infringement or unauthorized usage.

If you have reasons to believe that any materials in this thesis are deemed not suitable to be distributed in this form, or a copyright owner having difficulty with the material being included in our database, please contact lbsys@polyu.edu.hk providing details. The Library will look into your claim and consider taking remedial action upon receipt of the written requests.

The Hong Kong Polytechnic University

Department of Applied Biology and Chemical Technology

**Mass Spectrometric and Theoretical Studies on
Protonated and Potassium Cationized
Biological Molecules in the Gas Phase**

Cheng Man Kit

A thesis submitted in partial fulfillment of
the requirements for the degree of

Doctor of Philosophy

in

Chemistry

September 2007



CERTIFICATE OF ORIGINALITY

I hereby declare that this thesis is my own work conducted during the period 9.2003 - 8.2007 in the Department of Applied Biology and Chemical Technology, the Hong Kong Polytechnic University. The theoretical calculations reported in this thesis were all carried out by the author. Dr. Y. Tsang, Ms. Onyx O. Y. Chan and Ms. Toby P Y. Lau, who are members of Prof. Tsang's research group, provided exploratory or supplementary experimental measurement of some of the mass spectral data presented in this thesis, and due acknowledgements have been made in the relevant parts of the thesis. Other than these acknowledgements, and to the best of my knowledge, this thesis reproduces no material previously published or written that has been accepted for the award of any other degree or diploma. This thesis has not been submitted to this or any other institution for academic qualification purposes.

Cheng Man Kit

Date: 10, September, 2007

Abstract

α -/ β -amino acids are the constituent units of peptides and proteins, as well as important starting materials for the synthesis of pharmaceutically important intermediates and drugs. In particular, β -peptides are more resistant to enzymatic degradations than their α -analogues, and hold the key to a new generation of bacteria-resistance drugs. The recent surge in proteomics research also places high demands on peptide sequencing analysis by tandem mass spectrometry (MS/MS), which is based on the low-energy collision-induced dissociation (CID) mass spectra of protonated/alkali metal cationized peptides. However, the *intrinsic* properties of α -/ β -amino acids/peptides, e.g. proton (H^+) and potassium cation (K^+) affinities, and the mass spectrometric dissociation mechanisms of protonated amino acids and peptides, are not fully understood.

In the present study, the first set of reliable experimental K^+ affinities of the twenty naturally occurring α -amino acids were determined to be (in kJ mol^{-1}): Arg (163) > His (155) > Gln (154) > Trp (151) > Asn (149) > Lys (144) > Glu (140) > Tyr (140) > Phe (139) > Asp (137) > Thr (136) > Pro (135) > Met (135) > Ser (133) > Ile (129) > Leu (128) > Val (127) > Cys (124) > Ala (123) > Gly (119) using the mass spectrometric kinetic methods and estimated theoretically using the density functional theory (DFT) B3-LYP/6-311+G(3df,2p)//B3-LYP/6-31G(d) protocol. With the exception of lysine (Lys) and arginine (Arg), the experimental and theoretical potassium cation (K^+) affinities are found to agree to within $\pm 15 \text{ kJ mol}^{-1}$, with mean absolute deviation (MAD) of 4.9 kJ mol^{-1} only. The most stable K^+ binding to aliphatic amino acids (Gly, Ala, Val, Leu, Ile) involves a bidentate interaction in the **CS1** form involving the carboxylic C=O and OH sites, whereas for amino acids with functionalized side chain (namely, Ser, Thr,

Cys, Met, Phe, Tyr, Trp, Asp, Asn), a tridentate interaction in the **CS2** form involving the backbone O=C, N-terminal NH₂, and the O/N-heteroatom site of the functional group in the side chain is generally favored. The only exceptions are the K⁺-Pro/Glu/Gln/Lys/His/Arg complexes, which are found to be most stable in the zwitterionic **ZW1** form.

The H⁺/K⁺ affinities of five biologically important β-amino acids were determined to be (in kJ mol⁻¹, at 298K/0K): β-Abu 942.0/134.7, β-Leu 955.6/138.3, β-Phe 948.0/137.6, β-Tyr 955.4/138.7 and β-Glu 951.5/141.5. The H⁺ affinities (PA) of four model β-dipeptides and one biologically important β-dipeptide were determined to be (in kJ mol⁻¹ at 298K): Gly(β-Ala) 942.0, (β-Ala)Gly 971.3, Ala(β-Ala) 947.8, (β-Ala)Ala 970.3 and (β-Ala)His 1023.4. The experimental H⁺/K⁺ affinities for the β-amino acids and the H⁺ affinities for the β-dipeptides are found to be in very good agreement with values estimated by the DFT protocol, with MAD of 3.1/6.4 and 5.9 kJ mol⁻¹, respectively. The most stable sites of binding and conformations of the H⁺ and K⁺ bound complexes were found by theoretical calculations using the DFT protocol. The most stable proton binding site of the β-amino acids and β-dipeptides is at the N-terminal amino nitrogen (NH₂), while K⁺ binds to the two carboxylic oxygens [O=C and -OH] in the most stable charge-solvated **CS1** mode. For carnosine ((β-Ala)His), the most stable proton binding site is at the π-nitrogen of the imidazole ring of the histidine residue. The proton (H⁺) affinities (PA) of β-amino acids and β-dipeptides are generally larger than that of their α-analogues. This is attributed to a more stabilizing hydrogen bond or bonding network found in the β-amino acids and β-dipeptides. Unlike α-dipeptides, the PA enhancing effect is much more pronounced when β-Ala is located at the N-terminus than at the C-terminus of the β-dipeptides.

The potential energy surfaces for the dissociation of protonated β-alanine (β-Ala), and two model β-dipeptides, (β-Ala)Gly and Gly(β-Ala), including the reaction intermediates, transition

structures (energy barriers) and energetics of the reaction (ΔH_0 , ΔH_{298} , and ΔG_{298}) were found by theoretical calculations using the DFT protocol. For protonated β -Ala, the loss of H_2O , CH_2CO , and $(CH_2CO + H_2O)$ pathways are energetically preferred. The loss of $NH=CH_2$, NH_3 and $(NH_3 + CO)$ pathways have higher critical energies, and are observed under more energetic CID conditions. The loss of these small stable neutrals are not found in the dissociation of protonated α -Ala, and is directly related to the presence of the 'extra' $-CH_2-$ unit in the main carbon chain of β -Ala, separating the N-terminal $-NH_2$ group and C-terminal $-COOH$ group. The formation of β -Ala specific fragment ions is dependent of the location, C-terminus versus N-terminus, of β -Ala in the β -dipeptide. For Gly(β -Ala), formation of the unique b'_2 (oxazinone) ions is energetically favored over y_1 ion formation. The b'_2 (oxazinone) ion dissociates further by characteristic loss of $NH=CH_2$ and NH_3 , in contrast to the loss of CO only observed for b_2 (oxazolone) ions derived from α -dipeptides. For (β -Ala)Gly, formation of b_1 (protonated β -lactam) ions and fragment ions due to the loss of NH_3 , which are indicative of the presence and location of β -Ala in the β -dipeptide, are competitive (having comparable energy barriers) with y_1 ion formation. The theoretical findings are consistent with experimental observations, and could be used to rationalize the appearance threshold voltages and relatively abundances of different fragment ions in the CID-MS/MS spectra of protonated β -Ala, (β -Ala)Gly and Gly(β -Ala). The knowledge gained in the present study will be useful in sequence analysis of β -peptides by tandem mass spectrometry.

The dissociation mechanisms of protonated α -peptides containing histidine is known to be complicated due to the presence and active participation of the basic imidazole ring in the side chain of histidine. In the present study, the potential energy surfaces for the dissociation of protonated model dipeptides, $[GlyHis + H]^+$ and $[HisGly + H]^+$, were established by DFT

calculations. The formation of the $b_2(\text{oxazolone-His})$ ion is energetically and entropically favoured, but $b_2(\text{diketopiperazine-His})$ and $b_2(\text{bicyclic})$ ions could also be formed at higher critical energies. As the $b_2(\text{diketo-His})$ ion is much more stable, initially formed $b_2(\text{oxazolone-His})$ ions could further isomerize to $b_2(\text{diketopiperazine-His})$ ions if there is sufficient internal energy imparted to the b_2 ions by collisional activation. The energy difference between the barrier of the formation of $b_2(\text{oxazolone-His})$ and that of further isomerization to $b_2(\text{diketopiperazine-His})$ ion are 201 and 115 kJ mol^{-1} for protonated GlyHis and HisGly, respectively. The difference in isomerization energy barriers is consistent with experimental observations in energy-resolved and time-resolved tandem MS/MS studies: isomerization is only partially achieved for b_2 ions derived from protonated GlyHisGly, but complete isomerization is found for b_2 ions derived from protonated HisGlyGly in the millisecond time frame of the ion trap mass analyzer. As the initial peptide sequence information is lost in the $b_2(\text{diketopiperazine-His})$ ion (a protonated cyclo-peptide), the implication of b_2 ion isomerization to peptide sequencing by tandem mass spectrometry is discussed.

Research Publications

Journal Papers

1. Cheng, M.K., Chan, O.Y., Lau, P.Y., So, P.K., Ma, N.L. and Tsang, C.W. “Dissociation of Protonated β -Alanine: a Combined Experimental and Theoretical Study” to be submitted to *Journal of the American Society for Mass Spectrometry* (2007)
2. Lau, P.Y., Cheng, M.K., Wong, C.H.S, and Tsang, C.W. “The Formation and Structures of b_2 ions Derived from Protonated Histidine-containing Peptides with Histidine at the N-terminus” to be submitted to *Journal of the American Society for Mass Spectrometry* (2007)

Conference Papers

1. Cheng, M.K., Wong, C.L., Ma, N.L. and Tsang, C.W., “Fragmentation Pathways and Mechanisms of Alkali Metal Cationized Histidine”. *The Eleventh Symposium on Chemistry Postgraduate Research in Hong Kong*, The Hong Kong Polytechnic University, Hong Kong (2004)
2. Tsang, C.W., Tsang, Y., Wong, H.S., Siu, F.M., Cheng, M.K., Lee, H.M., Abirami, S. and Ma, N. L. “Potassium Cation Binding to α -Amino Acids and Dipeptides : A Combined Theoretical and Experimental Study” *Proceedings of the 52nd ASMS*

Conference on Mass Spectrometry and Allied Topics, May 23-27, 2004, Nashville, USA.

3. Cheng, M.K., Chan, O.Y., Abirami, S., Ma, N. L. and Tsang, C.W. “A Theoretical Study on Fragmentation Pathways and Mechanisms of Protonated β -Alanine” *The 229th American Chemical Society National Meeting*, San Diego, USA (2005)
4. Chan, O.Y., Cheng, M.K., Ma, N.L. and Tsang, C.W. “Mass Spectrometric Fragmentation of Protonated (H^+) Peptides Containing β -Amino Acids”. *The 229th American Chemical Society National Meeting*, San Diego, USA (2005)
5. Lau, P.Y., Cheng, M.K., Wong, C.L., Wong, C.H.S. and Tsang, C.W., “The Structure and Fragmentation of b_2 ions of Protonated (H^+) Peptides Containing Histidine”. *The Twelfth Symposium on Chemistry Postgraduate Research in Hong Kong*, The Hong Kong Polytechnic University, Hong Kong (2005)
6. Cheng, M.K., Chan, O.Y., Chan, W.K. and Tsang, C.W. “Determination of Proton Affinities of Model and Bioactive β -dipeptides: A Combined Experimental and Theoretical Study” *The Thirteenth Symposium on Chemistry Postgraduate Research in Hong Kong*, The Hong Kong Polytechnic University, Hong Kong (2006)
7. Cheng, M.K., Chan, O.Y., So, P.K., Lau, P.Y. and Tsang, C.W. “Fragmentation Pathways of Protonated β -Alanine and β -Peptides: An Energy-Resolved Tandem Mass Spectrometric and Theoretical Study” *Proceedings of the 54th ASMS*

Conference on Mass Spectrometry and Allied Topics (on CD ROM), May 28 - June 1, 2006, Seattle, U.S.A.

8. Lau, P.Y., Cheng, M.K., Wong, C.L., Wong, C.H.S. and Tsang, C.W., “The Competitive Formation and Dissociation of bn(dehydration, -H₂O) ions of Protonated (H⁺) Peptides Containing Histidine”. *The Thirteenth Symposium on Chemistry Postgraduate Research in Hong Kong*, The Hong Kong Polytechnic University, Hong Kong (2006)

Acknowledgment

I would like to thank my chief supervisor, Prof. C. W. Tsang, for his generous guidance, supervision and encouragement throughout the conduct of this project, especially his valuable comments on the manuscript of this thesis. Special thanks are extended to Dr. Ida N. L. Ma (my co-supervisor) and Dr. Carrie H. S. Wong, who very helpfully guided me in the understanding and execution of the theoretical calculations of my study.

The award of the Hong Kong Polytechnic University graduate studentship to me, and the funding support of the Research Grant Council of Hong Kong (CERG Project No. 5012/03P, 5012/04P and 5013/05P) for this project are gratefully acknowledged.

I would also like to thank all of my research group members, who have helped me in various ways during the years of my study. In particular, I would like to thank Miss O. Y. Chan, Miss P. Y. Lau and Mr. W. K. Chan of our research group who kindly provided me the experimental results. I also wish to express my gratitude to all academic and technical staff from the Department of Applied Biology and Chemical Technology for their support.

Finally, I would like to thank all the members of my family and friends for their continuous motivation and support during the course of my postgraduate study.

Table of Contents

Certificate of Originality	i
Abstract	ii
Research Publications	vi
Acknowledgement	ix
Table of Contents	x
List of Figures	xv
List of Tables	xxii
List of Schemes	xxiv
List of Abbreviations	xxv
Chapter 1 Introduction	
1.1 Biochemical Significance of α -/ β -Amino Acids and Peptides	1
1.2 Proton (H^+) and Potassium Cation (K^+) Affinities of Amino Acids and Peptides	4
1.3 Mass Spectrometric Fragmentation of Protonated Amino Acids and Peptides	8
1.4 Literature Review	13
1.5 Aim and Scope of Present Study	17
Chapter 2 Tandem Mass Spectrometry (MS/MS) and Experimental Methodologies	
2.1 Ionization Methods in Mass Spectrometry	
2.2.1 Fast Atom Bombardment (FAB)	19
2.2.2 Electrospray Ionization (ESI)	21

2.2	The Quasi-Equilibrium Theory (QET) of Mass Spectra	23
2.3	Tandem Mass Spectrometry (MS/MS)	
2.3.1	Unimolecular (Metastable) Ion Dissociation	30
2.3.2	Collision-Induced Dissociation (CID)	32
2.4	The Mass Spectrometric Kinetic Method	
2.4.1	The Standard Kinetic Method	34
2.4.2	The Extended Kinetic Method	36
2.5	Instrumentation and Experimental Procedures	
2.5.1	The Finnigan-MAT95S Double-Focusing (B-E) Mass Spectrometer	38
2.5.2	Waters-Micromass Quattro Ultima Triple Quadrupole Tandem Mass Spectrometer	41
2.5.3	Chemicals and Sample Preparation Procedures	43
2.5.4	Instrumental Conditions	45
Chapter 3 Computational Methodology		
3.1	<i>Ab Initio</i> Molecular Orbital (MO) Methods	
3.1.1	The Schrödinger Equation	50
3.1.2	The Born-Oppenheimer Approximation	51
3.1.3	The Slater Determinant	52
3.1.4	Koopmans' Theorem	53
3.1.5	Basis Set Approximation	54
3.1.6	Basis Set	54
3.1.7	Hartree-Fock (HF) Self-Consistent Field (SCF) Theory	57
3.2	Density Functional Theory (DFT)	
3.2.1	Hybrid Methods	61
3.3	Zero-point Corrections and Frequencies	62

3.4	Thermochemical Corrections	63
3.5	The Energetic Protocol Adopted in Present Study	64
3.6	Potential Energy Surface (PES) of Dissociation	67
Chapter 4	Potassium Cation Affinities of α-Amino Acids with Functionalized Side Chains: a Combined Experimental and Theoretical Study	
4.1	Background	70
4.2	Results and Discussion	
4.2.1	Experimental Determination of Potassium Cation Affinities of Amino Acids with Functionalized Side Chains (AAFSCs) and Their Methyl Esters	76
4.2.2	Theoretical K^+ Affinities and Binding Modes	94
4.2.3	Comparison between Experimental, Theoretical and Literature K^+ Affinity Values	96
4.2.4	Potassium Cation Binding to α -Amino Acids: Relative Stabilities of Charge-Solvated versus Zwitterionic Binding Modes	100
4.3	Conclusion	116
Chapter 5	Proton and Potassium affinities of Selected Biologically Significant β-Amino Acids	
5.1	Background	119
5.2	Results and Discussion	
5.2.1	Experimental Determination of <i>Absolute</i> Proton (H^+) Affinities of Selected β -Amino Acids	127
5.2.2	Experimental Determination of <i>Absolute</i> Potassium Cation (K^+) Affinities of Selected β -Amino Acids	131

5.2.3	Comparison between experimental and theoretical H ⁺ / K ⁺ affinity values	135
5.2.4	The H ⁺ and K ⁺ Binding Modes of Selected β-Amino Acids	138
5.2.5	Potassium Cation Binding to β-Amino Acids (<i>β-Abu</i> , <i>β-Leu</i> , <i>β-Phe</i> , <i>β-Tyr</i> , and <i>β-Glu</i>): Relative Stabilities of Charge-Solvated versus Zwitterionic Binding Modes	139
5.3	Conclusion	144
Chapter 6	Dissociation of Protonated β-Alanine and its Methyl Ester	
6.1.	Background	146
6.2	Results and Discussion	
6.2.1	Collision-induced Dissociation (CID) MS/MS Spectra of Protonated β-Alanine and its Methyl Ester	147
6.2.2	Dissociation of Protonated β-Alanine and its Methyl Ester: Proposed Fragmentation Pathways and Theoretical Potential Energy Surface (PES)	153
6.3	Conclusion	168
Chapter 7	Proton Affinities and Fragmentation Mechanism of Selected Model and Biologically Significant β-Dipeptides	
7.1.	Background	170
7.2	Results and Discussion	
7.2.1	Experimental Determination of Proton (H ⁺) Affinities of Selected β-Dipeptides	171
7.2.2	Comparison between experimental and theoretical proton affinity values of selected β-dipeptides	175
7.2.3	The proton (H ⁺) binding modes of β-dipeptides	177

7.2.4	Collision-induced Dissociation (CID) MS/MS Spectra of Protonated Gly(β -Ala) and Protonated (β -Ala)Gly	184
7.2.5	Proposed Pathway for Competitive Formation Pathway of b'_2 (oxazinone) and y_1 Ions from Protonated Gly(β -Ala)	188
7.2.6	Proposed Competitive Loss of NH_3 Pathway and Formation of b_1 Ion from Protonated (β -Ala)Gly	192
7.3	Conclusion	199
Chapter 8 Dissociation of Protonated Peptides Containing Histidine: Formation and Structure of b_2 Ions		
8.1	Background	201
8.2	Result and Discussion	
8.2.1	Collision-induced Dissociation (CID) of Protonated GlyHisGly and HisGlyGly	206
8.2.2	Dissociation of Protonated GlyHis: Theoretical Potential Energy Surface (PES) for Competitive Formation of b_2 (oxazolone-His), b_2 (diketo-His) and b_2 (bicyclic) ions	215
8.2.3	Dissociation of Protonated GlyHis: Proposed Pathway for Isomerization of b_2 (oxazolone-His) ion to b_2 (diketo-His) ion	225
8.2.4	Dissociation of Protonated HisGly: Theoretical Potential Energy Surface (PES) for Competitive Formation of b_2 (oxazolone-His) and b_2 (diketo-His) ions	228
8.2.5	Dissociation of Protonated HisGly: Proposed Pathway for Isomerization of b_2 (oxazolone-His) ion to b_2 (diketo-His) ion	233
8.3	Conclusion	237
Chapter 9 Suggestions for Further Works		239
References		242

List of Figures

- Figure 2.1 Ionization by fast atom bombardment (FAB)
- Figure 2.2 A schematic diagram of an electrospray ionization (ESI) source
- Figure 2.3 Generation of ions by electrospray ionization
- Figure 2.4 Potential energy diagram of a unimolecular dissociation reaction with a critical energy barrier (ϵ_0)
- Figure 2.5 Hypothetical $k(E)$ versus E curves for a simple bond cleavage reaction and a dissociation reaction involving molecular rearrangement
- Figure 2.6 Schematic diagram of MS/MS operation in the daughter ion scan mode
- Figure 2.7 A hypothetical internal energy distribution ($P(E)$) versus internal energy (E) of ions
- Figure 2.8 Schematic energy diagram of the dissociation of a potassium cation bound heterodimer $[L_1-K-L_2]^+$
- Figure 2.9 Schematic diagram of the Finnigan-MAT95S-B-E tandem mass spectrometer
- Figure 2.10 Schematic diagram of the Micromass Quattro Ultima triple quadrupole tandem mass spectrometer
- Figure 3.1 Iterative procedure of self-consistent field (SCF) calculations
- Figure 3.2 A potential energy surface (PES) of a simple dissociation reaction pathway
- Figure 4.1 Metastable (unimolecular) ion dissociation mass spectra of (a) $[\text{SerOEt-K-Phe}]^+$, (b) $[\text{SerOEt-K-Tyr}]^+$ and (c) $[\text{SerOEt-K-PheOMe}]^+$ heterodimers
- Figure 4.2 Experimentally measured $\ln(I_{[K-L_1]^+}/I_{[K-L_2]^+})$ values for metastable(unimolecular) ion decomposition of K^+ -bounded heterodimers of amino acids ($T_{\text{eff}} = 230 \text{ K}$)
- Figure 4.3 Experimentally measured $\ln(I_{[K-L_1]^+}/I_{[K-L_2]^+})$ values for metastable(unimolecular) ion decomposition of K^+ -bounded heterodimers of amino acids ($T_{\text{eff}} = 342\text{K}$)

- Figure 4.4 Triple quadrupole MS/MS spectra of the [CysOMe–K–AlaOMe]⁺ heterodimer using argon as collision gas at various collision energies (eV, laboratory frame)
- Figure 4.5 (a) Plot of $\ln(I_{[\text{Cys-OMe+K}]^+}/I_{[\text{Ln+K}]^+})$ versus $[\Delta H_{[\text{Ln+K}]^+} - \Delta H_{\text{Avg}}]$ at different collision energies, and (b) plot of $[(\Delta G)_{\text{app}}[\text{CysOMe} + \text{K}]^+ - \Delta H_{\text{Avg}}]/RT_{\text{eff}}$ against $1/RT_{\text{eff}}$ for the [CysOMe–K–L_n]⁺ heterodimers
- Figure 4.6 Plot of cumulative $\ln(I_{[\text{L+K}]^+}/I_{[\text{Ser+K}]^+})$ values obtained under metastable (MI) dissociation (Fig. 4.2) versus K⁺ affinity values of ligands at 0 K ($R^2 = 0.97$)
- Figure 4.7 Plot of cumulative $\ln(I_{[\text{L+K}]^+}/I_{[\text{Asp+K}]^+})$ values obtained under metastable (MI) dissociation (Fig. 4.3) versus K⁺ affinity values of ligands at 0 K ($R^2 = 0.99$)
- Figure 4.8 Schematic representation of charge-solvated (CS) and zwitterionic (ZW) binding modes of K⁺ bound α -amino acids
- Figure 4.9 The most stable K⁺ binding mode (CS1) of aliphatic amino acids (Gly/Ala/Val/Leu/Ile) optimized at the B3-LYP/6-31G(D) level. The K⁺ affinities at 0 K in kJ mol⁻¹ are shown in parenthesis. All the bond lengths are shown in Å
- Figure 4.10 The most stable CS and ZW K⁺ binding modes of Ser/Thr/Cys/Met, optimized at the B3-LYP/6-31G(D) level. The K⁺ affinities at 0 K in kJ mol⁻¹ are shown in parenthesis. All the bond lengths are shown in Å
- Figure 4.11 The most stable CS and ZW K⁺ binding modes of Phe/Tyr/Trp, optimized at the B3-LYP/6-31G(D) level. The K⁺ affinities at 0 K in kJ mol⁻¹ are shown in parenthesis. All the bond lengths are shown in Å
- Figure 4.12 The most stable CS and ZW K⁺ binding modes of Asn/Gln/Asp/Glu, optimized at the B3-LYP/6-31G(D) level. The K⁺ affinities at 0 K in kJ mol⁻¹ are shown in parenthesis. All the bond lengths are shown in Å
- Figure 4.13 The most stable ZW K⁺ binding modes of Pro/Lys/His/Arg, optimized at the B3-LYP/6-31G(D) level. The K⁺ affinities at 0 K in kJ/mol are shown in parenthesis. All the bond lengths are shown in Å

- Figure 5.1 Triple quadrupole MS / MS spectrum of the proton bound heterodimer [PA + H + (β -Phe)]⁺ using argon at a collision energy of 8 eV (laboratory frame) (β -Phe = β -Phenylalanine and PA = Propylamine)
- Figure 5.2 (a) Plot of $\ln(I_{[(\beta\text{-Phe})+\text{H}]^+}/I_{[\text{L}_n+\text{H}]^+})$ versus $[\Delta H_{[\text{L}_n+\text{H}]^+} - \Delta H_{\text{Avg}}]$ at different collision energies, and (b) plot of $[(\Delta G)^{\text{app}}_{[(\beta\text{-Phe})+\text{H}]^+} - \Delta H_{\text{Avg}}]/RT_{\text{eff}}$ against $1/RT_{\text{eff}}$ for the proton bound heterodimer $[(\beta\text{-Phe}) + \text{H} + \text{L}_n]^+$ heterodimers. ((β -Phe) = β -Phenylalanine, L_n = Propylamine, Isopropylamine and Triamylamine); numbers shown are *absolute* proton affinities
- Figure 5.3 Triple quadrupole MS / MS spectrum of the [SerOMe + K + (β -Phe)]⁺ heterodimer using argon as collision gas at a collision energy of 9 eV (laboratory frame) (β -Phe = β -Phenylalanine and SerOMe = Serine Methyl Ester)
- Figure 5.4 (a) Plot of $\ln(I_{[(\beta\text{-Phe})+\text{K}]^+}/I_{[\text{L}_n+\text{K}]^+})$ versus $[\Delta H_{[\text{L}_n+\text{K}]^+} - \Delta H_{\text{Avg}}]$ at different collision energies, and (b) plot of $[(\Delta G)^{\text{app}}_{[(\beta\text{-Phe})+\text{K}]^+} - \Delta H_{\text{Avg}}]/RT_{\text{eff}}$ against $1/RT_{\text{eff}}$ for the $[(\beta\text{-Phe}) + \text{K} + \text{L}_n]^+$ heterodimer. ((β -Phe) = β -Phenylalanine, L_n = Serine (Ser), Serine Methyl Ester (SerOMe) and Serine Ethyl Ester (SerOEt))
- Figure 5.5 Optimized geometries of most stable protonated β -Abu, β -Leu, β -Phe, β -Tyr and β -Glu complexes calculated at B3-LYP/6-311+G(3df,2p)//B3-LYP/6-31G+(D) level of theory
- Figure 5.6 Optimized geometries of most stable potassium cationized β -Abu, β -Leu, β -Phe, β -Tyr and β -Glu complexes calculated at B3-LYP/6-311+G(3df,2p)//B3-LYP/6-31G+(D) level of theory
- Figure 5.7 Optimized geometries of less stable potassium cationized β -Phe, β -Tyr and β -Glu complexes calculated at B3-LYP/6-311+G(3df,2p)//B3-LYP/6-31G+(D) level of theory

- Figure 6.1 Optimized structure of α -/ β -alanine (at B3-LYP/6-31G(d) level)
- Figure 6.2 Ion trap MS/MS spectra of (a) protonated β -alanine, $[(\beta\text{-Ala}) + \text{H}]^+$ (m/z 90) obtained at a RF activation voltage (V_{p-p}) of 0.66 V, and (b) protonated β -alanine methyl ester, $[(\beta\text{-AlaOMe}) + \text{H}]^+$ (m/z 104) obtained at a RF activation voltage (V_{p-p}) of 0.74V
- Figure 6.3 Ion trap energy resolved MS/MS breakdown graph of protonated β -alanine, $[(\beta\text{-Ala}) + \text{H}]^+$ (m/z 90)
- Figure 6.4 Triple quadrupole MS/MS spectra of (a) protonated β -alanine, $[(\beta\text{-Ala}) + \text{H}]^+$ (m/z 90), and (b) protonated β -alanine methyl ester, $[(\beta\text{-Ala})\text{OMe} + \text{H}]^+$ (m/z 104), obtained at a collision energy of 15 eV
- Figure 6.5 Potential energy surface (PES) of the dissociation of $[(\beta\text{-Ala})/(\beta\text{-Ala})\text{OMe} + \text{H}]^+$, leading to loss of (a) H_2O , (b) CH_2CO and $(\text{H}_2\text{O} + \text{CH}_2\text{CO})$ at 0K, calculated at the B3LYP/6-311+G(3df,2p)//B3LYP/6-31G+ level
- Figure 6.6 Optimized structures (at B3LYP/6-31G+ level) for the various species on the $[(\beta\text{-Ala}) + \text{H}]^+$ and $[(\beta\text{-Ala})\text{OMe} + \text{H}]^+$ dissociation potential energy surface. All species are stable intermediates / products, except those begin with “TS”, which are transition structures
- Figure 7.1 (a) Plot of $\ln(I_{[(\beta\text{-Ala})\text{His} + \text{H}]^+}/I_{[\text{L}_n + \text{H}]^+})$ versus $[\Delta H_{[\text{L}_n + \text{H}]^+} - \Delta H_{\text{Avg}}]$ at different collision energies, and (b) plot of $[(\Delta G)^{\text{app}}_{[(\beta\text{-Ala})\text{His} + \text{H}]^+} - \Delta H_{\text{Avg}}]/RT_{\text{eff}}$ against $1/RT_{\text{eff}}$ for the proton bound heterodimer $[(\beta\text{-Ala})\text{His} + \text{H} + \text{L}_n]^+$. ($(\beta\text{-Ala})\text{His}$ = β -Alanyl-Histidine, L_n = di-ethyl methyl amine, tri-ethylamine, tri-propylamine); numbers shown are *absolute* proton affinities
- Figure 7.2 Four possible optimized geometries protonated Gly(β -Ala) complexes calculated at B3-LYP/6-311+G(3df,2p)//B3-LYP/6-31G+(D) level of theory
- Figure 7.3 Optimized geometries of protonated (a) GlyAla, AlaGly and AlaAla, and protonated (b) Gly(β -Ala), (β -Ala)Gly, (β -Ala)Ala, Ala(β -Ala), and (β -Ala)(β -Ala) complexes calculated at B3-LYP/6-311+G(3df,2p)//B3-LYP/6-31G+(D) level of theory
- Figure 7.4 Three possible optimized geometries of protonated (β -Ala)His complexes

- calculated at B3-LYP/6-311+G(3df,2p)//B3-LYP/6-31G+(D) level of theory
- Figure 7.5 Optimized geometries of the most stable conformer of protonated AlaHis and $(\beta\text{-Ala})\text{His}$ complexes calculated at B3-LYP/6-311+G(3df,2p)//B3-LYP/6-31G+(D) level of theory
- Figure 7.6 (a) Ion trap MS/MS spectra of protonated Gly($\beta\text{-Ala}$) (m/z 147), obtained at a RF activation voltage (V_{p-p}) of 0.68V (ions of low intensities are: m/z 72 = $[\text{b}_2 - (\text{NH}=\text{CH}_2 + \text{CO})]^+$, m/z 84 = $[\text{b}_2 - (\text{CO} + \text{NH}_3)]^+$, m/z 87 = $[\text{b}_2 - \text{CH}_2\text{CO}]^+$, m/z 100 = $[\text{b}_2 - \text{NH}=\text{CH}_2]^+$ and m/z 112 = $[\text{b}_2 - \text{NH}_3]^+$), and (b) triple quadrupole MS/MS spectra of protonated $(\beta\text{-Ala})\text{Gly}$, $[(\beta\text{-Ala})\text{Gly} + \text{H}]^+$ (m/z 147) obtained at a collision energy of 18 eV
- Figure 7.7 Ion trap energy resolved MS/MS breakdown graph of protonated Gly($\beta\text{-Ala}$) (m/z 147). (Appearance threshold voltages are shown in parenthesis. For clarity of presentation, the ion intensity traces for $[\text{b}_2 - (\text{NH}=\text{CH}_2 + \text{CO})]^+$ (m/z 72), $[\text{b}_2 - (\text{CO} + \text{NH}_3)]^+$ (m/z 84), $[\text{b}_2 - \text{NH}=\text{CH}_2]^+$ (m/z 100) and $[\text{b}_2 - \text{NH}_3]^+$ (m/z 112) are omitted.)
- Figure 7.8 Potential energy surface (PES) of formation of y_1 ion and b'_2 (oxazinone) ion from protonated Gly($\beta\text{-Ala}$) at 0K, calculated at the B3-LYP/6-311+G(3df,2p)//B3-LYP/6-31G(d) level
- Figure 7.9 Optimized geometries (at B3-LYP/6-31G(d) level) of the various intermediates and transition species shown in the potential energy surface (PES) of formation of y_1 ion and b'_2 (oxazinone) ion from protonated Gly($\beta\text{-Ala}$)
- Figure 7.10 Potential energy surface (PES) of formation of b_1 ion and loss of NH_3 ($[\text{MH}-17]^+$) from protonated $(\beta\text{-Ala})\text{Gly}$ at 0K, calculated at the B3-LYP/6-311+G(3df,2p)//B3-LYP/6-31G(d) level
- Figure 7.11 Optimized geometries (at B3-LYP/6-31G(d) level) of the various intermediates and transition species shown in the potential energy surface (PES) of formation of b_1 ion and loss of NH_3 ($[\text{MH} - \text{NH}_3]^+$) from protonated $(\beta\text{-Ala})\text{Gly}$
- Figure 8.1 Ion trap MS/MS spectra of (a) protonated GlyHisGly, $[\text{GHG} + \text{H}]^+$ (m/z 270), obtained at a RF activation voltage (V_{p-p}) of 0.7 V, and (b) protonated

HisGlyGly, $[\text{HGG} + \text{H}]^+$ (m/z 270), obtained at a RF activation voltage (V_{p-p}) of 0.7 V

- Figure 8.2 Ion trap energy resolved MS/MS breakdown graphs of (a) b_2 ion of protonated GlyHisGly, $[\text{GHG} + \text{H}]^+$ (m/z 195), (b) protonated cyclo(GH), $[\text{cyclo}(\text{GH}) + \text{H}]^+$ (m/z 195), and (c) b_2 ion of protonated HisGlyGly, $[\text{HGG} + \text{H}]^+$ (m/z 195)
- Figure 8.3 Q-TOF energy resolved MS/MS breakdown graphs of (a) b_2 ion of protonated GlyHisGly, $[\text{GHG} + \text{H}]^+$ (m/z 195), (b) protonated cyclo(GH), $[\text{cyclo}(\text{GH}) + \text{H}]^+$ (m/z 195), and (c) b_2 ion of protonated HisGlyGly, $[\text{HGG} + \text{H}]^+$ (m/z 195)
- Figure 8.4 Ion trap time-resolved MS/MS study of b_2 of protonated GlyHisGly, $[\text{GHG} + \text{H}]^+$ (m/z 195) versus $[\text{cyclo}(\text{GH}) + \text{H}]^+$ (m/z 195)
- Figure 8.5 Ion trap time-resolved MS/MS study of b_2 ion of protonated HisGlyGly, $[\text{HGG} + \text{H}]^+$ (m/z 195) versus protonated cyclo(GH), $[\text{cyclo}(\text{GH}) + \text{H}]^+$, (m/z 195)
- Figure 8.6 (a) Potential energy surface (PES) of the dissociation of $[\text{GlyHis} + \text{H}]^+$, leading to the formation of $b_2(\text{oxazolone})$ and $b_2(\text{diketopiperazine})$ at 0K, calculated at the B3-LYP/6-31G(d)//B3-LYP/6-31G(d) level.
- Figure 8.6 (b) Potential energy surface (PES) of the dissociation of $[\text{GlyHis} + \text{H}]^+$, leading to the formation of $b_2(\text{bicyclic})$ at 0K, calculated at the B3-LYP/6-31G(d)//B3-LYP/6-31G(d) level
- Figure 8.7 (a) Optimized geometries (at B3-LYP/6-31G(d) level) of the various intermediates and transition species shown in the potential energy surface (PES) of formation of $b_2(\text{oxazolone})$ and $b_2(\text{diketopiperazine})$ from protonated GlyHis
- Figure 8.7 (b) Optimized geometries (at B3-LYP/6-31G(d) level) of the various intermediates and transition species shown in the potential energy surface (PES) of formation of $b_2(\text{bicyclic})$ from protonated GlyHis
- Figure 8.8 Potential energy surface (PES) of the dissociation of $[\text{GlyHis} + \text{H}]^+$, leading to the formation of $b_2(\text{oxazolone})$ and further isomerization to

$b_2(\text{diketopiperazine})$ at 0K, calculated at the B3-LYP/6-31G(d)//B3-LYP/6-31G(d) level

Figure 8.9 Optimized geometries (at B3-LYP/6-31G(d) level) of the various intermediates and transition species shown in the potential energy surface (PES) of further isomerization to $b_2(\text{diketopiperazine})$ from protonated GlyHis

Figure 8.10 Potential energy surface (PES) of the dissociation of $[\text{HisGly} + \text{H}]^+$, leading to the formation of $b_2(\text{oxazolone})$ and $b_2(\text{diketopiperazine})$ at 0K, calculated at the B3-LYP/6-31G(d)//B3-LYP/6-31G(d) level.

Figure 8.11 Optimized geometries (at B3-LYP/6-31G(d) level) of the various intermediates and transition species shown in the potential energy surface (PES) of formation of $b_2(\text{oxazolone})$ and $b_2(\text{diketopiperazine})$ from protonated HisGly

Figure 8.12 Potential energy surface (PES) of the dissociation of $[\text{HisGly} + \text{H}]^+$, leading to the formation of $b_2(\text{oxazolone})$ and further isomerization to $b_2(\text{diketopiperazine})$ at 0K, calculated at the B3-LYP/6-31G(d)//B3-LYP/6-31G(d) level

Figure 8.13 Optimized geometries (at B3-LYP/6-31G(d) level) of the various intermediates and transition species shown in the potential energy surface (PES) of further isomerization to $b_2(\text{diketopiperazine})$ from protonated HisGly

List of Tables

- Table 4.1 Experimental K^+ affinities at 0 K (kJ mol^{-1}) of amino acids (Group 1, 2, 3) measured by the extended kinetic method
- Table 4.2 Experimental and theoretical K^+ affinities at 0 K (kJ mol^{-1}) of α -amino acids
- Table 4.3 Experimental and theoretical K^+ affinities at 0 K (kJ mol^{-1}) of α -amino acids methyl esters
- Table 4.4 Literature values of experimental K^+ affinities at 0 K / 298 K (kJ/mol) of selected amino acids
- Table 5.1 Biological significance of the five selected β -amino acids in this study
- Table 5.2 Experimental proton (H^+) affinities at 298K, (ΔH_{298} , kJ mol^{-1}) and $\Delta(\Delta S_{H^+})^{\text{app}}$ ($\text{J mol}^{-1} \text{K}^{-1}$) of β -amino acids
- Table 5.3 Experimental potassium cation (K^+) affinities at 0 K, (ΔH_0 , kJ mol^{-1}) and $\Delta(\Delta S_{H^+})^{\text{app}}$ ($\text{J mol}^{-1} \text{K}^{-1}$) of β -amino acids
- Table 5.4 Experimental and theoretical proton (H^+) affinities of β -amino acids.
- Table 5.5 Experimental and theoretical K^+ affinities of β -amino acids at 0 K (kJ mol^{-1})
- Table 6.1 The relative enthalpies (ΔH_0 , ΔH_{298} at 0K and 298K), Gibbs free energies (ΔG_{298} at 298K, in kJ mol^{-1}) and entropies (ΔS_{298} at 298K, in J mol^{-1}) of the highest energy barriers for the loss of small neutrals on the $[(\beta\text{-Ala}) / (\beta\text{-Ala})\text{OMe} + H]^+$ potential energy surface.^a
- Table 6.2 The Relative Enthalpies at 0K (ΔH_0) and Relative Gibbs Free Energies at 298K (ΔG_{298}), in kJ mol^{-1} , with respect to species 1a (1b) for protonated β -Ala and (β -AlaOMe), respectively
- Table 7.1 Experimental proton (H^+) affinities at 0K, (ΔH_0 , kJ mol^{-1}) and $\Delta(\Delta S_{H^+})^{\text{app}}$ ($\text{J mol}^{-1} \text{K}^{-1}$) of α - and β -dipeptides determined by the extended kinetic method.

- Table 7.2 Comparison of experimental and theoretical proton (H^+) affinities of α - and β -dipeptides.
- Table 7.3 Energy barriers for competitive formation of (a) b_2' (oxazinone) and y_1 ions from $[Gly(\beta-Ala) + H]^+$, and (b) $[MH - NH_3]^+$ and b_1 ions from $[(\beta-Ala)Gly + H]^+$ ^a: the relative enthalpies (ΔH_0 , ΔH_{298} at 0K and 298K), Gibbs free energies ΔG_{298} at 298K, in $kJ\ mol^{-1}$) and entropies (ΔS_{298} at 298K, in $J\ mol^{-1}\ K^{-1}$)
- Table 7.4 Potential energy surface for the dissociation of (a) $[Gly-(\beta-Ala) + H]^+$ and (b) $[\beta-Ala-(Gly) + H]^+$: the relative enthalpies at 0K and 298K (ΔH_0 and ΔH_{298}) and Gibbs free energies at 298K (ΔG_{298}), in $kJ\ mol^{-1}$, with respect to species 1.
- Table 8.1 Energy barriers for the formation and further isomerization of different b_2 ions on the $[GlyHis / HisGly + H]^+$ potential energy surface: the relative enthalpies (ΔH_0 , ΔH_{298} at 0K and 298K), Gibbs free energies (ΔG_{298} at 298K, in $kJ\ mol^{-1}$) and entropies (ΔS_{298} at 298K, in $J\ mol^{-1}$)

List of Schemes

- Scheme 1.1 Chemical structures of (a) α -alanine and (b) β -alanine
- Scheme 1.2 Charge-solvated (CS) versus zwitterionic (ZW) alkali metal cation binding modes of amino acids in the gas phase
- Scheme 1.3 Fragmentation and nomenclature of protonated and alkali metal cationized peptides
- Scheme 1.4 Proposed mechanism for formation of b_1^- and y_1^- -ions
- Scheme 1.5 Formation of b'_2 (oxazinone) ion from $[\text{Gly}(\beta\text{-Ala}) + \text{H}]^+$
- Scheme 1.6 Hydrogen bonding patterns in protonated (a) α -Ala and (b) β -Ala
- Scheme 1.7 Chemical structure of b_2 (diketopiperazine-His) ion of $[\text{GlyHis} + \text{H}]^+$
- Scheme 4.1 Chemical structures of 20 amino acids
- Scheme 4.2 Schematic representation of zwitterionic (ZW) binding mode of K^+ and Tyr previously reported [Dunbar, 2000]
- Scheme 5.1 Chemical Structure of Selected Bioactive β -Amino Acids
- Scheme 6.1 The loss of CO from species $6a'$. Values in parentheses (ΔH_0 , in kJ/mol) are relative enthalpies respect to species 1a.
- Scheme 6.2 Loss of NH_3 from $[(\beta\text{-Ala}) + \text{H}]^+$
- Scheme 6.3 Loss of $(\text{NH}_3 + \text{CO})$ from $[(\beta\text{-Ala}) + \text{H}]^+$
- Scheme 6.4 Loss of $\text{NH}=\text{CH}_2$ from $[(\beta\text{-Ala}) + \text{H}]^+$
- Scheme 7.1 Formation of b'_2 (oxazinone) ion from $[\text{Gly}(\beta\text{-Ala}) + \text{H}]^+$
- Scheme 8.1 Chemical structure of histidine
- Scheme 8.2 Chemical structures of b_2 (oxazolone), b_2 (diketopiperazine) and b_2 (bicyclic) formed from $[\text{GlyHis} + \text{H}]^+$.
- Scheme 8.3 The proposed pathway of loss of NH_3 from b_2 (oxazolone-His) ion of $[\text{GlyHis} + \text{H}]^+$

List of Abbreviations

General

AC	Alternate current
B3LYP	Beck's three parameters exchange function (B3-) and the correlation functional Lee, Yang and Parr (-LYP)
BSSE	Basis Set Superposition Error
CGTOs	Contracted gaussian type orbitals
CID	Collision-induced dissociation
CS	Charge-solvated form
d.c.	Direct current
Da	Dalton
DFT	Density functional theory
E_{def}	Deformation energy
E_{elec}	Electronic energy
EP(K^+)	Energetic protocol for K^+
ESI	Electrospray Ionization
ESI-MS	Electrospray ionization-mass spectrometry
$E_{\text{stabilization}}$	Stabilization energy
GB	Gas phase basicity
GTO	Gaussian-type orbital
H/D	Hydrogen/Deuterium
H^+	Proton
HF	Hartree-Fock
m/z	Mass to charge ratio

M^+	Alkali metal cation, Li^+ , Na^+ or K^+
MAD	Mean absolute deviation
MCMM	Monte Carlo multiple minimum
MO	Molecular orbital
MP2	Second-order for Møller-Plesset
MS	Mass spectrometry
MS/MS	Tandem mass spectrometry
PA	Proton affinity
PCA	Potassium cation affinity
PES	Potential energy surface
PGTOs	Primitive gaussian type orbitals
R	gas constant, $8.31451 \text{ J K}^{-1} \text{ mol}^{-1}$
SCF	Self-consistent field
STO	Slater type orbitals
T_{eff}	Effective temperature
u	Atomic mass unit (amu)
V	Voltage
ZPE	Zero-point energy
ZW	Zwitterionic form
$\Delta(\Delta S)^{\text{app}}$	Apparent entropy change
$\Delta G_{0/298}$	Free energy at 0, 298K
ΔG^{app}	Apparent free energy
ΔH	Affinity or binding energy
$\Delta H_{0/298}$	Affinity or Binding Energy at 0, 298K

Abbreviations of Compounds

Me = -CH₃

Et = -C₂H₅

Chemical

Abu	Aminobutyric acid
AbuOMe	Amino isobutyric acid methyl ester
Ala	Alanine
Ala(β-Ala)	Alanyl(β-alanine)
AlaAla	Alanylalanine
AlaGly	Alanylglycine
AlaHis	Alanylhistidine
AlaOMe	Alanine methyl ester
Arg	Arginine
Asn	Asparagine
AsnOMe	Asparagine methyl ester
Asp	Asparatic acid
AspOMe	Asparatic acid methyl ester
Cys	Cysteine
CysOMe	Cysteine methyl ester
DMA	N,N-Dimethylacetamide
DMF	N,N-Dimethylformamide
F	Formamide
Gln	Glutamine
Gln	Glutamine methyl ester

Glu	Glutamic acid
GluOMe	Glutamic acid methyl ester
Gly	Glycine
Gly(β -Ala)	Glycyl(β -alanine)
GlyAla	Glycylalanine
GlyGly	Glycylglycine
GlyOMe	Glycine methyl ester
HCl	Hydrochloric acid
His	Histidine
HisOMe	Histidine methyl ester
Ile	Isoleucine
Leu	Leucine
LeuOEt	Leucine ethyl ester
LeuOMe	Leucine methyl ester
Lys	Lysine
LysOEt	Lysine ethyl ester
LysOMe	Lysine methyl ester
MA	N-Methylacetamide
MeOH	Methanol
Met	Methionine
MetOMe	Methionine methyl ester
MF	N-Methylformamide
Phe	Phenylalanine
PheOEt	Phenylalanine ethyl ester
PheOMe	Phenylalanine methyl ester

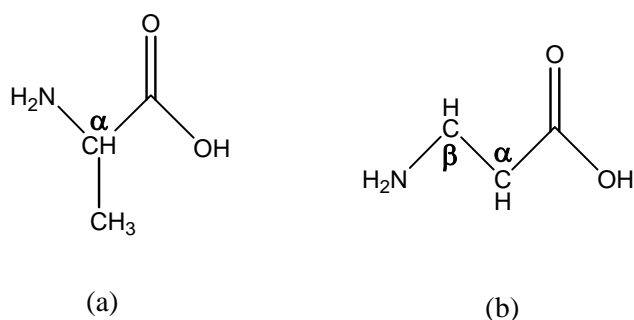
Pro	Proline
ProOMe	Proline methyl ester
Ser	Serine
SerOEt	Serine ethyl ester
SerOMe	Serine methyl ester
TCA	Trichloroacetic acid
TFA	Trifluoroacetic acid
Thr	Threonine
Trp	Tryptophan
Tyr	Tyrosine
TyrOMe	Tyrosine methyl ester
Val	Valine
ValOMe	Valine methyl ester
β -Ala	β -Alanine
β -AlaOMe	β -Alanine methyl ester
(β -Ala)(β -Ala)	β -Alanyl(β -alanine)
(β -Ala)Ala	β -Alanylalanine
(β -Ala)Gly	β -Alanylglycine
(β -Ala)His	β -Alanylhistidine (Carnosine)

Chapter 1 Introduction

1.1 Biochemical Significance of α -/ β -Amino Acids and Peptides

The twenty naturally occurring α -amino acids are fundamental building blocks for peptides and proteins, as well as for the synthesis of pharmaceutically important intermediates and drugs. [Zheng et al., 2006] Because of their biochemical significance, there are extensive past and on-going studies on the properties of α -amino acids and α -peptides.

In recent years, there are growing interests and studies on the properties of β -amino acids and peptides containing β -amino acids (named β -peptides in the present study).[Seebach et al., 2001; Rossi et al., 2003] In terms of chemical structure, the sole difference between α - and β -amino acids is the absence and presence, respectively, of an 'additional' $-\text{CH}_2-$ group between the N- and C-terminus of the amino acid. The most common and naturally occurring β -amino acid is β -alanine (**Scheme 1.1**). It is a constituent amino acid of the naturally occurring β -peptides carnosine and anserine, and also of pantothenic acid (vitamin B-5).[Davidson, 2003] β -alanylation of octapamine, tyramine or dopamine is suggested to lead to storage forms of these neurotransmitters in biological systems. β -alanine is also an important metabolite of the central nervous system and increased levels are associated with Cohen's syndrome.[Struys et al., 1999] Apart from being an indispensable component of coenzyme A, it is also a product of pyrimidine base degradation and a factor stimulating collagen synthesis in tissues. [Nagai and Suda, 1988; Boldyrev and Severin, 1990]



Scheme 1.1 Chemical structures of (a) α -alanine and (b) β -alanine

The insertion of a methylene group into the backbone of an α -amino acid has a clear structural impact. β -amino acids are stronger bases than α -amino acids,[Sewald, 1999] and are able to form stable secondary peptide structures with as few as four β -amino acid residues;[Seebach and Matthews, 1997] β -peptides containing β -amino acids exhibit additional degrees of conformational freedom as compared to their α -peptide counterparts. [Hook et al., 2004] The incorporation of a β -amino acid moiety into an α -peptide sequence can beneficially enhance proteolytic stability whilst still retaining significant original biological activity.[Steer et al., 2000, Gopi et al., 2003] With such enhanced stability and conformational flexibility, β -peptides are increasingly recognized to be an important class of compounds with potentially high biomedical and therapeutic values. [Seebach et al., 2001; Rossi et al., 2003]

A well-known example of β -peptide is carnosine ((β -Ala)-His), which is found to be widely distributed in vertebrates, and particularly abundant in muscle and nervous tissues. [Boldyrev and Severin, 1990] Carnosine is an established anti-aging agent because of its metal chelation and free-radical scavenging abilities.[Zatta et al., 2003; Tamba and Torreggiani, 1999] Another class of β -peptides is paralyisin (an example is (β -alanine)-tyrosine), which are toxins playing active roles in the metamorphosis of insects.[Kyrikou et al., 2003] In addition, the synthesis of a linear mPEG chain with methionine-(β -

alanine) (Met-(β -Ala) can be used as the ‘reporter spacers’ to assist the detection of the position of PEGylation within a peptide sequence. [Veronese et al., 2001; Guiotto et al. 2002]

The first part of the present study is an on-going investigative effort to determine the potassium cation (K^+) binding affinities of the 20 α -amino acids, and the proton (H^+) and potassium cation (K^+) binding energies (affinities) of biochemically important model β -amino acids and β -peptides. These are *intrinsic* properties of α -/ β -amino acids and α -/ β -peptides basic to the understanding of their chemical behaviour in the gas phase, and indirectly to their behaviour in the solution phase, in the presence of solvent effects. In addition, the H^+ and K^+ affinities of amino acids and peptides are also important factors governing their mass spectrometric dissociation patterns and pathways in the gas phase, and the relative stabilities of the dissociation products.

The recent surge in proteomic research requires sensitive and fast methods to determine the sequence of proteolytic peptides. [Rappsilber et al., 2003; Aebersold and Mann, 2003; Yates, 2004] Sequence information of α -peptides are now routinely obtained by tandem mass spectrometry (MS/MS), which is based on the low-energy (eV, laboratory scale) collision-induced dissociation (CID) of *protonated* peptides, [Paizs and Suhai, 2005] supplemented sometimes by that of alkali metal cationized peptides.[Tomlinson et al., 1999; Lin et al., 2000] However, the rules governing the dissociation behaviour of protonated α -peptides are not fully understood to-day. Compared to their α -analogues, the mass spectrometric dissociation behaviour of β -amino acids and β -peptides are even less studied and not well understood. The second part of the present study is to initiate a mechanistic study of the mass spectrometric dissociation of protonated model β -amino acids and β -peptides. Furthermore, a detailed study on the fragmentation pathways of

protonated α -peptides containing histidine was also carried out. The present study is intended, though in a limited way, as a comparative study of the H^+/K^+ affinities and mass spectrometric fragmentation behaviour of model α -/ β -amino acids and α -/ β -peptides.

1.2 Proton (H^+) and Potassium Cation (K^+) Affinities of Amino Acids and Peptides

Proton affinities (PA) of amino acids and peptides Protonation is a common and important process in biological systems. [Stryer, 1995] Amino acids and dipeptides have many functional groups and oxygen (O)/nitrogen (N) proton binding sites. The site of proton attachment significantly affects the intra-molecular hydrogen bonding, three dimensional structures and biological activities of peptides and proteins. The intrinsic properties of amino acids and peptides in the gas phase are often governed by its proton affinity (PA), or enthalpy of proton attachment. It is also a key parameter determining the occurrence and competitiveness of fragmentation pathways of protonated peptides, and hence the availability of sequence information derived from tandem mass spectrometry. Not surprisingly, there has been great interests in the gas phase proton affinities and site of protonation of amino acids and peptides. [Harrison and Yalcin, 1997]

The proton affinity (PA) of an amino acid/peptide is defined as the enthalpy change (ΔH) for the dissociation of the protonated complex, H^+L , as shown in Reaction [1.1], and calculated by Eqn. [1.2] for the enthalpy change at 0 K:



$$\Delta H = E_{H^+} + E_L - E_{H^+L} \quad [1.2]$$

where H^+ is the proton, L (ligand) is amino acid or peptide, and E represents the energy of H^+ , L and H^+L . The proton affinities at 0K and 298K are often denoted by ΔH_0 and ΔH_{298} , respectively. In order to assist the inter-comparison of theoretical and experimental values, standard statistical thermodynamic relations are employed to theoretically estimate the changes in enthalpy, free energy and entropy (e.g., ΔH_{298} , ΔS_{298} and ΔG_{298}) at temperatures higher than 0 K. [Delbene et al., 1983]

The intrinsic properties of molecules are best determined in the gas phase, in the absence of complicating solvent effects. The gas phase proton affinities of the 20 α -amino acids and selected di-/tri-peptides have been determined by different mass spectrometric techniques because protonated species can be easily generated and isolated under the vacuum conditions of a mass spectrometer. In the present study, the proton affinities of selected α -/ β -amino acids and dipeptides were determined by the mass spectrometric kinetic method (to be further elaborated in Section 2.4). The experimental measurement of proton affinities was supplemented by high level molecular orbital (M.O.) calculations, which provide information on the most stable proton binding sites and intra-molecular hydrogen bonding patterns of the selected protonated amino acids and dipeptides.

Potassium cation affinities of amino acids and peptide The potassium cation (K^+) is one of the most abundant metal cations found in biological systems. The non-covalent, mainly electrostatic binding interaction between K^+ and proteins can induce conformational changes in proteins. [Lippard and Berg, 1994; Stryer, 1995; Rodgers and Armentrout, 2000; Kohtani et al., 2000; Taraszka et al., 2001] The trans-membrane movement of K^+ underlies (electrical) signaling in the nervous system, generation of rhythmic signals by the heart, and unceasing sifting of toxic solutes in the blood by the kidney. [Miller, 1993; Kaim et al., 1994; Hille, 2001] Recent studies have shown that the

selective transport of K^+ across cell membranes depends on the binding interaction between K^+ and the main chain carbonyl oxygen atoms of the potassium ion channel (protein). [Doyle et al., 1998; Jiang et al., 2003; Zhou nad McKinnon, 2003] K^+ binding to the phenyl ring of aromatic amino acid residues, i.e., phenylalanine, tyrosine and tryptophan, have been suggested to affect the structure-functional aspects of some enzymes, e.g. tryptohanase, [Gokel et al., 2000] and the selectivity of K^+ ion channels. [Silverman et al., 1998; Nakamura et al., 1997]

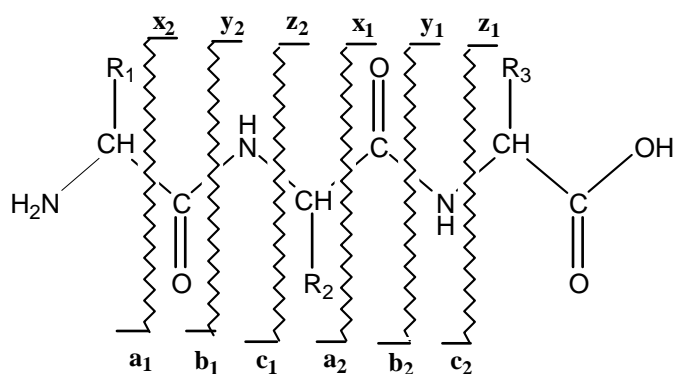
Hence, detailed knowledge of the structural and energetic aspects of the local binding interaction between K^+ and prototypical amino acid residues and peptides is essential for understanding the molecular basis of these important biological processes, serving as building blocks and links towards a detailed understanding of these interactions in the more complex and larger protein systems. Specifically, it is of fundamental importance to determine the binding energies and *preferred* sites of potassium binding to α/β -amino acids, and the relative stabilities of different K^+ binding modes. In addition, such knowledge is required in the interpretation of mass spectra of K^+ -peptide complexes, from which peptide sequencing information can be obtained, complimentary to that of protonated peptides. [Grese et al., 1989; Teesch and Adams, 1991; Loo and Muenster, 1999; Huang et al., 2002b]

When the proton is replaced by an alkali metal cation (e.g. $M^+ = K^+, Na^+$ and Li^+), Eqn. [1.2] can be equally applied to define the alkali metal cation (M^+) affinities (ΔH_0 and ΔH_{298}) and free energy of binding (ΔG_{298}) of α/β -amino acids and peptides. Amino acids and dipeptides are multi-dentate ligands with many possible oxygen (O) and nitrogen (N) alkali metal binding sites. Obviously, potassium (K^+) binding affinities of amino acids and dipeptides are dependent on how K^+ interacts with these plausible O/N-binding sites.

1.3 Mass Spectrometric Fragmentation of Protonated Amino Acids and Peptides

'Sequence-specific' fragment ions from amide (peptide) bond cleavage of peptides

At present, peptide sequencing by MS/MS is *mainly* based on the collision-induced dissociation (CID) of protonated peptides generated by electrospray ionization (ESI) and/or matrix-assisted laser desorption ionization (MALDI). Wysocki and co-workers, [Wysocki et al., 2000; Tsapraillis et al., 1999; Dongre et al., 1996b; Jones et al., 1994; McCormack et al., 1993] together with findings from other research groups, [Burlet et al., 1992a; Burlet et al., 1992b; Harrison and Yalcin, 1997; Cox et al., 1996; Dongre et al., 1996a; Thorne et al., 1990; Ballard and Gaskell, 1991] have demonstrated that the 'external' proton is 'mobile' upon collisional activation, and can be attached to various basic sites of the peptide, depending on the gas phase basicity (GB) / proton affinity (PA) of the protonation sites and internal energy distribution of the protonated peptide. Upon transfer/attachment of the proton to the amide nitrogens on the peptide backbone, the 'external' proton would decrease the bond order of the C-N amide bond and results in efficient cleavage of the peptide bond to yield either the b_i or the y_i ions (refer to **Scheme 1.3**). Usually, two series of 'sequence-specific' fragment ions are produced as a result of the amide (peptide) bond cleavage: (i) the a_i , b_i and c_i series of ions associated with the N-terminus, and (ii) the x_i , y_i (i.e. the '**Y+2H**' or "**y**") and z_i series of ions associated with the C-terminus of the peptides, where i = location of the amino acid residue counting from the C-terminus of the peptide as shown in **Scheme 1.3**. [Biemann, 1988; Roepstorff and J. Fohlman, 1984] Among these 'sequence-specific' fragment ions, the b_i and y_i ions are more commonly found in the MS/MS spectra of protonated peptides and useful in peptide sequencing. The mass difference between successive pairs of b_i/y_i and b_{i+1}/y_{i+1} fragment ions is related to the relative molar mass of the $(i + 1)$ amino acids, and is usually used to deduce the location (sequence) of individual amino acids in the peptide.



Scheme 1.3 Fragmentation and nomenclature of protonated and alkali metal cationized peptides.

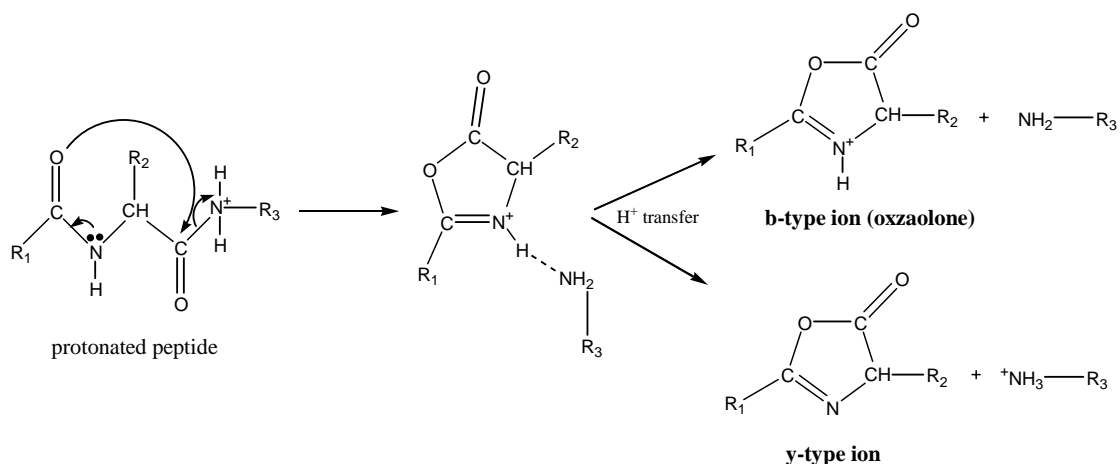
Loss of small stable neutrals) from protonated amino acids/peptides Fragment ions derived from loss of small neutrals, such as CO , CO_2 , NH_3 and H_2O , are found in the MS/MS mass spectra of protonated amino acids and small peptides, which may also appear, albeit partially, in the MS/MS spectra of larger peptides. They are generally regarded as ‘non-sequence specific’ (not derived from peptide bond cleavage) and previously regarded as not useful for peptide sequencing. However, their formation competes with the formation of sequence-specific \mathbf{b}_i and \mathbf{y}_i ions, leading to complications in the MS/MS spectrum of a protonated peptide, and may reduce the chance of a successful sequencing analysis. Therefore, an understanding of the factors governing the competitive formation of fragment ions by loss of neutrals versus the formation of \mathbf{b}_i and \mathbf{y}_i ions is essential in the interpretation of MS/MS spectra for peptide sequencing.

A number of experimental and theoretical studies on the loss of small stable neutrals from simple protonated α -amino acids/ α -peptides have been reported. [Rogalewicz et al., 2000; Rogalewicz and Hoppilliard, 2000; O’Hair et al., 2000; Reid et al., 1998; Klassen and Kebarle, 1997; Uggerud, 1997]. In fact, there is a growing awareness that fragment ions arising from the loss of small neutrals (e.g., loss of H_2O to yield the \mathbf{b}_n ions, where n is the

number of amino acid residues in the peptide) may fragment further to yield sequence specific ions. [Pingitore et al, 2004; Paizs and Suhai, 2001] This provides another justification for investigating the fragmentation mechanisms leading to loss of small neutrals from protonated peptides.

Fundamental studies on fragmentation mechanisms In practice, the ability of MS/MS in peptide sequencing depends strongly the formation/availability of ‘sequence-specific’ \mathbf{b}_i , \mathbf{y}_i and \mathbf{a}_i fragment ions: more number of \mathbf{b}_i , \mathbf{y}_i and \mathbf{a}_i ions in the MS/MS spectra would enhance the probability of a successful sequence determination. However, the occurrence of sequence-specific fragment ions is found to be not easily predictable among peptides, but depends very much on the composition and location of amino acids in the peptide.

In order to elucidate the governing rules leading to formation of diagnostic \mathbf{b}_i , \mathbf{y}_i and \mathbf{a}_i fragment ions, there have been some in-depth studies on the fragmentation mechanisms of protonated α -peptides in the past few years, as summarized in an excellent review by Paizs and Suhai.[Paizs and Suhai, 2005] At least for peptides comprised of amino acids with no O/N/S heteroatoms in their side chains (i.e. aliphatic amino acids and phenylalanine), the \mathbf{b}_i ions are found by Harrison and co-workers [Yalcin et al., 1995; Yalcin et al., 1996; Nold et al., 1997] to be a five-membered cyclic oxazolone structure initiated by intramolecular nucleophilic attack of an amide carbonyl oxygen on the N-terminal side at the neighboring carbonyl carbon, as shown in **Scheme 1.4.** [Schlosser and Lehmann, 2000]



Scheme 1.4 Proposed mechanism for formation of b_i - and y_i -ions

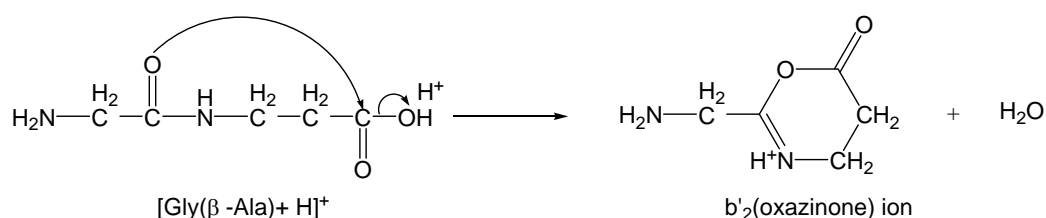
Theoretical studies by Paizs and Suhai further suggested that under the time-frame of low-energy (eV, laboratory scale) collision conditions, [Paizs and Suhai, 2005] the b_i or y_{n-i} (truncated protonated peptides) ions may actually be formed via the dissociation of a proton-bound dimer complex/intermediate between the oxazolone derivative and the truncated peptide. The competitive formation and relative ion abundances of the b_i and y_{n-i} ions is determined by the thermochemistry (proton affinity) of the species involved, and can be approximated by using a linear free-energy relationship: [Harrison, 1999; Paizs and Suhai, 2002; Paizs and Suhai, 2004]

$$\ln\left(\frac{b_i}{y_{n-i}}\right) \approx \left(\frac{PA_{N\text{-term}} - PA_{C\text{-term}}}{RT_{\text{eff}}}\right) \quad [1.3]$$

where b_i/y_{n-i} is the ion intensity ratio of the b_i and y_{n-i} ions, $PA_{N\text{-term}}$ ($PA_{\text{(oxazolone derivative)}}$) and $PA_{C\text{-term}}$ ($PA_{\text{(C-terminal peptide)}}$) are the proton affinities (PA) of the neutral species involved in the proton bound dimer, and T_{eff} (effective temperature) is a parameter related to the average internal energy of the dissociating dimer ions. This dissociation mechanism is named the b_x - y_z pathways by Paizs and Suhai. [Paizs and Suhai, 2005;

Yalcin et al., 1996; Nold et al., 1997; Paizs et al., 1999; Polce et al., 2000] However, related studies on β -amino acids/peptides have not been reported.

For β -peptides with β -alanine at the N-terminus, the $\mathbf{b}_x\text{-}y_z$ pathways would require the formation of a cyclic 6-membered oxazinone ring intermediate and product $\mathbf{b}_i(\text{oxazinone})$ ions, in competition with the formation of \mathbf{y}_{n-i} ions. **Scheme 1.5** shows the formation of $\mathbf{b}'_2(\text{oxazinone})$ ion from $[\text{Gly}(\beta\text{-Ala}) + \text{H}]^+$. It has been also noted that formation of the five-membered ring oxazolone structure as reaction intermediates and products is most favoured when compared to other ring sizes. An intermediate species of larger ring size will be entropically less favoured, while a smaller ring size would lead to greater enthalpy of activation due to ring constrains [Schlosser and Lehmann, 2000]. Hence, one of the objectives of the present study is to investigate the energetic/entropic factors governing the competitive formation of $\mathbf{b}_i(\text{oxazinone})$ versus \mathbf{y}_{n-i} fragment ions from protonated β -peptides, which are expected to be different from that of α -peptides. Also, the cyclic $\mathbf{b}_i(\text{oxazolone})$ ions usually dissociate further by characteristic loss of CO to yield \mathbf{a}_i ions which are also useful in sequence determination. [Yalcin et al., 1995; 1996; Biemann and Martin, 1987] A related issue to be investigated is whether $\mathbf{b}_i(\text{oxazinone})$ ions derived from β -peptides would further dissociate in a similar manner to yield \mathbf{a}_i ions, or to some other sequence-specific fragment ions.



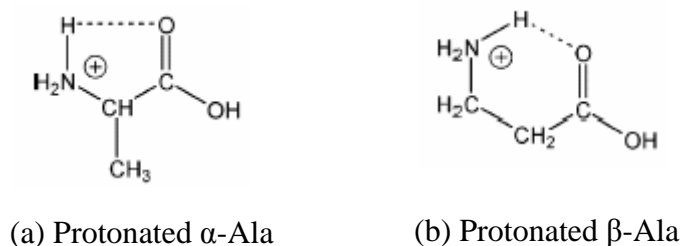
Scheme 1.5 Formation of $\mathbf{b}'_2(\text{oxazinone})$ ion from $[\text{Gly}(\beta\text{-Ala}) + \text{H}]^+$

1.4 Literature Review

In recent years, the free energies/affinities of Li^+ and Na^+ binding to the twenty naturally occurring α -amino acids have been reported, [Bojesen et al., 1993; Kish et al., 2003; Feng et al., 2003] with most of them obtained by the mass spectrometric kinetic method (KM). However, experimental data on the *intrinsic* K^+ binding energies (affinities) and binding modes of these biological model ligands remain not reported. As the potassium ion (ionic radius, 1.33 Å) is bigger than Li^+ (ionic radius 0.60 Å) and Na^+ (ionic radius 0.95 Å) ions, [Huheey et al., 1993] differences in their binding affinities and preferred modes of binding are expected. Given the biochemical significance of potassium, we have initiated and completed a mass spectrometric kinetic method and theoretical study on the K^+ affinity of the 20 α -amino acids and their methyl-esters. In addition, the relative stabilities of the charge-solvated (CS) and zwitterionic (ZW) K^+ binding modes are systematically investigated in this project.

The proton affinities (PA) and/or basicities of α -amino acids and model α -dipeptides in the gas phase have been determined in the past ten years. [Harrison, 1997] In contrast, there is virtually no information on the proton affinities of model β -amino acids and β -dipeptides. The only exception is the proton affinity (PA) of β -alanine recently reported by Wesdemiotis and co-workers using the mass spectrometric extended kinetic method [Hahn and Wesdemiotis, 2003]; the PA was found to be $924 \pm 4 \text{ kJ mol}^{-1}$ as compared to the PA of α -Ala at $902 \pm 4 \text{ kJ mol}^{-1}$. The higher PA of β -Ala is suggested to be the result of moving the electron-withdrawing $-\text{COOH}$ group further away from the amino ($-\text{NH}_2$) functional group and an improved hydrogen bonding arrangement with the β -substitution pattern as shown in **Scheme 1.6**. Hence, it would be interesting to learn

whether such structural effects on enhancement of PA from α - to β -alanine can be extended to other β -amino acids and the larger β -dipeptides.



Scheme 1.6 Hydrogen bonding patterns in protonated (a) α -Ala and (b) β -Ala

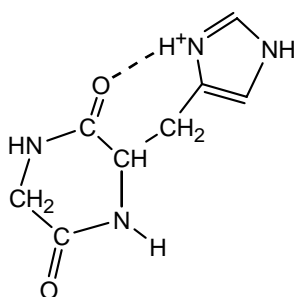
In order to differentiate α - and β -Ala containing tripeptides, Cooks and co-workers investigated the competitive dissociations of alkali metal cation ($M^+ = Li^+, Na^+, K^+, Rb^+$ and Cs^+) bound dimeric ions between an α - and β -tripeptide to their respective M^+ bound tripeptide complexes in an ion trap mass spectrometer.[Wu et al., 2004] Based on the large differences in relative intensities of the M^+ bound monomer (tripeptide) complexes observed, three pairs of isomers were successfully differentiated: (α -Ala)-Gly-Gly/ β -Ala)-Gly-Gly, Gly-(α -Ala)-Gly/Gly-(β -Ala)-Gly, and Gly-Gly-(α -Ala)/Gly-Gly-(β -Ala), with the Li^+ bound heterodimer complexes yielding the largest differences. The differences clearly reflect significant differences in the alkali metal cation affinities (ΔH_0 and ΔH_{298}) /free energy of binding (ΔG_{298}) of α - versus β -tripeptides, and structural features favoring zwitterionic (ZW) versus charge-solvation (CS) forms of the alkali metal-bound complexes was suggested to play a key role in the differentiation of the isomeric ion. However, there is no report on the *intrinsic* alkali cation affinities of β -amino acids/ β -dipeptides. As an exploratory and comparative study to the proton affinities of selected β -amino acids, the potassium cation affinities of selected β -amino

acids were experimentally measured and the relative stabilities of the CS versus ZW K^+ binding modes were investigated theoretically in the present study.

Unlike the case of α -amino acids/peptides, the fragmentation mechanisms of β -amino acids/peptides have not been systematically investigated. Seebach and co-workers reported the ESI-MS/MS fragmentation patterns of seven synthetic β -polypeptides comprised of all β -amino acids (β -alanine and its α -/ β -substituted 'homo'-derivatives. The largest β -polypeptides investigated contains 18 β -amino acids) and some of their methyl ester and N-acetyl derivatives.[Schreiber et al., 1999] Similar to α -peptides, they found sufficient number of b_i and y_i fragment ions due to amide (peptide) bond cleavage, allowing the sequence of β -amino acids in the β -polypeptide to be determined. On the other hand, the (i) $[b_i\text{-HN=CHR}]^+$ ($R=H, -CH_3$) and (ii) $[y_i\text{-NH}_3]^+$ fragment ions, which are not observed in the MS/MS spectra of protonated α -peptides, were also found. However, the underlying cause and fragmentation mechanisms leading to these similarities and differences between isomeric α - and β -peptides have not been explored. Furthermore, the case of β -peptides containing only one (or a few) β -amino acids among α -amino acids, presumably more common, has not been systematically investigated. Hence, in this study, the fragmentation pathway of β -alanine and its methyl ester, and model / biochemically significant β -dipeptides containing β -alanine are investigated using both tandem mass spectrometric (MS/MS) techniques and high level molecular orbital (M.O.) calculations.

Histidine-containing peptides are now widely developed as drugs for treatment on some diseases, e.g., as a ophthalmic drug for treating human cataracts. [Babizhayev et al., 2001] However, peptide sequencing of histidine-containing peptides by MS/MS is known to be complicated and its dissociation mechanisms are only partially understood. [Farrugia et al., 2001; Tsaprailis et al., 2004; Wysocki et al., 2000] O'Hair and co-workers first reported

that, experimentally, the ion trap MS/MS spectra (without defining detailed conditions, such as activation RF voltages used) of b_2 ions derived from protonated O-methyl esters of model di-/tripeptides containing histidine such as Glycyl-Histidine (GH) and Histidyl-Glycine (HG) are identical to that of cyclo-(GH) having the protonated diketopiperazine structure. [Farrugia et al., 2001] By using molecular orbital calculations, he was able to show that the b_2 (diketopiperazine-His) ion structure (**Scheme 1.7**; or abbreviated as b_2 (diketo-His)) was found to be thermodynamically more stable and favored over the b_2 (oxazolone) structure (refer to **Scheme 1.4**). [Farrugia et al., 2001] This finding is in contrast with the findings of previous studies that the formation of b_2 (oxazolone) ion has the lowest reaction barrier among the many dissociation pathways of α -peptides (which do not contain histidine) reported in the literature. [Yalcin et al., 1995; Yalcin et al., 1996; Paizs and Suhai, 2005; Paizs and Suhai, 2004; Schlosser and Lehmann, 2000] In other words, do protonated histidine-containing peptides behave differently from the b_x - y_z pathways, which are normally assumed to yield b_2 (oxazolone) ions? Hence, apart from the study of the dissociation pathways of β -amino acids/dipeptides, a systematic and study on the dissociation pathways of protonated His-containing dipeptides, including the associated energy barriers leading to the formation of the b_2 (diketopiperazine-His) and b_2 (oxazolone-His) ion structures, were carried out in the present study.



Scheme 1.7 Chemical structure of b_2 (diketopiperazine-His) ion of $[\text{GlyHis} + \text{H}]^+$.

1.5 Aim and Scope of Present Study

The first part of the present study is to apply the mass spectrometric kinetic method to determine the H^+ and/or K^+ affinities of twenty α -amino acids and their methyl-esters, selected model and biochemically important β -amino acids and β -dipeptides. In addition, high level density functional theory (DFT) molecular orbital calculations are also carried out to validate the experimental results, and to provide in sight on the relative stabilities of various H^+ or K^+ binding modes. The most stable H^+ binding structure of α -/ β -amino acids and dipeptides obtained in the first part of this study could also serve as the starting structures for the study of dissociation pathways of protonated model α -/ β -peptides in the second part of this project.

In the second part of the present study, we aimed to elucidate the dissociation pathways of protonated β -alanine and its methyl ester, selected model and biochemically significant β -dipeptides, and His-containing dipeptides. High level density functional theory (DFT) molecular orbital calculations were used to obtain the optimized structures and energetic of various intermediates and transition state involved in the dissociation pathway.

The specific objectives of the present study are:

1. to determine the potassium cation (K^+) affinities of 20 α -amino acids and their methyl esters by the mass spectrometric kinetic method, and to find out the relative stabilities of charge solvated (CS) versus zwitterionic K^+ binding modes by high level density function theory calculations (Chapter 4);
2. to determine the proton/potassium (H^+/K^+) binding affinities and modes of binding of selected biochemically important β -amino acids using the same methods as in (1) (Chapter 5);

3. to elucidate the dissociation pathways of protonated β -alanine and its methyl esters by tandem mass spectrometry and high level density functional theory calculations (Chapter 6);
4. to determine the proton (H^+) affinities and the dissociation pathways of protonated model and biochemically important β -dipeptides (Chapter 7); and
5. to elucidate the dissociation pathways of protonated His-containing α -dipeptides by high level density functional theory calculations, which are supplemented by experimental energy-resolved and time-resolved tandem mass spectrometric studies obtained by other members of Prof. Tsang's research group (Chapter 8).

Chapter 2 Tandem Mass Spectrometry (MS/MS) and Experimental Methodologies

In this chapter, the basic principles of tandem mass spectrometry and various mass spectrometric techniques used in the present study will be introduced. The different mass spectrometers used, the instrumental conditions and experimental procedures are described.

2.1 Ionization Methods in Mass Spectrometry

Fast atom bombardment (FAB) and electrospray ionization (ESI) were used in the present study for generating proton / potassium cationized amino acids/peptides for subsequent mass spectrometric kinetic method measurements and fragmentation studies. The two ionization methods have been widely applied to convert non-volatile amino acids and peptides to their protonated analogues prior to mass spectrometric analysis.

2.1.1 Fast Atom Bombardment (FAB)

In FAB ionization, a beam of cesium ion, Cs^+ , is accelerated at high kinetic energy (8-20 keV) and strike on a small plug of sample dissolved in a non-volatile glycerol matrix (Fig. 2.1). The kinetic energy of the atom or ion beam is transferred to the glycerol matrix, leading to ionization and self ion-molecule reactions of glycerol, producing protonated glycerol which serve as the protonating agent to the sample molecules. Protons transfer to the sample molecules could take place inside the liquid matrix or in the plasma (vapour phase) sputtered out of the liquid, resulting in the formation of the protonated sample

molecules. The glycerol matrix serves: (i) to maintain the long-lived FAB signals, and (ii) to refresh the bombarded surface with sample molecules. [De Hoffmann and Stroobant, 2001] Similarly, metal cationization of the sample molecule could take place if potassium iodide is added to the glycerol matrix. [Cedra and Wesdemiotis, 1996] Furthermore, the FAB-desorbed precursor ions, e.g. the protonated/potassium cationized heterodimer ions generated in the present study, were found to possess sufficient internal energies to undergo unimolecular (metastable) dissociation within the first field-free region of a B-E sector mass spectrometer, and yielding relatively intense metastable ions for mass spectrometric kinetic method measurements (refer to Section 2.4.1 for further discussions).

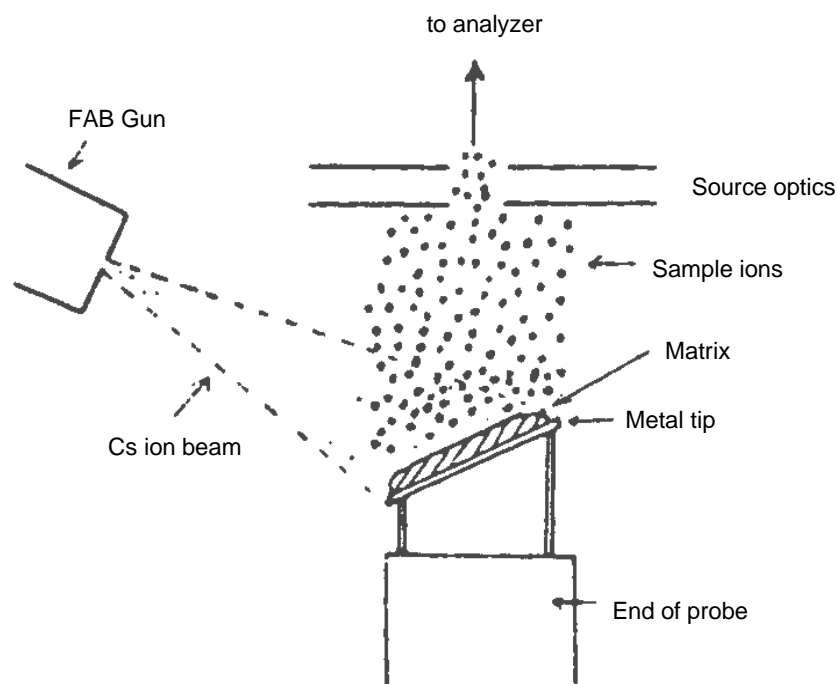


Figure 2.1 Ionization by fast atom bombardment (FAB)

In practice, the average internal energies of dissociating protonated / potassium cationized amino acids and peptides generated by FAB and monitored as metastable ions in a B-E sector mass spectrometer are found to be lower than that observed in low-energy collision-induced dissociation (CID) within a triple quadrupole mass spectrometer. In the present study, FAB ion generation in conjunction with metastable ion monitoring was used to measure the potassium cation affinities of selected α -amino acids by the standard kinetic method (refer to **Section 2.4.1**), and to supplement low-energy (eV scale, laboratory frame) CID results obtained with a triple quadrupole tandem mass spectrometer.

2.2.2 Electrospray Ionization (ESI)

Electrospray ionization (ESI) is a popular soft ionization technique to introduce neutral or ionic molecules in solution to a mass spectrometer in the gas phase. [Yamashita and Fenn, 1984a] Figure 2.2 shows a simplified schematic diagram of an electrospray ionization source. Before injection into the ESI source, the sample has to be dissolved in a mobile phase, such as 1:1 methanol:water (v/v), and the sample solution could be introduced by a syringe pump via a small diameter fine stainless steel capillary. Inside the ESI source, the tip of the capillary is at atmospheric pressure and is floated at a high potential (e.g., 3-4 kilovolts) relative to a counter electrode. The large potential different (voltage drop) creates an electrostatic spray of multiply charged droplets containing the sample molecules and ions. The subsequent ion formation processes are illustrated in Figure 2.3.

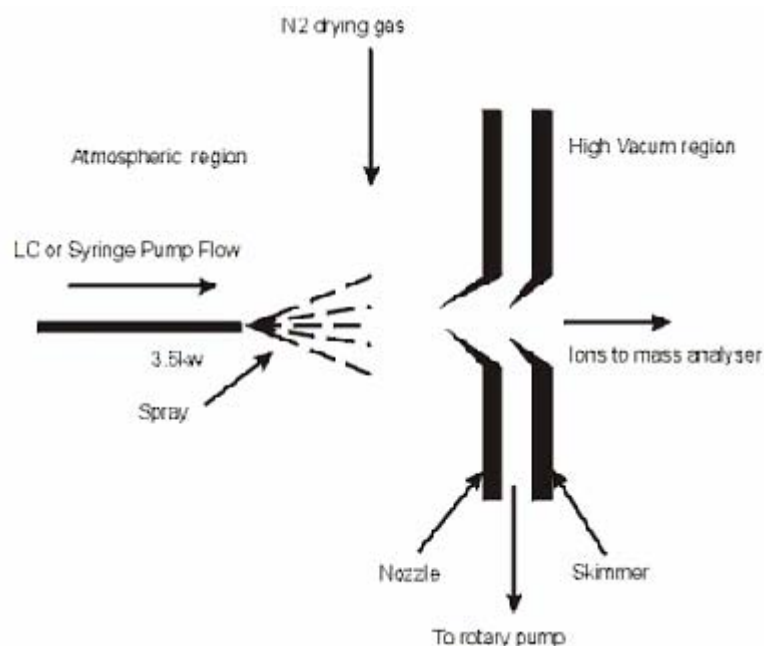


Figure 2.2 A schematic diagram of an electrospray ionization (ESI) source

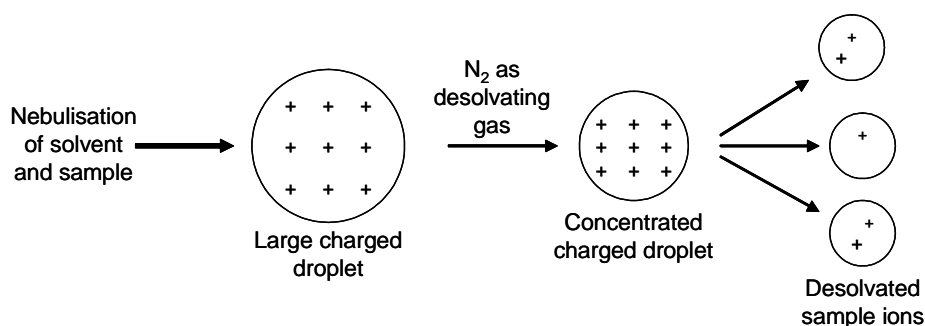


Figure 2.3 Generation of ions by electrospray ionization

The charged droplets are continuously reduced in size by solvent evaporation, usually with the assistance from elevated source temperatures and/or the flow of a drying gas, leading to an increase in surface charge density and a reduction in droplet radius. Finally, the electric field strength within the charged droplet reaches a critical point (the Rayleigh stability limit) when the ions at the surface of the droplets begin to be ejected into the gas phase due to columbic repulsion, yielding more droplets of smaller diameters. Eventually, sample ions are produced by successive fission of the charged droplets and completely desolvated by the nebulizing gas stream. The emitted ions are then sampled by a skimmer

cone and transmitted to the mass analyzer for subsequent m/z analysis. The detailed mechanism involved in the electrospray process is quite complicated, and have been reviewed by Kebarle and co-workers. [Kebarle and Tang, 1993; Kebarle and Ho, 1997; Kebarle, 2000]

Aside from pre-formed ions in solution, amino acids and peptides can be easily protonated under slightly acidic conditions (e.g. in the presence of 0.1 to 1.0 % v/v of formic acid) by electrospray ionization. Analysis of peptides in their protonated forms generated by ESI has become a routine method of analysis. Ions generated by ESI are found to possess lower internal energies than that produced by other ionization techniques, such as electron-impact ionization and FAB, [De Hoffmann and Stroobant, 2001] and therefore do not undergo extensive further dissociation unless additional internal energy imparted to them via a secondary process, such as collision with an inert gas (refer to **Section 2.3.2**).

2.2 The Quasi-Equilibrium Theory (QET) of Mass Spectra

Under the high vacuum conditions of a mass spectrometer, competitive unimolecular dissociations of the precursor ions result in different relative abundances of precursor and fragment ions recorded in the mass spectrum. The quasi-equilibrium theory (QET) of mass spectra is a simple theory useful in providing a conceptual and semi-quantitative framework to understand the relative ion intensities of precursor and fragment ions that appear in a mass spectrum.[Levsen, 1978] It was developed prior to the development of a more elaborate and quantitative theory, the Rice-Ramsperger-Kassel-Marcus (RRKM) theory of unimolecular dissociation to theoretically estimate numerically the rate constants, which are often required for a full understanding of the relative ion abundances in a mass spectrum.[Lorquet, 2000]

According to the QET, the extent of fragmentation depends on a number of physiochemical and instrumental parameters, including (i) the rate constants (k) of competitive unimolecular dissociations as a function of internal excitation energy (E), (ii) the time frame (t) of the dissociation reaction inside the mass spectrometer (i.e., $\sim 10^{-4} - 10^{-5}$ sec and \sim several tens of 10^{-3} sec for a triple quadrupole and ion trap mass spectrometer, respectively), and (iii) the internal energy distribution, $P(E)$, of the precursor ions.

According to the transition state (TS) theory, the rate constant, k , of a unimolecular dissociation reaction can be described by the equation [2.1] : [Holbrook et al., 1996]

$$k = \frac{k_B T}{h} \frac{Q^+}{Q} \exp(-\varepsilon_0 / RT) \quad [2.1]$$

where Q^+ and Q represent the partition functions of the activated complex (transition state) and the reactant (precursor ion), respectively, T is the temperature, k_B the Boltzmann constant, h the Planck's constant, R the ideal gas constant, and ε_0 the critical (activation) energy of the dissociation reaction (refer to Fig. 2.4). As the partition function refers to the number of micro-canonical states accessible to the ions, the Q^+/Q ratio is a measure of the entropy change of the transition state relative to the precursor ion. However, there is a limitation to this equation : it can be employed only when the system is under thermodynamic equilibrium, with a Boltzmann distribution to describe the population of the reactant, transition state and products, and characterized by a temperature T .

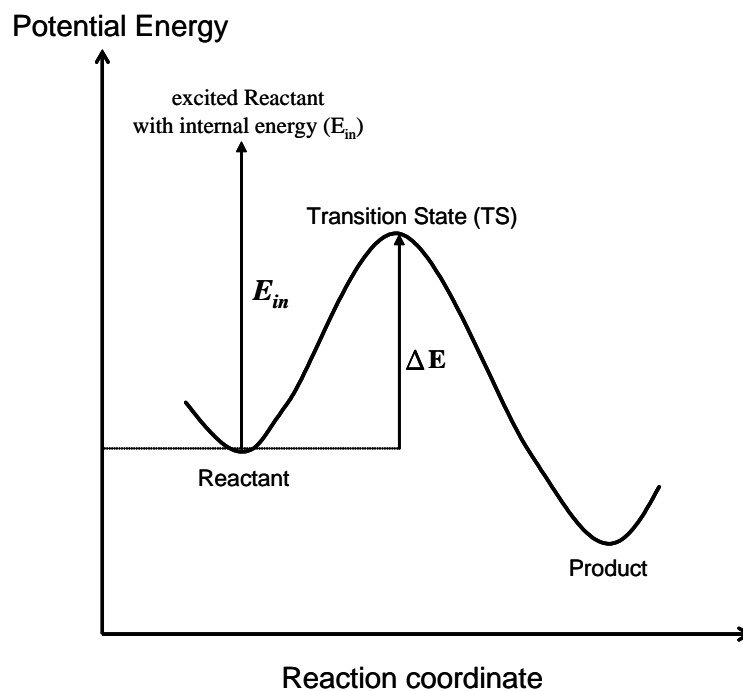


Figure 2.4 Potential energy diagram of a unimolecular dissociation reaction with a critical energy (ϵ_0)

Unlike condensed (solution) phase reactions, the internal energy of molecular ions undergoing unimolecular dissociation in a mass spectrometer under high vacuum (i.e., in the gas phase where no or very few ion-molecule collisions take place) may not follow a Maxwell-Boltzmann distribution, i.e., the ions are not decomposing under thermodynamic equilibrium conditions. If this is the case, then an ‘effective temperature’ term, T_{eff} , is used to replace the thermodynamic equilibrium temperature T to re-solve this issue. T_{eff} is defined as the ‘hypothetical temperature’ under thermodynamic equilibrium at which the identical fragmentation behaviour of the dissociating precursor ions is observed. [Vekey, 1996; Drahos and Vekey, 1999]

Since energy must be conserved in an isolated system (i.e., the precursor ion), another approach is to formulate the rate constant k of dissociation as a function of the total

internal excitation energy, E . According to the quasi-equilibrium theory of mass spectra,[Levsen, 1978; Holbrook et al., 1996] unimolecular dissociation occurs when a system of s classical oscillators with total energy E exceeds the critical energy of dissociation, ε_0 , of the bond to be broken (assumed to be a classical harmonic oscillator). In other words, ε_0 is the theoretical energy barrier of the unimolecular dissociation reaction, which is equal to the energy difference between the transition state and the dissociating precursor ion (the reactant). The rate constant $k(E)$ is then taken to be proportional to the probability of the precursor ion passing over the energy barrier, and is given by Eqn. [2.2] :

$$k(E) = \nu \left(1 - \frac{\varepsilon_0}{E} \right)^{s-1} \quad [2.2]$$

where ν is the frequency factor which is a ratio of product of frequencies of the energized molecule/ion (containing s oscillators/vibrational bonds) to the product of frequencies of the transition state (containing $s - 1$ oscillators/vibrational bonds), and is a measure of the entropic constrains of the reaction. In practice, s represents the number of degrees of freedom (effective number of oscillators), which is usually taken to be 1/2 to 1/5 of the actual vibrational degrees of freedom ($3N - 6$) of the dissociating precursor ion. The QET of mass spectra and the effect of $k(E)$ on relative ion abundance has been recently reviewed by Vekey . [Vekey, 1996]

The relationship between the magnitude of the frequency factor ν and the internal energy, E , or specifically how does ν change with increasing E , is of particular relevance to the present work. Generally speaking, it is an inverse function of the ‘looseness’ or ‘tightness’ of the activated complex, hence depending on the structure of the transition state involved. For a dissociation pathway involving re-arrangement of the bonds (i.e.,

bond formation and bond breaking at the same time) and a ‘tight’ transition state, ν is reduced and $k(E)$ generally increases more slowly with E when compared to pathway involving simple bond fissions only. The difference between rearrangement and simple bond cleavage reactions can be illustrated by the $k(E)$ versus E curves as shown in Figure 2.5. [Levsen, 1978; De Hoffmann and Stroobant, 2001] Thus, a dissociating pathway involving molecular re-arrangement has to display a lower critical energy in order to be able to compete with a pathway involving a bond cleavage with a higher frequency (more favourable entropy factor). The quasi-equilibrium theory of mass spectra and the effect of $P(E)$ on relative ion abundance has been reviewed recently. [Vekey, 1996]

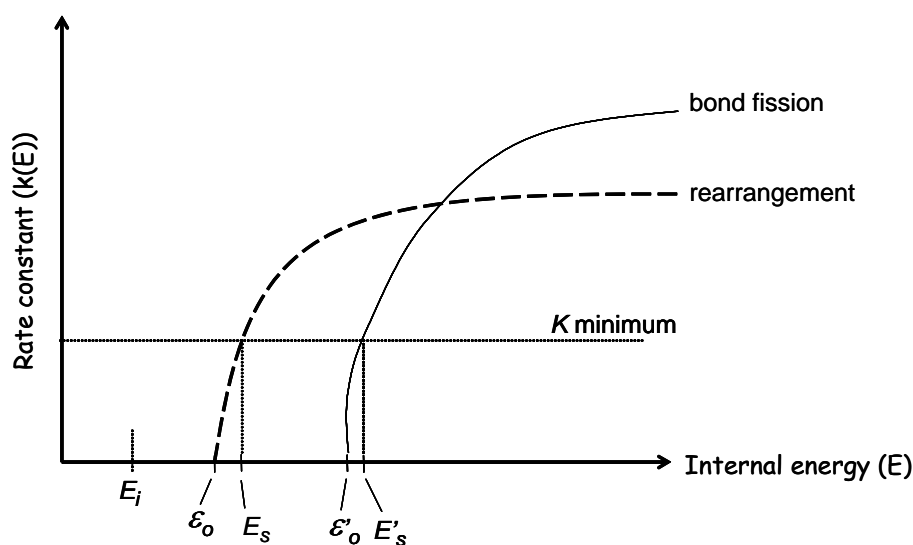


Figure 2.5 Hypothetical $k(E)$ versus E curves for a simple bond cleavage reaction and a dissociation reaction involving molecular rearrangement (E_i , is the energy required for generation of the parent ion; ϵ_0 , the parent ion contains enough excess energy to fragment but the reaction is not fast enough to allow observation of the fragment; E_s , the excess energy required for the ion to dissociate before leaving the ionization source. The difference of $\epsilon_0 - E_s$ is called the kinetic shift)

Kinetic Shift Equation [2.2] indicates that a precursor ion can proceed to dissociate if the internal energy (E) \geq the critical energy (ϵ_0). However, the onset or experimental threshold energy (appearance/threshold energy, AE) for observation of the dissociation (fragmentation) of the precursor ions is far greater than the critical energy (ϵ_0) because extra energy is required to drive the reaction fast enough to reach a detectable amount of ions within the time frame ($\sim 10^{-5}$ - 10^{-6} s and 10^{-5} ~ 10^{-4} s, respectively) of a magnetic sector or triple quadrupole mass spectrometer. The difference between AE and ϵ_0 , (AE - ϵ_0), is called the kinetic shift. [Levsen, 1978; De Hoffmann and Stroobant, 2001; Lifshitz, 2002]

For different mass analyzers operating with different time frames, the kinetic shift also differs in magnitude. Larger kinetic shifts are observed for the shorter time scale ($\sim 10^{-6}$ - 10^{-4} sec) and higher dissociation rate constants required for observing dissociating precursor ions in a magnetic sector and triple quadrupole mass spectrometers. [Lifshitz, 1992; Lifshitz, 2002] Generally, a larger kinetic shift is expected for larger precursor ions with more number of effective oscillators. A larger kinetic shift could possibly shift the internal energy required for dissociation to a region where the other higher critical energy dissociation pathways become possible. A larger kinetic shift is expected for a rearrangement reaction, which is associated with a slow increase of $k(E)$ with increasing E (Fig. 2.5). In the case of protonated glycinamide, $^+H_3NCH_2CONHCH_3$, the magnitude of the kinetic shift for dissociation yielding the immonium ion, $[H_2N=CH_2]^+$, in a triple quadrupole mass spectrometer was estimated to be as large as 0.45 eV. [Klassen and Kebarle, 1997] This suggested that the kinetic shift effect can shift the experimentally observed threshold voltage to a significantly higher value than the theoretically found ϵ_0 value.

On the other hand, the time scale of activation (dissociation) of an ion trap mass analyzer is approximately 100 times longer than that of a magnetic-sector or triple quadrupole systems. Previous studies have shown that the ion trap can detect unimolecular dissociation channels with rate constants as slow as $1 \times 10^3 \text{ sec}^{-1}$; the kinetic shift was observed to be much smaller, or even negligible for small ions. [Lifshitz, 1992; Lifshitz et al., 1983] In favourable cases, when the kinetic shifts are small, the order of appearance or threshold voltages (energies) observed with an ion trap mass analyzer is more likely to be consistent with the order of theoretical critical energies (ϵ_0) of dissociation calculated for the different pathways. [Abirami et al., 2005]

2.3 Tandem Mass Spectrometry (MS/MS)

MS/MS is a two-stage (separated by a collision cell) mass spectrometer that allows the study of dissociation reactions of a particular ion in a mixture of ions. [Busch et. al, 1988; De Hoffmann et. al, 1996]

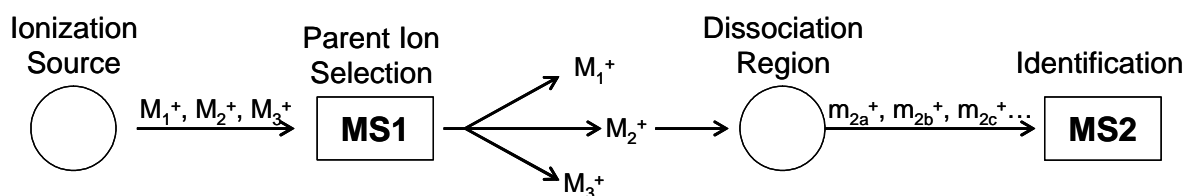


Figure 2.6 Schematic diagram of MS/MS operation in the daughter ion scan mode

As illustrate in Fig. 2.6, for a mixture of ions, M_1^+ , M_2^+ ,, M_3^+ generated in the ionization source of a mass spectrometer (MS1), a target ion of interest, generall named the parent or precursor ion, M_2^+ , is mass-selected by the first mass analyzer, MS1. With excess internal energy, the parent ion will undergo a number of competitive dissociations along the pathway of travel (e.g. inside the collision cell of a triple quadruole mass spectrometer), yielding daughter ions m_{2a}^+ , m_{2b}^+ , m_{2c}^+ and associated neutral fragments. The daughter ions are then mass analyzed by the second stage mass analyzer (MS2). This is known as the ‘daughter ion scan mode’ and is the most common scanning mode used in tandem mass spectrometry, as was performed with a B-E sector tandem mass spectrometer and/or with a triple quadrupole instrument in the present study.

2.3.1 Unimolecular (Metastable) Ion Dissociation

Ions observed and recoreded with a B-E sector mass spectrometer can usually be classified into three types: molecular (precursor) ion, metastable ion and daughter ion. [De Hoffmann and Stroobant, 2001] Molecular (stable) ions are formed in the ionization source and travel to the detector without dissociation. Metastable ions (of intermediate internal energies) are formed in the source and dissociate in the ‘field free’ region between the B and E sectors before reaching the detector. Ions possessing higher internal excitation energies exceeding the critical energy, ϵ_0 , would dissociate within the ionization source, and thus could only be detected as daughter ions. The relative portions of an energy distribution curve for yielding the molecular ions, metastable ions and daughter ions is shown for a hypothetical internal energy distribution curve, $P(E)$, in Fig. 2.7.

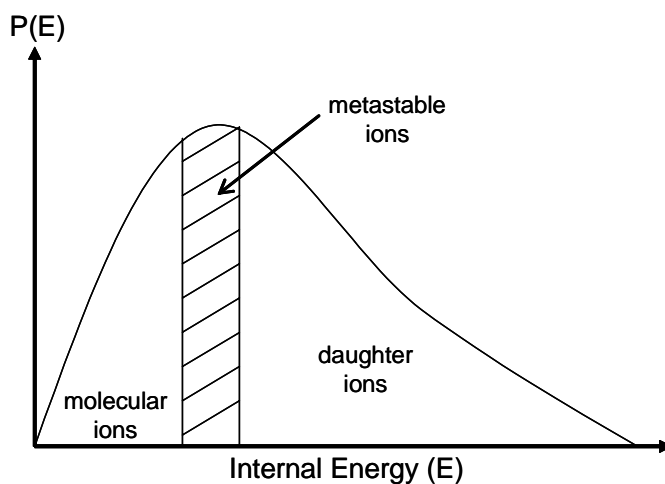


Figure 2.7 A hypothetical internal energy distribution ($P(E)$) versus internal energy (E) of ions

The metastable ions formed in the first field free region (1st FFR) of a magnetic (B) and electric (E) sector type mass spectrometer in the present study were detected by B/E linked scans, a technique to be described in more details in **Section 2.5.1**. Due to the narrow time window of the 1st FFR of a B-E sector instrument, metastable ions are characterized by a relatively narrow range of internal energies (Fig. 2.7), which are usually only slightly above the energy threshold for dissociation.

Previously, the parent-daughter relationship of radical molecular ions generated by electron-impact ionization could be established by recording the metastable ion spectrum for studies on ion dissociation pathways and mechanisms. However, metastable ions generally constitute less than 1 % of the total ion population, and are recorded with very low ion intensities. The problem is further aggravated for parent ions generated by electrospray ionization, which usually do not yield metastable ions at all. For this reason, studies on dissociating mechanisms and pathways of protonated amino acids and peptides

are now carried out by monitoring the low energy (eV scale) collision-induced dissociations occurring in the collision cell of a triple quadrupole mass spectrometer, or within an ion trap mass analyzer.

2.3.2 Collision-Induced Dissociation (CID)

Parent ions generated by ESI that do not have enough internal excitation energy to undergo dissociation can be mass selected by the first stage mass analyzer (MS1), activated (gaining more internal excitation energy) by collision with an inert gas in a collision cell, and then undergo further dissociations before reaching the detector of the mass spectrometer. In a low energy (eV scale, laboratory frame) collision process, parent ions are accelerated to a kinetic energy of 5 – 100 eV, and allowed to collide with a neutral/inert target gas (e.g. argon as collision gas used in the present study). During the collision, a fraction of the translational energy is converted into the internal energy of the parent ion. Once the internal energy (E) exceeds the critical energy (ϵ_0) of a dissociation reaction, collision-induced dissociation (CID) would occur. The amount of kinetic energy converted (the extent of dissociations) depends on a number of factors, such as collision velocity/energy (usually expressed in eV, the potential difference of ion acceleration) and the nature of collision gas. In general, the internal excitation energy imparted to the parent increases with the kinetic energy (eV) of ion acceleration; the maximum amount of kinetic energy available for conversion to internal energy of an ion in a single collision is given by Eqn.[2.2]: [Busch et al., 1988; De Hoffmann and Stroobant, 2001]

$$E_{\text{cm}} = \frac{E_{\text{lab}} m_{\text{target}}}{m_{\text{ion}} + m_{\text{target}}} \quad [2.2]$$

where E_{cm} is the maximum amount of collision energy in the centre of mass reference frame, E_{lab} is the ion kinetic energy of collision in the laboratory frame reference, m_{ion} is the mass of the parent ion and m_{target} is the mass of the collision gas (target gas).

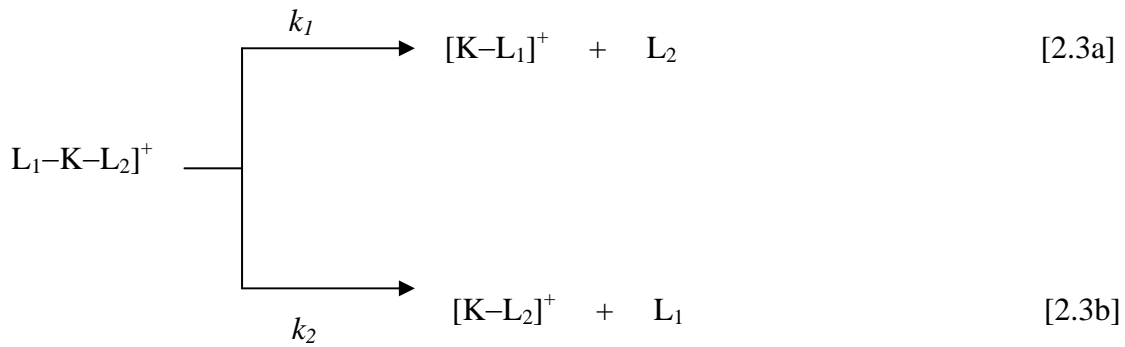
In the present study, low-energy CID experiments were performed with triple quadrupole tandem mass spectrometers (Waters-Micromass Quattro Ultima, Manchester, U.K.) for investigations into the dissociation pathways and mechanisms of protonated amino acids and peptides, as well as the determination of proton and potassium cation(s) affinities of β -amino acids and β -peptides.

2.4 The Mass Spectrometric Kinetic Method

The mass spectrometric kinetic method is developed by Cooks and co-workers [Cooks and Kurger, 1977; McLuckey et al., 1981; Cooks et al., 1994; Cooks and Wong, 1998] and applied to determine thermochemical information (e.g. ionization potentials) of a wide range of compounds. [Cooks et al., 1999] This method is further extended by Fenselau and co-workers [Cheng et al., 1993] and Wesdemiotis and co-workers [Cerdeja and Wesdemiotis, 1996; Cerdeja et al., 1998] to determine the thermochemical properties of structurally dissimilar compounds, or ligands with different metal cation binding modes (proton affinities and alkali metal cation affinities of amino acids and peptides). The first version of the method is now known as the ‘standard kinetic method’, while the version modified later is known as the “extended kinetic method”.

2.4.1 The Standard Kinetic Method

In the standard kinetic method, the relative K^+ affinity ($\Delta(\Delta H)$), between two neutral ligands, L_1 and L_2 , is measured from the rates of competitive unimolecular dissociations of the K^+ bound heterodimer complex, $[L_1-K-L_2]^+$, to its K^+ bound monomer complexes (Reactions [2.3a] and [2.3b]), where k_1, k_2 are the rate constants for the dissociations of the K^+ bound heterodimer to $[K-L_1]^+$ and $[K-L_2]^+$ monomers, with the corresponding critical energies ε_1 and ε_2 , and enthalpy change, ΔH_1 and ΔH_2 , of Reactions [2.3a] and [2.3b], respectively. The corresponding potential energy diagram for reactions [2.3a] and [2.3b] is shown in Fig. 2.8.



The natural logarithm of the relative rates of dissociation, $\ln(k_1/k_2)$, can be equated to the natural logarithm of the ion intensity ratio, $\ln(I_{[M-L_1]^+}/I_{[M-L_2]^+})$, by Eqn.[2.4] :

$$\ln\left(\frac{k_1}{k_2}\right) = \ln\left(\frac{I_{[K-L_1]^+}}{I_{[K-L_2]^+}}\right) = \ln\left(\frac{Q_1^*}{Q_2^*}\right) + \frac{(\varepsilon_2 - \varepsilon_1)}{RT_{\text{eff}}} \quad [2.4]$$

$$\approx \frac{\Delta(\Delta H)}{RT_{\text{eff}}} \quad [2.5]$$

where Q_1^* and Q_2^* are the partition functions of the two transition states of the competing reactions, $(\varepsilon_2 - \varepsilon_1)$ is the difference of activation energies of the two reactions. For ligands with similar structures and modes of binding, the $\ln(Q_1^*/Q_2^*)$ term is generally

taken to be zero (i.e., $Q_1^* = Q_2^*$). Assuming that the heterodimer dissociates with no reverse energy of activation, Eqn.[2.4] can be simplified to Eqn.[2.5], where the relative K^+ affinity between L_1 and L_2 , i.e., $\Delta(\Delta H) = \Delta H_{[K-L_2]^+} - \Delta H_{[K-L_1]^+}$, is now proportional to $\ln(I_{[K-L_1]^+}/I_{[K-L_2]^+})$. This standard kinetic method, usually expressed in the form of a relative K^+ affinity $\Delta(\Delta H)$ ladder, is applied in the present study to determine the *relative* potassium cation (K^+) affinities of 20 α -amino acids and their methyl-esters.

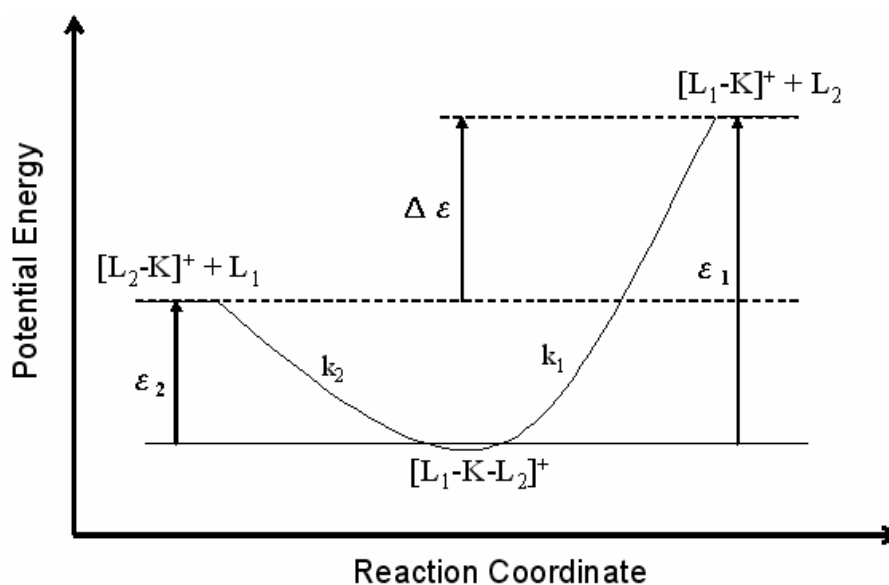


Figure 2.8

Schematic energy diagram of the dissociation of a potassium cation bound heterodimer $[L_1-K-L_2]^+$ (The rate constants (k_1 and k_2) can be approximated by a modified form of the canonical transition state with the thermodynamic temperature T replaced with an “effective temperature”, T_{eff} , which is defined as the temperature of a Boltzmann distribution of the activated complex (transition state) that fragments to give the same product ratio as observed for the non-Boltzmann distribution under chosen experimental conditions.[Vékey, 1996])

2.4.2 The Extended Kinetic Method

Consider the competitive unimolecular dissociations of K^+ bound heterodimers of a ligand L_1 (with unknown K^+ affinity, $\Delta H_{[K-L_1]^+}$) and reference compound L_n with known K^+ affinities ($\Delta H_{[K-L_n]^+}$), where L_1 and L_n are structurally dissimilar, the $\ln(Q_1^*/Q_n^*)$ term in Eqn [2.4] is generally non-zero but can be assumed to be a constant. The $\ln(Q_1^*/Q_n^*)$ term can then be expressed as in Eqn.[2.6], where $\Delta(\Delta S)^{app}$ is the difference in reaction entropies for the dissociation of the heterodimer to the $[K-L_1]^+$ and $[K-L_n]^+$ monomer complexes.

$$\ln\left(\frac{Q_1^*}{Q_n^*}\right) = -\frac{\Delta(\Delta S)^{app}}{R} \quad [2.6]$$

By drawing analogy with the thermodynamic related equation, $\Delta G = \Delta H - T\Delta S$, Eqn.[2.4] can then be re-formulated as Eqns.[2.7] and [2.8]:

$$\begin{aligned} \ln\left(\frac{k_1}{k_n}\right) &= \ln\left(\frac{I_{[K-L_1]^+}}{I_{[K-L_n]^+}}\right) = -\frac{\Delta(\Delta S)^{app}}{R} + \frac{\Delta(\Delta H)}{RT_{eff}} \\ &= \frac{\Delta G^{app}}{RT_{eff}} - \frac{\Delta H_{[K-L_n]^+}}{RT_{eff}} \end{aligned} \quad [2.7]$$

$$\text{where } \Delta G^{app} = \Delta H_{[K-L_1]^+} - T_{eff} \Delta(\Delta S)^{app} \quad [2.8]$$

$$\text{and } \frac{\Delta G^{app}}{RT_{eff}} = \frac{\Delta H_{[K-L_1]^+}}{RT_{eff}} - \frac{\Delta(\Delta S)^{app}}{R} \quad [2.9]$$

The ΔG^{app} , T_{eff} and $\Delta(\Delta S)^{\text{app}}$ terms are experimental values obtained according to the protocol of the extended kinetic method. Usually, the $\Delta(\Delta S)^{\text{app}}$ term is assumed to be constant for a series of structurally similar reference ligands, so that a plot of $\ln(I_{[\text{K-L}_1]^+}/I_{[\text{K-L}_n]^+})$ versus $\Delta H_{[\text{K-L}_n]^+}$ to (Eqn.[2.7]) will give $\Delta G^{\text{app}}/RT_{\text{eff}}$ as the y-intercept (y_o), and $-1/RT_{\text{eff}}$ as the slope (m). If the measurement is carried out at a number of different collisional excitation energies (T_{effs}), a second plot of y_o versus $-m$ will yield the K^+ affinity of L_1 , $\Delta H_{[\text{K-L}_1]^+}$, from the slope, and the entropic term $-\Delta(\Delta S)^{\text{app}}/R$ from the y-intercept of the plot.

However, the ΔG^{app} and $1/RT_{\text{eff}}$ terms (Eqn. [2.9]) are covariant so that the highly linearity of the second plot of the extended kinetic method could be an artifact in data analysis. [Armentrout, 2000] To remove this covariance, Armentrout suggested that the $\Delta H_{[\text{K-L}_n]^+}$ and ΔG^{app} terms can be replaced by $[\Delta H_{[\text{K-L}_n]^+} - \Delta H_{\text{Avg}}]$ and $[\Delta G^{\text{app}} - \Delta H_{\text{Avg}}]$, respectively, where ΔH_{Avg} is the average of the ΔH values of the reference compounds (L_n) [Armentrout, 2000]. The y-intercept of the first plot now becomes $[\Delta G^{\text{app}} - \Delta H_{\text{Avg}}]/RT_{\text{eff}}$ (slope $m = -1/RT_{\text{eff}}$ remains unchanged), and the slope of the second plot is then equal to $[\Delta H_{[\text{K-L}_1]^+} - \Delta H_{\text{Avg}}]$ (y-intercept = $-\Delta(\Delta S)^{\text{app}}/R$ remains unchanged), from which $\Delta H_{[\text{K-L}_1]^+}$ and $-\Delta(\Delta S)^{\text{app}}$ can be found. It should be pointed out that the T_{eff} , $(\Delta G_{\text{M}^+})^{\text{app}}$ and $(\Delta S_{\text{M}^+})^{\text{app}}$ terms are related to the properties of the dissociating heterodimer, and are dependent on the instrumental conditions under which the dissociation reactions are monitored. This method is known as the extended kinetic method, and is applied in the present study to determine the *absolute* potassium cation affinities of selected α -amino acids and their methyl-esters *when reference compounds of known and comparable potassium affinities are available for the experimental measurement.* Equations [2.7] to [2.9] are equally

valid when K^+ is replaced by proton (H^+), and the extended kinetic method is also used in the present study to determine the *absolute* proton/potassium cation affinities of selected β -amino acids and dipeptides.

The theoretical basis, assumptions and the methodology of the kinetic method have been critically reviewed and discussed recently. [Cooks and Wong, 1998; Cooks et al., 1999; Armentrout, 1999; Drahos and Vekey, 1999; Ervin, 2002; Ervin, 2000] The major advantage of the kinetic method for determining thermochemical properties is its simplicity, and the measurements can be carried out in commonly available tandem mass spectrometers.

2.5 Instrumentation and Experimental Procedures

In this section, the mass spectrometer and the experimental conditions used in the present study are described.

2.5.1 The Finnigan-MAT95S Double-Focusing (B-E) Mass Spectrometer

In this study, the unimolecular (metastable) ion dissociations mass spectra were obtained with the first stage B-E sector mass analyzers of the Finnigan-MAT95S-B-E tandem mass spectrometer [Huels et al., 1996; Schwartz et al., 1990] equipped with a cesium ion (Cs^+) FAB gun as ionization source.

The Finnigan-MAT95S-B-E mass spectrometer (MS1) is a reverse geometry (B-E) double focussing magnetic sector mass spectrometer with a 65° , 35 cm radius magnetic sector, B, followed by an electric sector, E as shown in Fig. 2.9. The full accelerating voltage is 5

keV, the maximum magnetic field strength is 1.7 Tesla, the maximum mass range is 3,500 Da, and the maximum resolution is 60,000 (10% valley) in the double focussing mode. Instrumental control and data acquisition are carried out via the Finnigan-MAT ICIS system software and a DEC Alpha workstation. Unimolecular (metastable) dissociations in the first field-free region (FFR-1) can be monitored by operating the instrument in the B/E linked-scans mode. [De Hoffmann and Stroobant, 2001]

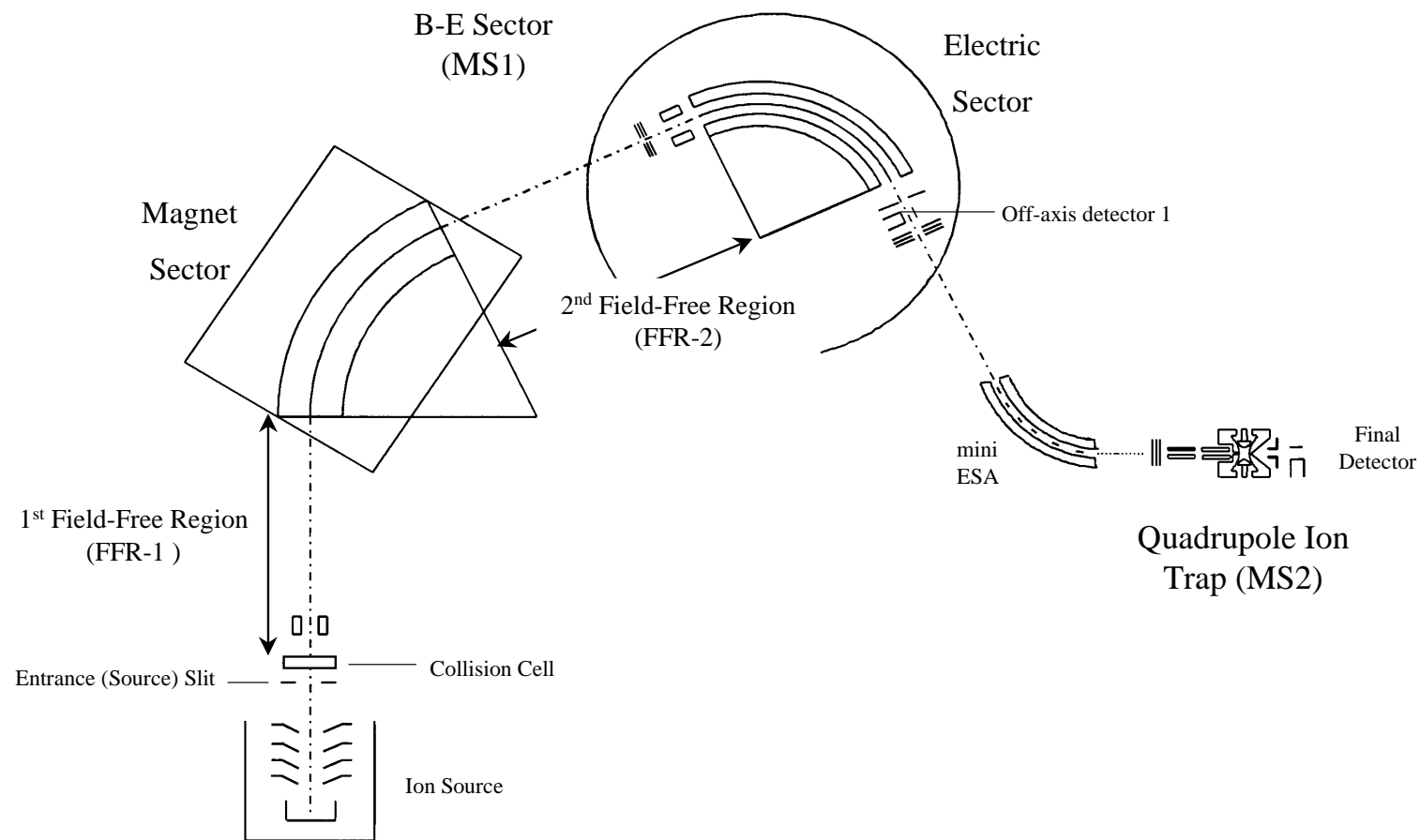


Figure 2.9 Schematic Diagram of the Finnigan-MAT95S-B-E tandem mass spectrometer

2.5.2 Waters-Micromass Quattro Ultima Triple Quadrupole Tandem Mass Spectrometer

A schematic diagram of the Waters-Micromass (Manchester, U.K.) Quattro Ultima triple quadrupole tandem mass spectrometer is shown in Figure 2.10.

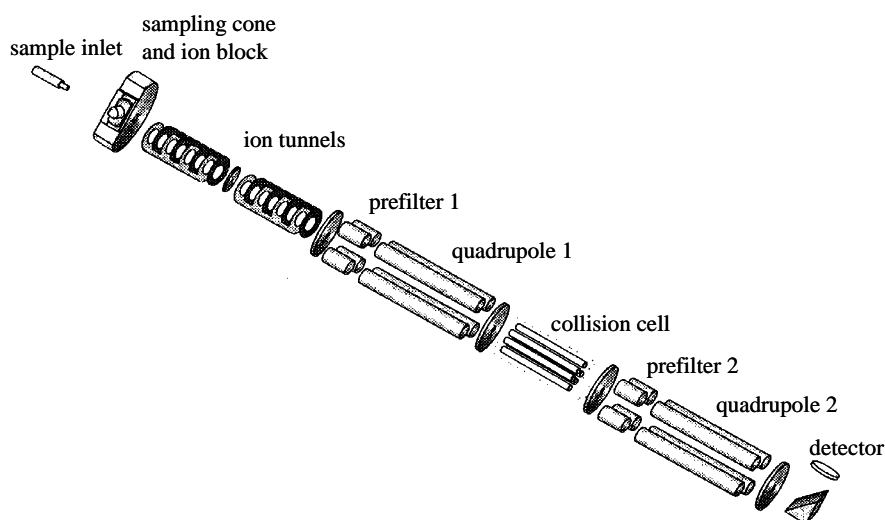


Figure 2.10 Schematic diagram of the Micromass Quattro Ultima triple quadrupole tandem mass spectrometer (taken from Micromass Quattro Ultima triple quadrupole tandem mass spectrometer user's manual)

The Quattro triple quadrupole mass spectrometer is equipped with a Z-spray electrospray ionization (ESI) source, [Herbert and Johnstone, 2003] and comprised of three main parts: two quadrupole mass analyzers (MS1 and MS2), and a central hexapole collision cell, to which a pressure of $\sim 1 \times 10^{-5} - 10^{-6}$ mbar of collision gas (argon) is generally introduced to perform effective CID of the precursor ions selected by MS1. Short-length hexapoles, prefilters and postfilters are located before and after the quadrupole analyzers to maximize the transmission of the ions to the detector. The ion detection system is consisted of a conversion dynode, phosphor and photomultiplier (650 V). The ion source (about 10^{-4} mbar) and analyzer ($10^{-5} - 10^{-6}$ mbar) regions are pumped by two turbo-molecular pumps

(Edwards) and two rotary pumps (Edwards). Data acquisition and processing are performed using the Micromass-MassLynx NT system software (version 3.5).

To obtain a MS/MS spectrum, the parent ion is first mass selected by the first quadrupole (MS1), accelerated by a potential difference (collision energy) of 0 - 200 V and then undergoes collision-induced dissociation (CID) by collision with the argon collision gas present in the RF-only hexapole collision cell. The fragment ions formed are mass analyzed by the second quadrupole mass analyzer (MS2) to yield a MS/MS mass spectrum. For the Quattro Ultima triple quadrupole mass spectrometer, the lowest detectable m/z value of ions is 2; it was employed in this study to confirm the absence/presence of low m/z ions ($\leq m/z$ 30) in the MS/MS spectra of protonated β -alanine and model β -dipeptides. Conversely, one of the product (daughter) ions can be mass selected by MS2, and MS1 can be scanned to provide a 'parent' MS/MS spectrum revealing the precursor ions of a particular daughter ion.

Another feature about the triple quadrupole MS system relevant to the present study is that it offers a wide range of adjustable collision energies (1 – 100 eV, laboratory scale) and variable pressures of collision gas pressure (10^{-5} – 10^{-4} milliBar) for low energy CID studies. Hence, the extended kinetic method measurements of the present project, which requires ion intensity ratio measurements over a wide range of effective temperatures (T_{eff}) or collision energies (eV) under suitable argon collision gas pressures, were conducted with the Quattro Ultima triple quadrupole MS system.

2.5.3 Chemicals and Sample Preparation Procedures

All chemicals and reagents were analytical grade (AR) and purchased from Acros, Aldrich and Sigma chemicals companies. Unless specified, they were used without further purification. The chemicals used in this study are listed below in the format: full chemical name (Abbreviation / Relative Molar Mass):

α -Amino Acids

Glycine (Gly / 75)	Alanine (Ala / 89)
Cysteine (Cys / 121)	Valine (Val / 117)
Leucine (Leu / 131)	Isoleucine (Ile / 131)
Serine (Ser / 105)	Methionine (Met / 149)
Proline (Pro / 115)	Threonine (Thr / 119)
Aspartic Acid (Asp / 133)	Phenylalanine (Phe / 165)
Tyrosine (Tyr / 181)	Glutamic Acid (Glu / 147)
Lysine (Lys / 146)	Asparagine (Asn / 132)
Tryptophan (Trp / 204)	Glutamine (Gln / 146)
Histidine (His / 155)	Arginine (Arg / 174)

Methyl/Ethyl Esters of α -Amino Acids

Glycine methyl ester (GlyOMe / 89)	Alanine methyl ester (AlaOMe / 103)
Cysteine methyl ester (CysOMe / 135)	Valine methyl ester (ValOMe / 131)
Leucine methyl ester (LeuOMe / 145)	Serine methyl ester (SerOMe / 119)
Methionine methyl ester (MetOMe / 163)	Proline methyl ester (ProOMe / 129)
Threonine methyl ester (ThrOMe / 133)	Aspartic Acid methyl ester (AspOMe / 147)
Phenylalanine methyl ester (PheOMe / 179)	Tyrosine methyl ester (TyrOMe / 195)
Glutamic acid methyl ester (GluOMe / 161)	Lysine methyl ester (LysOMe / 160)
Asparagine methyl ester (AsnOMe / 146)	Tryptophan methyl ester (TrpOMe / 218)

Glutamine methyl ester (GlnOMe / 160)	Histidine methyl ester (HisOMe / 169)
Leucine ethyl ester (LeuOEt / 159)	Phenylalanine ethyl ester (PheOEt / 193)

β -Amino Acids/ β -Amino Acids Methyl Esters

β -Alanine (β -Ala / 89)	β -Alanine methyl ester (β -AlaOMe/ 103)
---------------------------------------	---

α -/ β -Dipeptides

Glycylalanine (GlyAla / 146)	Alanylglycine (AlaGly / 146)
Alanylalanine (AlaAla / 160)	Glycylhistidine (GlyHis / 212)
Histidylglycine (HisGly / 212)	Alanylhistidine (AlaHis / 226)
Glycyl(β -alanine) (Gly(β -Ala) / 146)	Alanyl(β -alanine) (Ala(β -Ala) / 160)
β -Alanylglycine ((β -Ala)Gly / 146)	β -Alanylalanine ((β -Ala)Ala / 160)
β -Alanyl(β -alanine) ((β -Ala)(β -Ala) / 160)	
β -Alanylhistidine (Carnosine) ((β -Ala)His / 226)	

Generation of K^+ bound heterodimer ions by FAB For generation of abundant K^+ bound heterodimer ions by FAB, the samples were prepared by mixing saturated aqueous solutions of sample powders (or 20 μ L of liquid sample) with 20-40 μ L of 0.4 M aqueous potassium iodide (KI) solution, 10-20 μ L of 2.5 M trichloroacetic acid solution, and 20-40 μ L of glycerol matrix. Then, one drop (~2-5 μ L) of the mixture solution was transferred to the FAB probe tip for mass spectrometric analysis.

Generation of H^+/K^+ bound heterodimer ions by ESI For the generation of H^+/K^+ bound heterodimer ions by ESI, solution concentrations were optimized for maximum ion intensity by mixing different proportions of 2×10^{-4} M stock sample solutions (in methanol) with 50-200 μ L of methanol containing 1% v/v of formic acid or 0.04 M

potassium nitrate (KNO₃) solution (in methanol) to a final volume of 4 mL. For amino acids supplied in the HCl complexed form, NH₄OH solution (~28-30 % NH₃ in water) was added to the stock solution until the pH reached ~8-9. Methanol was used as solvent in all serial dilutions, if needed for the optimization steps. If the solubility of the chemicals in methanol was very low, then 100-300 μL of deionized water was added to the stock solution to increase the solubility. The resulting solution was introduced into the ESI interface by a syringe pump (Harvard Apparatus, model 22) at a flow rate of 5-10 μL/min. The procedure was equally applicable to the generation of protonated amino acids and peptides by ESI.

2.5.4 Instrumental Conditions

Fast atom bombardment-mass spectrometry (FAB-MS) conditions The typical Finnigan-MAT 95 ST conditions for acquiring a normal FAB mass spectrum are listed as follows:

Ionization method	:FAB, cesium ion gun as bombarding ion beam (~14 - 20 keV, emission current ~2 μA, heater current ~1.4 - 1.6 A)
Scan mode	:normal magnetic field scan (B scan)
Accelerating voltage	:4.7 kV
Scan rate	:5 - 15 sec/decade (depends on scanning mass range)
Mass resolution	:low resolution at approximately 800-1500 (M/ΔM, 10% valley)
Conversion dynode	:positive mode, 15 kV
Electron multiplier voltage	:1.6 - 1.8 kV, adjusted to a gain factor of 10 ⁴ - 10 ⁵

To perform the metastable measurement in the first field-free region (FFR-1) with reproducible ion intensity ratios, the ion intensity of metal cation bound heterodimers generated by FAB were tuned to be an intense signal $\geq 10,000 \mu\text{V}$ at a multiplier voltage of 1.3 kV by optimizing the FAB heater current, emission current and high voltage of the Cs^+ gun. However, careful sample preparation with the FAB matrix is also important. The mass spectrometric conditions were:

Acquisition mode	: LPROF
Accelerating voltage	: 4.7 kV
Multiplier	: 1.6-1.8 kV
Conversion dynode	: positive mode, 15 kV
Scan rate	: 10-15 sec/decade
Inter-scan time	: 0.5 sec
Vacuum conditions recorded by the ion gauge	
Ion source vacuum	: 4.0×10^{-8} - 2.0×10^{-7} mbar
Electrostatic analyzer vacuum:	$3.5 - 5.0 \times 10^{-8}$ mbar

A metastable spectrum measured was accumulated from 60-100 scans and repeated 3-4 times to obtain an averaged ion intensity ratio. The ion intensity ratios were typically reproducible to within $\pm 8\%$ (coefficient of variation, $n = 3-4$), and the uncertainty in logarithm of ratios were within ± 0.08 ($n = 3-4$).

Electrospray ionization-mass spectrometry (ESI-MS) conditions Argon (Ar) was used as the collision gas and introduced to the collision cell to yield 20-30 % attenuation of the precursor ion beam. The typical ion generation and mass spectrum acquisition conditions are shown as follows:

Electrospray ionization source

Capillary voltage	: 1 – 3 kV
Cone voltage	: 10 – 30 V
Hexapole 1	: 0.0 – 0.2 V
Aperature	: 0.0 – 0.2 V
Hexapole 2	: 0.0 – 0.2 V
Nebulizing gas	: N ₂ , fully opened
Cone gas and flow rate	: N ₂ , 50 – 70 L hr ⁻¹
Desolvation gas and flow rate	: N ₂ , 400 – 700 L hr ⁻¹
Source temperature	: 60 – 80 °C
Desolvation temperature	: 120 – 150 °C

MS1 / MS2 parameters

LM 1 resolution	: 15
HM 1 resolution	: 15
Ion energy 1	: 0.1 – 0.4 V
Entrance	: 1 – 7 V
Exit	: 2 – 5 V
LM 2 resolution	: 15
HM 2 resolution	: 15

Ion energy 2 : 0.5 – 0.7 V
Multiplier : 650 V

Mass spectrum acquisition conditions:

Ionization mode : ESI, +ve
Scan mode : daughter ion scan (MS/MS)
Collision gas : argon (99.99% purity)
Collision energy : 5 – 32 eV (laboratory frame)
Multiplier : 650 V
Scan rate : 350 – 450 Th/second
No. of scans : 50 – 100

Vacuum / pressure conditions (mbar):

Collision cell Pirani gauge (without collision gas introduced): $< 1.0 \times 10^{-4}$ mbar
Collision cell Pirani gauge (with collision gas introduced): $< 1.0 \times 10^{-4}$ mbar
Analyzer Penning gauge (without collision gas introduced): $1.48 - 1.52 \times 10^{-5}$ mbar
Analyzer Penning gauge (with collision gas introduced): $1.62 - 1.67 \times 10^{-5}$ mbar

When using the Quattro Ultima triple quadrupole mass spectrometer (which has a relatively long (18 cm) collision cell), the Ar gas in the collision cell had to be kept below the ‘normal’ operating pressure range to reduce the number of multiple-collisions occurring, and to minimize further fragmentation of the K^+ bound monomer complexes. Consequently, the introduction of Ar collision gas was monitored indirectly by reading the ‘Analyser Penning Gauge’ in the analyser region, and no direct reading of the ‘Collision Cell Pirani Gauge’ connected to the collision cell was taken.

For low energy CID experiments, the collision energy was adjusted in the range of 5-35 eV. Typically, 60-100 scans were accumulated to yield a mass spectrum and the average of the ion intensity ratios of 3-4 mass spectra was taken as the final result. The ion intensity (peak height) ratios so obtained was found to be reproducible to within $< \pm 8\%$ (coefficient of variation, $n = 4$) and the logarithm of ratios to within ± 0.08 ($n = 4$).

Chapter 3 Computational Methodology

In this chapter, the basic principles of the theoretical modeling methodologies used in current study will be introduced. All *ab initio* and density functional theory calculations have been carried out using the *Gaussian03* [Frisch et al., 2003] package of programs installed in Compaq XP900, Intel Pentium 4 and SGI Supercomputers workstations.

3.1 *Ab Initio* Molecular Orbital (MO) Methods

Ab initio is a Latin word which means “from the beginning” and molecular orbital (MO) theory uses one-electron functions to approximate the full molecular wavefunctions. Thus, the purpose of *ab initio* molecular orbital modeling is to predict the properties of atomic and molecular systems based on the laws of quantum mechanics, and using only fundamental physical constants, without reference to experimental data.

3.1.1 The Schrödinger Equation

The energy of a stationary state of a molecule can be obtained by solving the time-dependent Schrödinger equation, which in shorthand operator form given in Eqn. [3.1]: [Hehre et al., 1986]

$$\hat{H}\Psi = E\Psi \quad [3.1]$$

where \hat{H} is the Hamiltonian (a differential operator consisting of both kinetic and potential energies to represent the total energy); Ψ is the wavefunction (a function of the Cartesian

coordinates of all particles and spin coordinates in the atomic/molecular system); E is the energy of state of a system (relative to a state in which the constituent particles, nuclei and electrons are infinitely separated and at rest).

3.1.2 The Born-Oppenheimer Approximation

The Hamiltonian for a molecular system, \hat{H} , can be written as the kinetic and potential energy operator of the pairwise attraction and repulsion terms of nuclei and electrons: [Hehre et al., 1986]

$$\hat{H} = \hat{T}_n + \hat{T}_e + \hat{V}_{ne} + \hat{V}_{ee} + \hat{V}_{nn} \quad [3.2]$$

where \hat{T}_n and \hat{T}_e are the kinetic energy operators for nuclei and electrons; \hat{V}_{ne} , \hat{V}_{ee} and \hat{V}_{nn} are the potential energy operators for nuclei-electron attraction, inter-electronic repulsions and inter-nuclear repulsions, respectively.

Since no particles are moving independently of each other as implied in the Hamiltonian Eqn. [3.2], the Born-Oppenheimer approximation can simplify the problem by separating nuclear and electronic motions. This approximation is generally reasonable as the mass of the nucleus is about 1,800 times greater than that of an electron. The nuclei move very slowly with respect to the electrons, and the electrons react essentially instantaneously to the changes in nuclear positions. Thus, it is more convenient to construct an electronic Hamiltonian (\hat{H}_e) for *fixed* nuclear positions, then the kinetic energy term for the nuclei (\hat{T}_n) can be neglected:

$$\hat{H} \approx \hat{H}_e = \hat{T}_e + \hat{V}_{ne} + \hat{V}_{ee} + \hat{V}_{nn} \quad [3.3]$$

3.1.3 The Slater Determinant

A molecular orbital (ψ) is a function of the Cartesian coordinates (x, y, z) of a single electron. Its square (ψ^2) is the probability distribution of the electron in space. To describe an electron completely, the spin coordinates ($\xi = +1/2$ or $-1/2$ for spin function α or β , respectively) should also be included. Thus, a complete wavefunction for a single electron is the product of a molecular orbital (ψ) and a spin function (ξ), named as spin orbital.

For an N-electron system, the simplest way to approximate the full wavefunction (Ψ) is to present it as a Slater determinant, Ψ_{Slater} , which is represented by Eqn. [3.4].

$$\Psi_{\text{Slater}} = (N!)^{-\frac{1}{2}} \begin{vmatrix} \psi_1(1)\xi_\alpha(1) & \psi_2(1)\xi_\beta(1) & \dots & \psi_n(1)\xi_\beta(1) \\ \psi_1(2)\xi_\alpha(2) & \psi_2(2)\xi_\beta(2) & \dots & \psi_n(2)\xi_\beta(2) \\ & & \vdots & \\ & & \vdots & \\ \psi_1(N)\xi_\alpha(n) & \psi_2(N)\xi_\beta(n) & \dots & \psi_n(N)\xi_\beta(N) \end{vmatrix} \quad [3.4]$$

The first row of the Ψ_{Slater} included all the possible spin orbital assignments for electron 1, and similarly for the other electrons in other rows. On expansion, the Ψ_{Slater} becomes a sum of spin orbitals. In order to ensure the probability of finding the electron anywhere in space is unity, a normalization constant of $(n!)^{-1/2}$ is needed. The Ψ_{Slater} fulfills two crucial properties of molecular wavefunction; [Jensen, 1999]

- (i) It satisfies the antisymmetric requirement of a electronic wavefunction, i.e., when the coordinates of any pair of electrons are interchanged, it is equivalent to the interchange of the corresponding rows of these two electrons in the determinant, which have the effect of changing the +/- sign;

- (ii) It is also equivalent to satisfying the Pauli exclusion principle, i.e., no two electrons of the same spin may occupy the same molecular orbital. It is because the determinant vanishes when any two rows (spin orbitals) in Ψ_{Slater} are identical.

3.1.4 Koopmans' Theorem

When we consider the energy of an N-electron system and the corresponding system with one electron removed from orbital number k, and assume that the molecular orbitals for these two systems are identical, we have the following relationship: [Koopmans, 1933]

$$E_N^k - E_{N-1} = \varepsilon_k \quad [3.5]$$

where ε_k is exactly the orbital energy. The ionization energy within the “frozen MO” approximation is given as simple as the orbital energy, which is also known as Koopmans' theorem. The theorem suggests that: [Jensen, 2007]

(i) the eigenvalues of the Fock operator (the details will be discussed in **Section 3.1.7** below). corresponding to occupied molecular orbitals are well defined and they converge to a specific value as the size of the basis set (described in Section 3.1.5) is increased. In contrast, unoccupied orbitals in a sense are only the “left-over” functions in a given basis set, and their number increases as the basis set is made larger.

(ii) The lowest unoccupied eigenvalue usually converges to zero, corresponding to a solution for a free electron, described by a linear combination of the most diffuse basis functions.

3.1.5 Basis Set Approximation

Simply to say, a basis set is a set (collection) of mathematical functions used to solve the Schrödinger equation in order to represent molecular orbitals. Thus, the molecular orbitals (ψ) can be expressed as a linear combinations of a finite set of N prescribed one-electron functions represented by *known* basis functions (ϕ_x). Take Eqn. [3.6] as an example, the i^{th} molecular orbital can be represented by a linear combination of a series ($x=1, 2, 3, \dots, N$) basis functions (ϕ_x) with coefficient (c_{xi}) as the molecular orbital expansion coefficients,

$$\Psi_i = \sum_{x=1}^N c_{xi} \phi_x \quad [3.6]$$

where i , x and N represent a series of molecular orbitals, a series of basis functions, and the dimension of the basis function, respectively. The expansion coefficients in Eqn. [3.6] are determined by applying the variational principle in a self-consistent fashion (the details will be discussed in **Section 3.1.6** below).

3.1.6 Basis Set

Slater and Gaussian Type Orbitals

There are two types of basis functions: the Slater and Gaussian type orbitals. The Slater Type Orbitals (STO) describes exponential radial distributions of electron density. They are labeled like hydrogen atomic orbitals, $1s, 2s, 2p_x, \dots$, and have the normalized form. Take STO_{1s} as an example: [Hehre et al., 1986]

$$STO_{1s} = \left(\frac{\zeta_1^3}{\pi} \right)^{1/2} \exp(\zeta_1 r) \quad [3.7]$$

where ζ_1 is a constant determining the size of the orbitals. STOs provide reasonable representations of atomic orbitals with ζ values recommended by Slater. However, they are difficult to handle for computational calculations. Thus, the other commonly used type of basis functions, the Gaussian-type basis function, GTO, is introduced. The Gaussian basis function for the s-type atomic orbitals, GTO_s , which describe the angular distributions of electron density, is represented by the following equation: [Hehre et al., 1986]

$$GTO_s = \left(\frac{2\alpha}{\pi}\right)^{3/4} \exp(-\alpha r^2) \quad [3.8]$$

Pople Style Basis Sets

Pople style basis sets are used extensively in this work, and thus more details are introduced here. Pople style basis sets are one type of contracted basis sets. Their basis functions, also known as the primitive gaussian type orbitals (PGTO), are combined together by fixed linear combinations to form the contracted gaussian type orbitals (CGTOs). Here are some examples:

- (i) STO-nG basis set: where the Slater type orbital (STO) is approximated by n PGTOs. Usually, STO-3G is the widely used as a minimum basis set.
- (ii) k-nlmG basis set: split valence basis sets. The first part 'k' means k PGTO are used for representing the core orbitals, while the second part 'nlm' describes how many functions the valence orbitals (CGTO) are split into (now is three) with different sizes, and how many PGTO are used to represent the inner, medium, and outer valence orbitals (here the letters

'nlm' are representing n-, l- and m- PGTOs for inner, medium and outer valence orbitals, respectively).

- (iii) k-nlm++G(idf,jpd) basis set: more parameters are sometimes added before the G (for Gaussian) to indicate the addition of diffuse and polarization functions. The diffuse functions (denoted as '+') are larger size version of s- and p-type functions. They allow orbitals to occupy a larger region of space and directional characters. They are found to be important for systems where electrons are relatively far away from the nucleus, such as anions, molecules with lone pairs of electrons, systems in their excited states, and transition states, etc. The polarization functions are higher angular momentum functions, i.e., *idf, jpd* means *i* d and one f polarization functions are added to heavy atoms and *j* p and one d polarization functions are added to hydrogen atom. The diffuse and polarization functions are particularly useful in describing chemical bonds.

Generally speaking, as the number of basis functions increases, the accuracy of the molecular orbitals improves. Taking the highest basis set we used in the present study as an example, the 6-311+G(3df,2p) basis set indicates a triple split valence basis, where the core orbital is made up of a contraction of six PGTOs, and the valence orbitals is split into three functions, represented by three-, one- and one PGTOs, respectively. The '+' indicates the diffuse p-function are added to the heavy atoms. The polarization functions (3df,2p) indicate three d- and one f-functions are added to heavy atoms, and two p-functions are added to hydrogen atoms.

3.1.7 Hartree-Fock (HF) Self-Consistent Field (SCF) Theory

Variational Principle

To generate approximate solutions for the Schrödinger equation, the variational principle, which states that any approximate wavefunction has an energy above or equal to the true energy (i.e., $E_{\text{trial}} \geq E_{\text{true}}$), is employed. In other words, the variational principle is to minimize the energy of a single Slater determinant by varying the MO coefficient, under the constraint that the MOs remain to be orthonormal. By making a trial wavefunction containing a number of parameters, we can get the “best” approximation of the true energy at the energy minimum as a function of these parameters.

Hartree-Fock (HF) Self-Consistent Field (SCF) Theory

Hartree-Fock (HF) self-consistent field method is based on the Variational Principle. In simple terms, if a basis set is selected for orbital expansion, the coefficients (c_{xi} in Eqn. [3.6]) may then be varied repeatedly until there is no further change from one iteration to the next one, so as to minimize the expectation value of energy, E_{trial} . Thus, the best single-determinant wavefunction, Ψ_{HF} , is found by minimizing E_{trial} with respect to the coefficients c_{xi} , and their relationship are shown below: [Hehre et al., 1986]

$$\partial E_{\text{trial}} / \partial c_{xi} = 0 \quad [3.9]$$

Roothaan-Hall Equations

By applying the variational principle, a set of algebraic equations for c_{xi} can be formed. They can be solved independently by Roothaan-Hall equation for a closed shell molecules/atoms (Eqn. [3.10]). In other words, the Roothaan-Hall equations allow the

solution of HF equations using matrix techniques, as these equations can be considered as a matrix representation of the HF equation in an infinite basis. For practical reason (computational efficiency), the number of basis functions is limited. Hence, these calculations cannot reach the HF limit. The Roothaan-Hall equation is given as below: [Hehre et al., 1986]

$$\sum_{v=1}^N (\bar{F}_{\chi v} - \varepsilon_i \bar{S}_{\chi v}) c_{vi} = 0 \quad [3.10]$$

where $\bar{F}_{\chi v}$ and $\bar{S}_{\chi v}$ are the Fock matrix and overlap matrix of the basis functions, respectively, between χ and v basis functions. While ε_i is the one electron energy of the molecular orbital, ψ_i , and c_{vi} is the MO coefficients. For normalization conditions, the MO coefficient are given as

$$\sum_{\chi=1}^N \sum_{v=1}^N c_{\chi i}^* \bar{S}_{\chi v} c_{vi} = 1 \quad [3.11]$$

The Fock matrix, $\bar{F}_{\chi v}$, must be known in order to determine the unknown MO coefficients. On the other hand, the Fock matrix is only known if all the coefficients, c_{vi} , are known. Thus, an iterative process is required for testing the convergence within a certain threshold (energy and c_{vi}). If the iteration fails, then the next iteration will be initiated. If the iteration is successful (convergence achieved), the energy and c_{vi} are then solved. The whole iteration process is illustrated in Fig. 3.1.

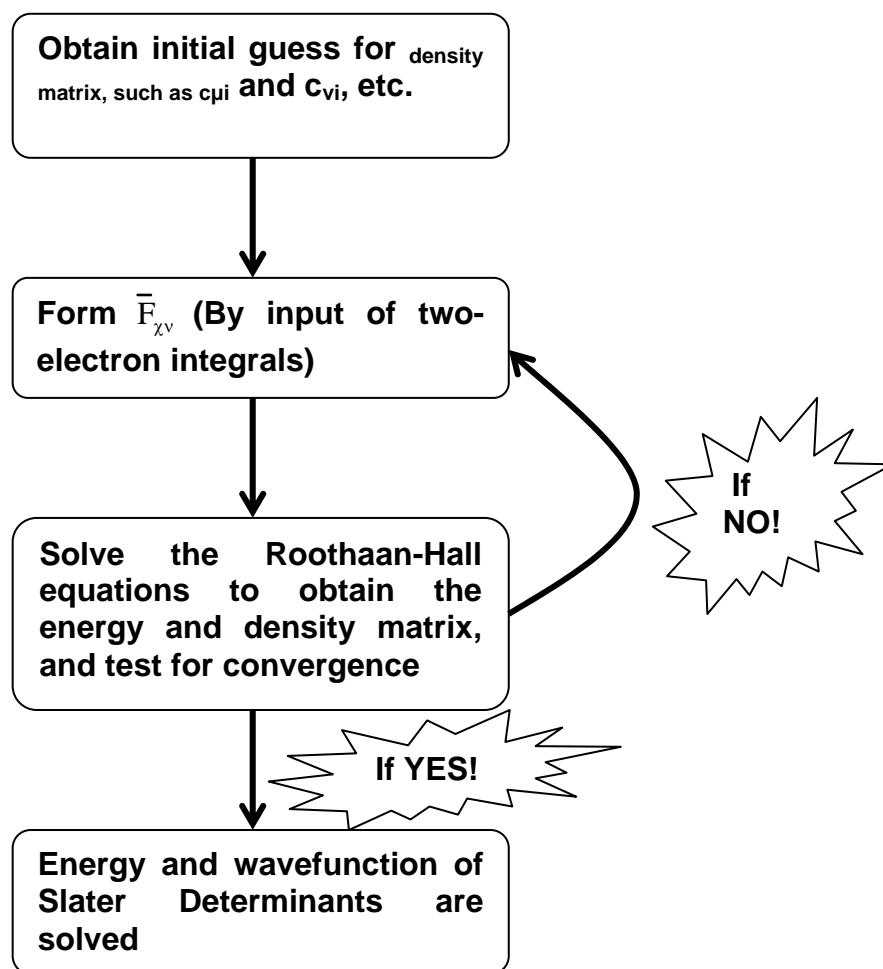


Figure 3.1 Iterative procedure of self-consistent field (SCF) calculations

3.2 Density Functional Theory (DFT)

In contrast to *ab initio* theory where all analyses are based on the wavefunction, Density Functional Theory (DFT) methods are mainly based on the electron density (ρ). In DFT, the electronic energy is expressed as a functional of density, $E[\rho]$; in other words, the aim of DFT methods is to design functionals connecting the electron density with energy. [Parr and Yang, 1989; Bartolotti and Flurchick, 1996; Baerends and Gritsenko, 1997]

Under the DFT formalism, the total energy is decomposed into three contributions: i) kinetic energy, ii) Coulomb energy (due to classical electrostatic interactions among all charged particles in the system), iii) exchange-correlation energy which captures all many-body interactions. [Koch and Holthausen, 2000]

According to Kohn and Holthausen,[Koch and Holthausen, 2000] the energy functional $E[\rho]$ can be calculated as follows,

$$\begin{aligned}
 E[\rho] &= T[\rho] + T_s[\rho] + E_{ne}[\rho] + E_{ee}[\rho] \\
 &= T[\rho] + T_s[\rho] + E_{ne}[\rho] + (J[\rho] + K[\rho]) \\
 &= T_s[\rho] + E_{ne}[\rho] + J[\rho] + (K[\rho] + T[\rho]) \\
 &= T_s[\rho] + E_{ne}[\rho] + J[\rho] + E_{xc}[\rho] \qquad [3.12]
 \end{aligned}$$

where the kinetic energy functional can be split into two parts: $T_s[\rho]$ is one part of the kinetic energy contribution that *can* be solve exactly, $T[\rho]$ is the other part of the kinetic energy with a small correction term that *cannot* be solved exactly, $E_{ne}[\rho]$ is the attraction between the nuclei and electrons, and $E_{ee}[\rho]$ is the electron-electron repulsion term arising from the combined effects of Coulombic interactions, $J[\rho]$, and the exchange interactions, $K[\rho]$. The part of the kinetic energy which *cannot* be solved, i.e., $T[\rho]$, can also be absorbed into the exchange contribution between electrons, $K[\rho]$, to form the exchange-correlation term of electron-electron repulsion, $E_{xc}[\rho]$.

Since $T_s[\rho]$, $E_{ne}[\rho]$ and $J[\rho]$ can be solved exactly, the first task for DFT is to derive suitable formulae for the exchange-correlation term, $E_{xc}[\rho]$, followed by the second task which is to determine a set of orthogonal (to enforce the Pauli principle) orbitals for the

energy minimization. Since both $J[\rho]$ and $E_{xc}[\rho]$ functional depends on the total density, an iterative procedure is needed. The $E_{xc}[\rho]$ is usually further partitioned into two parts: a pure exchange (E_x) and a pure correlation part (E_c), i.e., $E_{xc}[\rho] = E_x + E_c$. The difference between various DFT methods relies precisely in the choice of the functional form of the exchange and the correlation function (i.e. $E_{xc}[\rho]$). [Koch and Holthausen, 2000]

There are three types of DFT methods: Local Density Approximation (LDA) methods, Gradient Corrected Approximation (GGA) Method, and Hybrid Methods. In LDA, the density is treated locally as a uniform electron gas. For GGA, the exchange and correlation energies are dependent not only on the electron density, but also on derivatives of the density. The Hybrid method is among the commonly used DFT methodologies used by computational chemists, which is also widely used in this work with Becke's three parameters exchange function and the correlation functional of Lee, Yang and Parr (B3-LYP).

DFT is conceptually and computationally very similar to Hartree-Fock (HF) theory as discussed in **Section 3.1.7**. However, it provides much better results and has consequently become a very popular method. The main disadvantage of DFT lies in its inability to systematically describe certain important features, such as van der Waals' interaction.

3.2.1 Hybrid Methods

In the DFT hybrid method, the exchange energy of a Slater determinant is computed from the HF method. The B3-LYP functional employed in this work makes use of Becke's

three parameters exchange function (B3-) and the correlation functional of Lee, Yang and Parr (-LYP). [Lee, et al. 1988] The E_{xc} is given as below:

$$E_{xc}^{B3-LYP} = aE_x^{HF} + (1-a)E_x^{LSDA} + b\Delta E_x^B + cE_c^{LYP} + (1-c)E_c^{LSD} \quad [3.13]$$

The constants a, b and c are those determined by Becke who determined the values of the three parameters by fitting to the 56 atomization energies, 42 ionization potentials and 8 proton affinities and 10 first-row atomic energies in the G1 molecule set, and the computed values of a, b and c are found to be 0.80, 0.72 and 0.81, respectively. [Frisch et al., 2003]

Because of the parameterization, B3-LYP functionals perform almost as well as the highly accurate but more computationally-extensive G1/G2 model, with the unsigned error for energetics at about 2 kcal mol⁻¹ (8 kJ mol⁻¹). [Koch and Holthausen, 2000] The performance of the B3-LYP level of theory in term of geometries is also impressive. [Koch and Holthausen, 2000] For a set of 20 organic molecules, geometries optimized at the B3-LYP/6-31G(d) level were found to be in error by less than 0.005Å on average for bond lengths, and bond angles were accurate to within a few tenths of a degree, which was of the same order as the uncertainties in the experimental equilibrium structures for most polyatomic molecules. Thus, several authors suggested [Frisch et al., 2003] that the B3-LYP functional could be used instead of MP2 geometries for the highly accurate extrapolation schemes like the Gaussian-2 (G2) methodology.

3.3 Zero-point Corrections and Frequencies

According to the Heisenburg uncertainty principle, all molecules have some vibrational energy even at 0 Kelvin. Thus, a term called zero-point energy, ZPE, has to be added to

the calculated total energy (i.e., the electronic energies, E_{elec} , calculated above, which assume the system is completely at rest) to obtain the ‘true’ energy of the molecule, E_0 , that is:

$$E_0 = E_{\text{elec}} + \text{ZPE} \quad [3.14]$$

Molecular frequencies, ν , are equal to the second derivative of the energy with respect to the nuclear positions, r :

$$\nu = \partial^2 E / \partial r^2 \quad [3.15]$$

However, raw frequency values computed with the Hartree-Fock method (and other quantum mechanical methods) are known to contain some systematic errors: it generally overestimates the frequency for the Hartree-Fock method by 10%-12% when compared to the experimental data, similarly for the frequency values computed with the B3-LYP method.[Scott and Radom, 1996; Polfer et al., 2005] As a result, a scale factor of 0.8929 and 0.9806 is required to scale down frequencies predicted at the Hartree-Fock and B3-LYP level, respectively.

3.4 Thermochemical Corrections

A thermal energy correction must be added into the zero-point corrected electronic energy, E_0 (Eqn. [3.14]), in order to obtain the total energy of a system at higher temperatures other than 0 K. The thermal correction includes the effects of molecular translation (E_{trans}), rotation (E_{rot}), and vibration (E_{vib}), at the specified temperature (T), and pressure (P), that is:

$$E_{\text{tot}} = E_0 + E_{\text{vib}} + E_{\text{rot}} + E_{\text{trans}} \quad [3.16]$$

The E_{trans} , E_{rot} and E_{vib} can be estimated by statistical mechanics equation, assuming that the molecule is a rigid rotor and a harmonic oscillator. [McQuarrie and Simon, 1997] The enthalpy (H) is further deduced as:

$$H = E_{\text{tot}} + RT \quad [3.17]$$

, where R is a gas constant ($8.314 \text{ J K}^{-1} \text{ mol}^{-1}$). In order to obtain the Gibbs free energy (G):

$$G = H - T(\Delta S) \quad [3.18]$$

, where ΔS is the change of entropy that can be estimated from harmonic vibrational frequencies via statistical mechanics equations. [McQuarrie and Simon, 1997]

3.5 The Energetic Protocol Adopted in Present Study

In this work, the interaction between proton (H^+) / potassium cation (K^+) and α -/ β -amino acids and β -dipeptides in the gas phase was modeled with the ‘Energetic Protocol for H^+/K^+ ’, abbreviated as EP(H^+/K^+). The procedure is based on the energetics and structures determined with the hybrid Becke3-Lee-Yang-Parr (B3-LYP) [Becke, 1993] density functionals.

The computational procedures of the EP(H^+/K^+) protocol are listed as follows:

- (1) Geometry optimization at the HF level using the standard 6-31G(d), followed by frequency calculations in order to confirm to be real minima and obtain the zero-point-energy (ZPE) correction at this level;

(2) Geometries of these stable minima were further refined by the B3-LYP functional with the 6-31G(d) basis set in order to obtain the effect of electron correlation on structures of ligands and H⁺/K⁺-ligand complexes; [Becke, 1993]

(3) Energetics are obtained by using the B3-LYP functional with the large and flexible 6-311+G(3df,2p) basis set based on geometry determined in step (2), followed by frequency calculations at B3-LYP functional with the 6-31G(d) basis set, i.e., the energetic calculations were carried out at the B3-LYP/6-311+G(3df,2p)//B3-LYP/6-31G(d) level.

Proton (H⁺) / potassium cation (K⁺) affinities (PAs / PCAs) at 0K, ΔH_0 , are obtained using Eqn. [3.19], using K⁺ affinities as an example:

$$\Delta H_0 = [(E_{K^+} + E_L) - E_{K^+-L}] + [ZPE_L - ZPE_{K^+-L}] \times 0.9806 \quad [3.19]$$

, where E_{K^+} , E_L and E_{K^+-L} are the electronic energies of the potassium metal cation, the ligand and the K⁺-ligand complex, respectively, obtained from step (3); ZPE_L and ZPE_{K^+-L} are the zero-point-energy corrections for the ligand and the K⁺-L complex obtained from step (1), respectively, with a scaling factor of 0.9806 for the B3-LYP frequencies.[Scott and Radom, 1996; Polfer et al., 2005]

The EP(H⁺/K⁺) theoretical values at 0K (ΔH_0) are often converted to affinities at 298K (ΔH_{298}) for the purpose of comparison with experimental values at 298K. While the free energy of binding (ΔG_{298}) of different conformers/isomers is also calculated from the B3-LYP/6-31G(d) frequencies by applying standard statistical thermodynamics relations. [DelBene, 1983]

In summary, all theoretical studies reported in this work, except the study on protonated His-containing dipeptides in chapter 8, is modeled by the following levels of theory:

- (1) Geometries: B3-LYP/6-31G(d);
- (2) Single point energies: B3-LYP/6-311+G(3df,2p)//B3-LYP/6-31G(d);
- (3) Zero-point energy (ZPE) and thermal correction: B3-LYP/6-31G(d);

The B3-LYP hybrid method has been found to be the best overall performance for problems related to gas-phase ion chemistry [Alcami et al., 2001], with deviations from the experimental values typically by no more than 5 kJ mol⁻¹. [Wang et al., 1999; Rodriguez et al., 2000; Addario, 2002; Lau et al., 2003] We found this observation to be valid in the calculation of H⁺/K⁺ affinities, even though a relatively large basis set has to be used. [Dinadayalane et al., 2006; Aribi et al., 2003; Pingitore et al., 2004; Balta et al., 2003]. The agreement between the experimental and calculated ΔH_0 values lends credence to the optimized geometries and energetics obtained in this study. In addition, the basis set we used, 6-31G(d), is a medium size basis set which has been demonstrated to be adequate for geometry optimizations and excitation energy calculations on covalent molecules.[Nguyen and Pachter, 2001]. The 6-311+G(3df,2p) basis set were used because calculations without diffuse and polarization functions for the heavy and hydrogen atoms may be inadequate for calculations on ion-molecule complexes. [Bruyneel, 2003]

For the study on the dissociations of protonated dipeptides containing histidine (His) in chapter 8, the theoretical protocol adopted is generally the same as listed above, except that the single point energies of various species are calculated at the same level of as geometry optimization, i.e., at the B3-LYP/6-31G(d)//B3-LYP/6-31G(d) level, and also

the same for the ZPE correction. The reasons for adopting a lower level of theory in the theoretical calculations of His-containing dipeptides are:

- (i) the calculation on B3-LYP/6-311+G(3df,2p)//B3-LYP/6-31G(d) level on protonated His-containing dipeptides required very extensive computational time because, on average, there were more than 25 atoms in every species, each of which would require additional computation time of more than 24 hours in computation time if single point energies are calculated at this higher level for each species;
- (ii) the single point energies calculated at B3-LYP/6-31G(d)//B3-LYP/6-31G(d) level is shown to be consistent with our experimental observations; i.e., the order of theoretical critical energies for dissociation of various protonated/ionic fragments are, in the main, in agreement with the order of threshold voltages obtained experimentally (refer to **Section 6.2.2** for further discussion) ;
- (iii) the single point energies calculated at B3-LYP/6-31G(d)//B3-LYP/6-31G(d) level is widely adopted in literature for M.O calculations of relative large species like protonated dipeptides, and is proven to be of sufficient accuracy in most cases for determining at least the relative proton affinity as well as Rice-Ramsperger-Kassel-Marcus (RRKM) modeling of dissociation rate constants of protonated peptides. [Csonka et al., 2005]

3.6 Potential Energy Surface (PES) of Dissociation

The binding sites between proton/alkali metal cation and amino acids/peptides in the gas phase cannot be easily captured by x-ray crystallography. Moreover, it is also difficult

to detect experimentally the involvement of proposed reaction intermediates and transition species, and hence the verification of proposed reaction pathways/mechanisms in chemical research. As a result, the use of high-level Molecular Orbital calculations becomes very popular in order to find out the plausible proton/alkali metal cation binding modes to peptides and its detailed dissociation pathways.

In this work, the prediction of different dissociation pathways from H^+ - α -/ β -amino acids/dipeptides are expressed in the form of potential energy surface (PES). A PES of a simple dissociation reaction path according to the *Transition State Theory* (TST) is shown in Figure 3.2.

As shown in Fig. 3.2, a PES of a dissociation reaction is a plot of minimum potential energy (i.e., the electronic energy, ΔE) of the species (reactants and products) along the reaction coordinate. The activation or critical energy ΔE^* is the energy difference between the highest energy barrier (usually a TS, but could sometimes be the products (i.e., the fragment ion plus neutrals lost in the present study), which is also a major factor determining the rate of the reaction. Gibbs free energy of the reaction, ΔG^* , could also be calculated using the enthalpy (ΔE^*) and entropy (ΔS) obtained by Eqn. [3.21]:

$$\Delta G^* = \Delta E^* - T(\Delta S) \quad [3.21]$$

At energies exceeding the critical energy ΔE^* , the rate of dissociation, k_{rate} , is also affected by entropic factors of the TΔS or final products, which are related to the frequency factor, ν , of the dissociation reaction, and the difference in Gibbs free energies between the TS and reactant, i.e., ΔG^* , which in term could be estimated by Eqn. [3.22]. One of the basic assumption of the transition state theory is that the TS is in thermodynamic equilibrium with the reactants and products, and the probability of finding

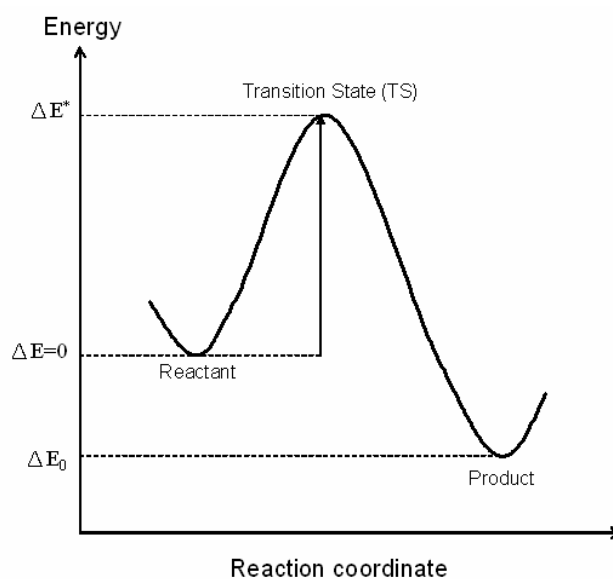


Figure 3.2 A potential energy surface (PES) of a simple dissociation reaction path

a molecule in the given quantum state is proportional to $e^{-\Delta G^*/RT}$ according to the Boltzmann distribution. Hence, the rate of dissociation reaction is given by Eqn [3.22]:

$$k_{rate} = \nu \cdot e^{-\Delta G^*/RT} \quad [3.22]$$

where ν is the frequency factor of the reaction, R is the gas constant, and T is the effective temperature. From Eqn [3.22], it could be seen that the rate of a chemical reaction generally increases with the a greater (negative) change in the free energy change of the TS and the reactants, a concept which will be used in our rationalization of experimental observations and PES predictions of dissociation of protonated β -alanine (Chapter 6), β -dipeptides (Chapter 7) and His-containing dipeptides (Chapter 8).

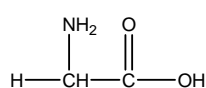
Chapter 4 Potassium Cation Affinities of α -Amino Acids with Functionalized Side Chains: a Combined Experimental and Theoretical Study

4.1 Background

The chemical structures of the 20 most common α -amino acids are shown in **Scheme 4.1**. While the Li^+ [Bojesen et al., 1993; Feng et al., 2003] and Na^+ [Bojesen et al., 1993; Gapeev and Dunbar, 2001; Kish et al., 2003; Moision and Armentrout, 2002] affinities of many α -amino acids have been experimentally measured and reported, there are only limited data on the corresponding K^+ affinities. Part of the underlying reasons is that K^+ affinities could not be easily measured as Li^+ and Na^+ affinities. Experimentally, Li^+ and Na^+ affinities of model organic ligands had been measured by high pressure mass spectrometry (HPMS) [Davidson and Kebarle, 1976] and Fourier-transformed-ion cyclotron resonance (FT-ICR) techniques, [Hoyau et al., 1999; Burk et al., 2000] both of which requires the establishment of an equilibrium reaction between the metal cation and the binding ligand under the vacuum and time frame (microseconds to milliseconds) of the mass spectrometer. Presumably because of the weaker K^+ binding, it was found that a much more longer time (more than a few hours) is required to reach binding equilibrium with potassium cation in the gas phase.[Gapeev and Dunbar, 2001] Consequently, it is not surprising that the first K^+ -glycine (Gly) affinity was determined by Kebarle and co-workers using the threshold collision-induced dissociation (threshold CID) method, [Klassen et al., 1996] a technique based on the unimolecular dissociation of the K^+ -ligand complex, with no involvement of a binding equilibrium reaction. The K^+ -glycine affinity was recently re-measured by a more refined threshold-CID protocol developed by Armentrout and co-workers.[Moision and Armentrout, 2002] Using a similar threshold-

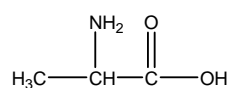
CID protocol, the K^+ affinities of the aromatic amino acids phenylalanine (Phe), tyrosine (Tyr) and tryptophan (Trp) were measured by Rodgers and co-workers.[Ruan and Rodgers, 2004] The K^+ affinities so determined are in general agreement with theoretical values obtained by M.O. calculations based on MP2/B3-LYP protocols. However, threshold-CID measurements are usually carried out with specially designed mass spectrometers dedicated for this particular purpose, which are not easily accessible to the average research laboratory. Aside from that of Gly, Phe, Tyr and Trp, the experimental K^+ affinities of other α -amino acids have not been reported in the literature.

(a) Aliphatic amino acids



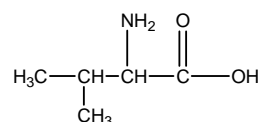
Glycine (Gly)

$M_\alpha = 75.03$



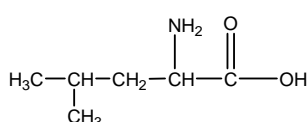
Alanine (Ala)

$M_\alpha = 89.05$



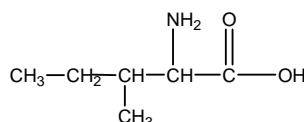
Valine (Val)

$M_\alpha = 117.08$



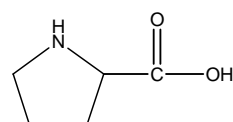
Leucine (Leu)

$M_\alpha = 131.09$



Isoleucine (Ile)

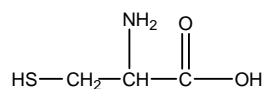
$M_\alpha = 131.09$



Proline (Pro)

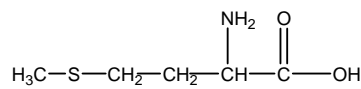
$M_\alpha = 115.06$

(b) Amino acids with -SH/ -SCH₃/-OH functionalized side chains



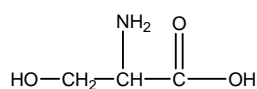
Cysteine (Cys)

$M_\alpha = 121.02$



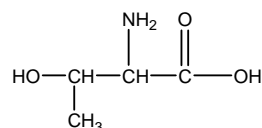
Methionine (Met)

$M_\alpha = 149.05$



Serine (Ser)

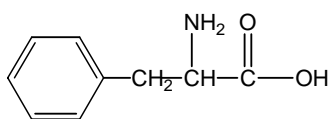
$M_\alpha = 105.04$



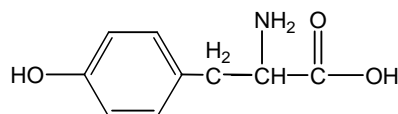
Threonine (Thr)

$M_\alpha = 119.06$

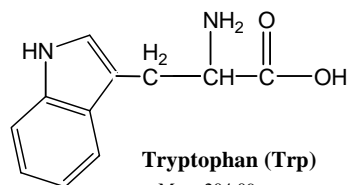
(c) Amino acids with aromatic side chain



Phenylalanine (Phe)
 $M_{\alpha} = 165.08$

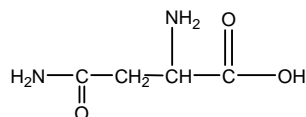


Tyrosine (Tyr)
 $M_{\alpha} = 181.07$

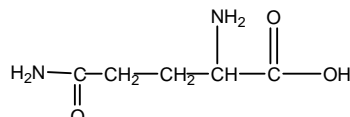


Tryptophan (Trp)
 $M_{\alpha} = 204.09$

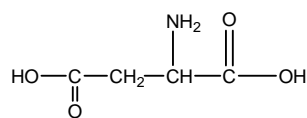
(d) Amino acids with carboxylic acid and amide functionalized side chains



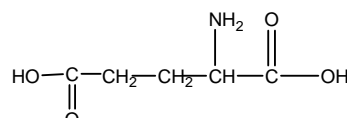
Asparagine (Asn)
 $M_{\alpha} = 132.05$



Glutamine (Gln)
 $M_{\alpha} = 146.07$

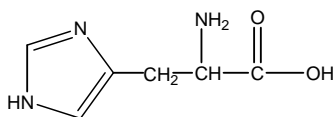


Aspartic acid (Asp)
 $M_{\alpha} = 133.04$

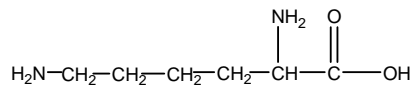


Glutamic acid (Glu)
 $M_{\alpha} = 147.05$

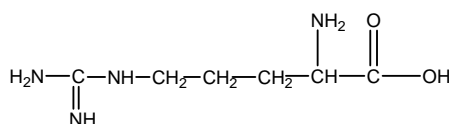
(e) Amino acids with basic side chain



Histidine (His)
 $M_{\alpha} = 155.07$



Lysine (Lys)
 $M_{\alpha} = 146.11$



Arginine (Arg)
 $M_{\alpha} = 174.11$

Scheme 4.1 Chemical structures of 20 α -amino acids

As a simple alternative to the threshold-CID method, the kinetic method (Section 2.4) is also capable of measuring alkali metal cation affinities of model ligands without the need of establishing a binding reaction equilibrium. In fact, the first study on Li^+ and Na^+ affinities of selected aliphatic amino acids was based on results from standard kinetic method measurements, though the accuracy of some of the reported Li^+ and Na^+ affinity values is in doubt due to uncertainty of the reference affinity values used in the calibration of the \ln intensity ratio measurements.[Bojesen et al., 1993] The Li^+ [Feng et al., 2003] and Na^+ [Kish et al., 2003] affinities of aliphatic amino acids and other amino acids were later re-explored using the kinetic method and *validated* theoretical affinity values of amides as reference values. The issue of availability of accurate reference values for kinetic method measurements is even more acute for the determination of K^+ affinities of amino acids because of the lack of accurate validated reference values. An earlier report on the determination of K^+ affinity of Phe, Tyr and Trp by using the extended kinetic method was found to be likely in serious error and in disagreement with theoretical values.[Ryzhov et al., 2000] The plausible causes of the serious error were later attributed to (i) inappropriate choice of *tautomeric* reference compounds (i.e. the DRN/RNA bases adenine, cytosine, guanine with many possible structures / K^+ affinities in the gas phase), and (ii) possibly wrong K^+ affinity values for the reference compounds in the kinetic method measurements. [Rodgers and Armentrout, 2000] This highlights the importance of availability of reference compounds of accurately known K^+ affinities in kinetic method measurements

Amino acids are molecules with many functional groups and O/N-heteroatom metal cation binding sites; the energetically favoured K^+ binding modes for each amino acid could only be determined by theoretical molecular modeling. In addition, with the dramatic increase in hardware computation capabilities in recent years, M.O. modeling using the

MP2 or B3-LYP protocol with large basis sets were found to be able to yield accurate alkali metal affinities (Li^+ , Na^+ and K^+) of model organic ligands to within $\pm 12 \text{ kJ mol}^{-1}$ range.[Hoyau et al., 1999; Rodgers and Armentrout, 2000; Siu et al., 2001a; Lau et al., 2003] Not surprisingly, the binding of alkali metal cations to the simplest amino acid, glycine, have been most extensively studied.[Jensen, 1992; Hoyau and Ohanessian, 1998; Wong et al., 2002] Again, most of the theoretical studies on binding modes and affinities were focused on the smaller Li^+ and Na^+ cations as analogous studies on the larger K^+ ion are computationally more demanding. Among the few studies on K^+ binding, the most stable binding mode for K^+ -glycine is the bidentate charge-solvated mode (CS) with K^+ -glycine binding to the amide carbonyl oxygen ($\text{O}=\text{C}$) and the carboxylic hydroxyl oxygen ($-\text{OH}$) sites.[Wong et al., 2002] For the K^+ -phenylalanine complex, the most stable binding mode is the tridentate CS mode with K^+ binding to the $\text{O}=\text{C}$, $-\text{NH}_2$, and the aromatic- π surface. [Siu et al., 2004] The relative stabilities of different CS and zwitterionic binding modes were found to be mainly the same for tyrosine and tryptophan, and for the small Li^+ / Na^+ ions as well. [Dunbar, 2000; Siu et al., 2001b; Ruan and Rodgers, 2004] The tridentate CS binding mode ($\text{O}=\text{C}$, $-\text{NH}_2$, and $-\text{SH}/-\text{OH}$) was also found to be most stable for Na^+ binding to cysteine (Cys) and serine (Ser), the amino acids with the $-\text{SH}$ and $-\text{OH}$ functional group in its side chain, respectively. [Hoyau et al., 1999] However, theoretical studies on the corresponding K^+ binding modes have not been reported.

Zwitterionic (ZW) modes of alkali metal binding to α -amino acids was suggested to be likely when the amino acid is sufficiently basic and the alkali metal cation is relatively large in ionic size.[Wytttenbach et al., 2000] Williams and co-workers first suggested that the K^+ -arginine (Arg) complex is likely to occur in the zwitterionic state as it showed preferential loss of NH_3 under FT-ICR CID conditions; the experimental evidence is

consistent with results obtained from theoretical calculations on the relative stabilities of proposed K^+ bound ZW and CS binding modes. [Jockusch et al., 1999] Ohanessian and co-workers also showed theoretically that the most stable Na^+/K^+ -proline complex, another basic α -amino acid, is in the zwitterionic (ZW) form, with Na^+ / K^+ bound to the two carboxylate oxygens and the proton bound to the cyclic secondary amino group in the gas phase.[Hoyau et al., 1999] Experimental evidence in support of the theoretical findings was found in the *relative* Na^+/K^+ affinity of proline and its methyl ester determined by the standard kinetic method: the Na^+/K^+ -Pro complex was found to show greater affinity than the Na^+/K^+ -ProOMe complex.[Talley et al., 2002] In the absence of a free hydroxyl functional group, Na^+/K^+ bound methyl esters of amino acids in general could only be found in the charge-solvated (CS) state, and should show greater affinity than its free acid because of its enhanced molecular polarizability (and hence ion-induced dipole interaction) due to the presence of the additional methyl group. The reversal in *relative* affinity found for the Na^+/K^+ -Pro and Na^+/K^+ -ProOMe complexes, as was found for the Na^+/K^+ -Arg and Na^+/K^+ -ArgOMe complexes, was not observed for 13 other amino acids studied. This is highly indicative that the Na^+/K^+ -Pro complex was found in the ZW form. This is followed by a detailed study of alkali metal cation (Li^+ , Na^+ and K^+) binding to proline by Marino et al. at the B3LYP/6-311++G** level [Marino et al., 2003]; the results also showed that among the many possible CS and ZW binding modes, the most stable binding mode is the K^+ -Pro complex in the ZW form. Aside from proline and arginine, the K^+ binding to other basic amino acids like lysine and histidine remained unexplored.

As part of an on-going effort to establish the K^+ affinities of model organic ligands, Prof. Tsang's research group has successfully established a set of validated K^+ affinities of six amides, which could be usefully employed as reference values in the determination of K^+

affinities of α -amino acids by the mass spectrometric kinetic method.[Tsang et al., 2004] In the present study, we measured the intrinsic potassium cation (K^+) binding affinities (energies) of the twenty naturally occurring α -amino acids by the mass spectrometric kinetic method, and conducted a systematic study on the many possible K^+ binding modes by high level hybrid density functional theory (DFT) calculations. Due to the limited studies on K^+ affinities and binding modes in the literature, our focus was on amino acid with functionalized side chains as well as their O-methyl esters. Specifically, we aim to obtain consistency in the experimental and theoretical affinity values, identify the most stable K^+ binding modes, and elucidate the factors governing the relative stabilities of the charge solvated (CS) versus zwitterionic (salt bridge) K^+ binding modes.

4.2 Results and Discussion

4.2.1 Experimental Determination of Potassium Cation Affinities of Amino Acids with Functionalized Side Chains (AAFSCs) and Their Methyl Esters

Relative K^+ Affinities. The K^+ affinities of aliphatic amino acids (glycine, alanine, valine, leucine, and iso-leucine) and their methyl esters (as listed in Table 4.1) have been determined by the standard kinetic method using the validated K^+ affinities of six amides (formamide, methyl foramide, N,N'-dimethyl formamide, acetamide, N-methyl acetamide, and N,N'-dimethyl acetamide) as reference values.[Tsang, 2003; Tsang et al., 2004] The experimental values were in excellent agreement with theoretically values calculated using the protocol, with a mean-absolute-deviation (MAD) of 0.9 kJ mol^{-1} only. Such excellent agreement provides confidence in the accuracy of the K^+ affinity values of the aliphatic

amino acids and their methyl esters, and they were used as the reference values in the determination of the K^+ affinity of the remaining α -amino acids in the present study.

Some exploratory work on kinetic method measurements of the K^+ affinities of selected amino acids with functionalized side chains (AAFSC) had been carried out by members of Prof. Tsang's research group. [Tsang, 2003] To ensure reproducibility and consistency of experimental results, all previous measurements were repeated in the present work, and the mass spectrometric measurements was extended to all of the twenty α -amino acids. After a series of trial measurements, we found that the entropic term ($\Delta(\Delta S)$) in the kinetic method measurements may or may not be significant (i.e. $\Delta(\Delta S) \approx 0$ and $\Delta(\Delta S) \neq 0$) for the AAFSCs and their methyl esters, so that a combination of the standard (when $\Delta(\Delta S) \approx 0$) and extended (when $\Delta(\Delta S) \neq 0$) kinetic method measurements had to be adopted in the present study. The standard kinetic method measurements were conducted under metastable ion (MI) dissociation conditions using the MAT-95S-B-E sector mass spectrometer (Fig. 2.9), while the extended kinetic method measurements were conducted under low-energy CID conditions (eV, laboratory frame) using the Quattro triple-quadrupole mass spectrometer (Waters, Manchester, U.K.)

Based on their mass spectrometric dissociation behavior (i.e., similar entropic effects in dissociation of the heterodimers) in the kinetic method measurements, the AAFSCs and their methyl (-OMe) esters (with ethyl esters (-OEt) included when necessary for building up of the relative K^+ affinity ladder) examined in this study can be grouped into three groups:

Group 1: Ser, Thr, Phe, Tyr and their -OMe esters

Group 2: Asp, Glu, Lys, Asn, Gln, Trp, His, Arg and their -OMe esters

Group 3: Cys, Met, Pro and their –OMe esters

For **Group 1** and **2** AAFSCs and their –OMe esters, an internally consistent relative K^+ affinity ladder could be obtained under metastable ion dissociation conditions. Typical metastable ion dissociation mass spectra of three heterodimers including (a) [SerOEt–K–Phe] $^+$, (b) [SerOEt–K–Tyr] $^+$ and (c) [SerOEt–K–PheOMe] $^+$ are shown in Fig. 4.1. The relative K^+ affinities, expressed in terms of the measured natural logarithm ion intensity ratios, $\ln(I_{[K-L_1]^+}/I_{[K-L_2]^+})$, of the **Group 1** and **Group 2** AAFSCs and their –OMe/OEt esters, are shown in Fig. 4.2 and Fig. 4.3, respectively, in the form of a relative K^+ affinity ladder.

As shown in Fig. 4.2 and Fig. 4.3, the $\ln(I_{[K-L_1]^+}/I_{[K-L_2]^+})$ values are internally consistent for all the K^+ -bound heterodimers of AAFSCs and their –OMe/-OEt esters. For example, the $\ln(I_{[K-L_1]^+}/I_{[K-L_2]^+})$ intensity ratio for the metastable dissociation of [PheOMe–K–SerOMe] $^+$ was 2.82 (Fig. 4.2), while a very similar value was obtained by summing the $\ln(I_{[K-L_1]^+}/I_{[K-L_2]^+})$ values of the four intermediate stair-steps, i.e., $2.91 = 0.51 + 0.46 + 0.09 + 1.85$. The result suggests that entropic effects are small in the metastable ion dissociation of the K^+ -bound heterodimers of AAFSCs and their –OMe/-OEt esters, and the $\ln(I_{[K-L_1]^+}/I_{[K-L_2]^+})$ ratio shown in Fig. 4.2 and Fig. 4.3 can be approximated to the $\Delta(\Delta H)/RT_{\text{eff}}$ term according to Eqn. [2.5], where $\Delta(\Delta H)$ is the difference of K^+ affinities between the ligands L_1 and L_2 . In practice, this means the entropic contribution to the measured relative K^+ affinity, i.e., the $T_{\text{eff}}\Delta(\Delta S)^{\text{app}}$ term in Eqn. [2.8], is not more than 0.5 kJ mol^{-1} (estimation based on the observed deviations in the $\ln(I_{[K-L_1]^+}/I_{[K-L_2]^+})$ ratios in the ‘additivity check’ for internal consistency), and can be approximated to zero. Based on

the relative affinity ladders shown in Fig. 4.1 and 4.2, the order of K^+ affinities among the AAFSCs is found as follows:

Group 1: Ser < Thr < Ser-OMe < Phe ~ Tyr < Ser-OEt < Phe-OMe

Group 2: Asp < Glu < Lys < Glu-OMe < Lys-OMe < Lys-OEt < Asn < Trp < Gln
< His < His-OMe < Arg

Because of the presence of entropic effects, the **Group 3** AAFSCs could not be included in the relative affinity ladders of **Group 1** and **Group 2** AAFSCs; as a result, their K^+ affinities have to be determined separately by extended kinetic method measurements as described in the following section.

Absolute K^+ Affinities. The absolute K^+ affinities of selected Group 1, 2 and 3 AAFSCs were first measured by the extended kinetic method using the K^+ affinities of aliphatic amino acids and their -OMe/-OEt esters as reference values (Table 4.1), which were established in previous studies by members of Prof. Tsang's research group. [Tsang, 2003; Wong, 2004] For example, the [CysOMe-K-L_n]⁺ heterodimer ion (L_n = GlyOMe, AlaOMe, ValOMe and LeuOMe as reference compounds) was subjected to different extents of collisional activation (10 - 30 eV collision energies) in a triple quadrupole mass spectrometer, and the intensity of the [K-CysOMe]⁺ and [K-L_n]⁺ fragment ions were measured (refer to MS/MS spectra shown in Fig. 4.4. for the case L_n=AlaOMe). A plot of $\ln(I_{[CysOMe-K-L_1]^+}/I_{[K-L_n]^+})$ intensity ratios values obtained from the MS/MS spectra (where L_n are the reference compounds) versus $[\Delta H_{[K-L_n]^+} - \Delta H_{Avg}]$ (where the ΔH s are the K^+ binding affinities of the reference compounds) yields a regression line whose slope and y-intercept render the effective temperature (T_{eff}) of the dissociating heterodimer [CysOMe-K-L_n]⁺ and the $[\Delta G^{app}_{[K-L_n]^+} - \Delta H_{Avg}]/RT_{eff}$ terms,

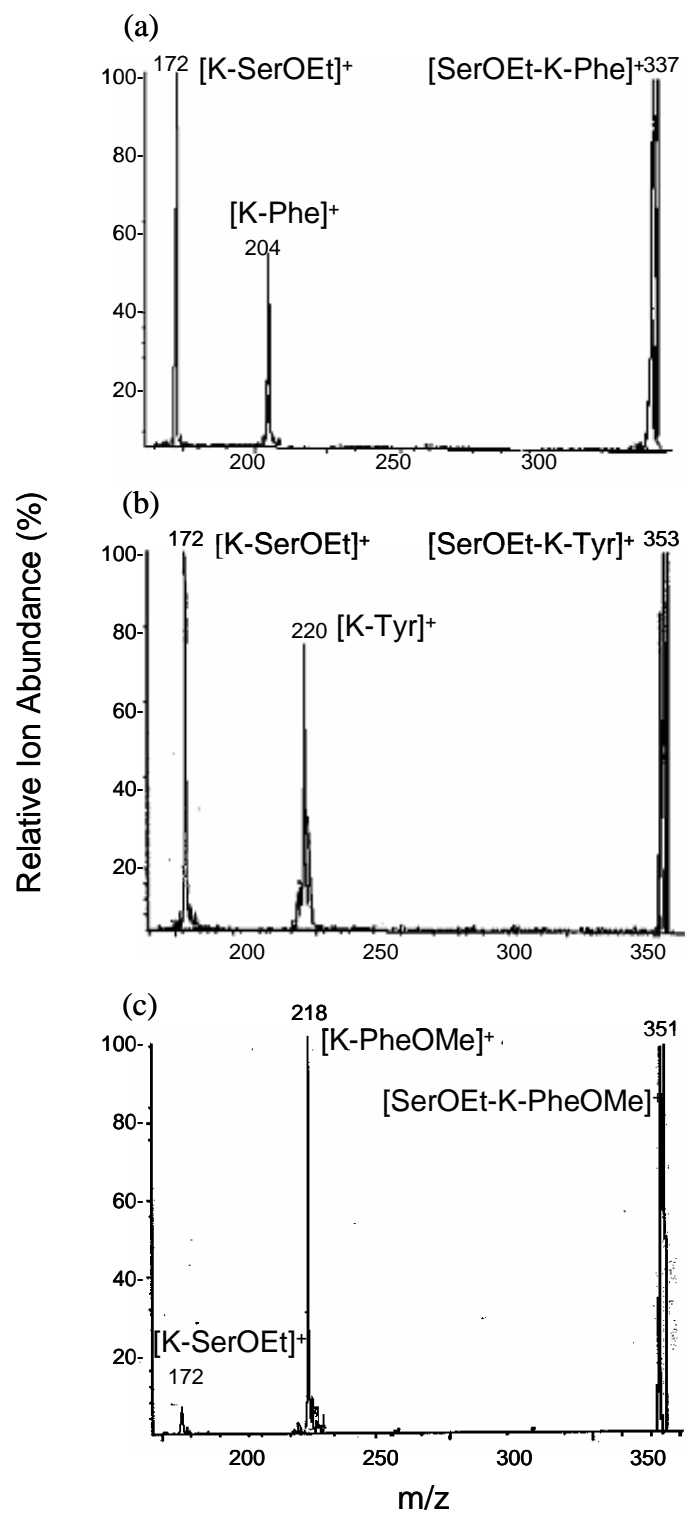


Figure 4.1 Metastable (unimolecular) ion dissociation mass spectra of (a) [SerOEt-K-Phe]⁺, (b) [SerOEt-K-Tyr]⁺ and (c) [SerOEt-K-PheOMe]⁺ heterodimers (Phe = Phenylalanine, Tyr = Tyrosine, PheOMe = Phenylalanine methyl ester and Ser-OEt = Serine ethyl ester.)

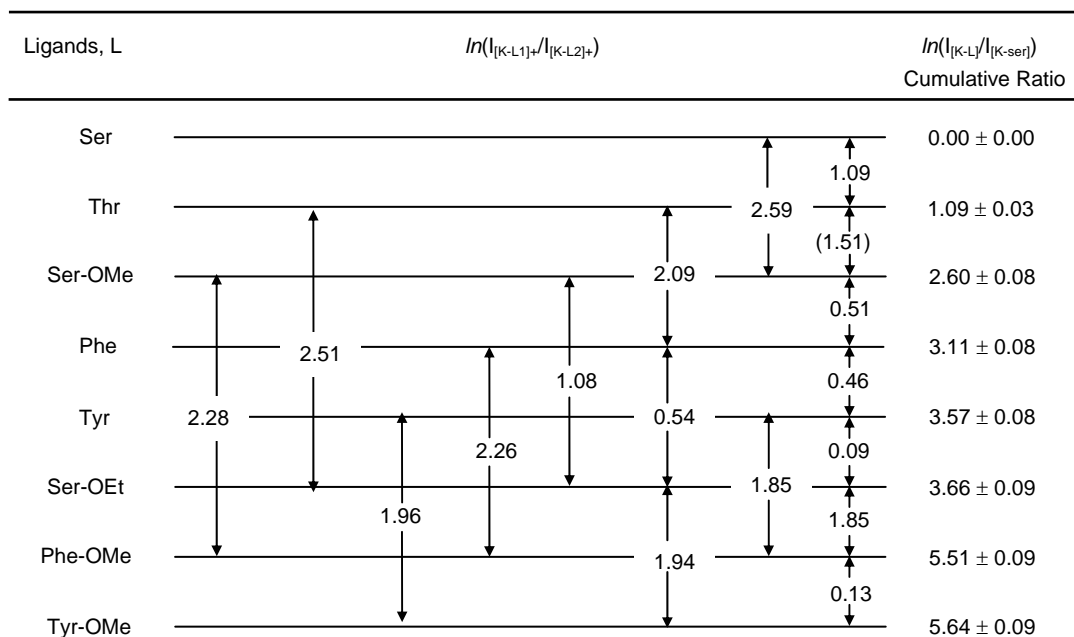


Figure 4.2 Experimentally measured $\ln(I_{[K-L_1]^+}/I_{[K-L_2]^+})$ values for metastable(unimolecular) ion decomposition of K^+ -bounded heterodimers of amino acids ($T_{\text{eff}} = 230$ K). The $\ln(I_{[K-L_1]^+}/I_{[K-L_2]^+})$ values are logarithm of ion intensity ratios. The data presented under the heading $\ln(I_{[K-L]}/I_{[K-Ser]^+})$ are average \pm standard deviation of cumulative values expressed relative to serine. The $\ln(I_{[K-L_1]^+}/I_{[K-L_2]^+})$ lines are not drawn to scale for clarity

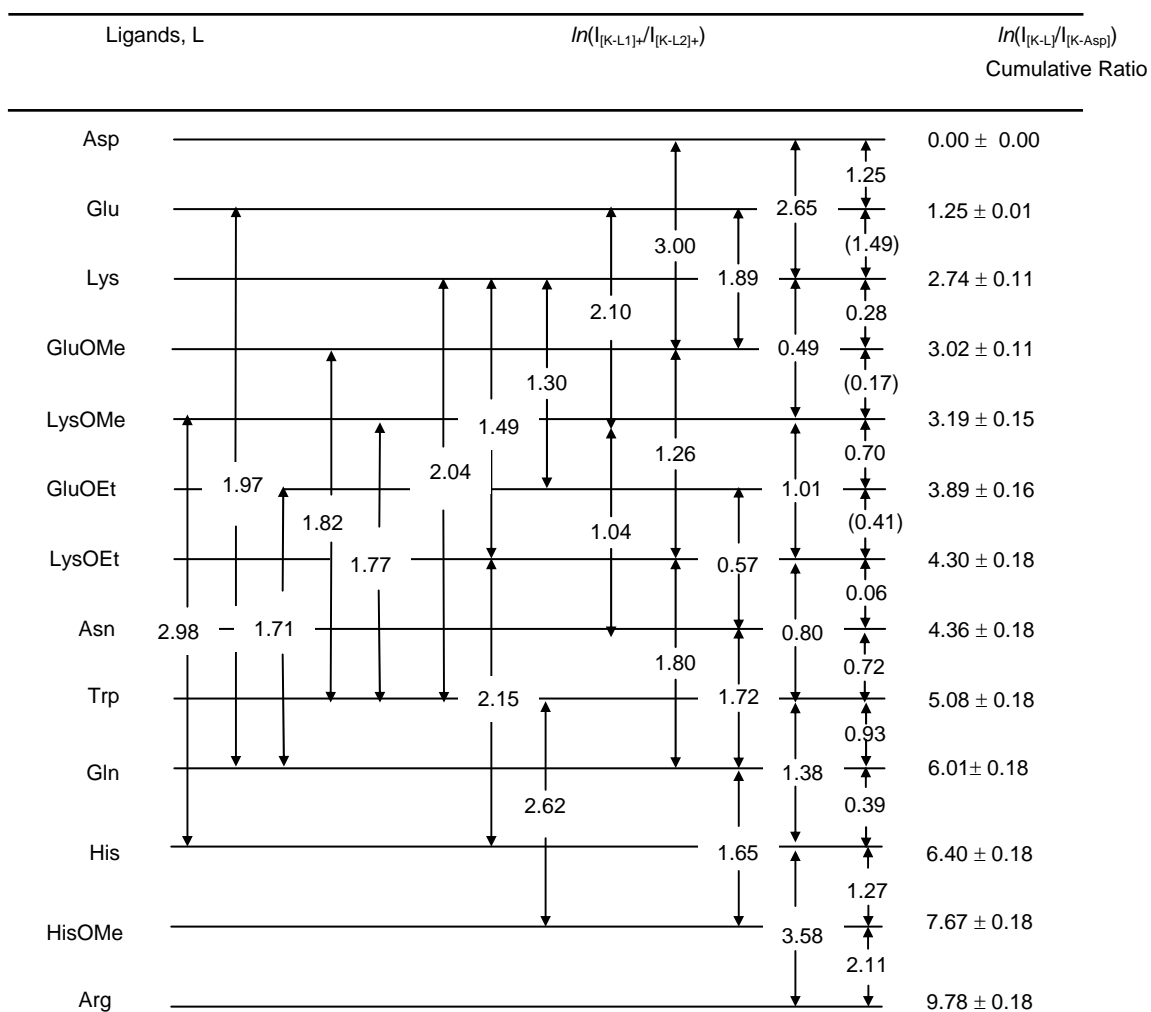


Figure 4.3 Experimentally measured $\ln(I_{[K-L_1]^+}/I_{[K-L_2]^+})$ values for metastable(unimolecular) ion decomposition of K^+ -bounded heterodimers of amino acids ($T_{\text{eff}} = 342\text{K}$). The $\ln(I_{[K-L_1]^+}/I_{[K-L_2]^+})$ values are logarithm of ion intensity ratios. The data presented under the heading $\ln(I_{[K-L]^+}/I_{[K-Asp]^+})$ are average +/- standard deviation of cumulative values expressed relative to aspartic acid. The $\ln(I_{[K-L_1]^+}/I_{[K-L_2]^+})$ lines are not drawn to scale for clarity

respectively (Fig. 4.5(a) and Eqn [2.7] and Section 2.4.2). By plotting the $[\Delta G^{\text{app}}_{[\text{K-L}_n]^+} - \Delta H_{\text{Avg}}]/RT_{\text{eff}}$ term against $1/RT_{\text{eff}}$ (Fig. 4.5(b), Eqn [2.9] and Section 2.4.2), the K^+ binding affinity for cysteine methyl ester, $\Delta H_{[\text{K-CysOMe}]^+}$, as well as the apparent entropic change term, $\Delta(\Delta S)^{\text{app}}$, for the dissociation of the $[\text{CysOMe-K-L}_n]^+$ heterodimer complex, were obtained from the slope and y-intercept of the plot. The K^+ affinities of a total of 16 α -amino acids and their $-\text{OMe}/-\text{OEt}$ esters were determined by the extended kinetic method, and the experimentally measured affinity values, together with the reference compounds/values adopted, are summarized in Table 4.1. The experimental uncertainty (\pm S.D.) of the extended kinetic method measurement is in the 0.1 to 1.4 kJ mol^{-1} range (Table 4.1), while the assigned uncertainty of the reference affinity values for the aliphatic amino acids Gly, Ala, Val, Leu and iso-Leu and their $-\text{OMe}/-\text{OEt}$ esters is $\pm 12 \text{ kJ mol}^{-1}$. [Tsang, 2003] Combining the errors from these two sources and taking a conservative approach of estimation, we tend to assign an overall uncertainty of $\pm 14 \text{ kJ mol}^{-1}$ for the α -amino acids and their $-\text{OMe}/-\text{OEt}$ esters determined by the extended kinetic method in the present work.

The K^+ affinities of amino acids and their $-\text{OMe}/-\text{OEt}$ esters found from the extended kinetic method measurements were in turn used as ‘calibration values’ to determine the K^+ affinities of the remaining AAFSCs and their $-\text{OMe} / -\text{OEt}$ esters that appear in the relative K^+ affinity ladders shown in Fig. 4.2, and Fig. 4.3. For example, a plot of the cumulative $\ln(I_{[\text{K-L}]^+}/I_{[\text{K-Ser}]^+})$ values of serine (Ser), threonine (Thr) and serine methyl ester (Ser-OMe) versus their experimental K^+ affinity values yields a straight line ($R^2 = 0.99$), with a slope equal to $1/RT_{\text{eff}}$ (according to Eqn. [2.5]) as shown in Fig. 4.6, from which an effective temperature (T_{eff}) of 230 K was obtained for the relative affinity ladder shown in Fig. 4.2. The K^+ affinities of Phe, Tyr, SerOEt, PheOMe and TyrOMe could

then be found by extrapolation of this calibration plot using the cumulative $\ln(I_{[K-L]^+}/I_{[K-Ser]^+})$ value of the individual amino acid or its -OMe/-OEt esters (Fig. 4.6). By the same token, another plot of cumulative $\ln(I_{[K-L]^+}/I_{[K-Asp]^+})$ values from the relative affinity ladder shown in Fig. 4.3 versus the newly found K^+ affinity of Asp, Lys, LysOMe and LysOEt (Table 4.1) yields a second calibration plot as shown in Fig. 4.7, from which the K^+ affinity of Glu, GluOMe, GluOEt, Trp, Gln, His, HisOMe and Arg could be found (Fig. 4.7).

The experimental K^+ affinities of **Group 1** and **Group 2** AAFSCs and their -OMe esters so obtained are summarized in Tables 4.2 and 4.3, respectively. The experimental uncertainty (\pm S.D.) of the standard kinetic method calibration plots shown in Fig. 4.6 and 4.7 are estimated to be 1.0 and 2.0 kJ mol^{-1} , respectively. Combining the estimated uncertainty of $\pm 14 \text{ kJ mol}^{-1}$ for the reference affinity values (i.e., the experimental affinity values listed in Table 4.1 obtained by extended kinetic method measurements) used to obtain the calibration plots, we tend to assign an overall uncertainty of $\pm 15 \text{ kJ mol}^{-1}$ and $\pm 16 \text{ kJ mol}^{-1}$ for the α -amino acids and their -OMe/-OEt esters determined by the standard kinetic method ladder shown in Fig. 4.2 and 4.3, respectively.

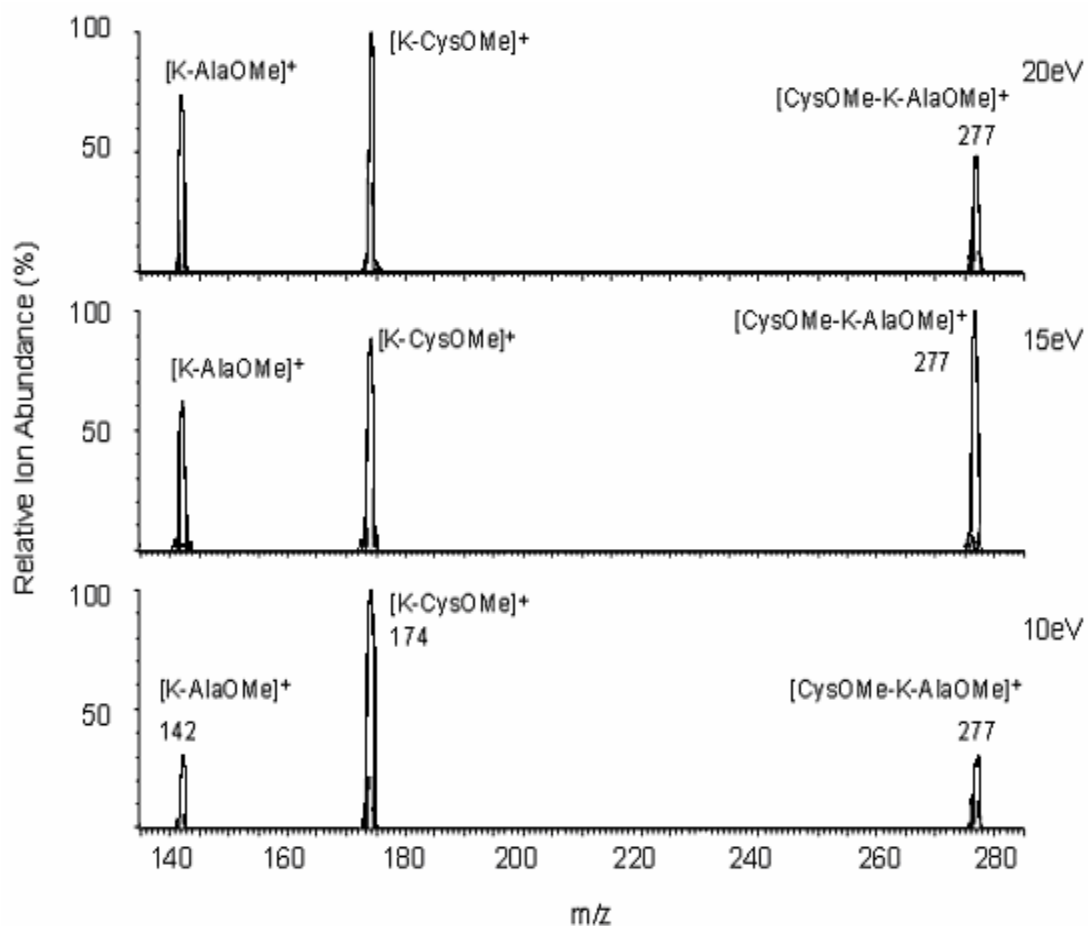


Figure 4.4 Triple quadrupole MS/MS spectra of the [CysOMe-K-AlaOMe]⁺ heterodimer using argon as collision gas at various collision energies (eV, laboratory frame). (CysOMe = Cysteine methyl ester and AlaOMe = Alanine methyl ester)

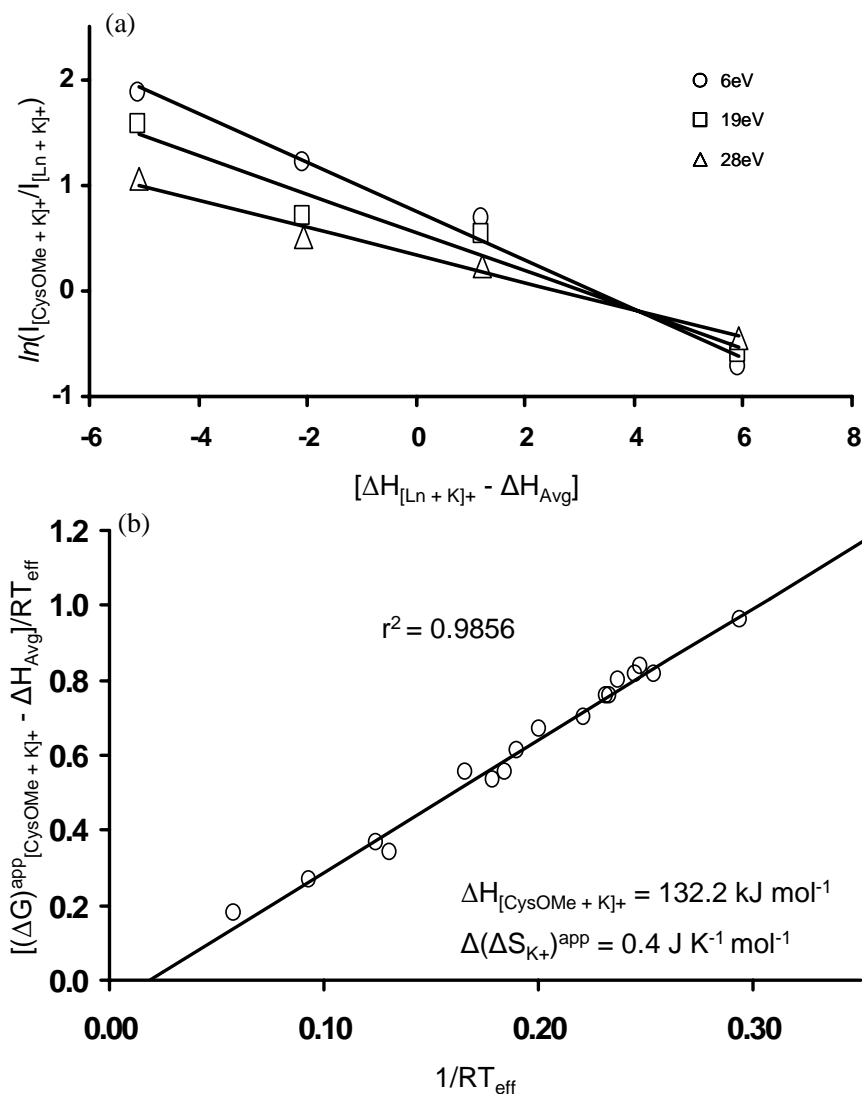


Figure 4.5 (a) Plot of $\ln(I_{[\text{Cys-OMe}+\text{K}]^+}/I_{[\text{L}_n+\text{K}]^+})$ versus $[\Delta H_{[\text{L}_n+\text{K}]^+} - \Delta H_{\text{Avg}}]$ at different collision energies, and (b) plot of $[(\Delta G)^{\text{app}}_{[\text{CysOMe} + \text{K}]^+} - \Delta H_{\text{Avg}}]/RT_{\text{eff}}$ against $1/RT_{\text{eff}}$ for the $[\text{CysOMe-K-L}_n]^+$ heterodimers. (CysOMe = cysteine methyl ester, L_n = GlyOMe, AlaOMe, ValOMe and LeuOEt); numbers are *absolute* affinities

Table 4.1 Experimental K⁺ affinities at 0 K (kJ mol⁻¹) of amino acids (**Group 1 , 2 , 3**) measured by the extended kinetic method

Amino Acid	This Work ^a		References (kJ mol ⁻¹)
	ΔH_0	$\Delta(\Delta S_{K^+})^{app}$	
Group 1 Serine (Ser)	132.8 ± 0.1 (0.1)	-0.6 ± 0.1 (0.1)	Leu (128.4), ValOMe (129.9),
Threonine (Thr)	135.6 ± 0.3 (0.5)	1.6 ± 0.5 (0.9)	LeuOMe (131.6), LeuOEt (134.6)
Serine methyl ester (SerOMe)	137.7 ± 0.2 (0.4)	-10.1 ± 0.4 (0.7)	
Threonine methyl ester (ThrOMe)	140.4 ± 0.1 (0.4)	0.62 ± 0.6 (1.7)	SerOMe (137.7), PheOMe (143.9), TyrOMe (144.3), PheOEt (145.5)
Group 2 Aspartic acid (Asp)	136.5 ± 0.3 (0.5)	2.0 ± 0.7 (1.2)	SerOMe (137.7), SerOEt (140.4),
Lysine (Lys)	144.3 ± 0.1 (0.1)	3.8 ± 0.1 (0.2)	PheOMe (143.9), TyrOMe (144.3), PheOEt (145.5)
Lysine methyl ester (LysOMe)	146.0 ± 0.1 (0.3)	3.6 ± 0.4 (0.6)	
Lysine ethyl ester (LysOEt)	148.5 ± 0.1 (0.2)	5.7 ± 0.3 (0.5)	
Aspartic Acid Methyl Ester (AspOMe)	141.0 ± 0.1 (0.1)	1.1 ± 0.1 (0.3)	SerOMe (137.7), SerOEt (140.4), PheOMe (143.9), TyrOMe (144.3), PheOEt (145.5)

	Asparagine (AsnOMe)	Methyl Ester	157.7 ± 0.9 (2.5)	3.4 ± 2.5 (7.4)	GluOMe (145.1), GluOEt (147.6), TrpOMe (155.1), HisOMe (158.2)
Group 3	Cysteine (Cys)		124.0 ± 0.1 (0.1)	4.3 ± 0.2 (0.3)	Ala (122.7), AlaOMe (126.6), Val (127.1), Leu (128.4), ValOMe (129.9), LeuOMe (131.6)
	Methionine (Met)		134.7 ± 0.1 (0.2)	3.6 ± 0.2 (0.4)	Val (127.1), Leu (128.4), ValOMe (129.9), LeuOMe (131.6), LeuOEt (134.6)
	Proline (Pro)		135.3 ± 0.1 (0.2)	-4.1 ± 0.3 (0.5)	Ser (132.8), SerOMe (137.7), SerOEt (140.4), PheOMe (143.9), TyrOMe (144.3), PheOEt (145.5)
	Methionine (MetOMe)	Methyl Ester	137.6 ± 0.5 (1.3)	6.3 ± 1.1 (3.3)	Ser (132.8), ThrOMe (140.4), SerOEt (140.4), PheOMe (143.9)
	Proline (ProOMe)	Methyl Ester	138.1 ± 1.4 (4.2)	-2.1 ± 3.2 (9.2)	AlaOMe (126.6), ValOMe(129.9), LeuOMe (131.6)
	Cysteine (CysOMe)	Methyl Ester	132.1 ± 0.1 (0.1)	0.3 ± 0.1 (0.2)	GlyOMe (123.6), AlaOMe (126.6), ValOMe(129.9), LeuOEt (134.6)

^a Determined by extended kinetic method in this work and the uncertainties are given as ±S.D. (90% confidence interval).

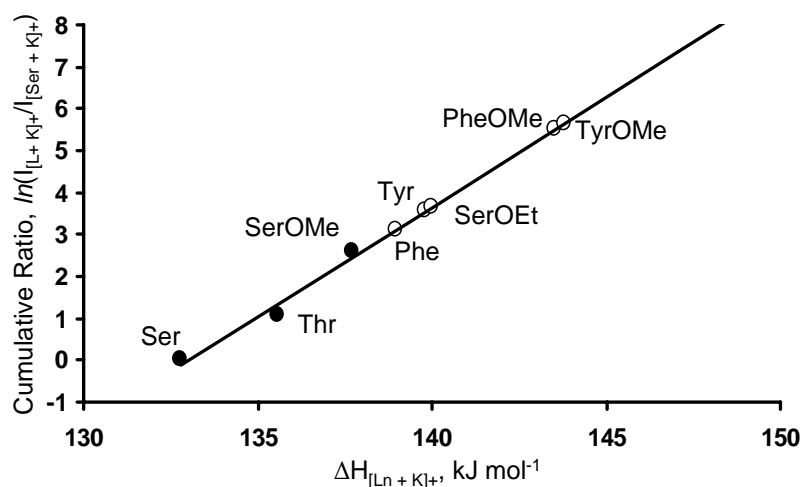


Figure 4.6 Plot of cumulative $\ln(I_{[L+K]^+}/I_{[Ser+K]^+})$ values obtained under metastable (MI) dissociation (Fig. 4.2) versus K^+ affinity values of ligands at 0 K ($R^2 = 0.97$). The $\ln(I_{[L+K]^+}/I_{[Ser+K]^+})$ values are with reference to Ser. The T_{eff} is equal to 230 K, which is calculated by Eqn. [2.5]. (Filled circles represent the reference compounds used to determine the K^+ affinity of AAFSCs (unfilled circles)

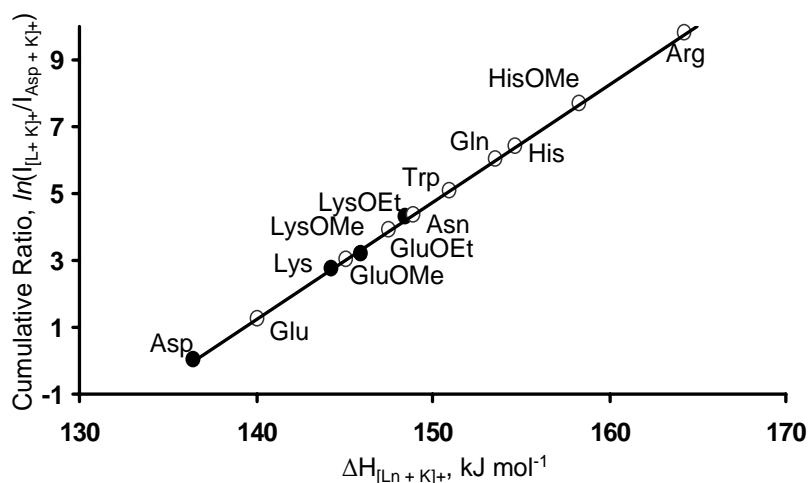


Figure 4.7 Plot of cumulative $\ln(I_{[L+K]^+}/I_{[Asp+K]^+})$ values obtained under metastable (MI) dissociation (Fig. 4.3) versus K^+ affinity values of ligands at 0 K ($R^2 = 0.99$). The $\ln(I_{[L+K]^+}/I_{[Asp+K]^+})$ values are with reference to Asp. The T_{eff} is equal to 342 K, which calculated by Eqn. [2.5]. (Filled circles represent the reference compounds used to determine the K^+ affinity of AAFSCs (unfilled circles)

Table 4.2 Experimental and theoretical K⁺ affinities at 0 K (kJ mol⁻¹) of α -amino acids

Amino acid	Potassium Cation Affinity, ΔH_0				ΔH_0 (Expt) - ΔH_0 (Theory) ^g
	Expt ^a	Theoretical ^c			
		CS1 (O=C, OH) ^d	CS2 (O=C, NH ₂ , X) ^e	ZW (COO ⁻) ^f	
Glycine (Gly)	119	117	115 (O=C, NH ₂)	105	2
Alanine (Ala)	123	123	118 (O=C, NH ₂)	116	0
Cysteine (Cys)	124 ^b	115	123 (X = S)	117	1
Valine (Val)	127	128	122 (O=C, NH ₂)	124	-1
Leucine (Leu)	128	128	121 (O=C, NH ₂)	124	0
Isoleucine (Ile)	129	129	123 (O=C, NH ₂)	126	0
Serine (Ser)	133 ^b	124	136 (X = OH)	122	-3
Methionine (Met)	135 ^b	127	143 (X = S)	140	-8
Proline (Pro)	135 ^b	130	---	143	-8
Threonine (Thr)	136 ^b	130	141 (X = OH)	122	-5
Aspartic Acid (Asp)	137 ^b	129	145 (X = O=C)	129	-8
Phenylalanine (Phe)	139	139 (O=C, π)	143 (X = π)	127	-4

Tyrosine (Tyr)	140	141 (O=C, π)	144 (X = π)	132	-5
Glutamic Acid (Glu)	140	142	142 (X = O=C)	148	-8
Lysine (Lys)	144 ^b	135	153 (X = NH ₂)	162	-18
Asparagine (Asn)	149	138	160 (X = O=C)	143	-11
Tryptophan (Trp)	151	153 (O=C, π)	152 (X = π)	135	-2
Glutamine (Gln)	154	146	159 (X = O=C)	167	-13
Histidine (His)	155	163 (O=C, N π)	162 (X = N π)	164	-9
Arginine (Arg)	163	178(O=C,NH _(side))	160 (X = NH)	188(CO⁻, NH_{2(side)})	-25

^a Experimental affinities at 0 K, $\Delta H_{0(\text{Expt})}$, measured by standard kinetic method in this work (Fig. 4.6 and 4.7).

^b Experimental affinities at 0 K, $\Delta H_{0(\text{Expt})}$, measured by extended kinetic method in this work (Table 4.1).

^c Theoretical affinities at 0 K, $\Delta H_{0(\text{Theory})}$, determined at the B3-LYP/6-311+G(3df,2p)//B3-LYP/6-31G(d) level, with ZPE corrections at B3LYP/6-31G(d) level and scaled by 0.9806. The most stable binding modes and associated K⁺ affinities are indicated by bold fonts.

^d CS1, charge-solvated (CS) conformer of K⁺-AA, with K⁺ binding bidentately to the two carboxylic oxygens.

^e CS2, charge-solvated (CS) conformer of K⁺-AA, with K⁺ binding tridentately to carbonyl oxygen, amino nitrogen and the O/N-heteroatom site (X) of the functionalized side chain.

^f ZW1, the most stable zwitterionic (ZW) conformer of K⁺-AA, with K⁺ binding bidentately to two carboxylic oxygens.

^g The difference between experimental and theoretical affinity for the most stable charge-solvated (CS) or zwitterionic form (ZW) binding mode (in **Bold**)

Table 4.3 Experimental and theoretical K⁺ affinities at 0 K (kJ mol⁻¹) of α -amino acids methyl esters

Amino acids methyl esters	Potassium Cation Affinity, ΔH_0			ΔH_0 (Expt) - ΔH_0 (Theory) ^f
	Expt. ^a	Theoretical ^c		
		CS1 ^d	CS2 ^e	
GlyOMe	124	124 (O=C, NH ₂)	78 (O=C, OMe)	0
AlaOMe	127	128 (O=C, NH ₂)	---	-1
CysOMe	132 ^b	135 (O=C, NH ₂ , S)	118 (O=C, NH ₂)	-3
ValOMe	130	131 (O=C, NH ₂)	---	-1
LeuOMe	132	133 (O=C, NH ₂)	---	-1
SerOMe	138 ^b	145 (O=C, NH ₂ , OH _(side))	126 (O=C, OH _(side))	-7
MetOMe	138 ^b	153 (O=C, NH ₂ , S)	136 (O=C, NH ₂)	-15
ProOMe	138 ^b	132 (O=C, NH ₂)	89 (NH ₂ , OMe)	-6
ThrOMe	140 ^b	150 (O=C, NH ₂ , OH _(side))	131 (O=C, OH _(side))	-10
AspOMe	141 ^b	156 (O=C, O=C, NH ₂)	139 (O=C, OH _(side))	-15
PheOMe	144	152 (O=C, NH ₂ , π)	137 (O=C, NH ₂)	-8

TyrOMe	144	154 (O=C, NH₂, π)	140 (O=C, NH ₂)	-10
GluOMe	145	151 (O=C, O=C, NH₂)	150 (O=C, OH _(side))	-11 ^f
LysOMe	146 ^b	160 (O=C, O=C, NH₂)	135 (O=C, NH ₂)	-14
AsnOMe	158 ^b	170 (O=C, O=C, NH₂)	141 (O=C, NH ₂)	-12
TrpOMe	155	166 (O=C, NH₂, π)	144 (O=C, π)	-11
GlnOMe	---	173 (O=C, O=C, NH₂)	153 (O=C, NH ₂)	---
HisOMe	158	179 (O=C, NH₂, N^π)	---	-21

^a Experimental affinities at 0 K, $\Delta H_{0(\text{Expt})}$, measured by standard kinetic method.

^b Experimental affinities at 0 K, $\Delta H_{0(\text{Expt})}$, measured by by extended kinetic method.

^c Theoretical affinities at 0 K, $\Delta H_{0(\text{Theory})}$, determined at the B3-LYP/6-311+G(3df,2p)//B3-LYP/6-31G(d) level, with ZPE corrections at B3-LYP/6-31G(d) level and scaled by 0.9806.

^d CS1, the most stable charge-solvated (CS) conformer of K⁺-AA complex

^e CS2, the second most stable charge-solvated (CS) conformer of K⁺-AA complex.

^f The difference between experimental affinities and theoretical affinities of the most stable conformer in charge-solvated form (CS1).

4.2.2 Theoretical K^+ Affinities and Binding Modes

In addition to the experimental measurements, we have carried out theoretical evaluation of K^+ affinities of the α -amino acids and their methyl esters using the density functional theory B3-LYP/6-311+G(3df,2p)//B3LYP/6-31G(d) protocol. Previous studies by Prof. Tsang's research group have shown that this protocol yields absolute K^+ affinities for 65 model organic ligands in excellent agreement with experimental affinities (mean absolute deviation of 4.5 kJ mol⁻¹). [Lau et al., 2003] Thus, the theoretical values could provide further confidence on the experimental values if such consistency between theoretical and experimental K^+ affinities could be extended to the larger amino acid molecules with functionalized side chains. Furthermore, the theoretical calculations could reveal the most stable K^+ binding mode, and the relative stabilities of the different CS and ZW modes

For the evaluation of K^+ affinities, the most stable conformations (geometries) of the free acids and its methyl esters were first found by optimization at the HF/6-31G(d) level, confirmed to be a minimum with frequency analysis, and refined at the B3LYP/6-31G(d). In general, the most stable conformations correspond to molecular structures in which the stabilizing intra-molecular hydrogen bonding patterns are maximized, and whenever available, the conformations that are found in the present work are in agreement with those reported in the literature.

For the K^+ bound aliphatic amino acid /methyl ester complexes, the geometries of two CS complexes and two ZW complexes as depicted in Fig. 4.8 were explored and optimized. **CS1** is a charge-solvated (CS) structure with K^+ bidentately binding to carbonyl oxygen (O=C) and hydroxyl oxygen (OH) or electron-donating atom such as O/N/S/ π sites of functionalized side chain *X*. **CS2** is another charge-solvated (CS) structure with K^+

tridentately binding to carbonyl oxygen (O=C), amino nitrogen (NH₂) and O/N/S/π sites of functionalized side chain *X*. **CS1** is reported to be the most stable binding mode of K⁺-Gly/Ala/Val/Leu/Ile,[Wong, 2004] while **CS2** is reported to be the most stable binding mode for K⁺-Phe/Tyr/Trp. [Dunbar, 2000; Siu et al., 2001b; Ruan and Rodgers, 2004] **ZW1** is a zwitterionic structure (ZW) in which K⁺ is bound to two carboxylate oxygen atoms (COO⁻) with the carboxylic proton intra-molecularly transferred to the amino nitrogen (-NH₂). This ZW binding mode is expected to be favored for basic amino acids, allowing the amino nitrogen to readily accept the proton from the carboxylate hydroxyl group (-OH) to become NH₃⁺. Alternatively, the carboxylic proton could be transfer to the O/N-heteroatom basic site in the side chain (*X*) instead of to the N-terminal amino nitrogen, yielding the **ZW1'** binding mode as suggested by William and his co-workers for the K⁺-Arg complex. [Jockusch et al., 1999]

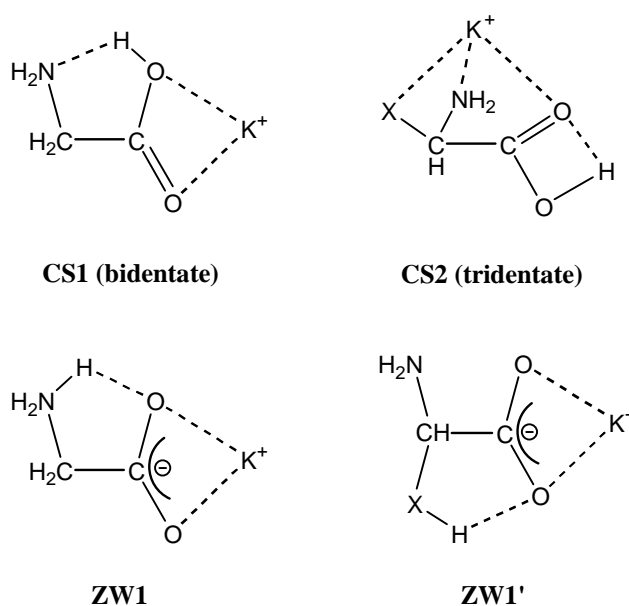


Figure 4.8 Schematic representation of charge-solvated (CS) and zwitterionic (ZW) binding modes of K⁺ bound α -amino acids.

Together with the experimental values, the theoretical K⁺ affinities for the CS and ZW binding modes of the twenty α -amino acids are summarized in Table 4.2, while the CS1

and CS₂ affinity values for the methyl esters are listed in Table 4.3. The geometries of the most stable CS and ZW K⁺ bound complexes are shown in Fig. 4.9 - 4.13. The theoretical results for the aliphatic amino acids were obtained in previous studies,[Wong, 2004] but they are included and presented here for the sake of completeness. In general, an assigned uncertainty of ± 12 kJ mol⁻¹ is acceptable in the theoretical evaluation of potassium metal cation affinities.[Siu et al. 2001a; Lau et al., 2003; Wong, 2004] The reliability and inter-consistency of the experimental and theoretical values obtained in this work is discussed further in the following section.

4.2.3 Comparison between Experimental, Theoretical and Literature K⁺ Affinity Values

There were only a few experimental K⁺ affinities, i.e., that of Gly, Phe, Tyr and Trp, have been reported in the literature; they are listed in Table 4.4 for comparison with the experimental values obtained in this work. Our experimental value for K⁺-Gly (at 119 kJ mol⁻¹) is in very good agreement with literature values of 125 kJ mol⁻¹ [Klassen et al., 1996] and 121 kJ mol⁻¹ [Moision and Armentrout, 2002] obtained by the threshold-CID technique; the difference of 6 or 3 kJ mol⁻¹ is significantly smaller than the claimed experimental uncertainty of ± 15 kJ mol⁻¹ in this work. For Phe, Tyr and Trp, the difference between the literature threshold-CID and our kinetic method values increases to 11 – 15 kJ mol⁻¹, but remains within the higher end of our claimed uncertainty of ± 15 kJ mol⁻¹. This relatively large difference is likely to be due to the combined errors arising from the threshold-CID and kinetic method measurements as the threshold-CID values were found to be systematically higher, while the kinetic method values are systematically lower than the theoretical values (Table 4.3 and 4.4). For the standard kinetic method measurements, greater error is expected with increasing affinity values usually associated

with larger amino acids arising from (i) increasing uncertainty (\pm S.D.) in the cumulative log intensity ratios towards the higher affinity end of the relative affinity ladder (Fig. 4.2 and 4.3), and (ii) increasing propagation of errors as more of the calibration (reference) affinity values used were obtained by separate extended kinetic method measurements. For the threshold-CID measurements, a likely source of error is derived from the significant correction term for the chemical shift, which is estimated theoretically based on the RRKM theory of unimolecular kinetics. Despite the difference between the two set of experimental data, the experimental order of K^+ affinity: Phe < Tyr < Trp is found to be the same for the threshold-CID and kinetic method measurements. Given the many approximations assumed in the kinetic method, we tend to conclude that the set of experimental affinity values obtained in the recent study is acceptable, and is reliable within the claimed limits of uncertainty of $\pm 15 \text{ kJ mol}^{-1}$.

As shown in Table 4.2 and 4.3, the experimental K^+ affinities ($\Delta H_{0(\text{Expt})}$) are in very good agreement with theoretical values at 0K ($\Delta H_{0(\text{Theory})}$), with a mean absolute deviation (MAD) of 6.6 kJ/mol for 20 α -amino acids and 8.1 kJ mol^{-1} for the 18 amino acids methyl esters. Except for the case of glycine with a positive deviation of 2 kJ mol^{-1} , all the experimental values are systematically lower than the theoretical values, suggesting that the experimentally values are likely to have under-estimated, and the theoretical values over-estimated the actual K^+ affinities. The difference between experimental and theoretical values is noticeably very small for the aliphatic amino acids and their methyl esters (with MAD of 0.6 kJ mol^{-1} ($n=5$) and 0.6 kJ mol^{-1} ($n=4$), respectively), but increases as the size of the amino acid increases. This general trend of increasing discrepancies with larger affinity values associated with larger amino acids is in line with the greater experimental errors expected in the kinetic method measurements. Furthermore, a recent report also suggested that greater errors are found in the theoretical proton affinities

of amino acids calculated by a similar DFT protocol.[Dinadayalane et al., 2006] Thus, the B3-LYP protocol is likely to yield greater uncertainties in the calculated K^+ affinities, and contributes, in part, to the increasing discrepancies between experimental and theoretical values as the amino acid molecules become larger.

Best agreement between experimental and theoretical binding affinities is obtained when the affinities for the most stable K^+ modes are adopted in the comparison. This suggests that experimentally, the K^+ bound amino acid and methyl ester complexes are found predominantly in their most stable CS or ZW forms under the experimental conditions of the present study. However, the occurrence of other low lying K^+ binding modes with comparable but less binding affinities cannot be excluded. While the methyl esters could only bind to K^+ in the CS form, the most stable K^+ form for free amino acids could be either in the CS or ZW forms. However, relatively large discrepancies of 18, 25 and 21 kJ mol^{-1} are found for the exceptional cases of Lys, Arg and HisOMe. We have conducted exhaustive searches for the most stable conformation of the free acid and their K^+ bound complexes in the theoretical computation. The discrepancy of 21 kJ mol^{-1} found for HisOMe, which shows the second highest K^+ affinity measured, is likely to be due to the combined errors in the experimental measurement ($\pm 15 \text{ kJ mol}^{-1}$) and theoretical calculations (at an estimated minimum of $\pm 6 \text{ kJ mol}^{-1}$ for the case of HisOMe). For the case of Lys and Arg, another plausible contributory cause is that their K^+ bound complexes might occur not only in their most stable ZW forms, but a significant portion may also be found in their less stable CS forms. A mixture of ZW and CS complexes would lead to lower experimental K^+ affinity values, leading to the greater than expected discrepancy found between the experimental and theoretical values. Further discussion on the relative stabilities of the ZW and CS forms of Lys and Arg are to be presented in the next section.

Table 4.4 Literature values of experimental K⁺ affinities at 0 K / 298 K (kJ/mol) of selected amino acids

Amino Acid	Potassium Cation Affinity at 0K / 298K (ΔH_0 / ΔH_{298})		
	Literature	Our Work ^a	$\Delta H_{(\text{Literature})} - \Delta H_{(\text{Our work})}$ ^b
Phenylalanine (Phe)	150 ± 6 ^c	139	11
Tyrosine (Tyr)	155 ± 9 ^c	140	15
Tryptophan (Trp)	165 ± 6 ^c	151	14
Glycine (Gly)	125 ± 6 ^d , 121 ± 4 ^e	119	6, 3

^a Experimental affinities at 0 K, $\Delta H_{0(\text{Expt})}$, measured by the standard kinetic method in this work.

^b The difference of experimental affinities between literature values and reported values in the present study, in kJ mol^{-1} .

^c Experimental affinities at 0 K, $\Delta H_{0(\text{Expt})}$, measured by the threshold-CID method [Ruan and Rodgers., 2004].

^d Experimental affinity at at 298 K, $\Delta H_{298(\text{Expt})}$, measured by the threshold-CID method [Klassen et al., 1996]. The difference between ΔH_{298} and ΔH_0 is theoretically estimated to be less than 1 kJ mol^{-1} .

^e Experimental affinity at 0 K, $\Delta H_{0(\text{Expt})}$, measured by the threshold-CID method [Moision and Armentrout, 2002].

4.2.4 Potassium Cation Binding to α -Amino Acids: Relative Stabilities of Charge-Solvated versus Zwitterionic Binding Modes

K⁺ - Aliphatic amino acids (Gly/Ala/Val/Leu/Ile) Complexes A brief review of the relative stabilities of the CS versus ZW binding modes of aliphatic amino acids (with no O/N-heteroatom functional group in their side chains, refer to Scheme 4.1) is included here because they serve as good references for understanding the behaviour of amino acids with functional groups in their side chains to be discussed later. The most stable binding mode of K⁺ with aliphatic amino acids (glycine (Gly)/ alanine (Ala) / valine (Val) /leucine (Leu) / iso-leucine (Ile)) were previously reported by our group [Tsang, 2003; Wong, 2004], with K⁺ bidentately bound to the carbonyl oxygen (O=C) and hydroxyl oxygen (OH) in the **CS1** mode (as shown in Table 4.2 and Fig. 4.9). It is the relatively strong ‘local’ ion-dipole interactions between K⁺ and the carbonyl oxygen (O=C) and hydroxyl oxygen (-OH), together with the strong hydrogen bonding between the carboxylic -OH and the N-terminal -NH₂ group that accounts for the extra stability in **CS1** complexes.

The **CS2** binding mode, with K⁺ bidentately bound to the carbonyl oxygen (O=C) and N-terminal amino nitrogen (-NH₂), is marginally less stable by 2 – 6 kJ mol⁻¹ (Table 4.2). It should be noted that the **CS2** mode becomes the most stable binding mode for Li⁺ and Na⁺, [Jensen, 1992; Hoyau and Ohanessian, 1998; Moision and Armentrout, 2004] indicating that ionic size does have an effect, though minor, on the relative stability of these two CS binding modes.

The zwitterionic K⁺ binding mode, **ZW1**, is found to be the least stable when compared to the **CS1** and **CS2** binding mode for K⁺-Gly, but its binding affinity is close to that of the **CS2** bind mode for Ala, Val, Leu and Ile (within 2-3 kJ mol⁻¹). Detailed analysis reveals that even though the positively charged K⁺ interacts more strongly with the negatively

charged carboxylate oxygens in the **ZW1** mode, this stabilizing effect is offset by the greater de-stabilizing ‘deformation energy’ required to transform the neutral ligand to the structurally more strained configuration in the K^+ bound complexed form.[Wong et al., 2004] The result is that the zwitterionic **ZW1** is *always* less stable than the charge-solvated **CS1** K^+ binding mode.

The study on K^+ -Gly/Ala/Val/Leu/Ile complexes reveals that it is the interplay of three major factors: (i) the stabilizing (attractive) ion-dipole and ion-induced dipole interaction between K^+ and the O/N-heteroatom binding sites (functional groups), (ii) stabilizing hydrogen bonding in the K^+ bound complex, and (iii) the magnitude of the ‘deformation energy’ that determine the relative stabilities of the CS versus ZW K^+ binding modes of aliphatic amino acids. As will be revealed in the following sections, these factors are equally applicable to the binding of K^+ to amino acids with functionalized side chains.

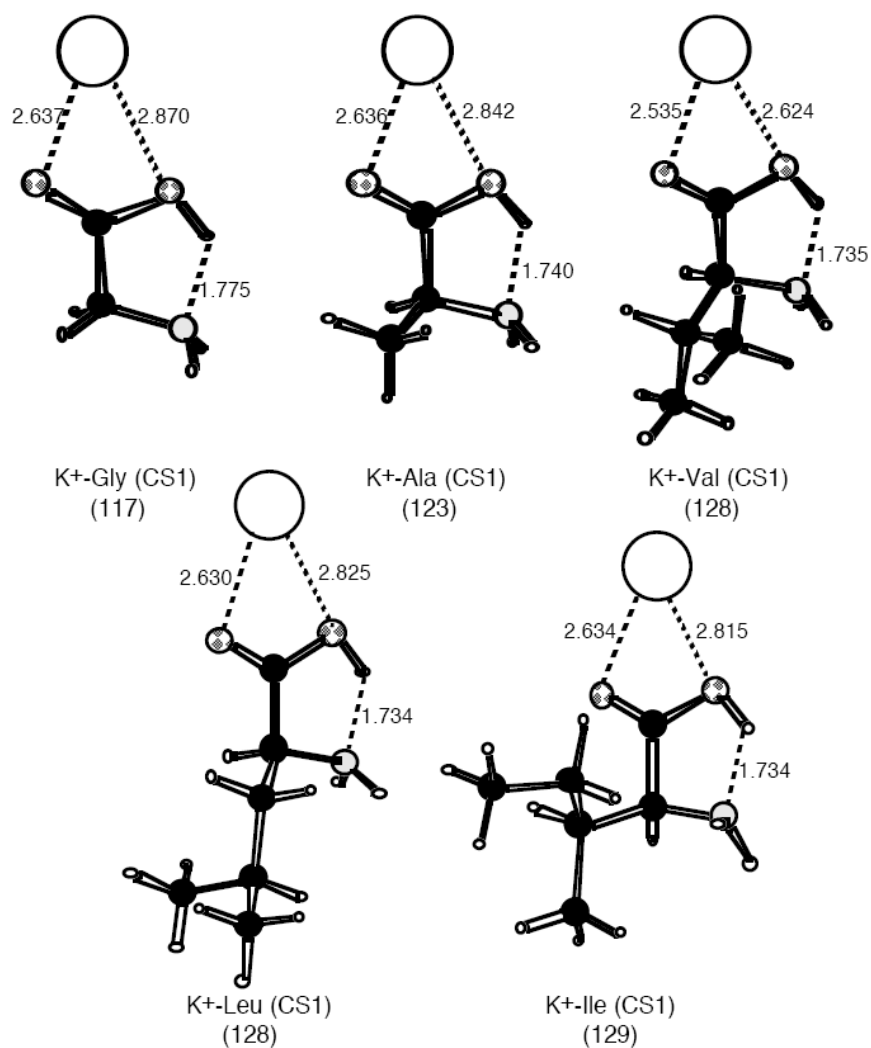


Figure 4.9 The most stable K⁺ binding mode (CS1) of aliphatic amino acids (Gly/Ala/Val/Leu/Ile), optimized at the B3-LYP/6-31G(D) level. The K⁺ affinities at 0 K in kJ mol⁻¹ are shown in parenthesis. All the bond lengths are shown in Å

K⁺ -Amino acids with -SH/ -SCH₃/-OH functionalized side chains (Ser/Thr/Cys/Met)

Complexes For serine (Ser, with -CH₂OH as side chain), threonine (Thr, with -CH(CH₃)OH as side chain), cysteine (Cys, with -CH₂SH as side chain) and methionine (Met, with -CH₂CH₂SCH₃ as side chain), K⁺ tridentate binding becomes possible due to the availability of an extra -SH/ -SCH₃/-OH binding site in the side chain. Previous

study have shown that for Na^+ , tridentate CS binding is the most stable binding mode for Ser and Cys, but the binding with Thr and Met have not been reported. [Hoyau et al., 1999; Kish et al., 2003]

Our theoretical results also indicate that the tridentate **CS2** binding mode ($\text{O}=\text{C}$, NH_2 , $\text{X}=\text{side chain functional group} = \text{OH}/\text{SH}/\text{SCH}_3$) is indeed the most stable K^+ binding mode for Ser, Thr, Cys, and Met; the detailed **CS2** binding geometries of the K^+ -Ser/Thr/Cys/Met complexes are shown in Fig. 4.10. The $\text{K}^+\dots\text{O}=\text{C}$ ($\sim 2.8 \text{ \AA}$) and $\text{K}^+\dots\text{NH}_2$ ($\sim 2.6 \text{ \AA}$) binding distances in the tridentate **CS2** binding mode of the K^+ -Ser/Thr/Cys/Met complexes are found to be very similar to that of the bidentate **CS2** binding mode of the K^+ -Ala/Val/Leu/Ile complexes [Wong, 2004], but the K^+ affinities of Ser/Thr/Met are greater than that of the aliphatic amino acids by $4 - 7 \text{ kJ mol}^{-1}$. The enhanced K^+ affinities could be attributed to the 'extra' bonding between K^+ and the $-\text{OH}$ ($\sim 2.7 \text{ \AA}$) for the K^+ -Ser/Thr complexes and between K^+ and $-\text{SCH}_3$ ($\sim 3.2 \text{ \AA}$) for the K^+ -Met complex, which more than compensates the significant deformation energy ($\sim 5-16 \text{ kJ mol}^{-1}$) involved in the tridentate binding mode. As threonine is a larger molecule than serine, it is expected to show greater K^+ affinity (experimentally and theoretically by 3 and 5 kJ mol^{-1} , respectively) due to its greater molecular polarizability (i.e., the ion-induced dipole interaction). By the same rationale, the experimental/theoretical K^+ -Met affinity is greater than K^+ -Cys by 9/10 kJ mol^{-1} . The significant increase in K^+ -Met affinity could also be partly attributed to its longer and flexible $-\text{CH}_2\text{CH}_2\text{SCH}_3$ side chain, leading to less deformation energy in K^+ -Met complex than in the K^+ -Cys complexed. As shown in Fig. 4.10, the $\text{K}^+\dots\text{OH}$ bonding distance ($\sim 2.7 \text{ \AA}$) is significantly shorter than the $\text{K}^+\dots\text{SCH}_3$ bonding distance ($\sim 3.2 \text{ \AA}$), indicating that the interaction of K^+ with the sulphur heteroatom site is much weaker than with the oxygen site. This could explain why the experimental K^+ -Cys affinity is significantly lower (by 9 kJ mol^{-1}) than the K^+ -Ser affinity,

and its theoretical tridentate **CS2** affinity (123 kJ mol^{-1} , Table 4.2) is comparable to that of the bidentate **CS2** affinity of K^+ -Val/Leu/Ile complexes.

Similarly, the $\text{K}^+ \dots \text{O}=\text{C}$ ($\sim 2.8 \text{ \AA}$) and $\text{K}^+ \dots \text{OH}$ ($\sim 2.6 \text{ \AA}$) bonding distances in the bidentate **CS1** binding mode of the K^+ -Ser/Thr/Cys/Met complexes are found to be very similar to that of the bidentate **CS1** binding mode of the K^+ -Ala/Val/Leu/Ile complexes (Fig. 4.9). For this reason, the bidentate **CS1** binding mode is found to be always $8 - 16 \text{ kJ mol}^{-1}$ less stable than the tridentate **CS2** binding mode. Similarly, the bidentately bound **ZW1** K^+ -Ser/Thr/Cys/Met complexes are found to be less stable than the corresponding tridentate **CS2** complexes by $3-19 \text{ kJ mol}^{-1}$.

K⁺ - Aromatic Amino acids (Phe/Tyr/Trp) Complexes Potassium cation binding to phenylalanine (Phe, with phenyl ring, $-\text{C}_6\text{H}_5$, as side chain), tyrosine (Tyr, with phenol, $-\text{C}_6\text{H}_4\text{OH}$, as side chain) and tryptophan (Trp, with indole as side chain) have been more extensively investigated because of their relevance to cation- π interactions in biological systems.[Dunbar,2000; Siu et al. 2001b, 2004; Ruan and Rodgers, 2004] In line with previously reported findings, we also found that at the B3-LYP/6-311+G(3df,2p)//B3LYP/6-31G(d) level of theory, the **CS2** binding mode, with K^+ tridentately bound to the carbonyl oxygen ($\text{O}=\text{C}$), amino nitrogen (NH_2), and the aromatic- π face of benzene/phenol in the side chain of Phe/Tyr, is the most stable binding

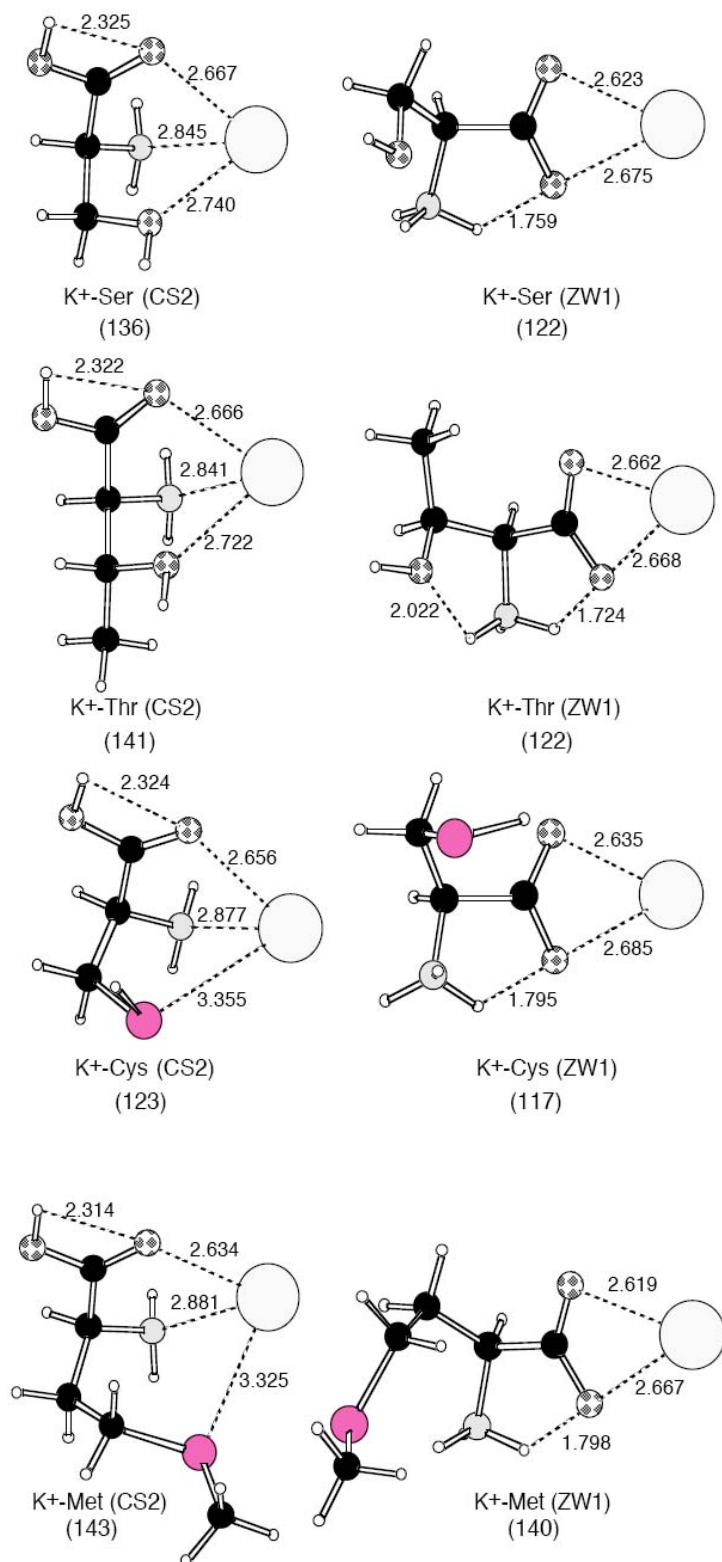


Figure 4.10 The most stable CS and ZW K^+ binding modes of Ser/Thr/Cys/Met, optimized at the B3-LYP/6-31G(D) level. The K^+ affinities at 0 K in kJ mol⁻¹ are shown in parenthesis. All the bond lengths are shown in Å

mode for the K^+ -Phe/Tyr complex. As shown in Fig. 4.11, the K^+aromatic- π bonding distance ($\sim 3 \text{ \AA}$) is comparable to that of the K^+O=C and K^+NH₂ ($\sim 2.6 - 2.8 \text{ \AA}$) bonding distances, indicating that K^+ - π interaction is strong and competitive with the other modes of non-covalent binding interaction.

For the K^+ -Trp complex, the bidentate **CS1** binding mode, with K^+ bound to the carbonyl oxygen (O=C) and the aromatic- π face of indole (the K^+ is located more on top of the phenyl ring), is numerically 1 kJ mol^{-1} more stable than the tridentate **CS2** mode (Fig. 4.11 and Table 4.2). As molecular modeling cannot be accurate down to this level of small differences, the bidentate **CS1** and tridentate **CS2** binding modes can be regarded to display very similar stabilities. Compared with the K^+ -Phe/Tyr complexes, the enhanced stability of **CS1** the binding mode of K^+ -Trp can be attributed to stronger cation- π interaction with the extended π -surface of the indole ring of tryptophan, and lesser deformation energy in the bidentate binding mode. Previous studies also showed that the **CS1** mode is the most stable binding mode for on K^+ -Trp, [Dunbar, 2000; Ruan and Rodgers, 2004] though a slightly different binding geometry (K^+ is sitting on top of and between the phenyl and indole ring) and lower affinity (by $\sim 3 \text{ kJ mol}^{-1}$) for the **CS2** binding mode was reported by Dunbar. In the zwitterionic binding mode (**ZW1**) of K^+ -Phe/Tyr/Trp complexes, K^+ is bound to the two carboxylate oxygens (COO⁻) with the carboxylic proton transferred to the amino nitrogen ($-\text{NH}_2$) (Fig. 4.11); the **ZW1** conformations are such that it involve minimal structural deformation from the free (un-complexed) forms of Phe, Tyr, and Trp. Furthermore, the **ZW1** structures can be viewed as having two linearly aligned local dipoles with the + - + - charge distribution pattern to maximize ion-dipole interaction: starting from K^+ (+), then onto the carboxylate COO⁻ group (-) and the protonated amino NH₃⁺ group (+), and finally ends at the π face of benzene/phenol/indole of Phe/Tyr/Trp (-). The result is a highly stabilizing zwitterionic

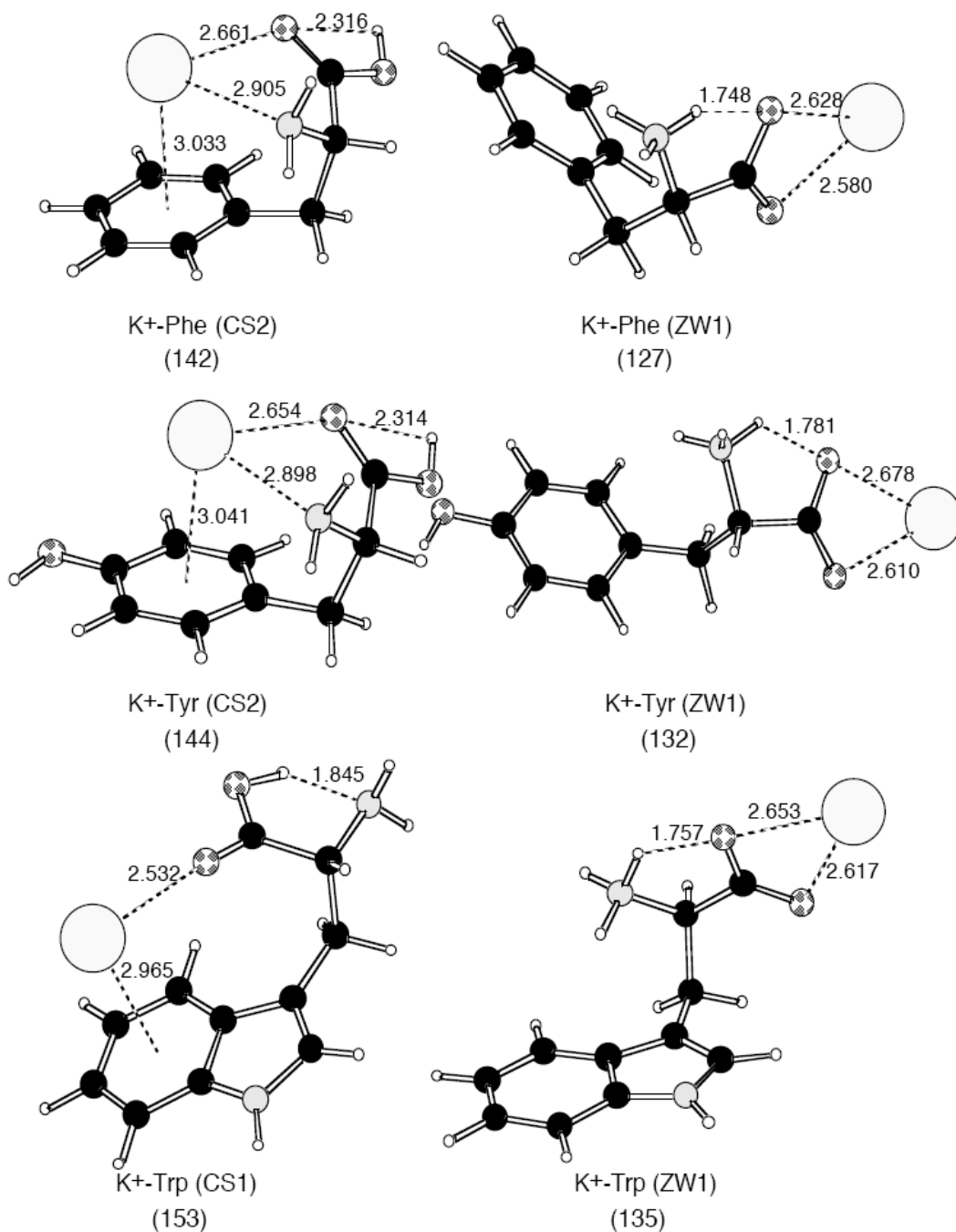
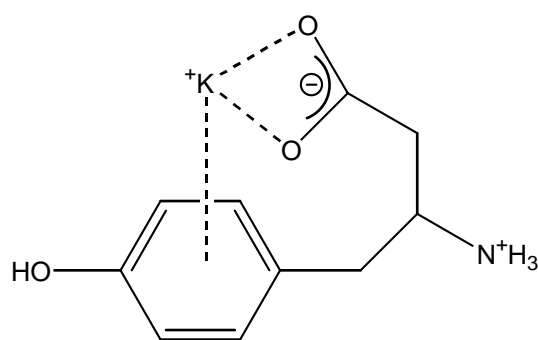


Figure 4.11 The most stable CS and ZW K⁺ binding modes of Phe/Tyr/Trp, optimized at the B3-LYP/6-31G(D) level. The K⁺ affinities at 0 K in kJ mol⁻¹ are shown in parenthesis. All the bond lengths are shown in Å

structure, as indicated by a short $K^+ \dots ^-OOC$ binding distance of $\sim 2.6 \text{ \AA}$ only. On the other hand, the **ZW1** structure has to bear the destabilization energy arising from the ‘charge-separation’ effect, i.e., the energy cost of maintaining a positive and negative charge apart at two opposite ends of a molecular structure. The overall result is that the **ZW1** structure is still less stable than the charge-solvated tridentate **CS2** structure by 12-18 kJ mol^{-1} , indicating that the higher K^+ co-ordination number remains the determining factor affecting the stability of K^+ -Phe/Tyr/Trp complexes. Although the detailed **ZW1** conformation of the K^+ -Phe complex was reported previously, [Siu et al., 2004] the **ZW1** conformations for the K^+ -Tyr/Trp complexes found in the present study have not been reported previously. Instead, Dunbar found an alternative, less stable ZW structure for K^+ -Phe/Tyr/Trp in which the K^+ is bound to the two carboxylate oxygens and located directly above the phenyl ring as shown in Figure 4.11., which are $\sim 21\text{-}28 \text{ kJ mol}^{-1}$ less stable than the **CS2** binding mode. [Dunbar, 2000]



Scheme 4.2 Schematic representation of zwitterionic (ZW) binding mode of K^+ and Tyr previously reported [Dunbar, 2000]

K⁺-Amino acids with carboxylic acid and amide functionalized side chains

(Asp/Asn/Glu/Gln) Complexes

The K⁺ bound complexes of aspartic acid (Asp, with –COOH in its side chain), glutamic acid (Glu, with –CH₂COOH in its side chain), asparagin(Asn, with –CONH₂ in its side chain) and glutamine (Gln, with –CH₂CONH₂ in its side chain) have not been reported previously. They are found to have similar CS and ZW binding modes and are grouped together in this section for convenience of discussion. In terms of structural difference, Glu/Gln contains one more –CH₂- unit than Asp/Glu, so that their backbone carbonyl group (O=C) is farther away from the carboxylic/amide carbonyl binding site (C=O_(side)) in the side chain. This structural difference is found to be the determining factor affecting the relative stabilities of the CS and ZW K⁺ binding modes. Theoretical results show that just like the case of aromatic amino acids, the charge-solvated tridentate structure **CS2** is the most stable K⁺ binding mode for Asn/Asp; however, to our surprise, the zwitterionic structure **ZW1** becomes the most stable K⁺ binding mode for the Gln/Glu. The detailed **CS2** and **ZW1** binding geometries of the K⁺-Asn/Gln/Asp/Glu complexes are shown in Fig. 4.12.

In the **CS2** binding mode of K⁺-Asn/Asp, K⁺ is tridentately bound to the backbone carbonyl oxygen (O=C), amino nitrogen (NH₂) and carboxylate/amide carbonyl oxygen (C=O_(side)) of the side chain (Fig. 4.12). Although K⁺-Asn and K⁺-Asp complexes have very similar CS2 binding geometries, K⁺-Asn is found to have a noticeably larger K⁺ binding affinity (~16 kJ mole⁻¹) than K⁺-Asp. In this regard, we note that the K⁺ bonding distances to the backbone carbonyl oxygen (O=C at 2.6 - 2.7 Å) and amino nitrogen (NH₂ at 2.9 Å) are more or less the same for both K⁺-Asn and K⁺-Asp complexes, but the K⁺ bonding distance to the amide carbonyl oxygen in the side chain of K⁺-Asn is noticeably shorter by 0.1 Å than that of K⁺-Asp. This is in line with our previous finding that for K⁺ binding to model di-peptide glycyl-glycine (GlyGly), local K⁺ binding

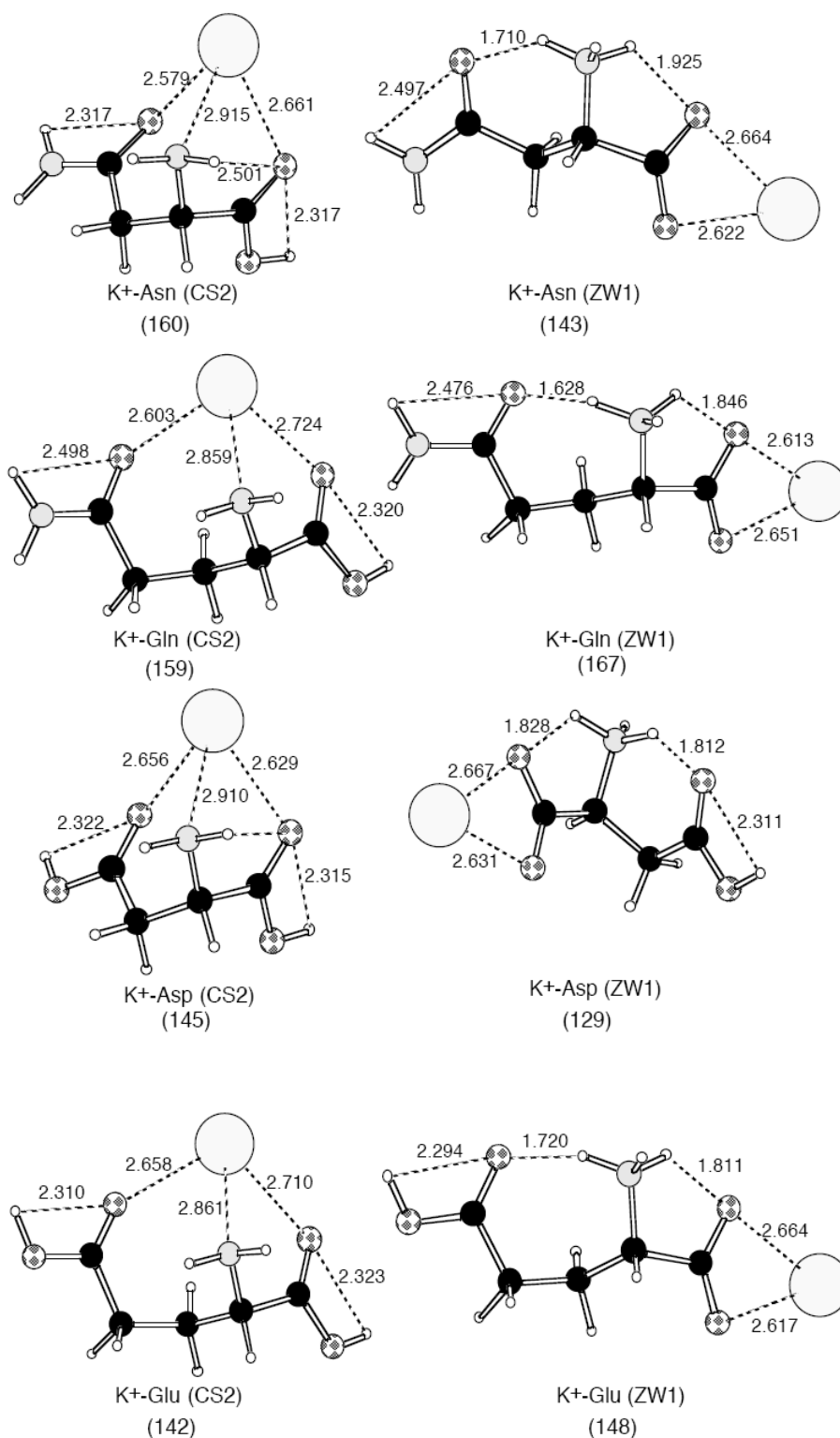


Figure 4.12 The most stable CS and ZW K⁺ binding modes of Asn/Gln/Asp/Glu, optimized at the B3-LYP/6-31G(D) level. The K⁺ affinities at 0 K in kJ mol⁻¹ are shown in parenthesis. All the bond lengths are shown in Å

with the amide carbonyl oxygen (O=C-NH) is significantly stronger than K⁺ binding to the carboxylate oxygen (O=C-OH).[Wong, 2004] Hence, it appears likely that the same rationale could be applied here to explain why K⁺-Asn displays significantly larger binding affinity (~16 kJ mole⁻¹) than K⁺-Asp.

As shown in Table 4.2, the bidentate **CS1** binding mode are less stable than the tridentate **CS2** mode by 13 – 22 kJ mole⁻¹ for the K⁺-Asp/Asn/Gln complexes, but is more or less the same affinity (at 142 kJ mole⁻¹) for the K⁺-Glu complex. It is likely that a more favorable hydrogen bonding pattern and lesser deformation energy are found for the **CS1** mode of K⁺-Glu, which might reduce the energy difference between the **CS1** and **CS2** binding modes.

As shown in Fig. 4.12, the **ZW1** binding geometries of the K⁺-Asn/Gln/Asp/Glu complexes are similar to each other, with K⁺ bound to the two carboxylate oxygen atoms (COO⁻) and the carboxylic proton attached to the amino nitrogen (-NH₂), which are linked by a ‘daisy-chain’ of hydrogen bonding network.

In particular, a six-membered ring and seven-membered ring structure are formed by hydrogen bonding between the N-terminal amino hydrogen and the amide/carboxylate carbonyl oxygen of the K⁺-Asn/Asp and K⁺-Gln/Glu complexes, respectively. The more flexible 7-membered ring allows a tighter hydrogen bond (shorter by 0.1 Å) to be formed between the N-terminal amino hydrogen and the amide/carboxylate carbonyl oxygen of the K⁺-Asn/Asp, leading to a more stabilizing network of hydrogen bonding pattern than in the K⁺-Gln/Glu complexes (Fig. 4.12). The result is that zwitterionic **ZW1** becomes the most stable binding mode for the K⁺-Gln/Glu complexes, with K⁺ affinity 8/6 kJ mole⁻¹ higher than that of the charge-solvated tridentate **CS2** binding mode. The pronounced effect of a ‘daisy-chain’ of hydrogen bonding network is also noted in the proton and K⁺

affinities of polyglycines [Zhang et al., 1993] and aliphatic amino acids [Wong, 2004], respectively. The case of K^+ -Gln/Glu complexes demonstrates that the presence of an additional methylene ($-CH_2-$) unit in the side chain of an α -amino acid could have a significant impact on the relative stabilities of the **CS** versus **ZW** K^+ binding modes.

K^+ - Basic Amino acids (Pro/Lys/His/Arg) Complexes Proline (Pro, with a cyclic secondary amine $-NH-$ site), lysine (Lys, with $-(CH_2)_4NH_2$ side chain), histidine (His, with an imidazole side chain) and arginine (Arg, with a guanidine, $-(CH_2)_3NHC(NH)NH_2$ side chain) are the four most basic α -amino acids, with proton affinities greater than 929 kJ mole^{-1} [Harrison, 1997; Hunter and Lias, 1998]. Previous studies have suggested that the formation of metal cationized **ZW** structures is favored for basic amino acids with high proton affinities (basicity).[Jockusch et al., 1999; Wyttenbach et al., 2000] Indeed, our theoretical results indicate that all the four K^+ -Pro/Lys/His/Arg complexes are zwitterionic in their most stable K^+ binding structures. The detailed **ZW1** binding geometries of the K^+ -Pro/Lys/His/Arg complexes are shown in Fig. 4.13.

In agreement with the recent findings of Russo and his co-workers,[Marino et al., 2003] the **ZW1** structure of K^+ -Pro is more stable than its bidentate **CS1** structure by 13 kJ mole^{-1} (Table 4.2). The good agreement between our experimental and theoretical values K^+ affinities (within 8 kJ mol^{-1}), reported for the first time, provide strong experimental evidence that the K^+ -Pro complex is likely to exist predominantly in the **ZW** form in the gas phase.

His and Lys are the second and third most basic α -amino acid, respectively. The theoretical alkali cation binding modes of these two amino acids have not been previously reported. Our theoretical result shows that the **ZW1** is the most stable binding mode for the K^+ -His/Lys complexes, where K^+ is bound to two carboxylate oxygen atoms (COO^-)

with the carboxylic proton attached to the amino nitrogen ($-\text{NH}_2$). However, the difference in K^+ affinities between the **ZW1** and tridentate **CS2** of K^+ -His is 2 kJ mol^{-1} only, which is noticeably smaller than that of Lys ($\sim 9 \text{ kJ mole}^{-1}$), indicating that the **ZW1** structure of K^+ -Lys complex is much more stable than its **CS2** structure when comparing with K^+ -His complex. Again, this difference can be explained in terms of the intra-molecular hydrogen bonding (interaction) formed in the two different **ZW1** complexes. In the **ZW1** form of K^+ -His, a six-membered ring linked by a hydrogen bond between the proton of the amino group ($-\text{NH}_3^+$) and the nitrogen of the imidazole ring (N^π) is formed, with an intra-molecular hydrogen bonding distance of 1.7 \AA which could be constrained by the rigidity of the imidazole ring. On the other hand, an eight-membered ring was formed between the proton of the N-terminal amino group ($-\text{NH}_3^+$) and the nitrogen of the amino nitrogen ($\text{NH}_{2(\text{side})}$) in the side chain of the **ZW1** of K^+ -Lys. Due to the greater flexibility of the eight-membered ring, a relatively shorter intra-molecular hydrogen bonding ($\sim 1.6 \text{ \AA}$) was found. As a result, the **ZW1** structure of the K^+ -Lys complex is much more stable than its **CS2** structure when compared with the K^+ -His.

Arg is the most basic α -amino acid which has a proton affinity of $1,024 \text{ kJ mole}^{-1}$ [Harrison, 1997; Hunter and Lias, 1998]. It is also the largest α -amino acid and hence theoretical K^+ binding studies with this amino acid is the most demanding when compared to other amino acids. Due to its large size, many more stable conformations could be found for in its free state and cation bound complexed state. The K^+ -Arg complex is expected to show higher K^+ affinity associated with its largest molecular polarizability; however, its absolute K^+ affinity has not been reported. In agreement with the previous study of Williams and co-workers, [Jockusch et al., 1999] we found the zwitterionic **ZW1** is the most stable binding mode; while the bidentate **CS1** and tridentate **CS2** binding mode are less stable by 10 and 28 kJ mol^{-1} , respectively. However, the our **ZW1** structure is

very different from that of Williams and co-workers, who reported a zwitterionic structure with the K^+ bound to the two carboxylate oxygen and the carboxylic proton is transferred to the N-terminal amino nitrogen. After exhaustive conformational optimization, we found the most stable zwitterionic mode is the **ZW1** structure as shown in Fig. 4.13, in which the K^+ is bound to the N-terminal nitrogen and one of the two carboxylate oxygens only, and with the carboxylic proton transferred to the secondary amine site ($NH_{(side)}$) in the guanidine side chain of Arg. The **ZW1** binding mode is stabilized by an efficient network of hydrogen bonds, including a short hydrogen bond ($\sim 1.6 \text{ \AA}$) between $NH_{(side)}$ and the N-terminal $-NH_2$ site in an eight-membered ring structure. Aside from the polarizability factor, this flexible eight-membered ring is an important structural factor leading to a highly stabilizing hydrogen network and reduced deformation energy in the **ZW1** binding mode of K^+ -Arg, which displays the highest K^+ affinity among all of the **CS** and **ZW** binding modes of α -amino acids. Regrettably, as explained in Section 4.2.3, we found the largest error (25 kJ mol^{-1}) among the theoretical and experimental K^+ affinity values of K^+ -Arg. However, we found good agreement between theory and experimental results for 18 of the 20 α -amino acids investigated. Furthermore, the relative stabilities of the **ZW1**, **CS1** and **CS2** K^+ binding modes of the K^+ -Arg complex can be rationalized in terms of the same stabilizing and de-stabilizing factors as in the case of the other amino acids. Hence, we are of the view that even though the absolute K^+ affinity values might show significant error, the relative stabilities of the **ZW1**, **CS1** and **CS2** K^+ binding modes of the K^+ -Arg complex found in the present study are most likely to be reliable.

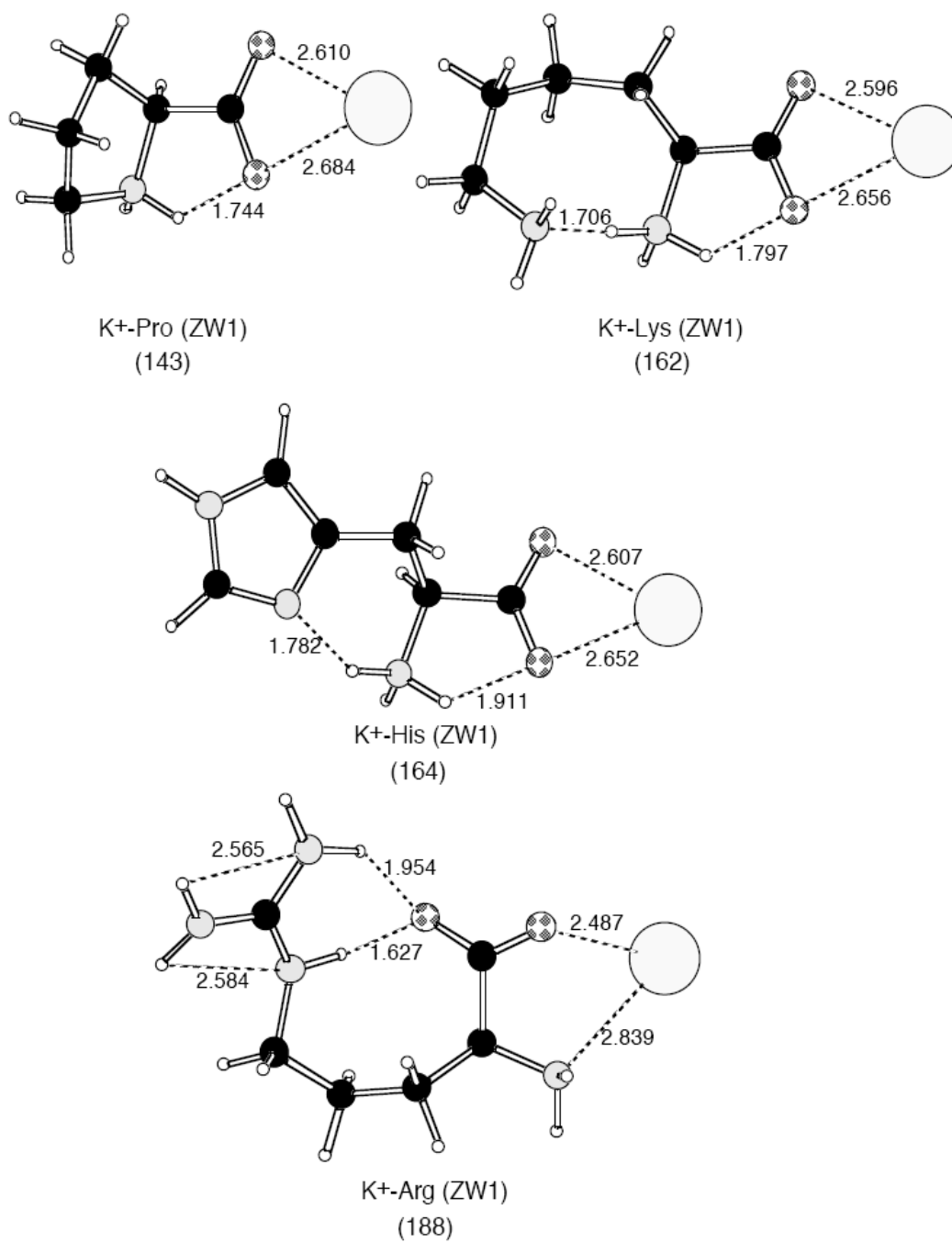


Figure 4.13 The most stable ZW K⁺ binding modes of Pro/Lys/His/Arg, optimized at the B3-LYP/6-31G(D) level. The K⁺ affinities at 0 K in kJ/mol are shown in parenthesis. All the bond lengths are shown in Å

K⁺-Methyl Esters of Amino Acids Complexes In the absence of a carboxylic proton, K⁺ could only be bound to methyl esters of amino acids in the charge-solvated **CS1** and **CS2** modes, but not in the zwitterionic **ZW1** mode. The purpose of including methyl esters in the present study is mainly to obtain experimental affinity values in support of the accuracy of the theoretical values obtained by the B3-LYP/6-311+G(3df,2p)//B3LYP/6-31G(d) protocol, without the complication of the competitive and possible occurrence of both the CS and ZW binding modes for some of the K⁺ bound amino acid complexes. As mentioned in the previous *Section 4.2.3*, very good agreement between our theoretical and experimental affinity values were obtained; the mean-average deviation (MAD) is 8.1 kJ mol⁻¹ for the 18 amino acids methyl esters studied. This is important experimental support for the validation and accuracies of the DFT protocol used also to evaluate K⁺ affinities and K⁺ binding geometries of similar studies on β -amino acids and β -dipeptides, which will be introduced in the following chapters.

The geometries of the **CS1** and **CS2** binding modes are found to be very similar to that of the free acids, and for this reason, they are not discussed in details here. For the 18 methyl esters studied, the tridentate **CS1** mode is found to be on average 22 kJ mol⁻¹ more stable than the **CS2** mode (Table 4.3), confirming that a K⁺ binding mode with higher coordination number is energetically more favored for methyl esters of amino acids.

4.3 Conclusion

With the exception of Lys and Arg, our study provides the first set of reliable experimental and theoretical potassium cation affinities (PCA) data for 18 of the 20 common α -amino acids. The experimental K⁺ affinities were determined to be (in kJ/mol): Arg (163) > His (155) > Gln (154) > Trp (151) > Asn (149) > Lys (144) > Glu (140) > Tyr (140) > Phe

(139) > Asp (137) > Thr (136) > Pro (135) > Met (135) > Ser (133) > Ile (129) > Leu (128) > Val (127) > Cys (124) > Ala (123) > Gly (119). Very good agreement between the experimental and theoretical potassium cation (K^+) affinities were obtained within ± 15 kJ mol⁻¹, with a mean absolute deviation (MAD) of 4.9 kJ/mol for the affinity values of the 18 α -amino acids. For Lys and Arg, the discrepancy between experimental and theoretical values is ± 15 and ± 25 kJ mol⁻¹, respectively, which can be attributed to the combined errors of the experimental determination and the theoretical modelling.

The most stable K^+ binding to aliphatic amino acids (Gly, Ala, Val, Leu, Ile) involves a bidentate interaction in the **CS1** form involving the carboxylic C=O and OH sites, whereas for amino acids with functionalized side chain (namely, Ser, Thr, Cys, Met, Phe, Tyr, Trp, Asp, Asn), a tridentate interaction in the **CS2** form involving the backbone O=C, N-terminal NH₂, and the O/N-heteroatom site of the functional group in the side chain is generally favored. This shows that a higher co-ordination number is the determining factors favoring the charge-solvated binding mode against the bidentate zwitterionic **ZW1** binding mode, in which the K^+ is bidentately bound to the carboxylate oxygens, and the carboxylic proton is transferred to the N-terminal nitrogen (NH₂) site. Aside from the co-ordination number factor, the ‘charge-separation’ effect, i.e., the energy required to maintain a positive (+) and negative (-) charge apart in the ZW structure, is also another de-stabilizing factor not favouring the ZW K^+ binding mode.

However, exceptions to this general rule are found in the K^+ -Glu/Gln complexes, which are found to be most stable in the **ZW1** form. An in-depth analysis of the bonding geometries in the K^+ -Glu/Gln complexes reveal that they are significantly stabilized by a ‘daisy-chain’ of hydrogen bonding network in the **ZW1** mode, together with a more flexible 7-membered ring hydrogen bonding structure as compared to that an analogous 6-

membered ring structure of the K^+ -Asn/Asp complexes. A larger ring size in the hydrogen bonding structure would also lead to less structural constraints and reduced deformation energy in the K^+ bound **ZW1** complex.

On the other hand, the **ZW1** mode is found to be the most stable K^+ binding mode for the four most basic amino acids, Pro, Lys, His and Arg. Clearly, the basicity of these amino acids are the driving force for the favored formation of the **ZW1** binding mode. The detailed conformations and relative stabilities of the **CS1**, **CS2** and **ZW1** modes of K^+ binding modes are found, for the first time, for Lys, His and Arg. The relative stabilities of the ZW versus CS modes are mainly governed by the interplay of the same stabilizing and de-stabilizing factors as found in other amino acids with functionalized side chains.

Contrary to literature reports, we have also found a new conformation for the most stable **ZW1** form of K^+ -Arg complex, in which K^+ is bound to the *N-terminal nitrogen* (NH_2) *site* and *one* of the two carboxylate oxygens only, and with the carboxylic proton transferred to the secondary amine site ($NH_{(side)}$) in the guanidine side chain of Arg. The stability of this exceptional **ZW1** conformation is rationalized in terms of the very strong intra-molecular hydrogen bonding pattern found in the K^+ complexed state.

The strong ‘local’ ion-dipole interactions between K^+ and $O=C$, the participation of the side-chain substituent in the coordination of the K^+ , the formation of an extra-strong hydrogen bonding and/or a ‘daisy-chain’ hydrogen bonding network, and the enhanced basicity (proton affinity) of the amino acid are the factors governing the relative stabilities of CS versus ZW forms.

Chapter 5 Proton and Potassium affinities of Selected Biologically Significant β -Amino Acids

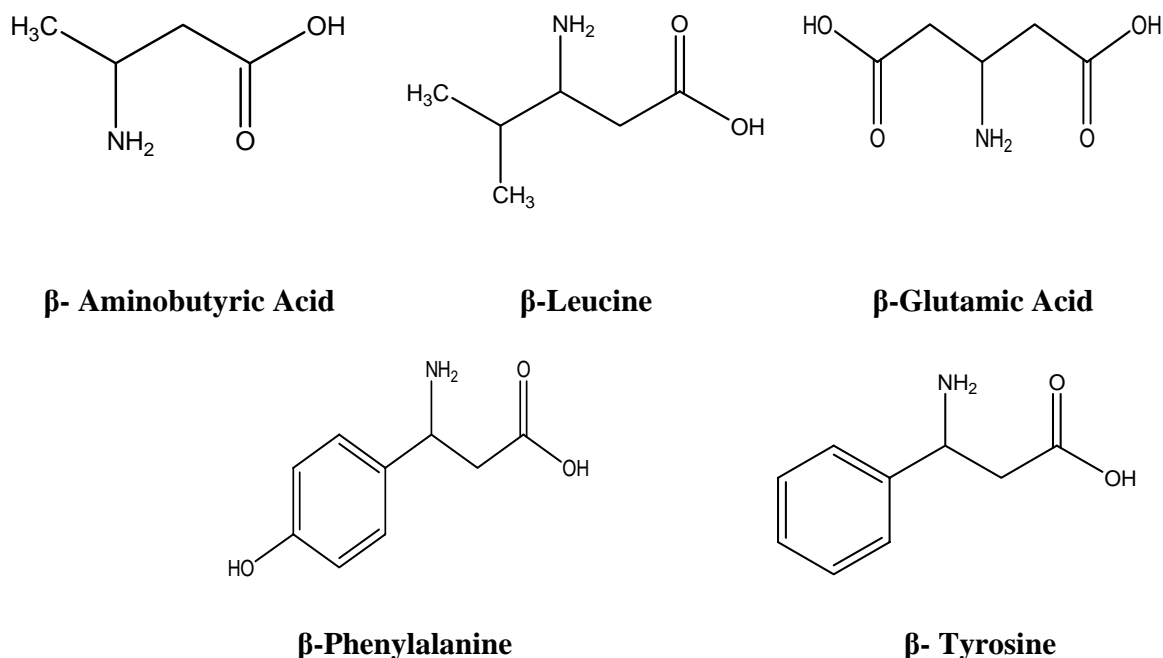
5.1 Background

In recent years, there is increasing recognition that the incorporation of critically positioned β -amino acids into peptides, cyclopeptides, glycopeptides, or alkaloids [Schmuck and Wennemers, 2004] would change the properties of these compounds, enabling them to survive in potent biological and physiological activities.[Ballard and Wang, 2002] For example, β -amino acids are found in the secondary metabolites of many bacteria, cyanobacteria, fungi and plants, which enable them to survive from the competition with other organisms.[Buchwaldt and Green, 1992; Engel et al., 2002]. The incorporation of these β -amino acid sub-structures could increase their stability against degradation by mammalian peptidases.[Steer et al., 2001] More specifically, it has been proposed that this is due to a lack of enzymes which could successfully cleave the peptidic bonds between an α -amino acid and a β -amino acid.[Pegova et al., 2000] Because of this special property, medicinal chemists are pursuing a strategy of screening many natural products and peptides incorporated with a β -amino acid moiety for the discovery and development of new drugs.[Steer et al., 2002] However, the influence of other properties of β -amino acids that could affect known enzyme functions, such as changes in the molecular/peptide conformation upon proton attachment and/or metal chelation, cannot be ruled out. Hence, basic knowledge and understanding on the proton and metal cation affinity of β -amino acids are required in drug discovery strategies employing the incorporation of one or more β -amino acids into peptides or other known molecular systems.

Previously, experimental and theoretical studies on proton affinities and alkali metal cation affinities have been focused on the simple α -amino acids, which serve as the building blocks for the understanding of more complex di-/tripeptide systems. Investigations into the proton affinity and alkali metal cation affinity of β -amino acids were reported only in the last five years. Not surprisingly, the first reported study is a combined experimental and theoretical study on the proton affinity of β -alanine, the most commonly found β -amino acid in nature.[Hahn and Wesdemiotis, 2002] This was followed by an experimental [Chan, 2006] and theoretical [Abirami et al., 2005] study on the alkali metal affinity and binding modes of β -alanine by members of Prof. Tsang's research group. For H^+/M^+ ($M = Li^+, Na^+$ and K^+) bound β -alanine, the H^+/M^+ affinity was found to be greater than that of α -alanine. This was attributed primarily to a more stabilizing intra-molecular hydrogen bond in H^+/M^+ bound β -alanine made possible by the presence of the extra $-CH_2-$ unit in the backbone of β -amino acids (refer to Section 1.1). Similar studies on other β -amino acids have not been reported.

Aside from β -alanine, there are many other β -amino acids that are found in nature either in free form or as part of a larger molecule. In particular, β -aminobutyric acid (β -Abu), β -leucine (β -Leu), β -glutamic acid (β -Glu), β -phenylalanine (β -Phe) and β -tyrosine (β -Tyr) (refer to **Scheme 5.1** for chemical structures) are found in many natural products and peptides of animals, plants, fungi, bacteria and protista, which are involved in many important biological functions. For example, (R)- β -aminobutyric Acid, which has a structure similar to that of β -alanine, is present in all living organisms and is directly involved in their primary metabolisms. [Griffith, 1986] (R)- β -Leucine (β -Leu) is generated by a non- B_{12} -dependent 2,3-aminomutase from (L)- α -leucine in the plant *Andrographis paniculata*. [Freer et al., 1981]

β -Glutamic acid (β -Glu) is accumulated as an osmolyte in archaea such as *M. thermolithotrophicus* [Robertson, 1989] and *Methanohalophilus portucalensis*. [Robinson, 2001] β -Glu is one of the compatible solutes which is balanced by intracellular K^+ ions and is probably intertwined with K^+ uptake and accumulation. In other words, K^+ and β -glutamic acid act as temporary osmolytes in the hyperosmotic response of *M. thermolithotrophicus*. β -phenylalanine (β -Phe) is found in peptides of the plant *Aster tartaricus* [Kelly et al., 1999; Davies et al., 1993] and the bacterium *Pseudomonas fluorescens* [Needham et al., 1994], and is shown to have anti-tumor and anti-bacterial properties. β -Tyrosine (β -Tyr) is found in peptides of marine sponges, and aside from its antifungal and insecticidal properties, [Coleman et al., 1999; Tinto et al., 1998] is found to be a potent cytotoxic against a number of human cancer cells. The biological essentiality and abundance in nature of the five selected β -amino acids are summarized in Table 5.1:



Scheme 5.1 Chemical Structure of Selected Bioactive β -Amino Acids

In this study, we aim to extend our previous studies on the intrinsic proton (H^+) and potassium cation (K^+) binding affinities of β -alanine (β -Ala) to the five biologically significant β -amino acids shown in **Scheme 5.1**.

Experimental H^+ binding affinities was determined by the extended mass spectrometric kinetic method, using aliphatic amines with known and comparable binding affinities as reference compounds. The kinetic method, both in the standard and extended version, and the amine reference compounds have been used in the determination of proton affinities of the five corresponding α -amino acids.[Harrison, 1999] For the kinetic method determination of K^+ affinities, methyl esters of α -amino acids the K^+ affinities of which had been determined as described in Chapter 4, were used as the reference compounds. In addition, hybrid density functional theory calculations using the established B3-LYP/6-311+G(3df,2p)//B3-LYP/6-31G(d) protocol was used to obtain the theoretical H^+/K^+ binding affinities and the most stable H^+/K^+ binding modes, and to aid in the proper interpretation of experimental results. Potassium cation is chosen as the probe metal ion in the present study because its binding modes with the corresponding α -amino acids have been elucidated in Chapter 4, and are available for comparison in the present study.

Table 5.1 Biological significance of the five selected β -amino acids in this study

β-Amino Acids	Sources	Biological Significance
β -Abu	(i) Phascosomine in the viscera of worms ^a (ii) sporophores of commercial mushroom, <i>Agaricus campestris</i> ^b	(i) constituent for phascosomine which is used for energetic muscular contraction in worms ^a (ii) nutritional, metabolic and physiological benefits ^b
β -Leu	(i) interconversion of leucine and β -leucine by leucine 2,3-aminomutase in human leukocytes, hair roots and rats' liver ^c	(i) decrease the function of the leucine 2,3-aminomutase ^c (ii) increase the catabolism of branched fatty acids ^c
β -Glu	(i) catabolic product through macromolecule breakdown in <i>M. thermolithotrophicus</i> ^d (ii) biosynthesis by <i>A. luteoviolacea</i> and by a unidentified facultative anaerobe ^{f,g,h}	(i) as a compatible solute in methanogenic bacteria ^{d,e} (ii) as temporary osmolytes with K ⁺ in the hyperosmotic response of <i>M. thermolithotrophicus</i> ^{d,e} (iii) as a substrate for glutamine synthetase in <i>Methanohalophilus</i> strain FDF1 ^{d,e}

<p>β-Phe</p>	<p>(i) constituent of cyclopentapeptides in roots of <i>Aster tartaricus</i>^{i,j}</p> <p>(ii) dipeptide in <i>Azolla caroliniana</i>^k</p> <p>(iii) metabolite andrimid and several moiramides of bacterium <i>Pseudomonas fluorescens</i>^m</p>	<p>(i) display antitumor nature in <i>Aster tartaricus</i>ⁱ</p> <p>(ii) display antibacterial and antimicrobial properties^m</p>
<p>β-Tyr</p>	<p>(i) Jaspamide, a modified peptide from a <i>Jaspis Sponge</i>^{n,o}</p> <p>(ii) Geodiamolides from the <i>Sponge Cymbastela sp.</i>^o</p>	<p>(i) as a β-amino acid unit in Jaspamide which exhibits potent insecticidal activity against <i>Heliothis virescens</i>, antimicrobial activity against <i>Candida albicans</i>, and antiproliferative activities, etc.^{p,q}</p> <p>(ii) as a β-amino acid unit in dipeptide of Geodiamolides which is potent cytotoxic against a number of human cancer cells , antifungal and insecticidal^{o,p}</p>

^a Yvonne Guillou; Yvonne Robin, Phascoline and Phascolosomine, Two New Guanidino Compounds from Sipunculid Worms: The Journal of Biological Chemistry, 1973, 248, 16, 5568-5672.

^b Mario R. Altamura, Frederick M. Robbins, Raymond E. Andreotti, Louis Long, Jr., Torsten Hasselstrom: Mushroom Ninhydrin-Positive Compounds, J. Agr. Food Chem., 1967, 15, 6, 1040-1043.

- ^c J. Michael Poston, Changes in Pernicious Anemia: *The Journal of Biological Chemistry*, 1980, 255, 21, 10067-10072.
- ^d Diane E. Robertson, David Noll, Mary F. Roberts, Free Amino Acid Dynamics in Marine Methanogens: *The Journal of Biological Chemistry*, 1992, 267, 21, 14893-14901.
- ^e Deana D. Martin, Rose A. Ciulla, Patrice M. Robinson, Mary F. Roberts, Switching Osmolyte Strategies: *Biochimica et Biophysica Acta*, 2000, 1524, 1-10.
- ^f Susan M. Henrichs, Russell Cuhel, Occurrence of beta-aminoglutaric Acid in Marine Bacteria: *Applied and Environmental Microbiology*, 1985, 50, 2, 543-545.
- ^g Susan M. Henrichs, John W. Farrington, Amino Acids in Interstitial Waters of Marine Sediments: *Nature*, 1979, 279.
- ^h J.C. Colombo, N. Silverberg, J.N. Gearing, Amino Acid Biogeochemistry in the Laurentian Trough: *Org. Geochem.*, 1998, 29, 4, 933-945.
- ⁱ Kelly K. Schumacher, Diane B. Hauze, Jianjun Jiang, J. Szewczyk, Rajarathnam E. Reddy, Franklin A. Davis, Madeleine M. Joullie, First Total Synthesis of Astin G: *Tetrahedron Letters*, 1999, 40, 455-458.
- ^j Stephen G Davies, Jamton Dupont, Robert J. C. Easton., Assignment of the Absolute Configuration to Winterstein's Acid: *Tetrahedron Letters*, 1993, 34, 8, 1291-1294.
- ^k James L. Corbin, Barry H. Marsh, Gerald A. Peters, *Azolla Caroliniana*: *Phytochemistry*, 1986, 25, 2, 527-528.
- ^m Judy Needham, Michael T. Kelly, Marie Ishige, Raymond J. Andersen, Andrimid and Moiramides A-C, Metabolites Produced in Culture by a Marine Isolate of the Bacterium *Pseudomonas fluorescens*: *J. Org. Chem.*, 1994, 59, 2058-2063.
- ⁿ T. Mark Zabriskie, James A. Klocke, Chris M. Ireland, Andrew H. Marcus, Tadeusz F. Molinski, D. John Faulkner, Chang Xu, Jon C. Clardy, Jaspamide, a Modified Peptide from a Jaspis Sponge, with Insecticidal and Antifungal Activity: *J. Am. Chem. Soc.*, 1986, 108, 3123-3124.

^o John E. Coleman, Rob Van Soest, Raymond J. Andersen, New Geodiamolides from the Sponge *Cymbastela* sp. Collected in Papua New Guinea: *J. Nat. Prod.*, 1999, 62, 1137-1141.

^p Winston F. Tinto, Alan J. Lough, Stewart McLean, William F. Reynolds, Margaret Yu, Wilfred R. Chan, Geodiamolides H and I, Further Cyclodepsipeptides from Marine Sponge *Geodia* sp.: *Tetrahedron*, 1998, 54, 4451-4458.

^q Angela Zampella, Clelia Giannini, Cecile Debitus, Christos Roussakis, Maria Valeria D'Auria, New Jaspamide Derivatives from the Marine Sponge *Jaspis splendama* collected in Vanuatu: *J. Nat. Prod.* 1999, 62, 332-33

5.2 Results and Discussion

5.2.1 Experimental Determination of *Absolute Proton (H⁺) Affinities of Selected β -Amino Acids*

The proton (H⁺) affinities of the selected five β -amino acids were determined using ethylamine, propylamine (PA), isopropylamine (IPA), t-amylamine (TAA), t-butylamine (TBA), n-methylethylamine (MEA), trimethylamine (TMA) as reference compounds as they have comparable H⁺ affinities at 298K to that of the β -amino acids. Similar measurements on α -amino acids showed that entropic effects (i.e., the $\Delta(\Delta S)^{\text{app}}$ term in Eqn. [2.9] is non-zero) are present in the dissociation of the H⁺ bound heterodimers, thus the extended kinetic method has to be adopted in the present study.

At typical low-energy CID MS/MS mass spectrum of the $[(\beta\text{-Phe}) + \text{H} + \text{PA}]^+$ heterodimer is shown in Figure 5.1. The heterodimer (m/z 225) dissociates by competitive bond fission to yield protonated β -phenylalanine ($\beta\text{-Phe}$) and protonated propylamine fragment ions at m/z 60 and m/z 166, respectively. The dissociation of the $[(\beta\text{-Phe}) + \text{H} + \text{PA}]^+$ heterodimer was measured at different collision energies (eV), which corresponds to excitation at different effective temperatures (T_{eff}). A plot of $\ln([\text{H} + \beta\text{-Phe}]^+ / [\text{H} + \text{Ln}]^+)$ versus $[\Delta H_{[\text{H}+\text{Ln}]^+} - \Delta H_{\text{Avg}}]$ (where Ln = propylamine (PA), isopropylamine (IPA) and t-amylamine (TAA)) yields a regression line with the slope and intercept of $-1 / RT_{\text{eff}}$ and $[\Delta G_{[\text{H}+\text{Ln}]^+} - \Delta H_{\text{Avg}}] / RT_{\text{eff}}$, respectively (Fig. 5.2(a)). A second plot is obtained by plotting the $[(\Delta G)^{\text{app}}_{[\beta\text{-Phe} + \text{H}]^+} - \Delta H_{\text{Avg}}] / RT_{\text{eff}}$ term versus $1/RT_{\text{eff}}$ (Fig. 5.2(b)); the slope and y-intercept of the second plot yields the H⁺ affinity at 298K (kJ mol⁻¹) of $\beta\text{-Phe}$ and the $\Delta(\Delta S)^{\text{app}}$ term, respectively (Eqn. [2.9]). The absolute H⁺ affinity for $\beta\text{-Phe}$ at 298K, $\Delta H_{[\text{H}-\beta\text{-Phe}]^+}$, as well as the apparent

entropy change were obtained from the second plot and found to be $948.0 \text{ kJ mol}^{-1}$ and 18.2 J mol^{-1} respectively. By the same token, the H^+ affinities of β -leucine (β -Leu), β -aminobutyric acid (β -Abu), β -glutamic acid (β -Glu) and β -tyrosine (β -Tyr) were determined in a similar way. The proton affinities of five selected β -amino acids so determined are summarized in Table 5.2.

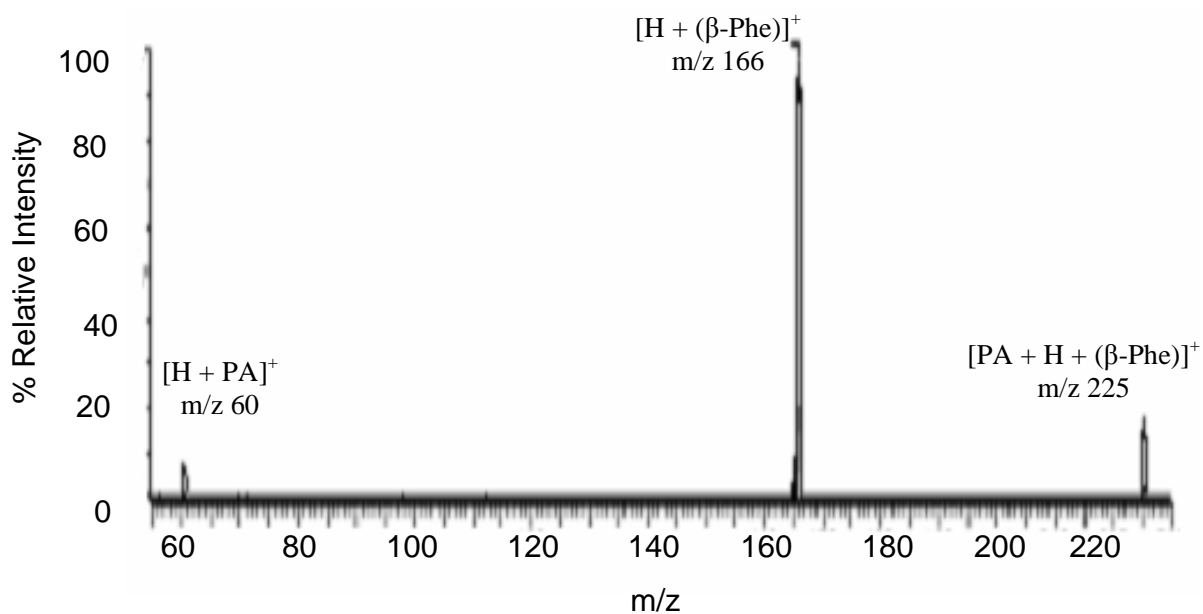


Figure 5.1 Triple quadrupole MS / MS spectrum of the proton bound heterodimer $[\text{PA} + \text{H} + (\beta\text{-Phe})]^+$ using argon at a collision energy of 8 eV (laboratory frame) (β -Phe = β -Phenylalanine and PA = Propylamine)

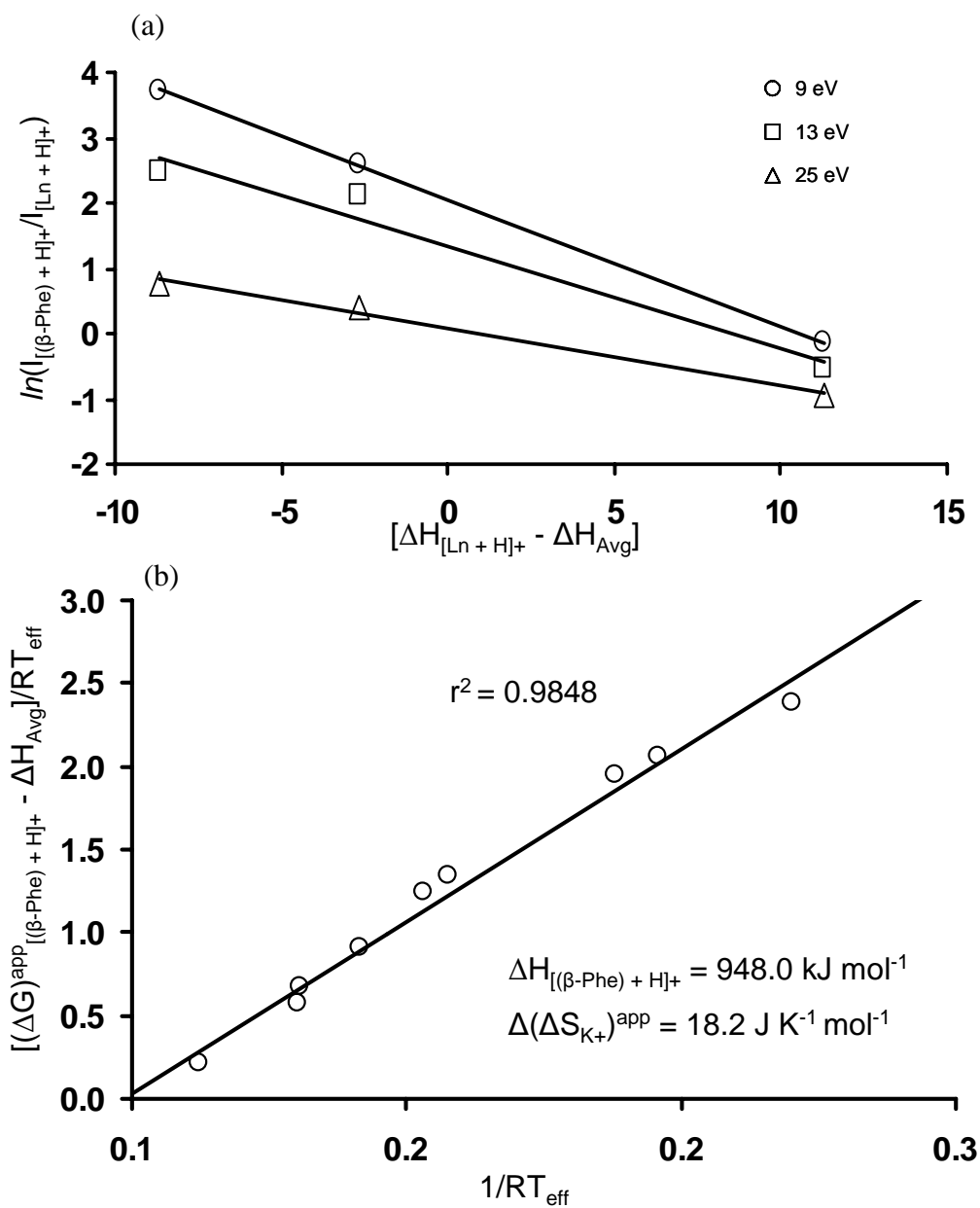


Figure 5.2 (a) Plot of $\ln(I_{[(\beta-Phe)+H]^+}/I_{[L_n+H]^+})$ versus $[\Delta H_{[L_n+H]^+} - \Delta H_{Avg}]$ at different collision energies, and (b) plot of $[(\Delta G)^{app}_{[(\beta-Phe)+H]^+} - \Delta H_{Avg}]/RT_{eff}$ against $1/RT_{eff}$ for the proton bound heterodimer $[(\beta-Phe) + H + L_n]^+$ heterodimers. ((β -Phe) = β -Phenylalanine, L_n = Propylamine, Isopropylamine and Triamylamine); numbers shown are *absolute* proton affinities

Table 5.2 Experimental proton (H^+) affinities at 298K, (ΔH_{298} , kJ mol^{-1}) and $\Delta(\Delta S_{H^+})^{\text{app}}$ ($\text{J mol}^{-1} \text{K}^{-1}$) of β -amino acids determined by the extended kinetic method.

β -amino acids	This Work ^a		References (kJ mol^{-1}) ^b
	ΔH_{298}	$\Delta(\Delta S_{H^+})^{\text{app}}$	
β -Abu	942.0 ± 1.0 (1.9)	22.3 ± 0.8 (1.6)	ethylamine (912.0), propylamine (917.8), isopropylamine (923.8)
β -Leu	955.6 ± 0.8 (1.4)	28.6 ± 1.8 (3.3)	n-methylethylamine (942.2), trimethylamine (948.9), diethylamine (952.4)
β -Phe	948.0 ± 0.7 (1.3)	18.2 ± 0.9 (1.6)	propylamine (917.8), isopropylamine (923.8), t-amylamine (937.8)
β -Tyr	955.4 ± 5.3 (9.9)	24.1 ± 7.4 (13.7)	isopropylamine (923.8), t-butyamine (934.1), trimethylamine (948.9)
β -Glu	951.5 ± 1.9 (3.6)	21.18 ± 2.3 (4.4)	isopropylamine (923.8), t-butyamine (934.1), n-methylethylamine (942.2)

^a Determined by extended kinetic method on this work and the uncertainties are given as \pm S.D.(90% confidence interval).

^b Proton Affinities are taken from: Hunter, E.P. and Lias, S.G., *Evaluated Gas Phase Basicities and Proton Affinities of Molecules: An Update*, *J. Phys. Chem. Ref. Data*, **1998**, 27, 3, 413-656.)

5.2.2 Experimental Determination of *Absolute* Potassium Cation (K^+) Affinities of Selected β -Amino Acids

The potassium cation (K^+) affinities of the selected five β -amino acids were determined using the extended kinetic method and similar experimental procedure as described in Chapter 4 for determination of K^+ affinities of twenty α -amino acids. Leucine methyl ester (LeuOMe), leucine ethyl ester (LeuOEt), valine methyl ester (ValOMe), serine (Ser), serine methyl ester (SerOMe), serine ethyl ester (SerOEt), asparagines(Asn), lysine methyl ester (LysOMe), lysine ethyl ester (LysOEt) and glutamic acid methyl ester (GluOMe) were used as the reference compounds as they have comparable K^+ affinities at 0K to that of β -amino acids.

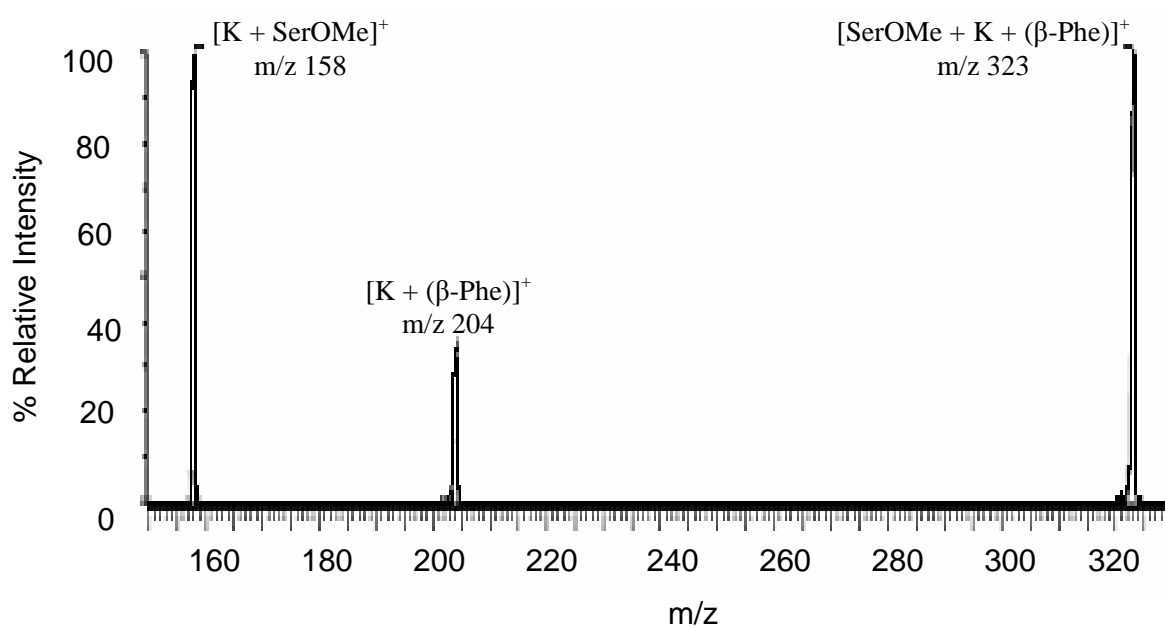


Figure 5.3 Triple quadrupole MS / MS spectrum of the $[SerOMe + K + (\beta\text{-Phe})]^+$ heterodimer using argon as collision gas at a collision energy of 9 eV (laboratory frame) ($\beta\text{-Phe}$ = β -Phenylalanine and SerOMe = Serine Methyl Ester)

A typical low-energy CID MS/MS mass spectrum of $[(\beta\text{-Phe}) + \text{K} + \text{SerOMe}]^+$ heterodimer is shown in Figure 5.3. The corresponding first and second plots of the extended kinetic method measurements are shown in Figure 5.4. The absolute K^+ affinity for $\beta\text{-Phe}$ at 0K, $\Delta H_{[\text{K}-\beta\text{-Phe}]^+}$, as well as the apparent entropy change are found to be $137.6 \text{ kJ mol}^{-1}$ and 0.94 J mol^{-1} , respectively. In addition, the K^+ affinities of $\beta\text{-leucine}$ ($\beta\text{-Leu}$), $\beta\text{-aminobutyric acid}$ ($\beta\text{-Abu}$), $\beta\text{-glutamic acid}$ ($\beta\text{-Glu}$) and $\beta\text{-tyrosine}$ ($\beta\text{-Tyr}$) were determined in a similar way. The potassium cation affinities of the five selected $\beta\text{-amino acids}$ so determined are summarized in Table 5.3.

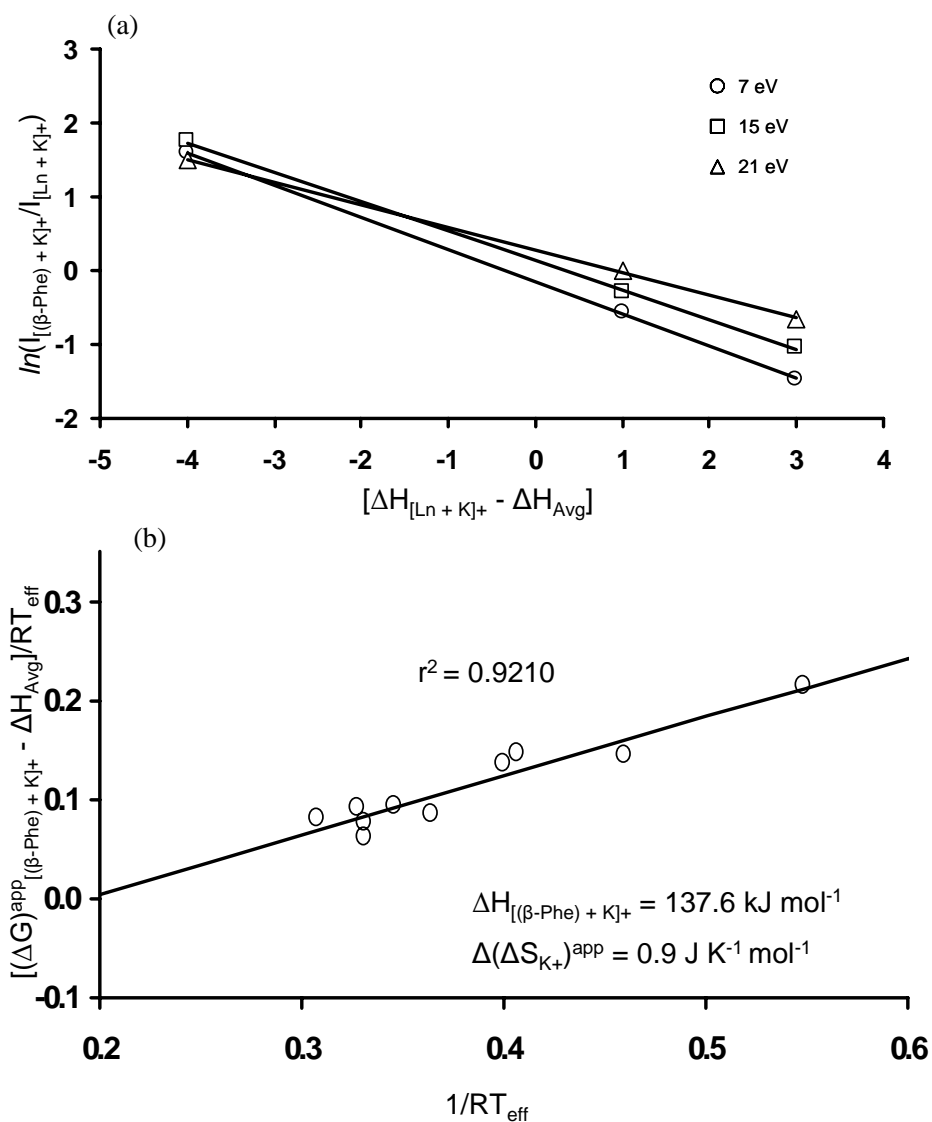


Figure 5.4 (a) Plot of $\ln(I_{[(\beta-Phe)+K]^+}/I_{[L_n+K]^+})$ versus $[\Delta H_{[L_n+K]^+} - \Delta H_{Avg}]$ at different collision energies, and (b) plot of $[(\Delta G)_{[(\beta-Phe)+K]^+}^{app} - \Delta H_{Avg}]/RT_{eff}$ against $1/RT_{eff}$ for the $[(\beta-Phe) + K + L_n]^+$ heterodimer. ((β -Phe) = β -Phenylalanine, L_n = Serine (Ser), Serine Methyl Ester (SerOMe) and Serine Ethyl Ester (SerOEt))

Table 5.3 Experimental potassium cation (K^+) affinities at 0 K, (ΔH_0 , kJ mol^{-1}) and $\Delta(\Delta S_{H^+})^{\text{app}}$ ($\text{J mol}^{-1} \text{K}^{-1}$) of β -amino acids

β -amino acids	This Work ^a		References (kJ mol^{-1}) ^b
	ΔH_0	$\Delta(\Delta S_{H^+})^{\text{app}}$	
β -Abu	134.7 ± 0.1 (0.2)	-1.1 ± 0.3 (0.6)	Ser (132.8), SerOMe (137.7), SerOEt (140.0)
β -Leu	138.3 ± 1.3 (2.4)	-16.2 ± 0.2 (0.3)	ValOMe (129.9), LeuOMe (131.6), LeuOEt (134.6)
β -Phe	137.6 ± 0.1 (0.2)	0.9 ± 0.3 (0.5)	Ser (132.8), SerOMe (137.7), SerOEt (140.0)
β -Tyr	138.7 ± 0.4 (0.8)	3.1 ± 1.1 (2.1)	Ser (132.8), SerOMe (137.7), SerOEt (140.0)
β -Glu	141.5 ± 0.5 (1.1)	3.4 ± 1.1 (2.0)	Asp (136.5), GluOMe (145.1), LysOMe (146.0), LysOEt (147.6)

^a Determined by extended kinetic method on this work and the uncertainties are given as \pm S.D.(90% confidence interval).

^b Potassium cation affinities determined in the present study (Chapter 4).

5.2.3 Comparison between experimental and theoretical H^+ / K^+ affinity values

Theoretical proton (H^+) and potassium (K^+) affinities of β -amino acids have not been reported in the literature. Density functional theory calculations have been shown earlier to be able to yield accurate proton affinities of 20 α -amino acids, [Maksic and Kovacevis, 1999] and to yield reasonably accurate potassium cation (K^+) affinities in the present work (Chapter 4) as well. In order to obtain information on the preferred site of proton (H^+) and potassium cation (K^+) binding and compare to that of corresponding α -amino acids, theoretical calculations on the binding modes and H^+ / K^+ affinities by hybrid density functional theory (DFT) calculations were carried out. The most stable conformations for the H^+ / K^+ -(β -amino acids) complexes were optimized at the B3-LYP/6-31G+(d) level, and the absolute H^+ / K^+ affinities were calculated at the B3-LYP/6-311+G(3df,2p)//B3-LYP/6-31G+(d) level of theory.

The theoretical H^+ and K^+ affinity values of the selected five β -amino acids are summarized and compared with experimental values in Table 5.4 and Table 5.5, respectively. Excellent agreements between the experimental and theoretical affinity values were obtained: the mean-absolute deviation (MAD) for proton affinities of five selected β -amino acids is only 3.1 kJ mol⁻¹ (Table 5.4), while the MAD for potassium cation (K^+) affinities is only 6.4 kJ mol⁻¹ (Table 5.5). Such consistency provides the necessary confidence that the experimental / theoretical H^+ / K^+ affinities, and the protonated and potassiated binding modes of the β -amino acids found in the present study are reliable and accurate.

Table 5.4 Experimental and theoretical proton (H^+) affinities of β -amino acids

β -amino acids	Proton Affinity, ΔH_{298}		$\Delta H_{298(\text{Expt})} - \Delta H_{298(\text{Theory})}^c$
	Experimental ^a	Theoretical ^b	
β -Aminobutyric acid (β -Abu)	942	943	-1
β -Leucine (β -Leu)	956	953	3
β -Phenylalanine (β -Phe)	948	952	-4
β -Tyrosine (β -Tyr)	955	959	-4
β -Glutamic acid (β -Glu)	952	955	-3

^a Experimental affinities at 298 K, $\Delta H_{298(\text{Expt})}$, measured by extended kinetic method in this work (Table 5.1).

^b Theoretical affinities at 298 K, $\Delta H_{298(\text{Theory})}$, determined at the B3-LYP/6-311+G(3df,2p)//B3-LYP/6-31G(d) level, with ZPE corrections at B3LYP/6-31G(d) level and scaled by 0.9806.

^c The difference between experimental and theoretical affinity of the most stable H^+ binding mode.

Table 5.5 Experimental and theoretical K^+ affinities of β -amino acids at 0K (kJ mol^{-1})

β -Amino acid	Potassium Cation Affinity, ΔH_0				ΔH_0 (Expt) –
	Expt ^a	Theoretical ^b			
		CS1 (O=C, OH) ^c	CS2 (O=C, NH ₂ , X) ^d	ZW (COO ⁻) ^e	
β -Aminobutyric acid (β -Abu)	135	143	126 (O=C, NH ₂)	139	-8
β -Leucine (β -Leu)	138	147	130 (O=C, NH ₂)	143	-9
β -Phenylalanine (β -Phe)	138	143	124 (X = cation- π)	139	-5
β -Tyrosine (β -Tyr)	139	146	126 (X = cation- π)	143	-7
β -Glutamic acid (β -Glu)	142	144	132 (O=C, NH ₂)	143	-2

^a Experimental affinities at 0 K, $\Delta H_{0(\text{Expt})}$, measured by extended kinetic method in this work (Table 5.2).

^b Theoretical affinities at 0 K, $\Delta H_{0(\text{Theory})}$, determined at the B3-LYP/6-311+G(3df,2p)//B3-LYP/6-31G(d) level, with ZPE corrections at B3LYP/6-31G(d) level and scaled by 0.9806. K^+ affinities for the most stable binding modes are indicated by fonts.

^c CS1, charge-solvated (CS) conformer of K^+ -(β -amino acid), with K^+ binding bidentately to the carbonyl oxygen.

^d CS2, charge-solvated (CS) conformer of K^+ -(β -amino acid), with K^+ binding tridentately to the carbonyl oxygen, amino nitrogen and the O/N heteroatom site (X) of the functionalized side chain.

^e ZW1, the most stable zwitterionic (ZW) conformer of K^+ -(β -amino acid), with K^+ binding bidentately to the two carboxylic oxygens.

^f The difference between experimental and theoretical affinity of the most stable charge-solvated CS1 binding mode. (in bold)

5.2.4 The H⁺ and K⁺ Binding Modes of Selected β -Amino Acids

Most Stable Binding Modes and Geometries of H⁺-(β -Abu) / (β -Leu) / (β -Phe) / (β -Tyr) / (β -Glu) Complexes

Density functional theory calculations at the B3-LYP/6-311+G(3df,2p)//B3-LYP/6-31G(d) level of theory show that the most stable proton binding conformations of the five bioactive β -amino acids (β -Abu, β -Leu, β -Phe, β -Tyr and β -Glu) have the proton bound to the amino nitrogen (N) (Fig. 5.5). The protonated conformers are stabilized by the hydrogen bonding between the ammonium hydrogen and amide oxygen (NH₂H⁺.....O=C) in a 6-membered ring pattern. The NH₂H⁺.....O=C bonding distances are relatively short in the 1.74 - 1.86 Å range, indicating that the hydrogen bonding is strong and significantly enhance the stability of the complexes.

The proton affinities (PA) of the five model β -amino acids are generally larger than that of their α -analogues. For examples, the experimental PA of β -Phe (948.0 kJ mol⁻¹) is greater than its α -analogue (α -Phe, 924.0 kJ mol⁻¹) [Harrison, 1997] by 24 kJ mol⁻¹. The enhanced PA could be attributed to the formation of the shorter (by 0.1 Å) and more stabilizing intramolecular NH₂H⁺.....O=C hydrogen bond of the complexes. The same hydrogen bonding pattern is also found in protonated β -Ala, which has a PA ~27 kJ mol⁻¹ higher than that of α -Ala. [Hahn and Wesdemiotis, 2002]

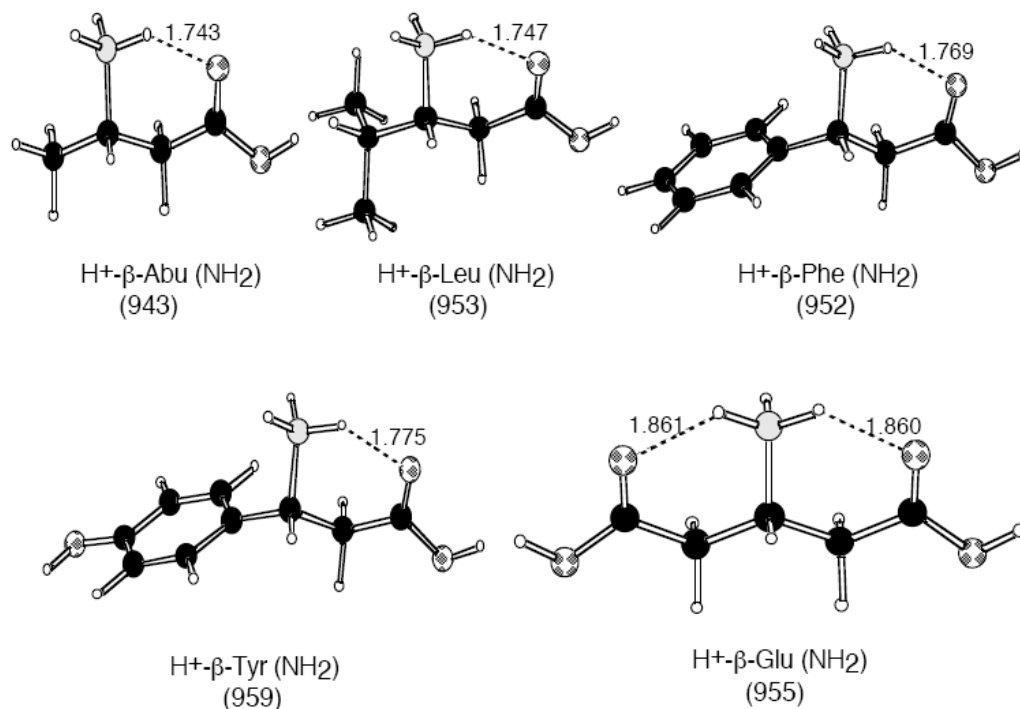


Figure 5.5 Optimized geometries of most stable protonated β -Abu, β -Leu, β -Phe, β -Tyr and β -Glu complexes calculated at B3-LYP/6-311+G(3df,2p)//B3-LYP/6-31G+(D) level of theory

5.2.5 Potassium Cation Binding to β -Amino Acids (β -Abu, β -Leu, β -Phe, β -Tyr, and β -Glu): Relative Stabilities of Charge-Solvated versus Zwitterionic Binding Modes

The CS1 Binding Mode The optimized geometries of the K^+ -(β -Abu)/(β -Leu)/(β -Phe) / (β -Tyr)/ (β -Glu) complexes in the **CS1** binding mode are shown in Figure 5.6. In the **CS1** binding mode, K^+ binds to the two carboxylic oxygens (CO, OH), with a very small deformation energy (E_{def} , 1-3 kJ mol^{-1}) due to minimum structural distortion of the free ligand. As in the case of K^+ binding to β -alanine,[Abirami et al., 2005] **CS1** is found to be the most stable K^+ binding mode for the five β -amino acids, with greater K^+ affinities than its α -

analogues. The enhanced stability of the **K⁺-CS1** binding mode could be attributed mainly to the presence of the ‘additional’ –CH₂– unit in the carbon chain of the β-amino acids, allowing the formation of a very short (1.5-1.6 Å) and stabilizing intramolecular hydrogen bond (–OH.....NH₂) between the hydroxyl and amino site in a 6-membered ring configuration. An analogous but weaker hydrogen bonding pattern is also found in their α-analogues in a 5-membered ring configuration, but with significantly shorter bonding distances (by ~0.20 Å). For example, the hydrogen bonding distance in the K⁺-(β-Leu) complex is 1.56 Å while that of K⁺-(α-Leu) is 0.17 Å shorter at 1.73 Å (Fig. 4.9 in Chapter 4), making **CS1** the most stable K⁺ binding mode for β-Leu.

The CS2 Binding Mode In the **CS2** binding mode, K⁺ binds to the carbonyl oxygen (O=C) and N-terminal amino (–NH₂) sites in the K⁺-(β-Abu)/(β-Leu)/(β-Glu) complexes, and tridentately with additional binding to the aromatic-π surface in the K⁺-(β-Phe)/(β-Tyr) complexes. The carbonyl oxygen (O=C) and N-terminal amino (–NH₂) sites are further apart in β-amino acids due to the presence of the ‘additional’ –CH₂– unit in its main carbon chain. Consequently, the **CS2** binding mode induces the most structural strain on the β-amino acids in the K⁺ complexed form when compared to the free ligand form, making it the least stable when compared to the **CS1** and zwitterionic **ZW1** binding modes (refer to Table 5.4). The situation is most acute for the tridentately bound K⁺-(β-Phe)/(β-Tyr) complexes, in which K⁺ is forced obliquely further away (~ 3.4 – 3.5 Å) from the aromatic-π surface in order to be more closely bound to the carbonyl oxygen (O=C) (Fig. 5.7). With weakened cation-π interaction and significant de-stabilizing deformation energy, the tridentate **CS2** is 18 – 20 kJ mol⁻¹ less stable than the bidentately bound **CS1** binding mode for the K⁺-(β-Phe)/(β-Tyr) complexes. On the contrary, in the absence of the ‘additional’ –CH₂– unit, the binding

geometries in the corresponding α -analogues are such that the tridentate binding mode (cation- π , CO, NH₂) is the most stable (refer to Table 4.2 and Fig. 4.11, Chapter 4). Because of enhanced structural deformation, a stable tridentate CS2 binding mode involving additional binding to one of the carboxylic oxygens in the side chain cannot be located in the K⁺-(β -Glu) complex, but can be found for the K⁺-(α -Glu) complex.

The ZW1 binding mode In the zwitterionic **ZW1** binding mode, the K⁺ is bound to the two carboxylate oxygens (COO⁻) with the proton transfer to the N-terminal -NH₂ site with minimum distortion of the conformation of the free ligand. The **ZW1** binding mode is further stabilized by a strong NH₂H⁺.....O=C hydrogen bonding in a six member-ring configuration as compared to an analogous but longer hydrogen bonding pattern in a 5-membered ring configuration in the α -analogues. Consequently, the energy difference between the **ZW1** and most stable **CS1** binding mode is narrowed to only 3-4 kJ mol⁻¹ for the K⁺-(β -Abu)/(β -Leu)/(β -Phe)/(β -Tyr) complexes (Table 5.5), and a marginal 1 kJ mol⁻¹ for the K⁺-(β -Glu) complex. For the corresponding K⁺-(α -Glu) complex, the stability of the **ZW1** binding mode is enhanced by a daisy chain of hydrogen bonds with adjacent 7-membered (more flexible and shorter/stronger hydrogen bonding) and 5-membered ring configurations (refer to Fig. 4.12, Chapter 4), so that it becomes the most stable with greater K⁺ binding affinity (by 6 kJ mol⁻¹) than the tridentate CS2 (O=C, NH₂, X = O=C) binding mode (refer to Table 4.2, Chapter 4). In the K⁺-(β -Glu) complex, an analogous hydrogen bonding pattern involving two adjacent 6-membered rings is formed (refer to Fig. 5.7), which is less flexible with longer (by ~ 0.1 Å) and weaker hydrogen bonding than the 7-membered ring configuration. As a result, the stability of the **ZW1** bonding mode for K⁺-(β -Glu) is reduced to marginally lower than that of the CS2 binding mode.

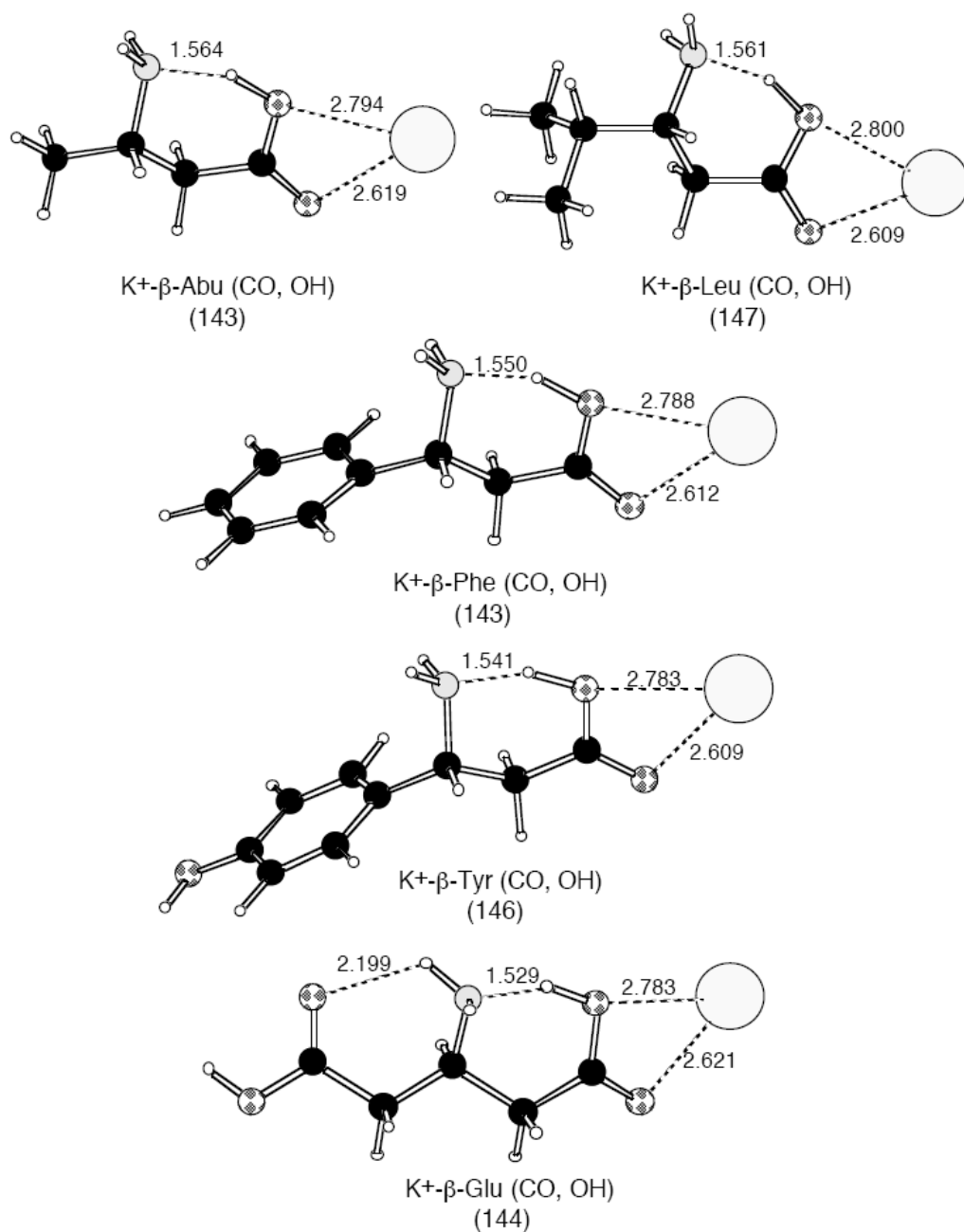


Figure 5.6 Optimized geometries of most stable potassium cationized β-Abu, β-Leu, β-Phe, β-Tyr and β-Glu complexes calculated at B3-LYP/6-311+G(3df,2p)//B3-LYP/6-31G+(D) level of theory

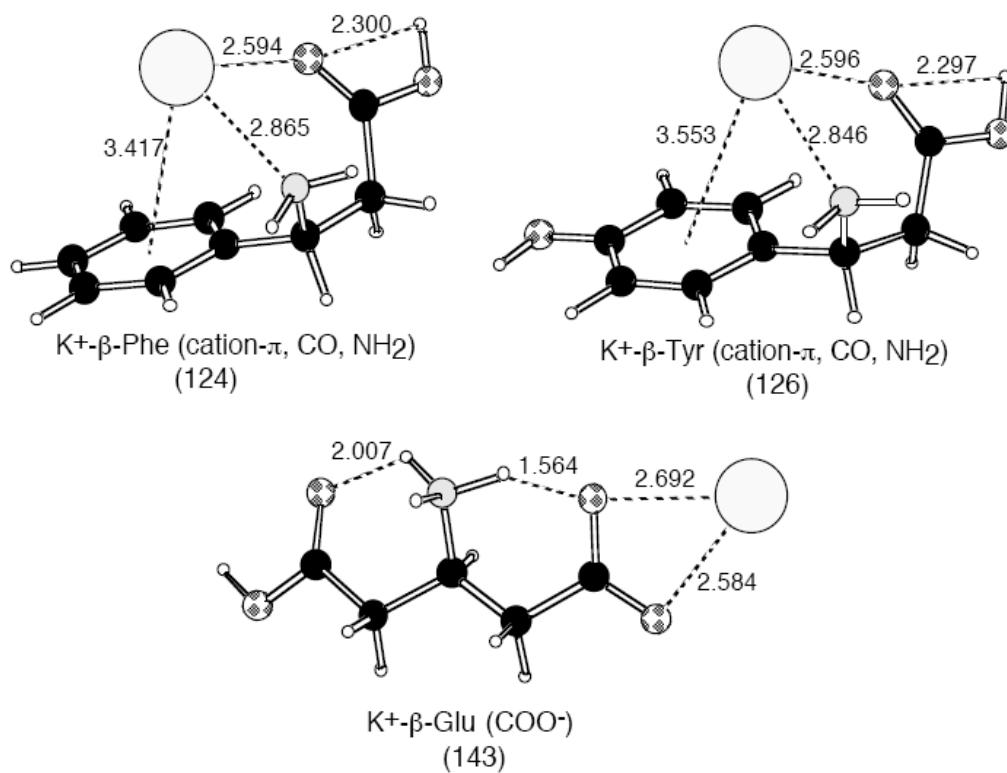


Figure 5.7 Optimized geometries of less stable potassium cationized β-Phe, β-Tyr and β-Glu complexes calculated at B3-LYP/6-311+G(3df,2p)//B3-LYP/6-31G+(D) level of theory

5.3 Conclusion

For the first time, the proton affinities and the potassium cation affinities of five biologically important β -amino acids have been determined by the mass spectrometric kinetic method. The H^+ affinities of the five β -amino acids (298K, in kJ mol^{-1}) are: β -Abu 942.0, β -Leu 955.6, β -Phe 948.0, β -Tyr 955.4 and β -Glu 951.5; while the K^+ affinities of the five β -amino acids (0K, in kJ mol^{-1}) are: β -Abu 134.7, β -Leu 138.3, β -Phe 137.6, β -Tyr 138.7 and β -Glu 141.5. The experimental values for both the H^+ affinities and K^+ affinities are found to be in very good agreement with theoretical affinities calculated at the B3-LYP/6-311+G(3df,2p)//B3-LYP/6-31G+(d) level with mean-absolute-deviation (MAD) of 3.1 and 6.4 kJ mol^{-1} only, respectively. The most stable proton binding site is found to be the same for both the α - and β -amino acids at the N-terminal nitrogen, while the charge-solvated **CS1** binding mode with K^+ bidentately bound to the carboxylic O=C and -OH sites is the most stable.

In the present study, we found both the proton affinity (PA) and potassium cation affinity of β -amino acids is generally larger than that of their α -analogues. The primary underlying cause is the same for the both findings: the ‘additional’ $-\text{CH}_2-$ unit in β -amino acids introduces greater flexibility in the main carbon chain of the β -amino acids, allowing more stabilizing intra-molecular hydrogen bonding patterns to be formed than their corresponding α -analogues.

The presence of the ‘additional’ $-\text{CH}_2-$ unit in β -amino acids also leads to subtle changes in the relative stabilities of the charge-solvated (CS) and zwitterionic (ZW) binding modes for β -amino acids with functionalized side chains when compared to its analogues. For α -Phe and α -Tyr, the tridentate **CS2** K^+ binding mode (cation- π , CO, NH_2) is the most stable, but it

becomes the least stable binding mode for β -Phe and β -Tyr due to greater structural deformation in the K^+ complexed form. The zwitterionic **ZW1** is the most stable K^+ binding mode for α -Glu, but it becomes marginally less stable than the charge-solvated tridentate **CS2** binding mode for β -Glu. This is due to the fact that a very stabilizing daisy chain of hydrogen bonding network involving a 7-membered ring adjacent to a 5-membered ring bonding configuration adjacent in the $K^+(\alpha\text{-Glu})$ complex is being replaced by a less stabilizing network involving two adjacent 6-membered ring bonding configurations in the case β -Glu. Thus, our theoretical studies indicate that the metal chelation properties of β -amino acids may differ from that of their α -analogues. However, metal chelation in real-life biological systems are affected by the 3-dimensional conformation of the peptides/proteins, and not just the intrinsic properties of the β -amino acid. Nevertheless, the basic information obtained in the present study may be relevant and useful in the rationalization of experimental observations on the biological activities of β -amino acids and β -peptides in future studies.

Chapter 6 Dissociation of Protonated β -Alanine and its Methyl Ester

6.1. Background

The mass spectral fragmentation behaviour of protonated peptides is dependent on the nature of their constituent amino acids. The characteristic fragmentation reactions of protonated amino acids, e.g. the preferred loss of small stable neutrals (H_2O , CO , NH_3 etc.), are often reflected in the MS/MS spectra of protonated α -peptides. Hence, detailed studies on the dissociation pathways of protonated amino acids are the building blocks towards a better understanding of the mass spectrometric fragmentation behaviour of the more complex peptide systems. For this reason, the dissociation pathways of the simplest protonated α -amino acids, glycine and alanine, have been extensively studied both experimentally [Rogalewic et al., 2000; van Dongen et al., 1996; Dookeran et al., 1996; Beranová, et al., 1995; Bouchoux et al., 2003; Kulik and Heerma, 1988] and theoretically. [O'Hair et al., 2000; Rogalewicz and Hoppilliard, 2000; Uggerud, 1997; van Dongen et al., 1996; Bouchoux et al., 2003]

On the other hand, there are very few reports on the fragmentation pathways of β -amino acids. Tsang and Harrison first reported on the major dissociation pathways of protonated β -alanine (β -ala) generated by chemical ionization in 1976, [Tsang and Harrison, 1976] but no further mechanistic study has been reported since then.

Given the growing recognition of the biochemical significance of β -amino acids and β -peptides in recent years, and the rapidly expanding use of tandem mass spectrometry in the determination of peptide sequence, it is timely to re-activate the mechanistic study on the

dissociation of the simplest β -amino acid, β -alanine. The aim of the present study is to elucidate the dissociation mechanisms and pathways of protonated β -alanine and its methyl ester by high level density functional theory (DFT) calculations, which is supplemented by experimental measurements on low energy collision induced dissociation (CID) carried out with an ion trap mass analyzer and a triple quadrupole tandem mass spectrometer. The focus of the present study is to find out the effect of the extra $-\text{CH}_2-$ unit in the main backbone of β -Ala / (β -Ala)OMe on the dissociation behaviours, such as the introduction of new pathways of fragmentation and products when compare to that of α -Ala / (α -Ala)OMe (refer to Figure 6.1).

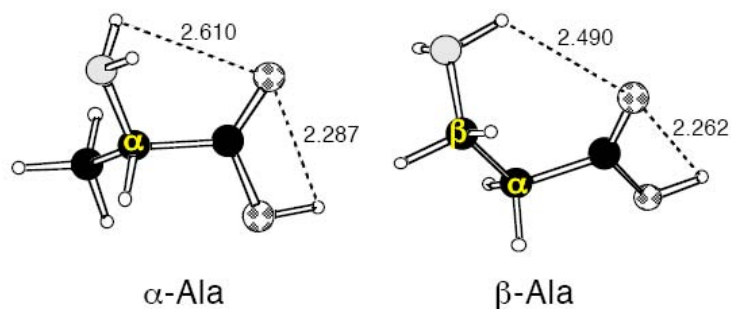


Figure 6.1 Optimized structure of α -/ β -alanine (at B3-LYP/6-31G(d) level)

6.2 Results and Discussion

6.2.1 Collision-induced Dissociation (CID) MS/MS Spectra of Protonated β -Alanine and its Methyl Ester

CID MS/MS spectra and the energy resolve MS/MS breakdown graph of protonated β -Alanine The dissociation of protonated β -alanine (β -Ala) and β -alanine methyl

ester (β -AlaOMe) are revealed by their ion trap and triple quadrupole mass spectrometer CID MS/MS spectra, which were obtained by Miss O. Y. Chan of our research group.

In the ion trap CID MS/MS spectrum of protonated β -alanine (Fig. 6.2(a)), $[(\beta\text{-Ala}) + \text{H}]^+$ (m/z 90), an intense peak at m/z 72 and two minor peaks at m/z 48 and m/z 30 are observed. The base peak is attributed to the loss of water (H_2O), leading to formation of a b_1 ion at m/z 72. The m/z 48 peak is due to the loss of ketene (CH_2CO); the consecutive loss of CH_2CO and H_2O leads to the fragment ion at m/z 30. The b_1 ions (m/z 72) are not observed in the CID MS/MS spectrum of protonated α -Ala [Rogalewic et al., 2000]. Comparison with the MS/MS spectrum of protonated β -lactam (m/z 72) reveals that the m/z 72 (b_1) fragment ion is likely to have the protonated β -lactams structure, which is much more stable than the corresponding three-membered ring ion if an analogous structure is formed from α -Ala. [Rode et al, 2002]

The ion trap energy resolved breakdown graph of protonated β -Ala, i.e., a plot of % relative fragment ion abundances versus the collision RF activation voltage (Fig. 6.3), shows that the predominant b_1 ion at m/z 72 is first formed with the lowest RF threshold voltage of 0.38 V, followed by the appearance of the m/z 48 and m/z 30 minor fragment ions at a higher RF activation voltage of 0.46 V. The b_1 ion remains to be the dominant fragment ion throughout the whole RF activation voltage range.

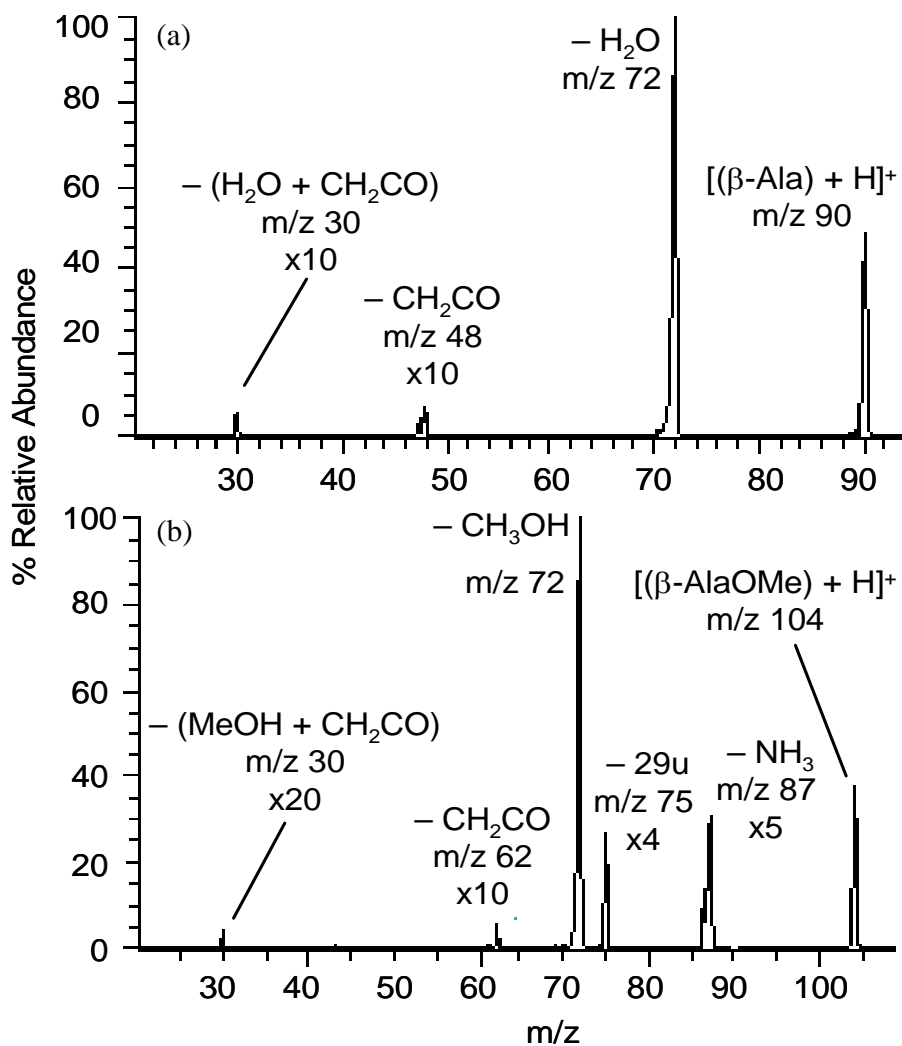


Figure 6.2 Ion trap MS/MS spectra of (a) protonated β -alanine, $[(\beta\text{-Ala}) + \text{H}]^+$ (m/z 90) obtained at a RF activation voltage (V_{p-p}) of 0.66 V, and (b) protonated β -alanine methyl ester, $[(\beta\text{-AlaOMe}) + \text{H}]^+$ (m/z 104) obtained at a RF activation voltage (V_{p-p}) of 0.74V (ion trap mass analyzer conditions: ‘low mass’ scan mode; ion activation time, 5 ms; main RF set for optimum trapping and detection of m/z 30; trap offset at -5 V, qz at 0.3)

Under the more energetic collisional activation conditions of a triple quadrupole tandem mass spectrometer, two additional fragment ions at m/z 45 and m/z 61 are newly observed: they are attributed to the consecutive loss of carbon monoxide and ammonia ($\text{CO} + \text{NH}_3$) and methanimine ($\text{NH}=\text{CH}_2$), respectively (Fig. 6.4(a)). These two fragment ions are likely to be derived from dissociation pathways with relatively higher critical energy barriers.

CID MS/MS spectra of protonated β -Alanine Methyl Ester

Like β -Ala, the ion trap

MS/MS spectrum of β -AlaOMe shows a major fragment ion (b_1) peak at m/z 72, a protonated β -lactam formed by loss of a methanol (CH_3OH) neutral (Fig. 6.2(b)). Two minor fragment ions arising from the loss of CH_2CO at m/z 62 and the consecutive loss of ($\text{CH}_2\text{CO} + \text{CH}_3\text{OH}$) at m/z 30, analogous to that of β -Ala, are also found.

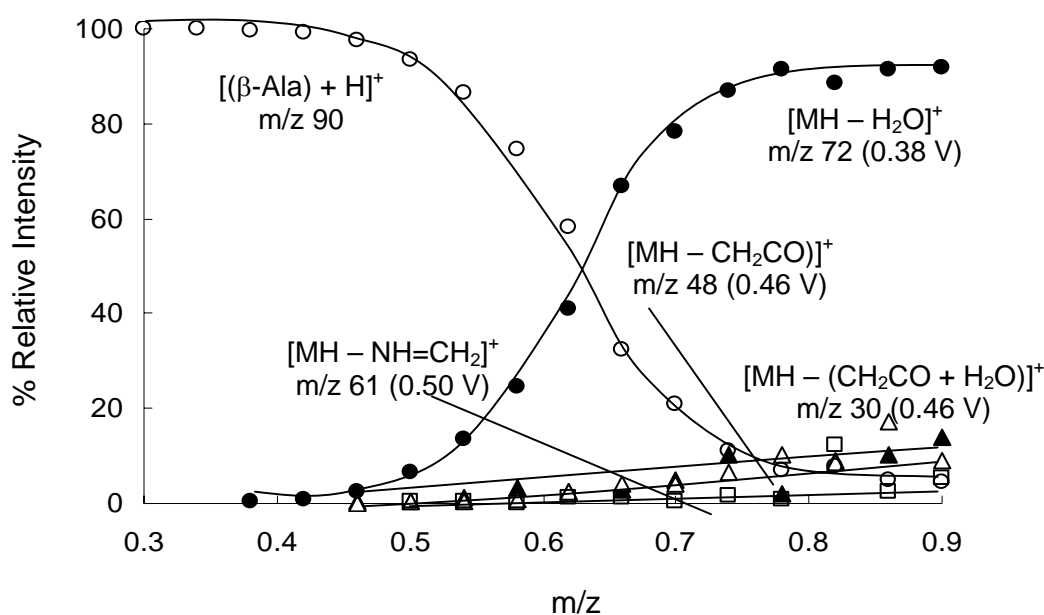


Figure 6.3 Ion trap energy resolved MS/MS breakdown graph of protonated β -alanine, $[(\beta\text{-Ala}) + \text{H}]^+$ (m/z 90) (Ion trap mass analyzer conditions: are same as those shown in Figure 6.2)

In addition, two minor fragment ions due to loss of ammonia (NH_3) at m/z 87 and methanimine ($\text{NH}=\text{CH}_2$) at m/z 75, which are not present in the ion trap MS/MS spectrum of protonated β -Ala, are also found. These two peaks are found in higher abundances in the CID MS/MS spectrum obtained with a triple quadrupole mass spectrometer, and are likely derived from dissociation pathways with higher critical energies.

Under the more energetic CID conditions of the triple quadrupole mass spectrometer, another fragment ion due to the loss of ($\text{CO} + \text{NH}_3$) from protonated (β -Ala)OMe appearing at m/z 59, which are absent in the corresponding ion trap MS/MS spectra, is observed (Fig. 6.4 (b)). The loss of ($\text{CO} + \text{NH}_3$) is likely to derive from another dissociation pathway of $[(\beta\text{-Ala)OMe} + \text{H}]^+$ with relatively higher critical energies.

The ion trap breakdown graph obtained for the dissociation of protonated (β -Ala)OMe, $[(\beta\text{-Ala)OMe} + \text{H}]^+$, was also obtained. As in the case of β -Ala, the dominant fragment ion at m/z 72 due to the loss of CH_3OH shows the lowest appearance threshold voltage at 0.38 V, followed by minor fragment ions due to loss of NH_3 (m/z 87, appearing at 0.46 V), $\text{NH}=\text{CH}_2$ (m/z 75, appearing at 0.46 V), CH_2CO (m/z 62, appearing at 0.50 V) and ($\text{CH}_2\text{CO} + \text{H}_2\text{O}$) (m/z 30, appearing at 0.50 V).

In summary, the experimentally observed major dissociation pathways (with relatively lower critical energy) for β -Ala / (β -Ala)OMe are due to (i) loss of H_2O / CH_3OH , (ii) loss of ketene (CH_2CO), and (iii) loss of ($\text{CH}_2\text{CO} + \text{H}_2\text{O}$ / CH_3OH). Dissociation pathways with higher critical energies involving (i) the loss of NH_3 , (ii) the loss of ($\text{NH}_3 + \text{CO}$), and (iii) the loss of $\text{NH}=\text{CH}_2$ are observed under more energetic CID conditions of a triple quadrupole mass spectrometer.

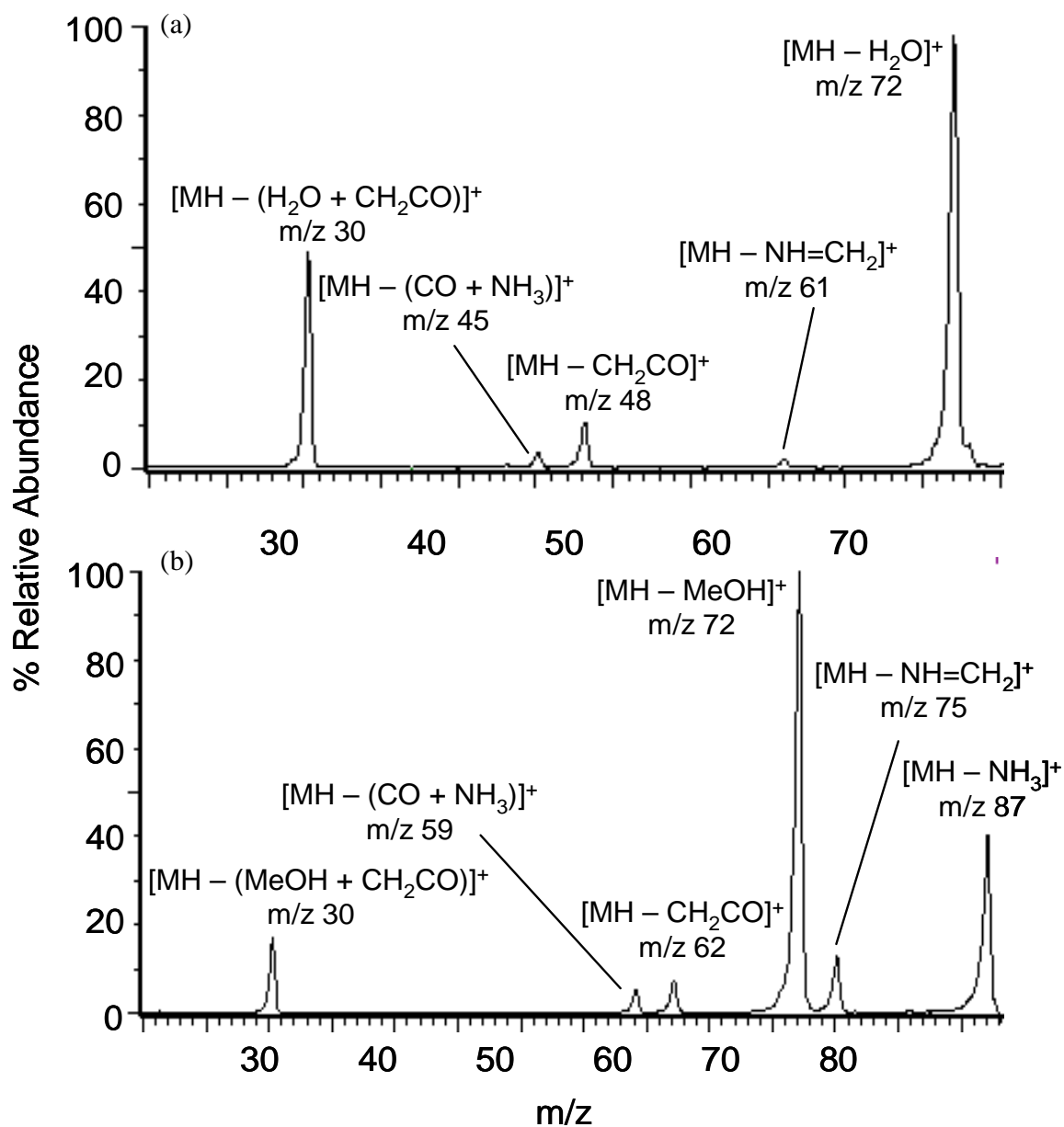


Figure 6.4 Triple quadrupole MS/MS spectra of (a) protonated β -alanine, $[(\beta\text{-Ala}) + \text{H}]^+$ (m/z 90), and (b) protonated β -alanine methyl ester, $[(\beta\text{-Ala})\text{OMe} + \text{H}]^+$ (m/z 104), obtained at a collision energy of 15 eV (at ~5 % attenuation of the precursor ion beam intensity)

6.2.2 Dissociation of Protonated β -Alanine and its Methyl Ester: Proposed Fragmentation Pathways and Theoretical Potential Energy Surface (PES)

In this section, high level density functional theory (DFT) calculations on the energetics of plausible dissociation pathways of protonated β -Alanine and its methyl esters (β -Ala and β -AlaOMe) were carried out to rationalize the experimental observations as described in the previous section. The geometries of all structures involved in the dissociation pathways (Figure 6.6) were fully optimized at the B3-LYP/6-31G(d) level, with single point energy calculations performed at the B3-LYP/6-311+G(3df,2p) level. At this level of theoretical calculation, the proton affinity for β -Ala is found to be 925 kJ mol^{-1} , in excellent agreement with the experimental value of 928 kJ mol^{-1} reported by Hahn and Wesdemiotis [Hahn and Wesdemiotis, 2003]. This suggests that the DFT protocol adopted in the present study is reliable and able to provide reliable information on the energetics of dissociation of protonated β -Ala and (β -Ala)OMe, consistent with experimental observations.

Previous studies have shown that for dissociation pathways involving loosely bound ion-neutral complexes as transition structures (e.g. species **TS6a** in Fig. 6.5) [Aribi et al, 2003; Balta et al., 2003; Grewal et al., 2004], and reactions leading to cyclized products in the present study (e.g. species **5a** and **6a'** in Fig. 6.7), entropic effects are important in affecting the occurrence (e.g., appearance threshold voltages) [Klassen and Kebarle, 1997; Aribi et al., 2003] and the rate of dissociations (i.e., relative fragment ion abundances). [Balta et al., 2003] In other words, the Gibbs free energy changes of the reactions at 298K, ΔG_{298} , which includes the consideration of the entropic factor in the $T\Delta S_{298}$ term, may be a more accurate indication of both the energetic and entropic requirements of the dissociation reactions. Hence, we

have included the calculation of ΔG_{298} and ΔS_{298} values of the highest energy barriers of the proposed pathways for dissociation of $[(\beta\text{-Ala})/(\beta\text{-Ala})\text{OMe} + \text{H}]^+$. In the present study, the fragmentation mechanism leading to the loss of H_2O / CH_3OH , CH_2CO and $(\text{CH}_2\text{CO} + \text{H}_2\text{O}/\text{CH}_3\text{OH})$, NH_3 , $(\text{NH}_3 + \text{CO})$ and $\text{NH}=\text{CH}_2$ from protonated $(\beta\text{-Ala})/(\beta\text{-Ala})\text{OMe}$ were explored and elucidated by DFT calculations. The theoretical energy barriers for the proposed pathways are compared to the experimentally observed appearance threshold voltages in Table 6.1. Energetic and free energy information (ΔH_0 , ΔH_{298} and ΔG_{298} with respect to the most stable protonated $\beta\text{-Ala}/(\beta\text{-Ala})\text{OMe}$ species **1a**/**1b**) for other key transition structures, stable intermediates and products of the proposed dissociation pathways are summarized in Table 6.2. In the following discussion, notations **1a**, **2a** etc. refer to stable intermediates (minima) on the dissociation potential energy surface (PES) of $[(\beta\text{-Ala}) + \text{H}]^+$ (Fig. 6.7), while labels such as **TS2a**, **TS4a** etc. denote the various transition structures (TS) between the minima. By replacing **a** with **b**, similar notations are used to denote the various structures on the PES of $[(\beta\text{-Ala})\text{OMe} + \text{H}]^+$.

Table 6.1 The relative enthalpies (ΔH_0 , ΔH_{298} at 0K and 298K), Gibbs free energies (ΔG_{298} at 298K, in kJ mol^{-1}) and entropies (ΔS_{298} at 298K, in J mol^{-1}) of the highest energy barriers for the loss of small neutrals on the $[(\beta\text{-Ala}) / (\beta\text{-Ala})\text{OMe} + \text{H}]^+$ potential energy surface.^a

neutral loss	$[(\beta\text{-Ala}) + \text{H}]^+$				$[(\beta\text{Ala})\text{OMe} + \text{H}]^+$			
	ΔH_0	ΔH_{298}	ΔG_{298}	ΔS_{298}	ΔH_0	ΔH_{298}	ΔG_{298}	ΔS_{298}
$\text{H}_2\text{O} / \text{CH}_3\text{OH}^b$	170 (<i>0.38</i>)	177	129	161	201 (<i>0.38</i>)	203	153	168
CH_2CO^c	163 (<i>0.46</i>)	167	158	30	182 (<i>0.50</i>)	185	177	27
$(\text{CH}_2\text{CO} + \text{H}_2\text{O} / \text{CH}_3\text{OH})^d$	234 (<i>0.46</i>)	244	144	336	265 (<i>0.50</i>)	272	167	352
NH_3	264 ^e (<i>-^f</i>)	271	253	60	256 (<i>0.46</i>)	263	242	70
$(\text{CO} + \text{NH}_3)^g$	485 (<i>-^f</i>)	496	466	101	506 (<i>-^f</i>)	517	489	94
NHCH_2^h	471 (<i>-^f</i>)	472	470	7	470 (<i>-^f</i>)	472	467	17

^a Theoretical calculated ΔH_0 , ΔH_{298} , ΔG_{298} and ΔS_{298} values are based on the potential energy surface at 0K shown in Figure 6.6 and 6.7. The appearance threshold energy (in V) for observation of the corresponding fragment ions under ion trap CID conditions is shown in italics in parenthesis.

^b Formation of protonated β -lactam, structure **6a'**/(**6b'**).

^c Via transition structure **TS4a**/(**TS4b**).

^d Formation of methan-iminium ion, structure **10a**/(**10b**)

^e Via transition structure **TS12a**/(**TS12b**) of Pathway 1 (Fig. 6.7).

^f Not observed under ion trap CID conditions, but observed under triple quadrupole CID conditions.

^g Formation of oxiranium ion **19a**/**19b** via transition structure **TS15a**/(**TS15b**).

^h Via transition structure **TS23a**/(**TS23b**).

Table 6.2 The relative enthalpies at 0K (ΔH_0) and gibbs free energies at 298K (ΔG_{298}), in kJ mol^{-1} , with respect to species **1a (1b)** for protonated β -Ala and (β -AlaOMe), respectively

Species	Energetics	
	ΔH_0	ΔG_{298}
TS2a (TS2b)	44 (49)	44 (48)
3a (3b)	30 (33)	28 (32)
TS4a (TS4b)	163 (182)	158 (177)
5a (5b)	108 (128)	100 (116)
TS6a (TS6b)	159 (185)	148 (171)
7a (7b)	140 (161)	124 (138)
8a + CH₂CO (8b + CH₂CO)	163 (181)	105 (120)
9a + H₂O (9b + CH₃OH)	200 (230)	147 (171)
10a + CH₂CO + H₂O (10b + CH₂CO + CH₃OH)	234 (265)	144 (167)
11a (11b)	50 (54)	44 (47)
TS12a (TS12b)	264 (256)	253 (242)
13a (13b)	262 (197)	245 (184)
14a + NH₃ (14b + NH₃)	312 (230)	264 (185)

TS15a (TS15b)	485 (506)	466 (489)
16a (16b)	273 (283)	250 (255)
17a + CO (17b + CO)	310 (288)	256 (234)
18a + NH₃ (18b + NH₃)	312 (321)	260 (263)
19a + CO + NH₃	354 (327)	269 (242)
(19b + CO + NH₃)		
6a' + H₂O	170 (201)	129 (153)
(6b' + CH₃OH)		
TS11a' (TS11b')	268 (286)	262 (279)
12a' (12b')	164 (157)	165 (144)
13a' + NH₃ (13b' + NH₃)	210 (189)	167 (144)
20a (20b)	24 (34)	24 (34)
22a (22b)	121 (116)	119 (113)
TS23a (TS23b)	471 (470)	470 (467)
24a (24b)	141 (150)	140 (149)
TS25a (TS25b)	333 (335)	324 (327)
26a (26b)	115 (127)	114 (126)
27a + NHCH₂	312 (290)	259 (236)
(27b + NHCH₂)		

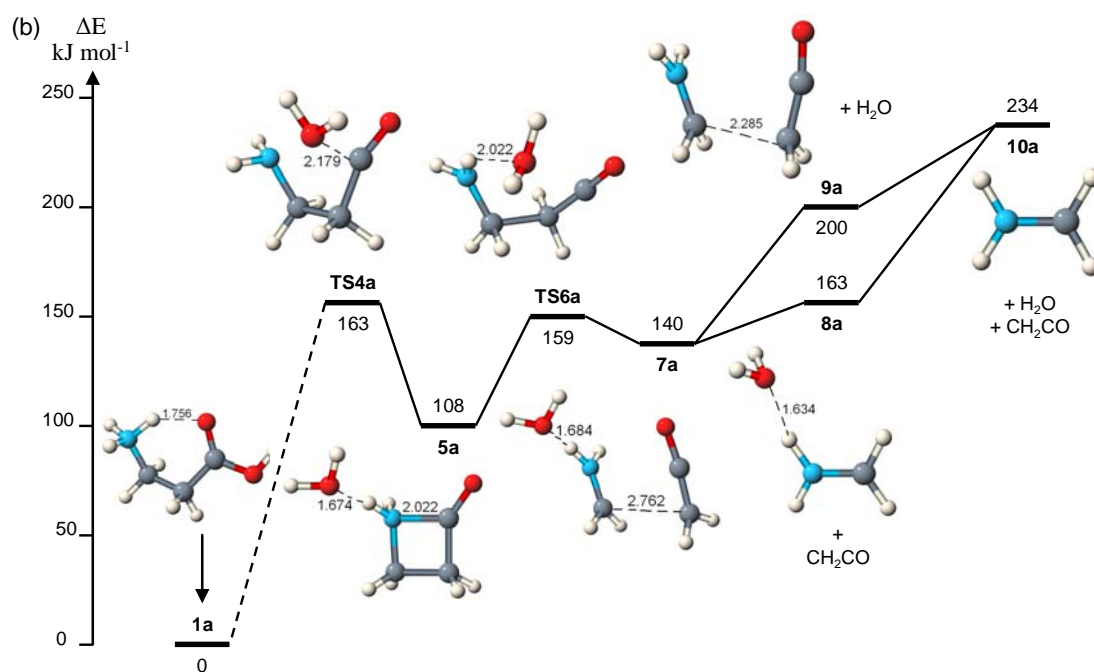
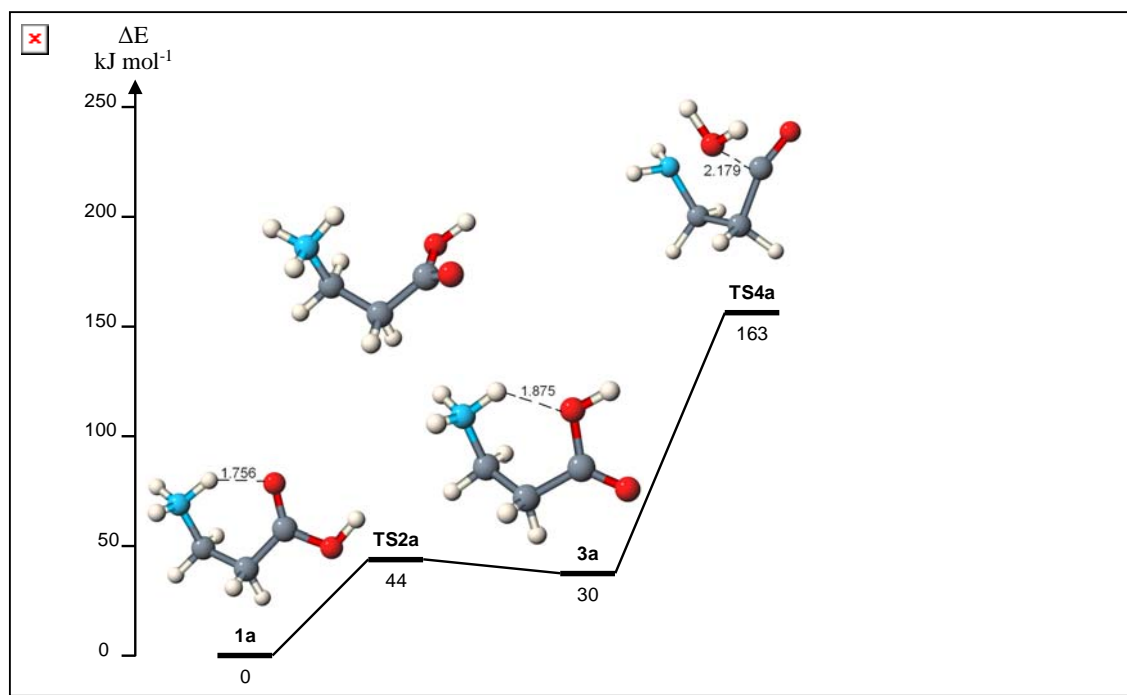


Figure 6.5 Potential energy surface (PES) of the dissociation of $[(\beta\text{-Ala})/(\beta\text{-Ala})\text{OMe} + \text{H}]^+$, leading to loss of (a) H_2O , (b) CH_2CO and $(\text{H}_2\text{O} + \text{CH}_2\text{CO})$ at 0K, calculated at the B3LYP/6-311+G(3df,2p)//B3LYP/6-31G+ level

Proposed pathway for formation of b_1 ion protonated (β -lactam ring) by loss of H_2O/CH_3OH

The loss of H_2O/CH_3OH from $[(\beta\text{-Ala})/[(\beta\text{-Ala})\text{OMe} + H]^+]$ leads to the predominant formation of protonated β -lactam (m/z 72), the only high intensity and base peak in the ion trap MS/MS spectra (Fig. 6.2) over the entire range of collision energies (Fig. 6.3). For protonated β -Ala, the most stable species (**1a** in Fig. 6.5(a)), with the proton initially attached to the nitrogen of the amino group ($-\text{NH}_3^+$), goes through a C-C bond rotation to yield species **3a**, so that the hydroxyl oxygen (O_H) of the $-\text{COOH}$ group is positioned to accept the proton from the amino ($-\text{NH}_3^+$) group. Then, proton transfer proceeds via **TS4a** to form a 2-oxoazetidinium... H_2O ion-neutral complex (species **5a**), which could easily lose H_2O to form a stable 4-membered ring protonated β -lactam, or the 2-oxoazetidinium ion (species **6a'**). The energy barrier for this process, i.e., the enthalpy change between **1a** and (**6a'** + H_2O) at 0K, is 170 kJ mol^{-1} , is about 7 kJ mol^{-1} higher in energy than the barrier of the transition species **TS4a**.

Under ion trap CID conditions, no further dissociation of protonated β -lactam was observed. According to the study of Rode and co-workers, the β -lactam ring and its derivatives are thermodynamically stable at 0K [Rode et al., 2002]. As a result, species **6a'** is unlikely to undergo further dissociation, such as the loss of CO to form the a_1 ion. Our single point energy calculation carried out at the same level of theory also showed that the barrier for the loss of CO from species **6a'** is associated with a high energy barrier relative to the species **1a** ($\sim 312 \text{ kJ/mol}$) (Scheme 6.1), indicating that the loss of CO is not feasible energetically. On the other hand, a similar mechanism for the loss of H_2O is found to be not feasible in the case of $[(\alpha\text{-Ala}) + H]^+$, the formation of a three-membered alpha-lactam ring from $[\alpha\text{-Ala} + H]^+$ is not as stable as species **6a'** (with $\sim 60 \text{ kJ mol}^{-1}$ higher energy barrier) according to our calculation results.

(0.38 V) < -CH₂CO (0.46 V) ~ -(CH₂CO + H₂O) (0.46 V). Furthermore, the fragment ion due to loss of H₂O, [(β-Ala) + H - H₂O]⁺ (m/z 72), is the only predominant ion in the MS/MS spectrum, while the fragment ion due to loss of CH₂CO is very low in ion intensity (< 5 % of total fragment ion intensity) throughout the entire range of ion trap collision energies. A similar reversal of trends is observed in the corresponding loss of CH₂CO, CH₃OH and (CH₂CO + CH₃OH) from [(β-Ala)OMe + H]⁺ (Table 6.1). Such apparent discrepancies could be resolved if entropic effects on dissociation rates as a function of internal energy of the dissociating [(β-Ala) + H]⁺ ions (assumed to increase with increasing collision energy), and associated kinetic shift effects on appearance threshold voltages are taken into consideration. Firstly, it is very likely that the loss of CH₂CO pathway shows a larger kinetic shift than the loss of H₂O pathway, so that the observed appearance threshold voltage for loss of H₂O (0.38 V) becomes lower than that of CH₂CO (0.46 V) for [(β-Ala) + H]⁺. The magnitude of the kinetic shifts is related to the free energy changes in the rate-determining step of the two competitive processes, as indicated by the ΔG₂₉₈ values for (**6a'** + H₂O) at 129 kJ mol⁻¹ and **TS4a** at 144 kJ mol⁻¹ in the case of [(β-Ala) + H]⁺, favoring the loss of H₂O over the loss of CH₂CO. That means once the energy threshold for loss of H₂O is exceeded, it becomes the entropically (kinetically) favored dissociation channel (ΔS₂₉₈ = 64 J mol⁻¹ K⁻¹), with the rate constant k(E) rising faster with increasing internal energy than the loss of CH₂CO pathway (ΔS₂₉₈ = 30 J mol⁻¹ K⁻¹ for **TS4a**).

As the loss of H₂O pathway is associated with a more steep rising k(E) versus E curve (refer to Fig. 2.5), a small kinetic shift and a lower appearance threshold voltage was observed than the loss of CH₂CO pathway (Fig. 6.5). [Levsen, 1978; De Hoffmann and Stroobant, 2001]. As the loss of H₂O is kinetically favored with a faster dissociation rate constant, the protonated β-lactam fragment product ion (m/z 72) becomes the dominant

peak in the ion trap MS/MS spectrum of $[(\beta\text{-Ala}) + \text{H}]^+$, while the peak due to loss of CH_2CO appears with much lower intensity at m/z 48 (Fig. 6.2(a)). Similarly, the favored loss of CH_3OH over the loss of CH_2OH from $[(\beta\text{-Ala})\text{OMe} + \text{H}]^+$ appearing at a lower threshold voltage (refer to table 6.1, 0.38V versus 0.5V, respectively) could be explained by the same rationale. As shown in Fig. 6.5 (b), the loss of CH_2CO is followed by the facile loss of $\text{H}_2\text{O}/\text{CH}_3\text{OH}$ from the loosely bound $\text{H}_2\text{O}/\text{CH}_3\text{OH}\dots$ methaniminium ion-neutral complex (species **8a/8b**), yielding the methaniminium ion **10a/10b** at the same appearance threshold voltage (0.46/0.50 V) as **8a/8b** (Table 6.1). Indeed, our theoretical results show that the sequential loss of $\text{H}_2\text{O}/\text{CH}_3\text{OH}$ from **8a/8b** is very much entropically favored (as indicated by the exceptionally large ΔS_{298} value of 336/352 $\text{Jmol}^{-1}\text{K}^{-1}$ for **(10a + CH₂CO + H₂O/CH₃OH)**), so that the dissociation reaction could proceed with very little kinetic shift and virtually no extra input of collisional energy for the observed appearance of the reaction (Table 6.1 and Fig. 6.3). As the $\text{H}_2\text{O}/\text{CH}_3\text{OH}\dots$ methaniminium fragment ions (species **8a/8b**) are formed in very low abundance, it follows that the subsequent methaniminium fragment ions (species **10a/10b**) formed by sequential loss of ($\text{H}_2\text{O}/\text{CH}_3\text{OH}$) are likely of low intensity (Fig. 6.2(a) and 6.2(b)). A similar approach invoking the entropic effect has been used previously to rationalize the dominant formation of the y_1 ion over the b_2 ion in the dissociation of protonated diglycine. [Balta et al., 2003] Eventually, more elaborate RRKM calculations on the rate constant $k(E)$ – internal energy (E) dependence of these dissociating pathways are required to verify our proposed rationalization.

Proposed pathways for loss of NH_3 , ($\text{NH}_3 + \text{CO}$) and $\text{NH}=\text{CH}_2$ The loss of NH_3 , ($\text{NH}_3 + \text{CO}$) and $\text{NH}=\text{CH}_2$ from $[(\beta\text{-Ala}) + \text{H}]^+ / [(\beta\text{-Ala})\text{OMe} + \text{H}]^+$ are likely pathways with higher dissociation critical energies when compared to the loss of H_2O and / or CH_2CO pathways. Indeed, we found two possible pathways of similar but high critical

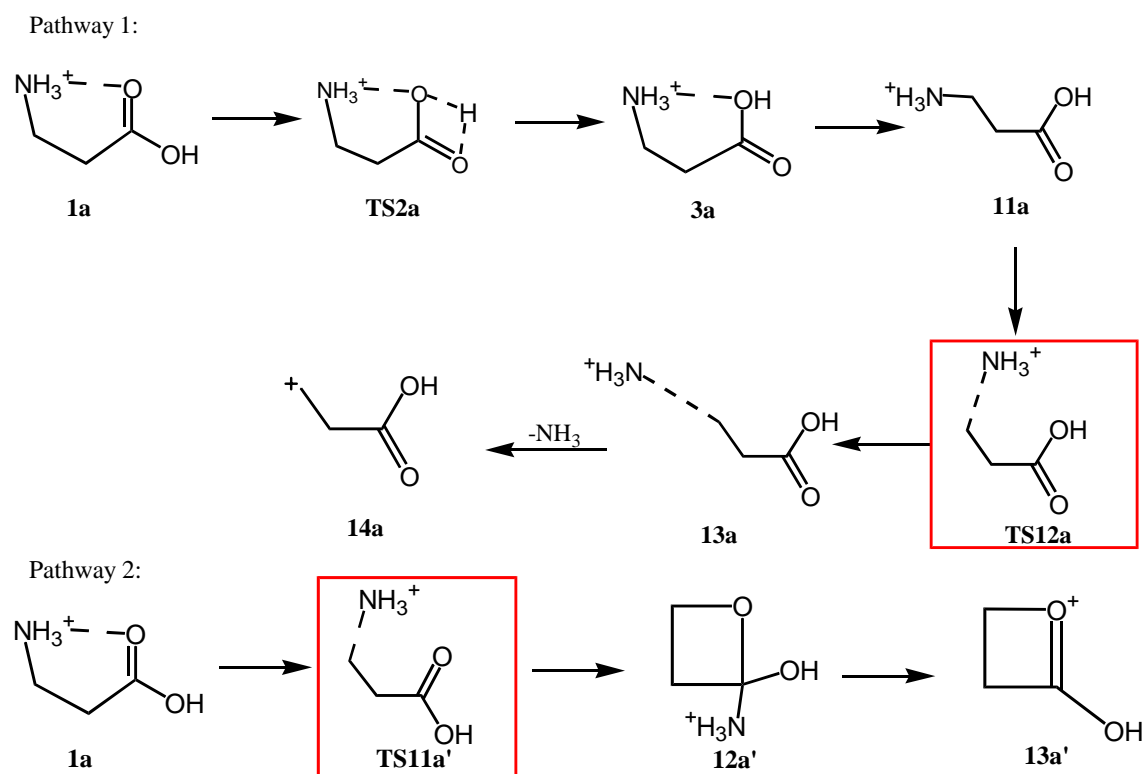
energies for loss of NH₃ from [(β-Ala) + H]⁺; the stable intermediates and transition structures involved are shown in **Scheme 6.2**. The first pathway (Pathway 1) starts from species **3a** (a conformer of protonated β-Ala with the proton attached to the –NH₂ site) with a bond rotation so that the ammonium (–NH₃⁺) group is *trans* to the carbonyl (C=O) group in species **11a**. Lengthening of the C–NH₃⁺ bond (~2.02 Å) yields the energy barrier **TS12a** (264 kJ mol⁻¹ at 0K with reference to species **1a**) and the species **13a** ion-neutral complex, with the ammonia molecule weakly attached to the cation fragment (HOOCCH₂CH₂⁺). This is followed by facile loss of NH₃ to yield the fragment (product) ion **14a** (a carbocation of propionic acid, m/z 73).

Comparing Pathway 1 to Pathway 2, Pathway 1 is found to have a slightly lower energy (264 versus 268 kJ mol⁻¹) and more favored reaction entropy ((ΔS₂₉₈ = 70 versus 34 J mol⁻¹ K⁻¹) than Pathway 2. Hence, it is likely that Pathway 1 is the major pathway contributing to the loss of NH₃ from [(β-Ala) + H]⁺.

Unlike β-Ala, protonated (β-Ala)OMe showed a loss of NH₃ peak even under the less energetic CID conditions of the ion trap mass analyzer (Fig. 6.2(b)). This could be attributed to the enhanced competitiveness of Pathway 1 relative to the loss of CH₃OH /CH₂CO pathways for [(β-Ala)OMe + H]⁺; the difference in critical energies (ΔH₀ at 0K) is reduced from 94/104 kJ mol⁻¹ of β-Ala to 55/74 kJ mol⁻¹ of (β-Ala)OMe (Table 6.1).

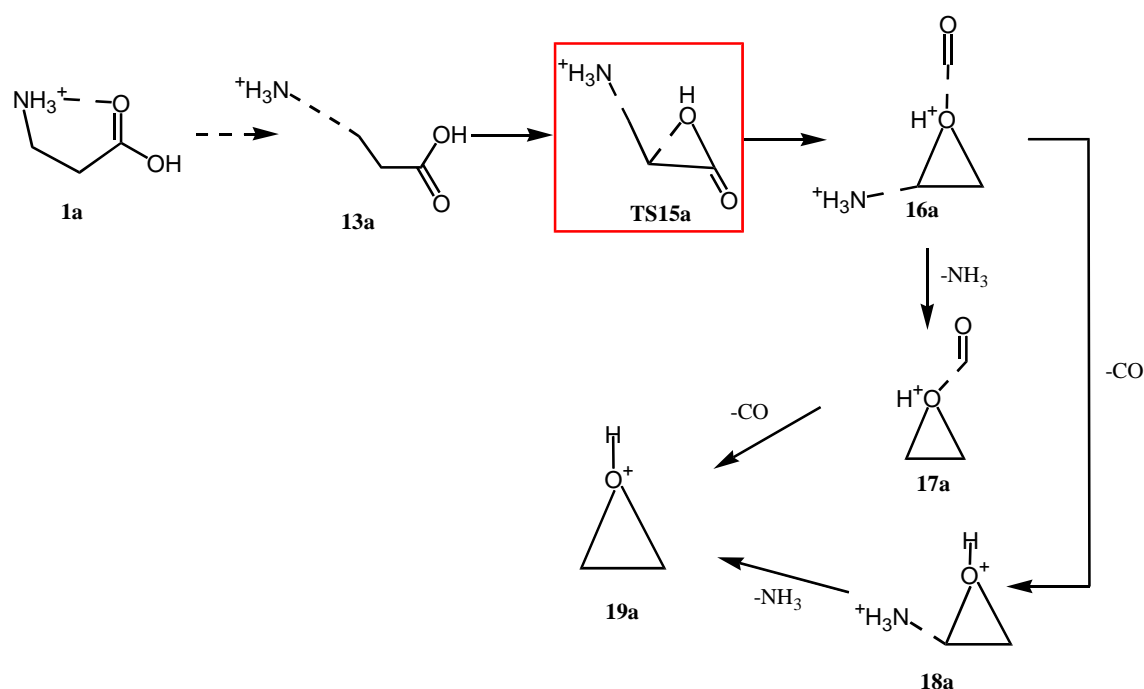
For loss of (NH₃ + CO) from [(β-Ala) + H]⁺, the proposed pathway is shown in **Scheme 6.3**. Starting from species **13a**, a high energy barrier **TS15a** (485 kJ mol⁻¹ at 0K) was formed when the hydroxyl oxygen (O_H) attacks the -CH₂- group to form a loosely-bound 3-membered ring intermediate **16a**, a NH₃... oxiranium...CO ion-neutral complex. This is followed by sequential loss of NH₃ and CO, or CO and NH₃, from species **16a** to yield firstly (**17a** + CO) or (**18a** + NH₃), respectively, and finally species **19a** (an

oxiranium ion) + NH₃ + CO. Among the proposed dissociation pathways investigated for [(β-Ala) + H]⁺ / [(β-Ala)OMe + H]⁺, the loss of (NH₃ + CO) with energy barrier **TS15a**/(**TS15b**) shows the highest critical energy of 485/506 kJ mol⁻¹. This is followed by a second hydrogen transfer from the amino nitrogen to the carboxylic carbon to form a 5-membered ring with energy barrier **TS23a** (471 kJ mol⁻¹ at 0K). A further C-C bond lengthening leads to formation of a NH=CH₂.....ethanediol cation ion-neutral complex **24a**. The third hydrogen transfer takes place, leading to the formation of a stable ion-neutral complex **26a**, followed by facile loss of NH=CH₂ (methanimine) to yield the final fragment (product) ion **27a**, an ethanediol carbocation with resonance stabilization of the positive charge around the carboxylic functional group.

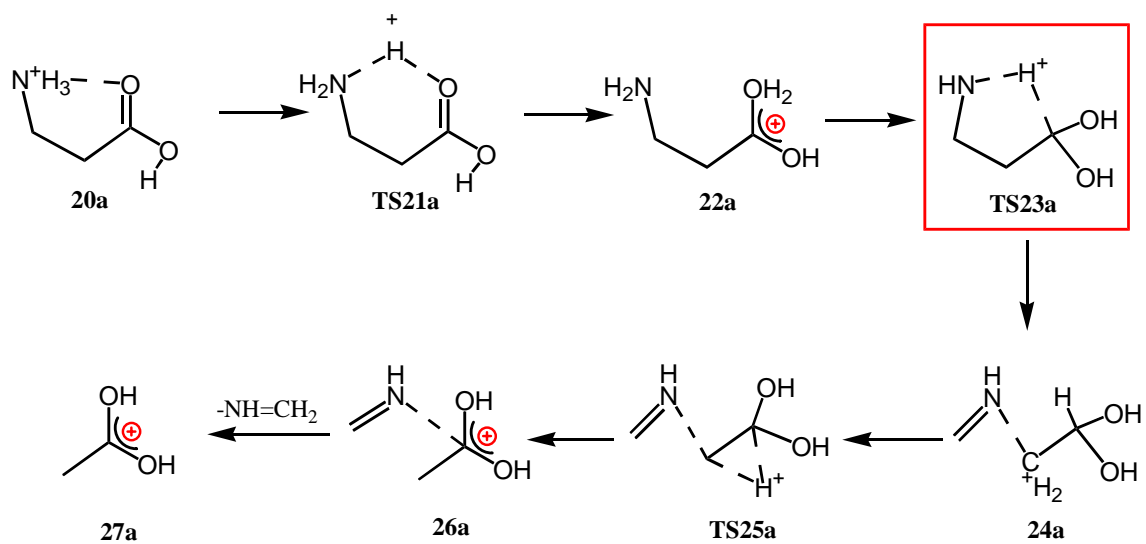


Scheme 6.2 Loss of NH₃ from [(β-Ala) + H]⁺ (Energy barriers are indicated by enclosing in a square box)

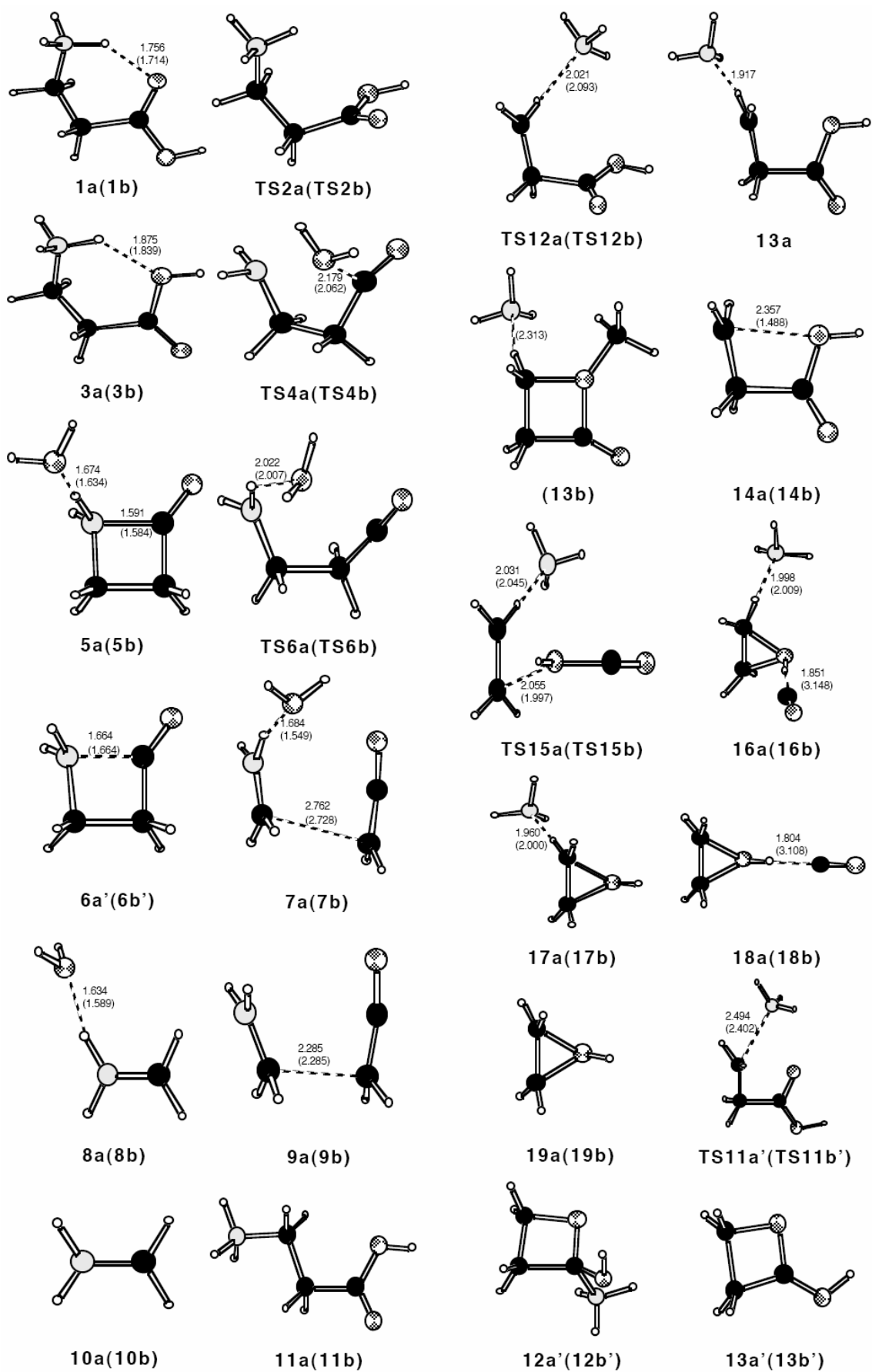
A proposed pathway for the loss of $\text{NH}=\text{CH}_2$ from $[(\beta\text{-Ala}) + \text{H}]^+ / [(\beta\text{-Ala})\text{OMe} + \text{H}]^+$ is shown in **Scheme 6.4**. Starting from the most stable binding mode of $[(\beta\text{-Ala}) + \text{H}]^+$ (species **20a**), a proton is transferred from the amino ($-\text{NH}_3^+$) group to a carboxylic oxygen ($\text{C}=\text{O}$), yielding the 3-aminopropane-1,1-diol (**22a**) carbocation with resonance stabilization of the positive charge around the carboxylic functional group. The loss of $\text{NH}=\text{CH}_2$ (methanimine) from protonated β -peptides has been reported and reviewed [Nguyen et al., 1996; Tang et al., 2004; El Aribi et al., 2004]; however, the energetics of the proposed pathway for $[(\beta\text{-Ala}) + \text{H}]^+ / [(\beta\text{-Ala})\text{OMe} + \text{H}]^+$ is first found in the present study.



Scheme 6.3 Loss of $(\text{NH}_3 + \text{CO})$ from $[(\beta\text{-Ala}) + \text{H}]^+$ (Energy barriers are indicated by enclosing in a square box)



Scheme 6.4 Loss of $\text{NH}=\text{CH}_2$ from $[(\beta\text{-Ala}) + \text{H}]^+$ (Energy barrier is indicated by enclosing in a square box)



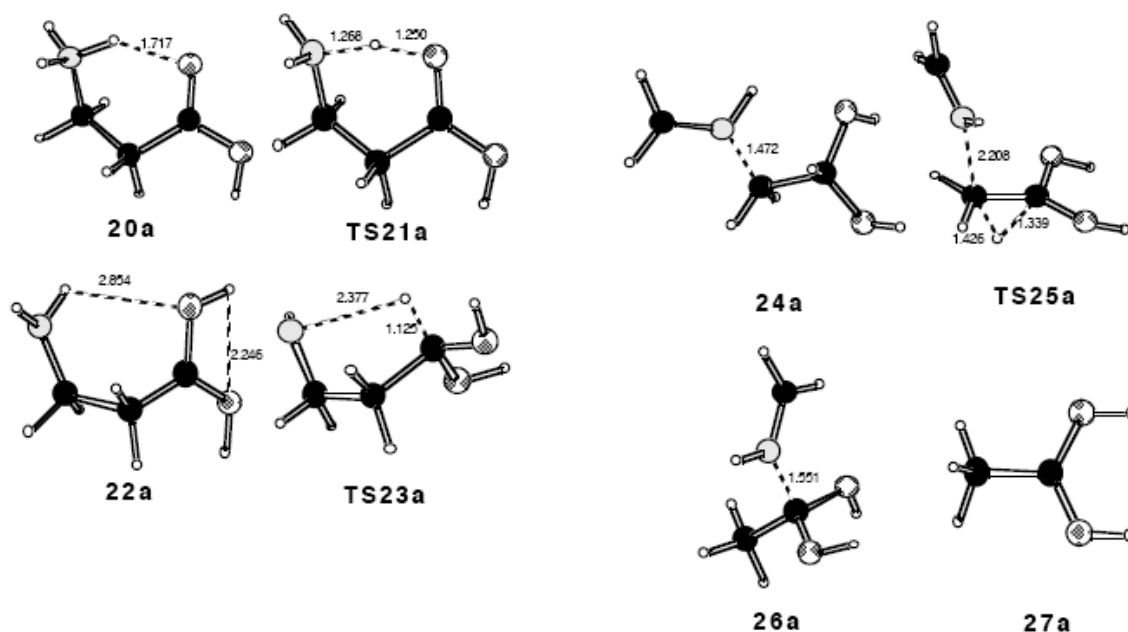


Figure 6.6 Optimized structures (at B3LYP/6-31G+ level) for the various species on the $[\beta\text{-Ala} + \text{H}]^+$ and $([\beta\text{-AlaOMe} + \text{H}]^+)$ dissociation potential energy surface. All species are stable intermediates / products, except those begin with “TS”, which are transition structures

6.3 Conclusion

The dissociations of protonated $\beta\text{-Ala}$ and $(\beta\text{-Ala})\text{OMe}$ are found to be very different from that of $\alpha\text{-Ala}$ and $(\alpha\text{-Ala})\text{OMe}$. The major dissociation pathways with relatively low critical energies are due to loss of H_2O , CH_2CO and $(\text{CH}_2\text{CO} + \text{H}_2\text{O})$, while the pathways leading to the loss of $\text{NH}=\text{CH}_2$, NH_3 and $(\text{NH}_3 + \text{CO})$ are found to have relatively higher critical energies. The mechanisms and energetics of the dissociation pathways are found by high level density functional theory calculations, and are consistent with experimental observations.

The dissociation pathways found for protonated β -Ala and (β -Ala)OMe are influenced significantly by the presence of the “extra” $-\text{CH}_2-$ unit separating the N-terminal $-\text{NH}_2$ group and the C-terminal $-\text{COOH}$ group of β -Ala. For example, the loss of H_2O / CH_3OH leading to the predominant formation of the protonated β -lactam fragment ion at m/z 72 is due to the stability of the 4-membered β -lactam ring, which could not be formed in the case of protonated α -Ala /(α -Ala)OMe due to the absence of the extra $-\text{CH}_2-$ unit. The pathways leading to the loss of CH_2CO and $\text{NH}=\text{CH}_2$ are also directly related to the presence of the “extra” $-\text{CH}_2-$ unit in β -ala.

Aside from the loss of stable neutrals not found in the dissociation of α -Ala /(α -Ala)OMe, the presence of the extra $-\text{CH}_2-$ unit also affects the relative stabilities of intermediates and transitional structures of the newly found pathways. Our theoretical study also found that free energy changes (as indicated by the calculated ΔG_{298}) can be suitably applied to rationalize the appearance threshold voltages and relative abundances of different fragment ions in the MS/MS spectrum of protonated β -ala and (β -ala)OMe. The fragmentation mechanisms of (β -ala)OMe are similar to that of β -ala except the relative energy barriers for loss of different neutrals are ‘reduced’ or ‘compressed’. This could explain why the higher energy pathways arising from the loss of $\text{NH}=\text{CH}_2$ and NH_3 are observed even under mild CID conditions of the ion trap mass analyzer.

As loss of small neutrals is commonly found in the MS/MS spectra of protonated small peptides, it is likely that the loss of some of these characteristic neutrals could be found in the MS/MS spectra of protonated small β -peptides. Thus the findings in the present chapter could provide the basis for understanding analogous fragment ion peaks in the MS/MS spectra of small β -peptides.

Chapter 7 Proton Affinities and Fragmentation Mechanism of Selected Model and Biologically Significant β -Dipeptides

7.1 Background

Model dipeptides, such as GlyAla, AlaGly and AlaAla, are the simplest molecular system containing a peptide bond. They are the starting point and link to the understanding of the binding of proton (H^+) to larger peptides. As a result, the proton affinities of some model di-/tri-peptides containing different α -amino acids have been experimentally determined [McKiernan et al., 1994; Cassady et al., 1995; Ewing et al., 1996; Bouchoux et al., 2003], theoretically studied, [Cassady et al., 1995; Ewing et al., 1996] and reviewed. [Harrison, 1997]

To our knowledge, the proton affinities (PA) of model β -dipeptides containing β -alanine (β -Ala) have not been reported in the literature. Following the study of proton (H^+) binding modes and affinities of selected β -amino acids in Chapter 5, it would be of fundamental interest to investigate whether the intrinsic proton binding properties of β -amino acids are reflected and extended to β -dipeptide systems.

Many studies on mass spectrometric fragmentation mechanisms of protonated peptides were first carried out with simple protonated model dipeptides because complications arising from the side chain functional groups can be minimized. The behavior of “real life” peptides could then be interpreted as consistency and/or deviations from these model peptides. [Paizs and Shuai, 2005]

There are very few reports on the fragmentation mechanisms of β -dipeptides. Talaty et al. recently reported the CID – MS/MS spectrum of linear tetrapeptide with a β -Ala in different position of the peptide.[Talaty et al., 2006] They found that for β -Ala located at N-terminus of the tetrapeptide, b_i ions and y_i are preferably formed with lesser collisional activation energies. However, the dissociation of β -peptides with β -Ala at the C-terminus, and the energetics of the dissociation pathways, remain unexplored.

In the present study, we aimed to determine the proton affinities of selected model β -dipeptides containing β -Ala by the mass spectrometric kinetic method. A biologically important β -dipeptide, carnosine ((β -Ala)His), was included in the study. High level density functional theory calculations was carried out to find out the most stable proton (H^+) binding conformation of the β -dipeptide and associated proton affinities (PA). The mass spectrometric fragmentation of two protonated model β -dipeptides, (β -Ala)Gly and Gly(β -Ala), with β -Ala at the C-terminus and N-terminus, respectively, were examined both experimentally and theoretically. The effect of the “additional” $-CH_2-$ unit in the main carbon chain of β -amino acids on (i) proton affinity (PA) of β -dipeptides and (ii) the dissociation pathways specific or indicative of the presence of β -Ala in the peptide will be investigated.

7.2 Results and Discussion

7.2.1 Experimental Determination of Proton (H^+) Affinities of Selected β -Dipeptides

The experimental procedure used to determine the proton (H^+) affinities (PA) of β -amino acids described in Section 5.3.1 could be equally applied to determine the H^+ affinities of

larger β -dipeptide systems. The extended kinetic method was adopted using alkyl amines with known and comparable H^+ affinities at 298K as the dipeptides were used as reference compounds. The proton affinities of four model β -dipeptides, Gly(β -Ala), (β -Ala)Gly, Ala(β -Ala) and (β -Ala)Ala, were measured in an exploratory study by Miss O. Y. Chan of our research group using ethylmethylamine, 2-propanamine, t-butylamine, t-amylamine, pyridine, piperazine, 3-methylpyridine and cyclohexylamine as reference compounds. In the present study, the proton affinity of the biologically important β -dipeptide, (β -Ala)His (carnosine) was determined. In addition and for comparative purposes, the H^+ affinities of analogous α -dipeptides, i.e., GlyAla, AlaGly, AlaAla, and AlaHis, were also determined in this work using the same experimental procedures.

Proton (H^+) Affinities of (β -Ala)His and AlaHis After some trial measurements, we found di-ethyl methyl amine, tri-ethylamine, tri-propylamine and tri-butylamine have comparable H^+ affinities at 298K to that of ((β -Ala)-His) and Ala-His. The low-energy CID MS/MS mass spectra of [$(\beta$ -Ala)-His-H-Ln] $^+$ heterodimer (where Ln = di-ethyl methyl amine, tri-ethylamine, tri-propylamine) were obtained at different collisional energies. A plot of $\ln(I_{[H+(\beta-Ala)His]^+}/I_{[H-Ln]^+})$ versus $[\Delta H_{[Ln+H]^+} - \Delta H_{Avg}]$ yields a regression line with slope of $-1/RT_{eff}$ and y-intercept of $[(\Delta G)_{[H+(\beta-Ala)His]^+}^{app} - \Delta H_{Avg}]/RT_{eff}$, respectively (Fig. 7.1(a)). A second plot is obtained by plotting the $[(\Delta G)_{[H+(\beta-Ala)His]^+}^{app} - \Delta H_{Avg}]/RT_{eff}$ term versus $1/RT_{eff}$ (Fig. 7.1(b)); the slope and y-intercept of the second plot yields the H^+ affinity at 298K (kJ mol^{-1}) of (β -Ala)-His and the $\Delta(\Delta S)^{app}$ term, which is equal to $1,023.4 \text{ kJ mol}^{-1}$ and 0.4 kJ mol^{-1} , respectively (Eqn. [2.9]). Similarly, the H^+ affinities of its α -analogue, AlaHis, and other α -dipeptides were determined in a similar way.

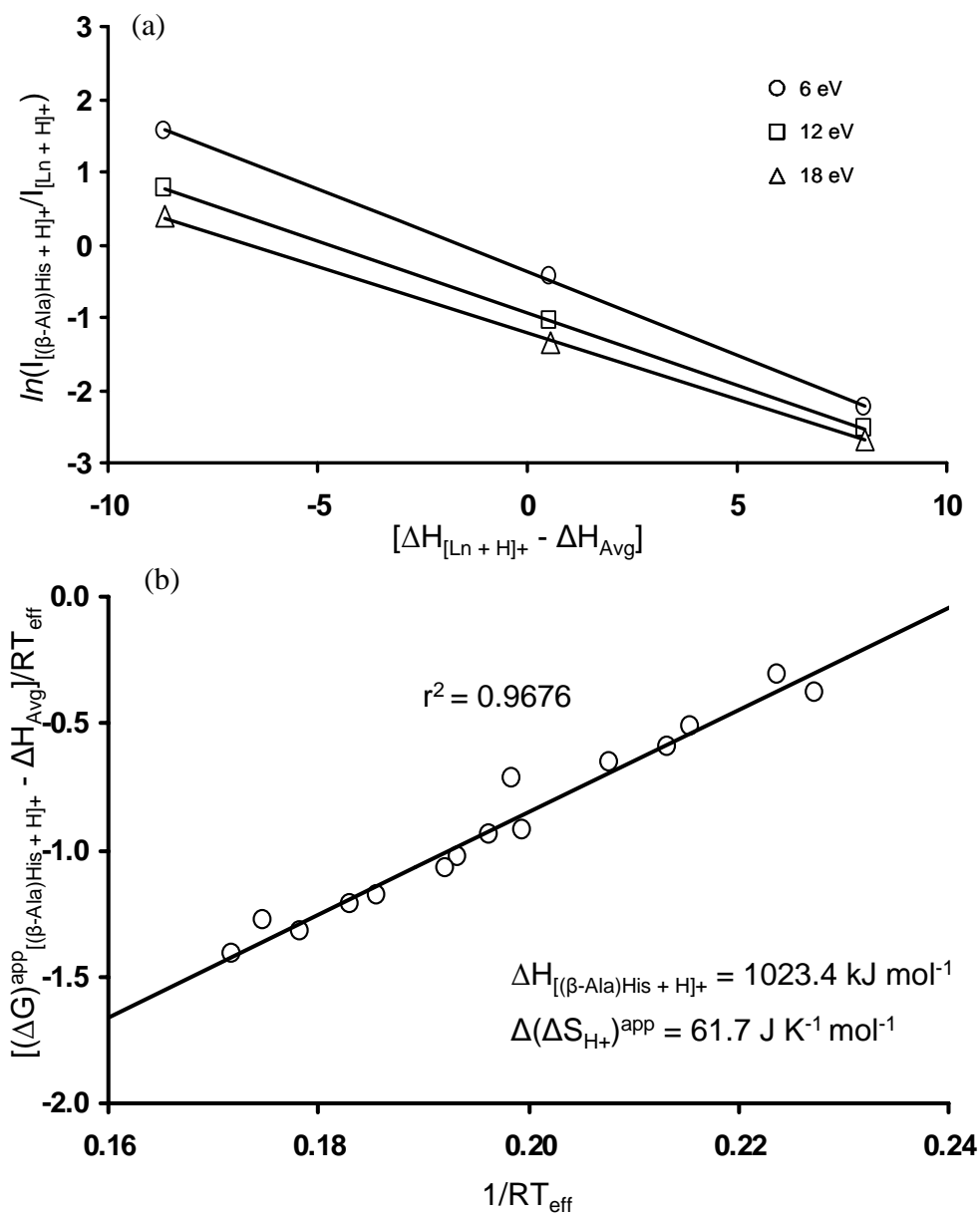


Figure 7.1 (a) Plot of $\ln(I_{[(\beta-Ala)His+H]^+}/I_{[L_n+H]^+})$ versus $[\Delta H_{[L_n+H]^+} - \Delta H_{Avg}]$ at different collision energies, and (b) plot of $[(\Delta G)^{app}_{[(\beta-Ala)His+H]^+} - \Delta H_{Avg}]/RT_{eff}$ against $1/RT_{eff}$ for the proton bound heterodimer $[(\beta-Ala)His + H + L_n]^+$. ($(\beta-Ala)His = \beta-Alanyl-Histidine$, $L_n = di-ethyl \text{ methyl amine, tri-ethylamine, tri-propylamine}$); numbers shown are *absolute* proton affinities.

Table 7.1 Experimental proton (H^+) affinities at 298K, (ΔH_{298} , kJ mol^{-1}) and $\Delta(\Delta S_{H^+})^{\text{app}}$ ($\text{J mol}^{-1} \text{K}^{-1}$) of α - and β -dipeptides determined by the extended kinetic method.

Dipeptides	This Work ^a		Reference Compound (proton affinity in kJ mol^{-1}) ^b
	ΔH_0	$\Delta(\Delta S_{H^+})^{\text{app}}$	
Gly(β -Ala)	942.0 ± 9.0 (1.0)	27.5 ± 1.8 (3.1)	t-butylamine (934.1), t-amylamine (937.8), N-Methylethylamine (942.2)
GlyAla	933.7 ± 8.6 (0.7)	17.9 ± 1.0 (1.8)	2-propanamine (923.8), t-butylamine (934.1), t-amylamine (937.8)
(β -Ala)Gly	971.3 ± 9.9 (2.6)	29.5 ± 2.0 (3.6)	t-butylamine (934.1), t-amylamine (937.8), Diethylamine (952.4)
AlaGly	937.7 ± 8.5 (0.7)	13.2 ± 0.9 (1.5)	2-propanamine (923.8), t-butylamine (934.1), t-amylamine (937.8)
Ala(β -Ala)	947.8 ± 8.7 (0.6)	26.8 ± 0.8 (1.4)	Pyridine (930.0), 3-methylpyridine (943.4), Piperazine (943.7)
(β -Ala)Ala	970.3 ± 12.9 (8.1)	15.2 ± 3.1 (5.6)	Pyridine (930.0), 3-methylpyridine (943.4), Piperazine (943.7)
AlaAla	939.5 ± 9.0 (1.0)	23.44 ± 1.3 (2.4)	2-propanamine (923.8), Cyclohexylamine (934.4), t-amylamine (937.8)
(β -Ala)His	1023.4 ± 0.3 (0.4)	61.7 ± 0.4 (0.7)	Tri-ethylamine (981.8), Tri-propylamine (991.0), Tri-butylamine (998.5)
AlaHis	1010.1 ± 0.7 (1.2)	38.2 ± 1.5 (2.6)	Di-ethyl methyl amine (960.1), Tri-ethylamine (981.8), Tri-propylamine (991.0)

^a Determined by extended kinetic method in this work and the uncertainties are given as \pm S.D.(90% confidence interval).

^b Proton Affinities are taken from: Hunter, E.P. and Lias, S.G., *Evaluated Gas Phase Basicities and Proton Affinities of Molecules: An Update*, *J. Phys. Chem. Ref. Data*, **1998**, 27, 3, 413-656.

The H^+ affinity determined by the extended kinetic method in this chapter is assumed to be 298K as the references' affinities are reported at 298K. [Hunter and Lias, 1998; Cooks et al., 1999; Cooks and Wong, 1998] The proton affinities of ((β -Ala)-His), Ala-His, and other α - and β -dipeptides so determined are summarized in Table 7.1. Combining the experimental uncertainties of the reference affinity values at 8.4 kJ mol⁻¹ (2 kcal/mol), the uncertainties of the H^+ affinities of α -/ β -dipeptides determined in this work are in the range of ± 11.0 kJ mol⁻¹ (Table 7.2).

7.2.2 Comparison between experimental and theoretical proton affinity values of selected β -dipeptides

To our knowledge, experimental proton affinities of β -dipeptides have not been reported in the literature. In order to obtain information on the preferred site of proton binding and theoretical H^+ affinities, theoretical calculations on the most stable H^+ binding modes and H^+ affinities were carried out. The theoretical affinity values of the four model β -dipeptides and (β -Ala)His (carnosine) and their α -analogues are summarized and compared with experimental values in Table 7.2. Excellent agreement between the experimental and theoretical affinity values was obtained; the mean-absolute deviation (MAD) for the nine protonated dipeptides in this study is only 5.9 kJ mol⁻¹. Such consistency provides the necessary confidence to the experimental / theoretical proton affinities, and the preferred site of protonation of the α -/ β -dipeptides found in the present study.

Table 7.2 Comparison of experimental and theoretical proton (H^+) affinities (ΔH_{298} , kJ mol^{-1}) of α - and β -dipeptides.

Dipeptides	Proton Affinity, ΔH_{298}		$\Delta\text{H}_{298(\text{Expt})} - \Delta\text{H}_{298(\text{Theory})}$
	Experimental ^a	Theoretical ^b	
Gly-Ala	933.7 ± 8.6	936.3	-2.6
Gly-(β -Ala)	942.0 ± 9.0	946.6	-4.6
Ala-Gly	937.7 ± 8.5	942.9	-5.2
(β -Ala)-Gly	971.3 ± 9.9	974.7	-3.4
Ala-Ala	939.5 ± 9.0	947.6	-8.1
Ala-(β -Ala)	947.8 ± 8.7	957.4	-9.6
(β -Ala)-Ala	970.3 ± 12.9	978.4	-8.1
AlaHis	1010.1 ± 0.7	1021.1	-11.0
(β -Ala)His	1023.4 ± 0.3	1026.7	-3.3

^a Determined in this work by the kinetic method ; uncertainties are given as \pm S.D.

^b Established at 298K by B3-LYP calculations with the 6-311+G(3df,2p) basis set.

7.2.3 The proton (H⁺) binding modes of β -dipeptides

A peptide has many proton binding sites. Consequently, there are many stable conformations that could be theoretically found when a proton binds to a dipeptide. In the preliminary stage of this study, we have conducted exhaustive conformational search, at B3-LYP/6-31G(d) level of geometry optimization, to explore various possible binding modes between the proton and the selected α - and β -dipeptides.

Protonated Model β -dipeptides Figure 7.2 shows some possible H⁺ binding modes for Gly(β -Ala), including proton attachment to the N-terminal nitrogen (-NH₂), amide oxygen (-OC) and C-terminal carboxylic oxygens (-COO). Four different conformations of [H + Gly(β -Ala)]⁺ were formed and their relative energies to the most stable form (where H⁺ is bound to the -NH₂ site) are shown in the brackets (Fig. 7.2). The proton affinities of the other three possible binding modes are 4 - 61 kJ mol⁻¹ lower than that of the most stable binding mode. By the same token, the most stable binding mode of all the four model β -dipeptides and their α -analogues were found and confirmed.

For comparative purposes, the conformations of five protonated model β -dipeptides and three of the corresponding protonated α -dipeptides (GlyAla, AlaGly and AlaAla) are shown in Figure 7.3. For both α - and β -dipeptides, the protonated conformers are stabilized by two intra-molecular hydrogen bonds: (i) hydrogen bonding between the N-terminal ammonium hydrogen and the amide oxygen (NH₂H⁺.....O=C), and (ii) hydrogen bonding between the carboxylic carbonyl oxygen and the amide hydrogen (C=O.....HN). The NH₂H⁺.....O=C bonding distances are about 0.36 - 0.39 Å and 0.27 - 0.52 Å shorter than the C=O.....HN bonding distances for α - and β -dipeptides, respectively, indicating that the hydrogen bonding

at the N-terminal site is significantly stronger and much more stabilizing than the hydrogen bonding at the C-terminal end.

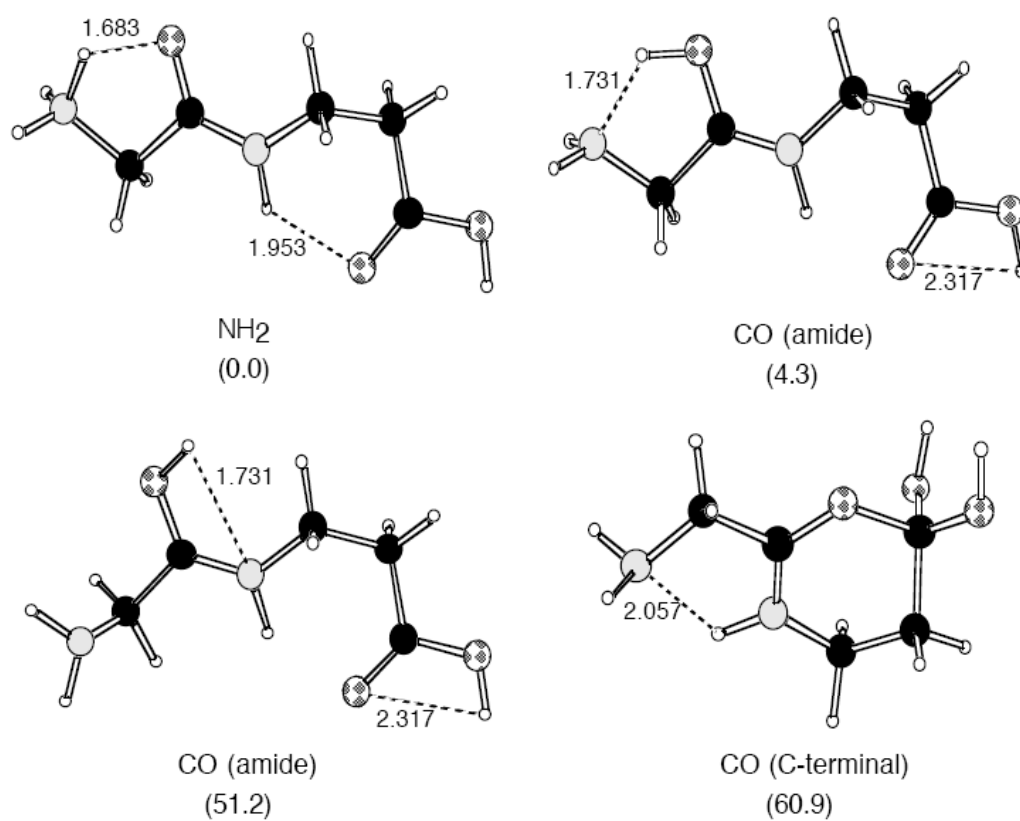


Figure 7.2 Four possible optimized geometries protonated Gly(β-Ala) complexes calculated at B3-LYP/6-311+G(3df,2p)//B3-LYP/6-31G+(D) level of theory

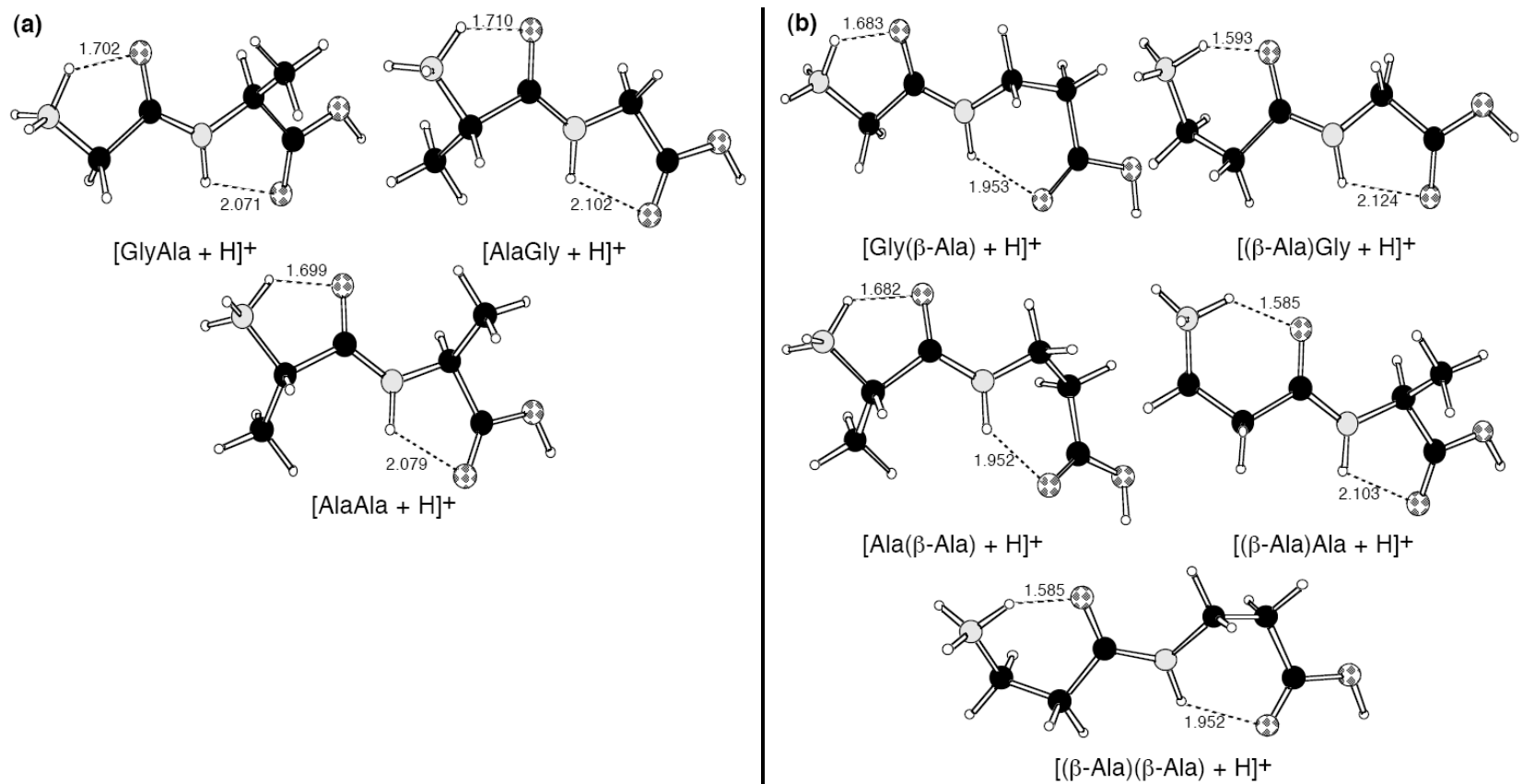


Figure 7.3 Optimized geometries of protonated (a) GlyAla, AlaGly and AlaAla, and protonated (b) Gly(β-Ala), (β-Ala)Gly, (β-Ala)Ala, Ala(β-Ala), and (β-Ala)(β-Ala) complexes calculated at B3-LYP/6-311+G(3df,2p)//B3-LYP/6-31G+(D) level of theory

The proton affinities (PA) of the five model β -dipeptides are generally larger than that of their α -analogues. For example, the experimental PA of $(\beta\text{-Ala})\text{Gly}$ is 33.6 kJ mol^{-1} greater than that of AlaGly (Table 7.1). The enhanced PA could be attributed to the formation of a shorter (by $\sim 0.1 \text{ \AA}$) and more stabilizing $\text{NH}_2\text{H}^+\cdots\text{O}=\text{C}$ hydrogen bond in a 6-membered ring configuration at the N-terminal $\beta\text{-Ala}$, versus a more loosely bound 5-membered ring configuration in AlaGly (Fig. 7.3). The hydrogen bonding pattern is similar to that found in $\beta\text{-Ala}$ alone, which also shows a PA $\sim 27 \text{ kJ mol}^{-1}$ higher than that of $\alpha\text{-Ala}$. [Hahn and Wesdemiotis, 2002]

When $\beta\text{-Ala}$ is located at the C-terminus in $\text{Gly}(\beta\text{-Ala})$, the $\text{C}=\text{O}\cdots\text{HN}$ hydrogen bond is formed in a 6-membered ring configuration, and is also shorter (by $\sim 0.1 \text{ \AA}$) when compared to the less stabilizing 5-membered ring hydrogen bonding pattern in GlyAla . At the same time, the $\text{NH}_2\text{H}^+\cdots\text{O}=\text{C}$ hydrogen bond is also shortened slightly (by $\sim 0.02 \text{ \AA}$), presumably due to less torsional strain in the $\text{O}=\text{C}-\text{N}$ amide bond, allowing the amide $\text{C}=\text{O}$ oxygen to be in closer contact with the ammonium hydrogen at the N-terminus. As a result, the combined effect is that $\text{Gly}(\beta\text{-Ala})$ shows an experimental PA 5.1 kJ mol^{-1} higher than that of GlyAla . Similar reasoning could explain why $(\beta\text{-Ala})\text{Ala}$ or $\text{Ala}(\beta\text{-Ala})$ shows higher PA than AlaAla .

Protonated carnosine (($\beta\text{-Ala}$)His) An exhaustive conformational search have been conducted to find out the most stable proton binding conformation of $(\beta\text{-Ala})\text{His}$ and its α -analogue, AlaHis . Compare to aliphatic model β -dipeptides, a very basic imidazole ring is present in $(\beta\text{-Ala})\text{His}$ and AlaHis . It implies that there are two more possible H^+ binding sites, π -nitrogen (N^π) and τ -nitrogen (N^τ) of the imidazole ring. To our knowledge, among all the possible binding site, which include the N-terminal nitrogen ($-\text{NH}_2$), amide oxygen ($-\text{OC}$) and C-terminal carboxylic oxygens ($-\text{COO}$), the N^π site has the largest basicity. Thus the H^+

bound complex with the proton bound to N^π is likely to show the largest proton affinity. Nevertheless, conformational search is conducted to find out the global minimum or the most stable H^+ binding site of (β -Ala)His and AlaHis. The optimized geometries of three protonated conformers of (β -Ala)His with the proton attached to the N-terminal nitrogen ($-NH_2$), amide oxygen ($-OC$) and π -nitrogen (N^π) of the imidazole ring are shown in Figure 7.4; their relative energies (in kJ mol^{-1}) with reference to the most stable form (where H^+ is bound to the N^π of the imidazole ring) are shown in brackets. The PA of the other two possible binding modes (at N-terminal $-NH_2$ and amide $O=C$) are 79 - 160 kJ mol^{-1} less stable than that of the most stable binding mode, indicating that protonation at the imidazole N^π leads to the formation of a very stable protonated conformer of (β -Ala)His.

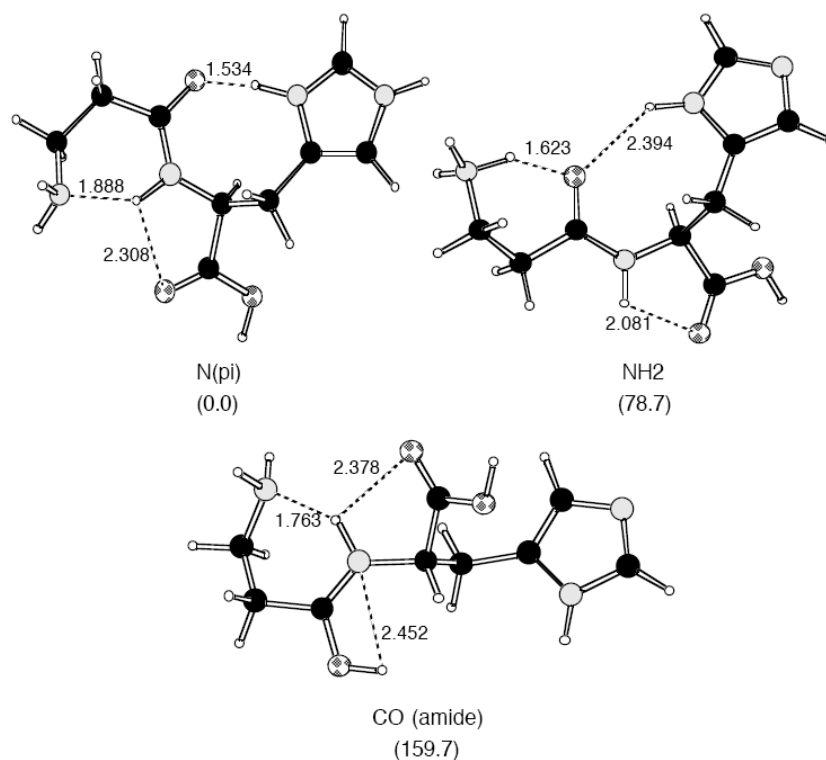


Figure 7.4 Three possible optimized geometries of protonated (β -Ala)His complexes calculated at B3-LYP/6-311+G(3df,2p)//B3-LYP/6-31G+(D) level of theory

Similarly, the most stable conformer of protonated AlaHis was found to have the proton attached to the N $^{\pi}$ of the imidazole ring of histidine. To facilitate inter-comparison, the optimized geometries of the most stable conformer of protonated (β -Ala)His and AlaHis are shown in Figure 7.5. For both AlaHis and (β -Ala)His, the protonated conformers are stabilized by three intra-molecular hydrogen bonds: (i) hydrogen bonding between the π -nitrogen of the imidazole ring and the amide oxygen (N $^{\pi}$ H $^+$O=C), (ii) hydrogen bonding between the amide hydrogen and N-terminal nitrogen (NH.....NH $_2$), and (iii) hydrogen bonding between the carboxylic carbonyl oxygen and the amide hydrogen (C=O.....HN). Among the three intra-molecular hydrogen bonds, the N $^{\pi}$ H $^+$O=C bond shows the shortest bonding distance (1.534-1.542 Å), indicating that it is the strongest and most stabilizing than the other two hydrogen bonds in the two conformers.

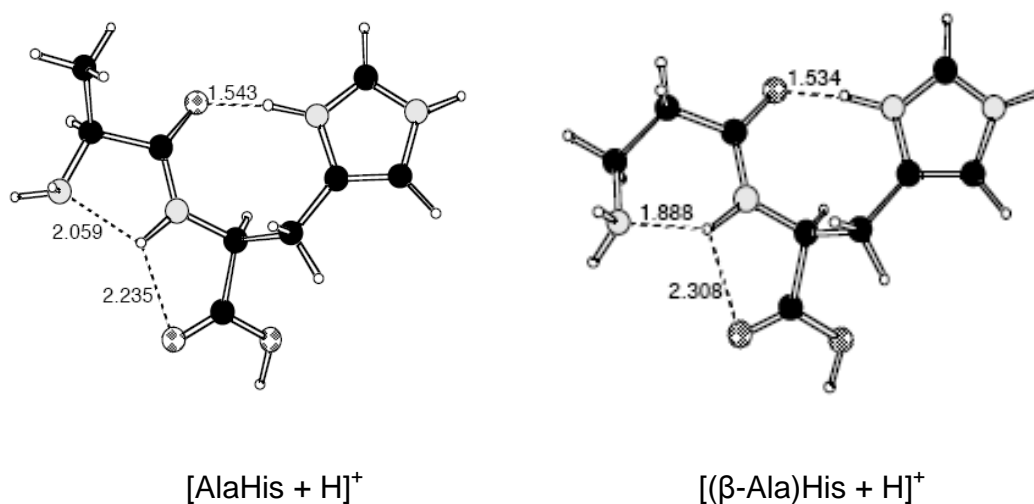


Figure 7.5 Optimized geometries of the most stable conformer of protonated AlaHis and (β -Ala)His complexes calculated at B3-LYP/6-311+G(3df,2p)//B3-LYP/6-31G+(D) level of theory

Once again, the experimental PA of (β -Ala)His is larger than that of AlaHis by 13.4 kJ mol⁻¹ (Table 7.1). Similar to the case of model β -dipeptides, the enhanced PA can be attributed to the formation of a shorter (by 0.1 Å) and more stabilizing NH \cdots NH₂ hydrogen bond in a 6-membered ring configuration at the N-terminal β -Ala, versus a more loosely bound 5-membered ring pattern in AlaGly (Fig. 7.3).

As shown in Table 7.2, both the experimental and theoretical affinities indicate that for the four α -dipeptides studied, the PA increases with the size of the α -dipeptides, i.e., PA (AlaHis) > PA (AlaAla) > PA (AlaGly) or PA (GlyAla). The situation is analogous to that found in aliphatic α -amino acids, i.e., PA (Ala) > PA (Gly). [Harrison, 1997] This is probably due to the greater molecular polarizability of the larger α -amino acids/peptide and its ability to stabilize the proton positive charge. This is also found to be true for β -dipeptides in general, as (β -Ala)His has the largest PA among all the β -dipeptides in this study. However, for β -dipeptides with similar molecular sizes, the PA is found to be more dependent on the location of β -Ala in the β -dipeptide than the size of the peptide. For example, the PA of (β -Ala)Gly at 971.3 kJ mol⁻¹ is significantly greater than that of Ala(β -Ala) at 947.8 kJ mol⁻¹, not to mention the smaller PA of Gly(β -Ala) at 942.0 kJ mol⁻¹. This indicates that the location of β -Ala in β -dipeptides has a significant effect on the PA of β -dipeptides, with much higher PA (by ~20 – 30 kJ mol⁻¹) when β -Ala is located at the N-terminus. This phenomenon could be explained by the much shorter and more stabilizing N-terminal NH₂H⁺ \cdots O=C hydrogen bond formed if β -Ala is located at the N-terminal than a much weaker O=C \cdots HN hydrogen bond if β -Ala is located at the C-terminal. In other words, positional effect on proton affinities is much more pronounced in β -dipeptides than in α -dipeptides.

7.2.4 Collision-induced Dissociation (CID) MS/MS Spectra of Protonated Gly(β -Ala) and Protonated (β -Ala)Gly

The CID MS/MS spectra and energy resolve MS/MS breakdown graph of these two protonated model β -dipeptides were obtained by Miss O. Y. Chan of our research group. As indicated in the previous section, the position of β -Ala in model β -dipeptides would have a great effect on their proton affinities. It is likely that the position of β -Ala in β -dipeptides, at C-terminus versus N-terminus, could affect their mass spectrometric fragmentation behaviors as well. To investigate this issue, we have attempted to rationalize the CID MS/MS spectra of protonated model β -dipeptides, Gly(β -Ala) and (β -Ala)Gly, with β -Ala at the C-terminus and N-terminus, respectively, by dissociation pathways obtained by high level density functional theory calculations.

CID MS/MS Spectra of Protonated Gly(β -Ala) The ion trap CIDMS/MS spectrum of protonated Gly(β -Ala) (m/z 147) is shown in Figure 7.6 (a). An intense b'_2 (oxazinone) ion at m/z 129 (refer to **Scheme 7.1**, a six-membered cyclic structure formed via a b_2 (oxazolone)-like pathway), and a y_1 ion at m/z 90 of moderate intensity are found. Further dissociation of the b'_2 ions yield fragment ions arising from the loss of NH_3 , ketene (CH_2CO), ($\text{NH}_3 + \text{CO}$) and ($\text{NH}=\text{CH}_2 + \text{CO}$), which are the characteristic neutral losses from protonated β -alanine (refer to Chapter 6), are also present (MS/MS spectrum of b'_2 ion is not shown).

As formation of the b'_2 (oxazinone) ion is unique and characteristics of protonated β -dipeptides with β -Ala at the C-terminus, we have explored its competitive formation from the model β -dipeptide, Gly(β -Ala), versus the formation of y_1 and other fragment ions as a function of ion trap collision energies. The energy resolve MS/MS breakdown graph of

Gly(β -Ala) obtained is shown in Figure 7.7. The b'_2 (oxazinone) ion (m/z 129) appears at the lowest RF threshold voltage of 0.40 volt, and remains to be dominant throughout the whole collisional activation RF voltage range. The formation of y_1 ion (m/z 90) is the second dominant fragment ion, appearing at a higher threshold voltage of 0.48 volt. Thus, the formation of b'_2 (oxazinone) and y_1 ions is competitive for β -dipeptides with β -Ala at the C-terminus.

CID MS/MS Spectrum of Protonated (β -Ala)Gly

For protonated (β -Ala)Gly, intense fragment ions characteristic of β -alanine are observed under the more energetic CID conditions of a Q-TOF tandem mass spectrometer. The Q-TOF CID-MS/MS spectrum of [(β -Ala)Gly + H]⁺ is shown in Figure 7.6 (b). The dissociation of protonated Gly(β -Ala) yields a dominant y_1 ion at m/z 76 and a less intense b_2 ion at m/z 129 arising from the well established $b_x - y_z$ pathway. Under more energetic CID conditions, fragment ion due to loss of NH₃, [MH - NH₃]⁺ (m/z 130), and a b_i ion (a protonated β -lactam at m/z 72) are observed, which are characteristics of the presence of β -Ala at the N-terminus of the β -dipeptide. These two fragment ions are likely to derived from dissociation pathways of [(β -Ala)Gly + H]⁺ with higher critical energies. A peak at m/z 118 due to loss of NH=CH₂ from the protonated β -dipeptide, a characteristic neutral loss from protonated β -alanine, is also found.

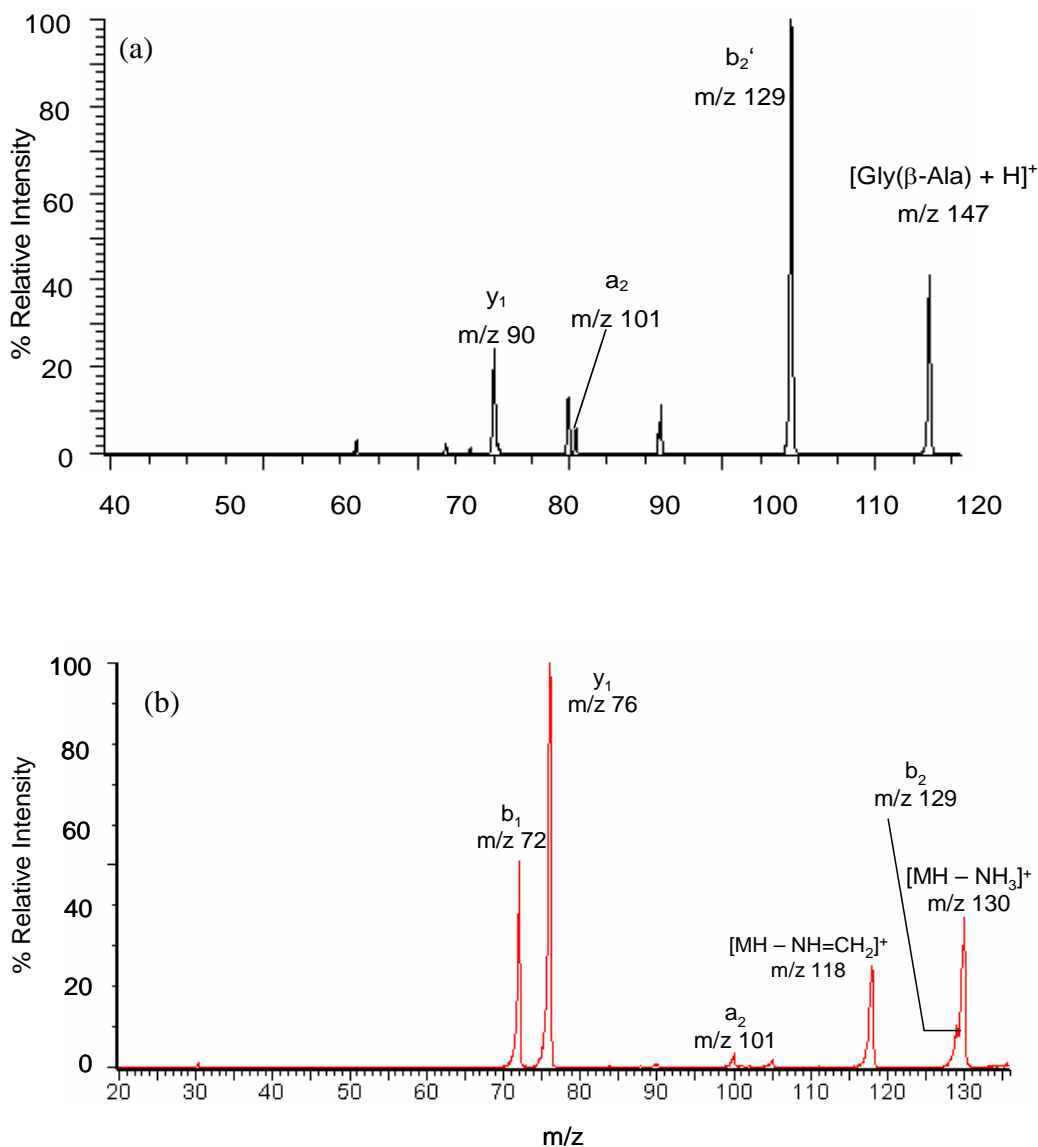
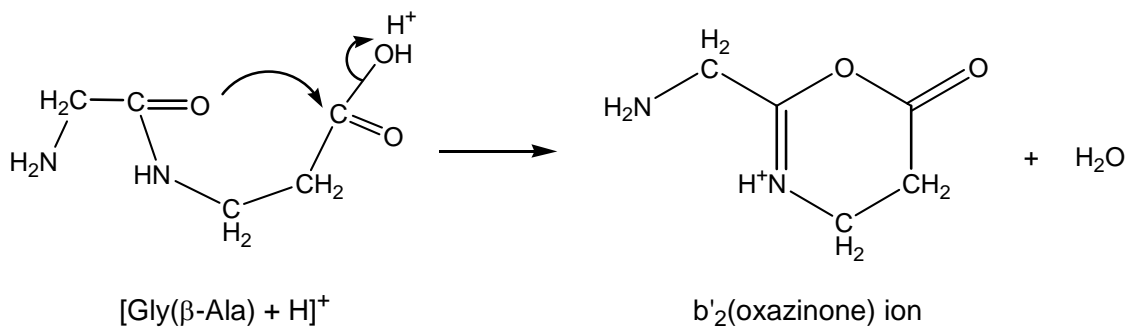


Figure 7.6 (a) Ion trap MS/MS spectra of protonated Gly(β -Ala) (m/z 147), obtained at a RF activation voltage (V_{p-p}) of 0.68V. (ions of low intensities are: m/z 72 = $[\text{b}_2 - (\text{NH}=\text{CH}_2 + \text{CO})]^+$, m/z 84 = $[\text{b}_2 - (\text{CO} + \text{NH}_3)]^+$, m/z 87 = $[\text{b}_2 - \text{CH}_2\text{CO}]^+$, m/z 100 = $[\text{b}_2 - \text{NH}=\text{CH}_2]^+$ and m/z 112 = $[\text{b}_2 - \text{NH}_3]^+$.) (Ion trap mass analyzer conditions: normal scan mode; ion activation time, 10 ms; trap offset at -10 V; q_z at 0.25), and (b) triple quadrupole MS/MS spectra of protonated (β -Ala)Gly, $[(\beta\text{-Ala})\text{Gly} + \text{H}]^+$ (m/z 147) obtained at a collision energy of 18 eV. (at $\sim 5\%$ attenuation of the precursor ion beam intensity)



Scheme 7.1 Formation of $\text{b}'_2(\text{oxazinone})$ ion from $\text{[Gly}(\beta\text{-Ala)} + \text{H}]^+$

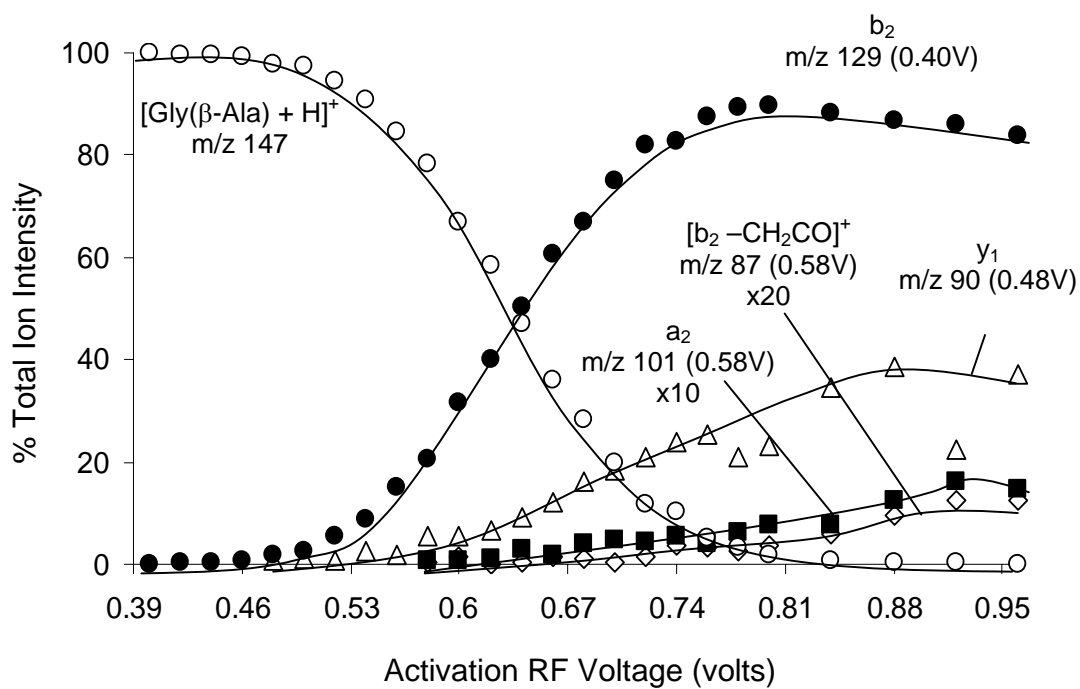


Figure 7.7 Ion trap energy resolved MS/MS breakdown graph of protonated Gly(β -Ala) (m/z 147). (Appearance threshold voltages are shown in parenthesis. For clarity of presentation, the ion intensity traces for $[\text{b}_2 - (\text{NH}=\text{CH}_2 + \text{CO})]^+$ (m/z 72), $[\text{b}_2 - (\text{CO} + \text{NH}_3)]^+$ (m/z 84), $[\text{b}_2 - \text{NH}=\text{CH}_2]^+$ (m/z 100) and $[\text{b}_2 - \text{NH}_3]^+$ (m/z 112) are omitted.)

7.2.5 Proposed Pathway for Competitive Formation Pathway of b'_2 (oxazinone) and y_1 Ions from Protonated Gly(β -Ala)

According to the CID MS/MS spectrum of protonated Gly(β -Ala), formation of the b'_2 (oxazinone) ion is unique and characteristics of protonated β -dipeptides with β -Ala at the C-terminus (Fig. 7.6 (a)). Furthermore, the energy-resolve MS/MS breakdown graph of protonated Gly(β -Ala) (Fig. 7.7) shows the formation of b'_2 (oxazinone) and y_1 ions at the threshold voltage of 0.40 and 0.48 V, respectively, are competitive for β -dipeptides with β -Ala at the C-terminus. For this reason, we have explored theoretically the energetics of competitive formation of the b'_2 (oxazinone) versus y_1 ions from protonated Gly(β -Ala). The proposed pathways and the corresponding potential energy surface (PES) are shown in Figure 7.8.

Using the same notations adopted in the previous Chapter 6, the labels **1**, **3**, etc. denote the various minima (stable intermediates), and the labels **TS2**, **TS4**, etc. denote the various transition structures (TS) between the minima on the PES. The same theoretical protocol adopted in Chapter 6 is applied here to locate all the optimized structures of various intermediates and transition structures, which are shown in Figure 7.9. With the optimized structures, single point energy calculations at 0K were obtained at the B3-LYP/6-311+G(3df,2p)//B3-LYP/6-31G(d) level of theory, with zero-point energy correction, as mentioned in chapter 6.[Scott and Radom, 1996]

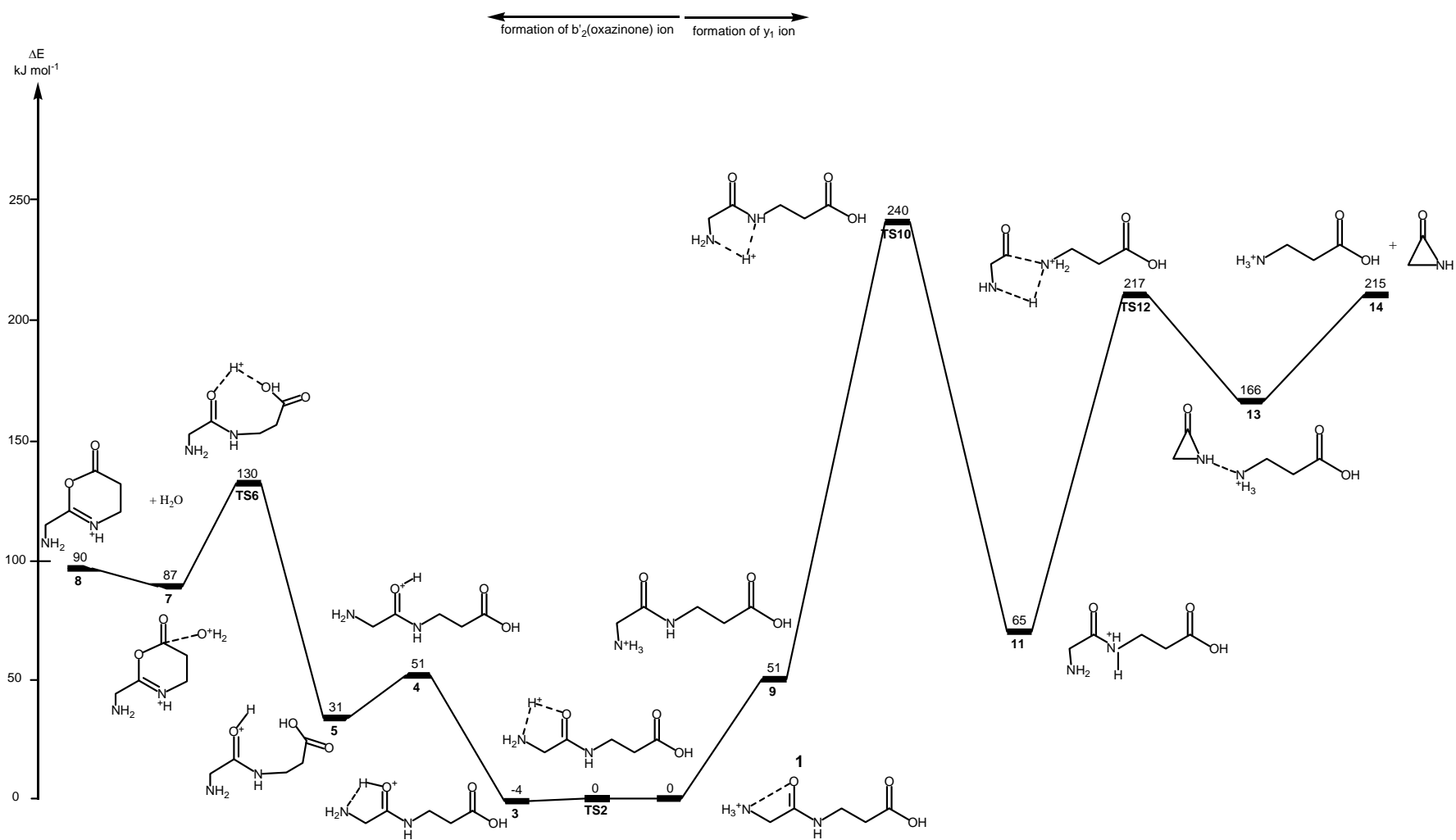


Figure 7.8 Potential energy surface (PES) of formation of y_1 ion and b'_2 (oxazinone) ion from protonated Gly(β -Ala) at 0K, calculated at the B3-LYP/6-311+G(3df,2p)//B3-LYP/6-31G(d)level

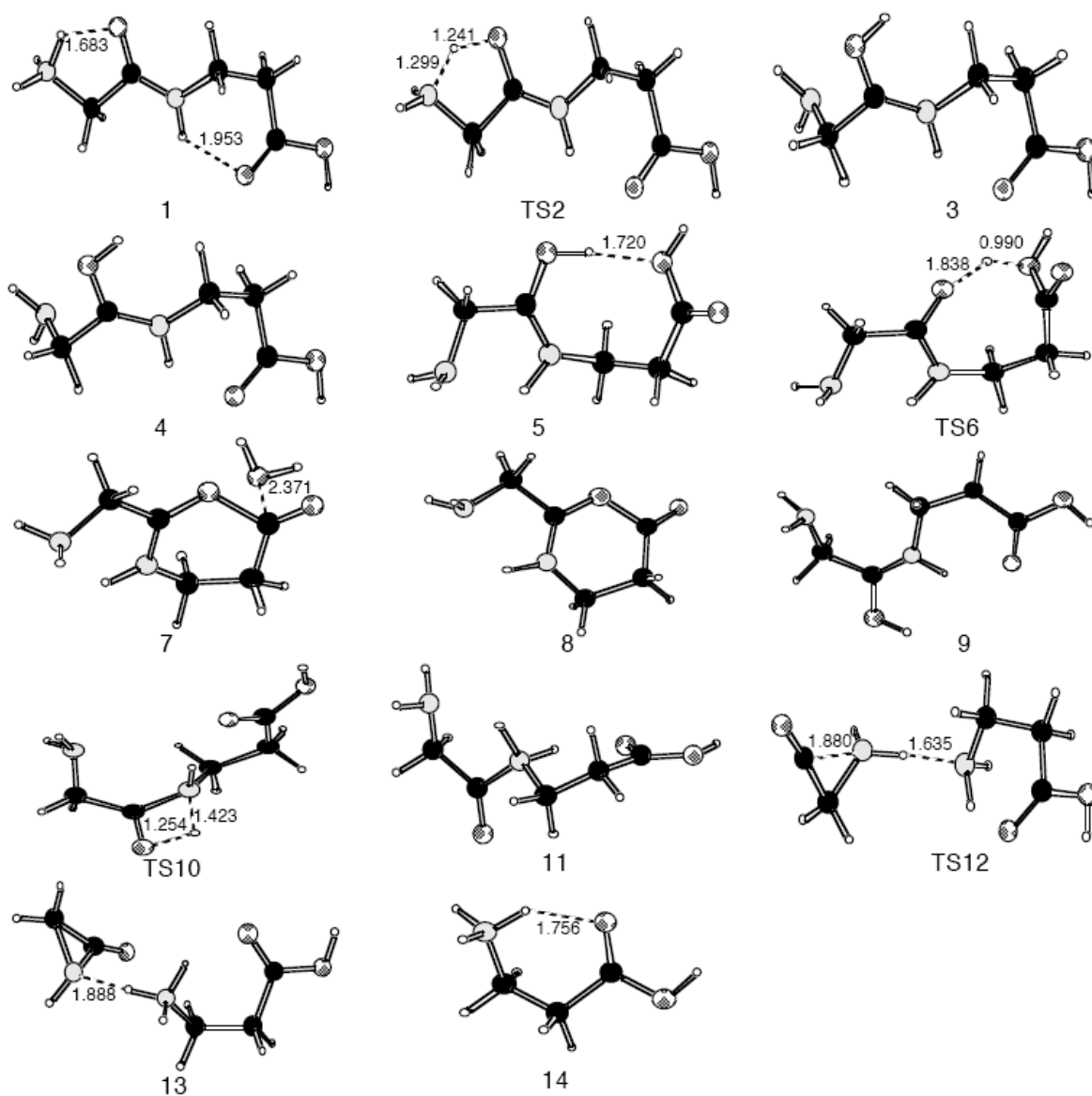


Figure 7.9 Optimized geometries (at B3-LYP/6-31G(d) level) of the various intermediates and transition species shown in the potential energy surface (PES) of formation of y_1 ion and b'_2 (oxazinone) ion from protonated Gly(β -Ala)

From the most stable form of protonated Gly(β -Ala) (species **1** in Figure 7.8), a proton is transferred from the amino nitrogen (N-terminal $-\text{NH}_2$) to the amide bond oxygen of **TS2** to yield species **3**. Species **4** is then formed by simple bond rotation with the proton facing the carbonyl oxygen of the carboxylic function (COOH) group at the C-terminus. Following bond rotations along the main carbon chain, a stable species **5** with the hydroxyl oxygen (O_H) at the C-terminus positioned to accept the proton from the amide bond oxygen is formed. A proton transfer then takes place via **TS6** to form a 2-(aminomethyl)-6-oxo-5,6-dihydro-4H-1,3-oxazin-3-ium... H_2O ion-neutral complex (species **7**). The ion-neutral complex (species **7**) then loses H_2O to yield a stable 6-membered ring b'_2 (oxazinone) ion, the 2-(aminomethyl)-6-oxo-5,6-dihydro-4H-1,3-oxazin-3-ium ion (an oxazinium ion, species **8**). The 0K enthalpy of reaction of this process, i.e., the energy difference between species **1** and species (**8** + H_2O), is 90 kJ mol^{-1} , with an energy barrier at **TS6** of 130 kJ mol^{-1} .

The formation of the γ_1 ion starts from species **1**, which is followed by a bond rotation so that the proton at the amino nitrogen can readily be transferred to the amide nitrogen. A proton transfer then takes place via **TS10**, and a stable species **11** with the proton now attached to the amide bond nitrogen. A second proton transfer from the amino nitrogen at the N-terminus to the amide bond nitrogen then takes place via **TS12** to yield an ion-neutral complex (species **13**), a protonated β -alanine...aziridin-2-one ion. The aziridin-2-one (a three-membered ring neutral is then detached from the ion-neutral complex (species **13**), and the protonated β -alanine ion (species **14**) is formed. The enthalpy of reaction at 0K of this process, i.e., the energy difference **1** and (**14** + **aziridin-2-one**) is 215 kJ mol^{-1} , with an energy barrier of 240 kJ mol^{-1} at **TS10**.

The theoretically estimated energy barriers at 0K and 298K (ΔH_0 , ΔH_{298} , ΔG_{298} and ΔS_{298}) for formation of the b'_2 (oxazinone) and y_1 , together with the experimental ion trap appearance threshold voltages for the two reaction channels, are listed in Table 7.3. The ΔH_0 , ΔH_{298} and ΔG_{298} values for other intermediate and TS structures of the proposed pathway are listed in Table 7.4. As shown in Table 7.3, the order of critical energies (in kJ mol^{-1}) / threshold voltage (in volts): b'_2 (oxazinone) (130 / 0.4) < y_1 ion (240 / 0.48), is in agreement with each other, indicating that the formation of b'_2 (oxazinone) ion is energetically preferred over the formation of y_1 ions. Furthermore, once the critical energies are exceeded, both dissociation pathways are slightly entropically disfavored, as indicated by the negative ΔS_{298} values of -10 and $-7 \text{ J mol}^{-1} \text{ K}^{-1}$ for the energy barriers of b'_2 and y_1 ions respectively. Taken together, the competitive formation of b'_2 (oxazinone) versus y_1 ions is mainly energetically-controlled, so that b'_2 ion intensity is significantly higher than that of the y_1 ion in the whole range of ion trap collision energies (Figure 7.7).

7.2.6 Proposed Competitive Loss of NH_3 Pathway and Formation of b_1 Ion from Protonated (β -Ala)Gly

Our proposed pathways for loss of NH_3 and b_1 ion formation from protonated (β -Ala)Gly are shown in Figure 7.10, while the optimized geometries of the various intermediates and TS are shown in Figure 7.11. The calculated energetics (ΔH_0 , ΔH_{298} , ΔG_{298} and ΔS_{298}) of the two pathways are listed in Table 7.3 and Table 7.4 respectively. The mechanism leading to b_1 ion formation is first introduced. Starting the most stable form of protonated (β -Ala)Gly species (**1** in Figure 7.10), simple bond rotations along the main carbon chain yield a species **5**

in which the amide bond nitrogen is positioned to accept the proton from the amino nitrogen at the N-terminus. A proton transfer then takes place via **TS6** to yield species **7** with the proton now attached to the amide bond nitrogen. A bond formation between the amide nitrogen and amide carbon via **TS8** follows, and an ion-neutral complex (species **9**), 2-oxoazetidinium (protonated β -lactam).....glycine, is formed. After the detachment of glycine, a stable 2-oxoazetidinium (ion species **10**) is formed. The enthalpy of reaction at 0K of this dissociation channel, i.e., the energy difference between species **1** and species **10** + Gly, which is also the energy barrier, is 227 kJ mol⁻¹. The b₁ ion at m/z 72 is the predominant and characteristic fragment ion of protonated β -Ala (refer to Chapter 6). Our results here are further evidence that the dissociation characteristics of protonated β -Ala are also reflected in the dissociation of protonated β -dipeptides with β -Ala at the C-terminus.

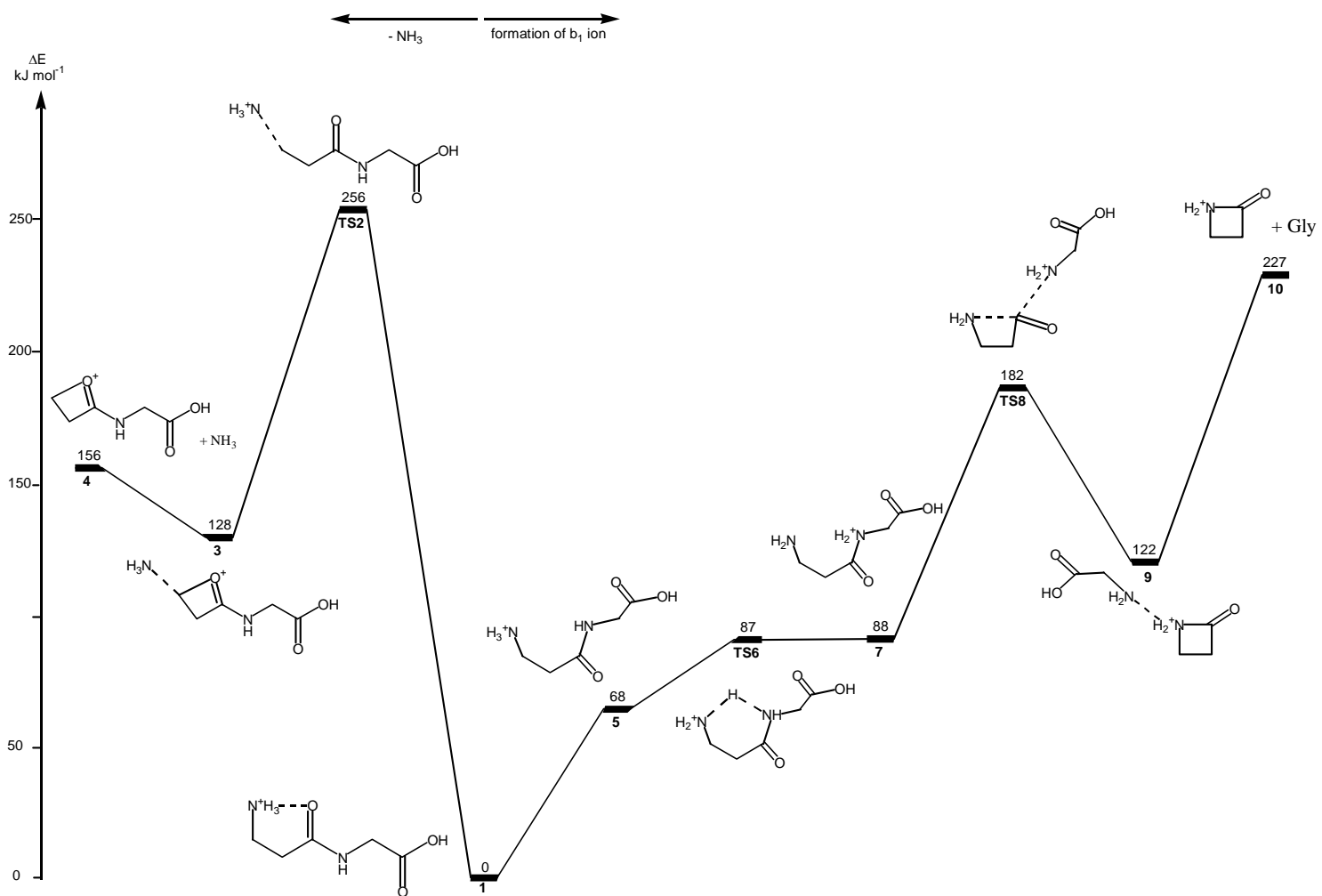


Figure 7.10 Potential energy surface (PES) of formation of b_1 ion and loss of NH_3 ($[\text{MH}-17]^+$) from protonated $(\beta\text{-Ala})\text{Gly}$ at 0K, calculated at the B3-LYP/6-311+G(3df,2p)//B3-LYP/6-31G(d) level

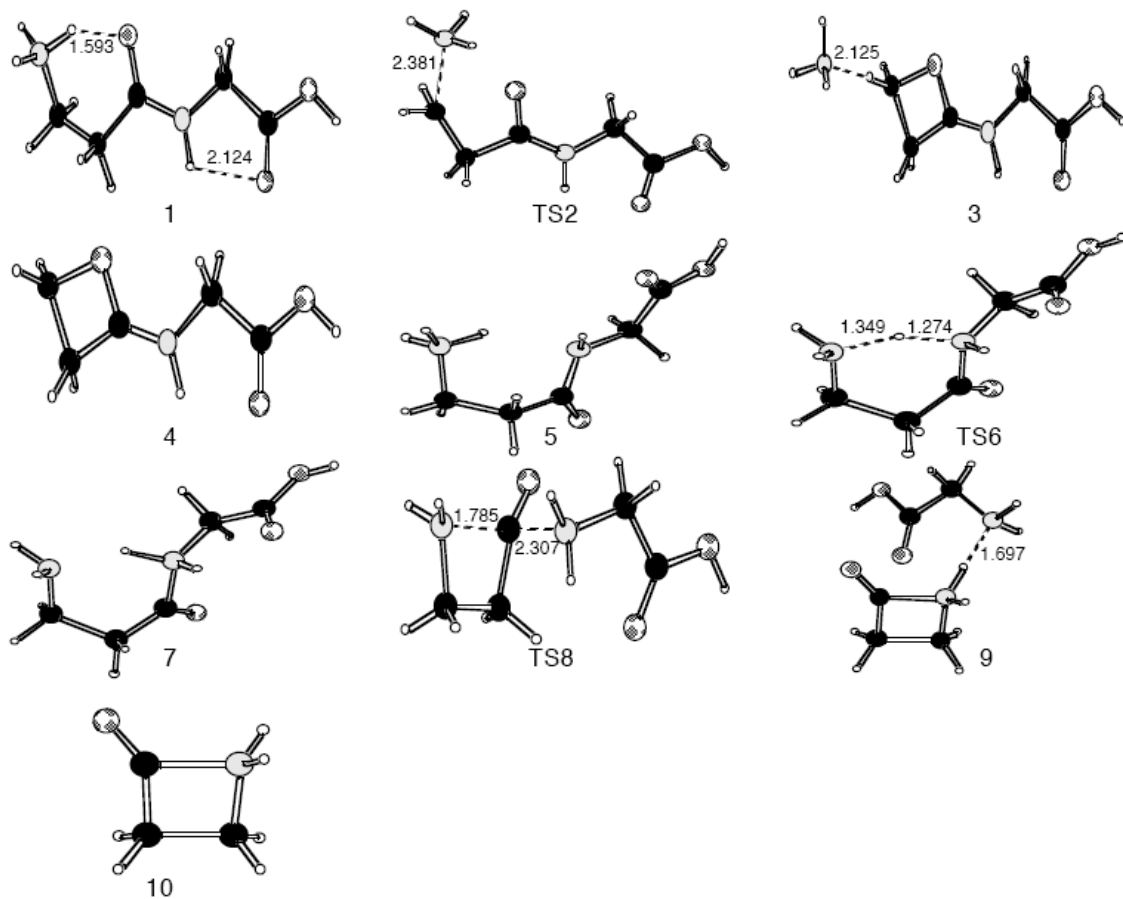


Figure 7.11 Optimized geometries (at B3-LYP/6-31G(d) level) of the various intermediates and transition species shown in the potential energy surface (PES) of formation of b_1 ion and loss of NH_3 ($[\text{MH} - \text{NH}_3]^+$) from protonated (β -Ala)Gly

Table 7.3 Energy barriers for competitive formation of (a) b_2' (oxazinone) and y_1 ions from $[\text{Gly}(\beta\text{-Ala}) + \text{H}]^+$, and (b) $[\text{MH} - \text{NH}_3]^+$ and b_1 ions from $[(\beta\text{-Ala})\text{Gly} + \text{H}]^+$ ^a: the relative enthalpies (ΔH_0 , ΔH_{298} at 0K and 298K), Gibbs free energies ΔG_{298} at 298K, in kJ mol^{-1}) and entropies (ΔS_{298} at 298K, in $\text{J mol}^{-1} \text{K}^{-1}$)

Formation of ions	$[\text{Gly}-(\beta\text{-Ala}) + \text{H}]^+$				$[(\beta\text{-Ala})\text{-Gly} + \text{H}]^+$			
	ΔH_0	ΔH_{298}	ΔG_{298}	ΔS_{298}	ΔH_0	ΔH_{298}	ΔG_{298}	ΔS_{298}
b_2' (oxazinone) ^b	130 <i>(0.40)</i>	131	134	-10	--- ^c	--- ^c	--- ^c	--- ^c
y_1 ^d	240 <i>(0.48)</i>	240	242	-7	--- ^c	--- ^c	--- ^c	--- ^c
$[\text{MH-NH}_3]^+$ ^e	--- ^c	--- ^c	--- ^c	--- ^c	256 <i>(0.54)</i>	260	252	27
b_1 ^f	--- ^c	--- ^c	--- ^c	--- ^c	182 <i>(0.54)</i>	183	182	3

^a: The appearance threshold energy (in V) for these fragments ions under ion trap CID conditions is shown in italics in parenthesis.

^b: Via transition structure **TS6** of Figure 7.8.

^c: Not observed under triple quadrupole CID conditions.

^d: Via transition structure **TS10** of Figure 7.8.

^e: Via transition structure **TS2** of Figure 7.10.

^f: Via transition structure **TS8** of Figure 7.10.

Table 7.4 Potential energy surface for the dissociation of (a) [Gly-(β -Ala) + H]⁺ and (b) [β -Ala-(Gly) + H]⁺: relative enthalpies at 0K and 298K (ΔH_0 and ΔH_{298}) and Gibbs free energies at 298K (ΔG_{298}), in kJ mol⁻¹, with respect to species **1**

Species	Energetics		
	ΔH_0	ΔH_{298}	ΔG_{298}
3	-4	-5	-3
4	51	53	50
5	31	30	33
7	87	92	86
8 + H ₂ O	90	94	55
11	65	65	65
14 + azirindin-2-one	215	215	168

Species	Energetics		
	ΔH_0	ΔH_{298}	ΔG_{298}
3	128	134	115
4 + NH ₃	156	161	114
5	68	68	66
TS6	87	86	89
9	122	124	120
10 + Gly	227	230	176

The loss of NH_3 from protonated (β -Ala)Gly involves the energy barrier **TS2**, an ion-molecule complex in which the NH_3 is only loosely bound to the peptide backbone (Figure 7.10). Following the detachment of NH_3 from the ion-molecule, cyclization to a more stable 4-[(carboxymethyl)amino]-2,3-dihydrooxetium ion to form species **4** takes place. It is the stability of the 4-membered ring species **4** that drives the loss of NH_3 from protonated (β -Ala)Gly.

The loss of NH_3 shows a higher energy barrier (256 kJ mol^{-1} at 0K) than b_1 ion formation (182 kJ mol^{-1} at 0K). However, loss of NH_3 is entropically (kinetically) favored once the internal energy of $[(\beta\text{-Ala)Gly} + \text{H}]^+$ exceeds the critical energy of dissociation, as indicated by the ΔS_{298} values of 27 and $3 \text{ J mol}^{-1} \text{ K}^{-1}$ for loss of NH_3 and b_1 ion formation, respectively (Table 7.3). This could explain why the % abundance of the $[\text{MH} - \text{NH}_3]^+$ ion (m/z 130) is significantly higher under the more energetic CID conditions of a Q-TOF tandem mass spectrometer.

As shown in Table 7.3, the $[\text{MH} - \text{NH}_3]^+$ ion appears at the same ion trap appearance threshold of 0.54 volt as the b_1 ion, even though the loss of NH_3 pathway has a higher critical energy than the b_1 ion formation pathway. Our theoretical results could also explain such apparant discrepancies. Compared to b_1 ion formation, the loss of NH_3 pathway is associated with a larger entropy change (ΔS_{298}) and therefore a smaller chemical shift (lowered threshold voltage) is expected for observation of the loss NH_3 of reaction channel.

7.3 Conclusion

In this study, the proton affinities (298K, in kJ mol^{-1}) of four model β -dipeptides and one bioactive β -dipeptide were determined by the mass spectrometric kinetic method: Gly(β -Ala) 942.0, (β -Ala)Gly 971.3, Ala(β -Ala) 947.8, (β -Ala)Ala 970.3 and (β -Ala)His 1023.4. The experimental values are found to be in very good agreement with theoretical affinities calculated the B3-LYP/6-311+G(3df,2p)//B3-LYP/6-31G+(d) level, with mean-absolute-deviation (MAD) of 5.9 kJ mol^{-1} only.

Theoretical studies reveal that the most stable proton binding site is the N-terminal amino nitrogen ($-\text{NH}_2$) for the model β -dipeptides and at the N^π -nitrogen of the imidazole ring for carnosine ((β -Ala)His). The enhanced proton affinity (PA) of β -alanine (β -Ala) versus that of α -alanine (α -Ala) can be extended to β -dipeptides, which show higher PA (by $6 - 30 \text{ kJ mol}^{-1}$) than their α -analogues. The underlying cause for the enhancement in PA is attributed to the 'additional' $-\text{CH}_2-$ unit in the carbon backbone of β -amino acids which introduces greater flexibility in the peptide backbone, allowing more stabilizing hydrogen bonding patterns to be found in β -dipeptides than their corresponding α -analogues. Furthermore, unlike α -dipeptides, the PA enhancing effect is much more pronounced when β -Ala is located at the N-terminus than at the C-terminus of the β -dipeptides.

Using protonated (β -Ala)Gly and Gly(β -Ala) as model β -dipeptides, the energetics and mechanisms of the major dissociation pathways characteristic of the presence of β -Ala in the dipeptide were established by high level density functional theory calculations. The formation of β -Ala specific fragment ions is dependent of the location, C-terminus versus N-terminus, of β -Ala in the β -dipeptide. For protonated Gly(β -Ala), formation of the unique

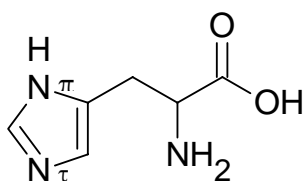
b'_2 (oxazinone) ions is energetically favored over y_1 ion formation. The b'_2 (oxazinone) ion dissociates further by characteristic loss of $\text{NH}=\text{CH}_2$ and NH_3 in contrast to the loss of CO only observed for b_2 (oxazolone) ions derived from α -dipeptides. For protonated (β -Ala)Gly, loss of NH_3 and formation of b_1 (protonated β -lactam) ions was established. The experimental observation of ion trap appearance threshold voltages and % relative ion abundances in the CID – MS/MS spectra are consistent with theoretical predictions, and can be rationalized in terms of the energy barriers (ΔH_0 and ΔH_{298}) and change in reaction free energy (ΔG_{298}) and entropy (ΔS_{298}) of the proposed pathways.

Most of these β -Ala specific fragment ions found in the MS/MS spectra of protonated (β -Ala)Gly and Gly(β -Ala) are different from that of the corresponding protonated α -dipeptides, indicating that the presence of the extra backbone $-\text{CH}_2-$ unit in β -Ala does have a structural effect on the dissociation mechanisms of protonated β -dipeptides

Chapter 8 Dissociation of Protonated Peptides Containing Histidine: Formation and Structure of b_2 Ions

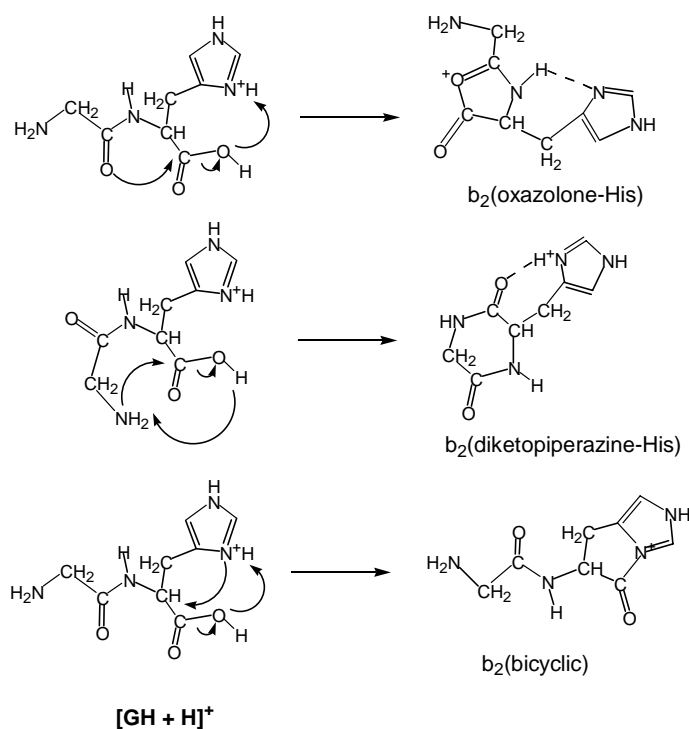
8.1 Background

Histidine (His, PA = 981 kJ/mol) (**Scheme 8.1**), with a very basic N^π site at the imidazole ring in its side chain, is the second most basic amino acid after arginine (PA = 1,036 kJ/mol) [Mann and Wilm, 1994; Yates et al., 1995; Yates et al., 1996]. Enzymes/proteins comprised of histidine-containing peptides are found to have many important biological functions, e.g., as a proton-relay between serine and aspartate in serine proteases [Wysocki et al., 2000], as metal chelating agents for the central ions of heme groups [Dongre et al., 1996], as nucleic acid vectors [Midoux et al., 2002] and the sequence recognition for a large number of DNA-binding proteins. A well known example of histidine-containing peptides is the angiotension and related family of peptides, which are responsible for regulation of blood pressure, endothelial function, and many other physiological functions in humans. [Ferrario et al., 1998; Inagami et al., 1999] In addition, histidine-containing peptides are now widely developed as drugs for treatment on some diseases, e.g., as an ophthalmic drug for treating human cataracts. [Babizhayev et al., 2001]



Scheme 8.1 Chemical structure of histidine

Due to the presence of basic imidazole ring of histidine, the \mathbf{b}_i ions ($i < n$, where $n = \text{number of amino acid residues in the peptide}$) are often the major fragment ions for histidine-containing peptides, as reported by O'Hair, and Wysocki and coworkers.[Farrugia et al., 2001; Tsapralis et al., 2004] It is generally accepted that, at least for peptides comprised of amino acids with no O/N/S heteroatoms in their side chains, the \mathbf{b}_i ions have the five-membered cyclic oxazolone structure [Yalcin et al., 1995; Yalcin et al., 1996], which is formed by intramolecular *nucleophilic attack of an amide carbonyl oxygen at the neighboring amide carbon on the C-terminal side*. [Paizs and Suhai, 2005; . Paizs and Suhai, 2004; Schlosser and Lehmann, 2000] The formation of the \mathbf{b}_2 (oxazolone-His) ion by this mechanism from the protonated model peptide HG (Histidine-glycine) is illustrated in **Scheme 8.2**.



Scheme 8.2 Chemical structures of \mathbf{b}_2 (oxazolone-His), \mathbf{b}_2 (diketopiperazine-His) and \mathbf{b}_2 (bicyclic) formed from $[\text{GlyHis} + \text{H}]^+$

However, the b_2 ions formed from histidine-containing peptides could have three possible structures, namely $b_2(\text{oxazolone-His})$, $b_2(\text{diketopiperazine-His})$ (for simplicity, denoted as $b_2(\text{diketo-His})$ hereafter) and $b_2(\text{bicyclic})$ (for peptides with histidine located at the C-terminus only). O'Hair and co-workers first reported that the ion trap MS/MS spectra (without defining detailed conditions, such as collisional activation RF voltages used) of b_2 ions derived from protonated O-methyl esters of model di-/tripeptides GH, HG, GHG and HGG were found to be very similar to that of cyclo-(GH). Furthermore, by using *ab initio* calculations, they showed that the structure of the $b_2(\text{diketo-His})$ ions of protonated GH and HG are more stable than that of the $b_2(\text{oxazolone-His})$ ions by 19.9 and 21.6 kJ mol⁻¹, respectively.[Farrugia et al., 2001] This suggests that the presence of histidine/imidazole ring in peptides facilitates proton transfer, favoring the formation of the $b_2(\text{diketo-His})$ ion. Formation of $b_2(\text{diketo-His})$ involves *nucleophilic attack of the N-terminal amino (-NH₂-) nitrogen on the amide/carboxylic carbon on the C-terminal side*, leading to the formation of a 6-membered ring $b_2(\text{diketo-His})$ ion (**Scheme 8.2**). It should be noted that the $b_2(\text{diketo-His})$ ion has the same ion structure as protonated cyclo-(GH), an ion that could be easily generated by ESI of cyclo-(GH). Hence, the further dissociation of $b_2(\text{diketo})$ ion, as monitored by its CID-MS/MS daughter spectrum, should resemble the MS/MS spectrum of protonated cyclo(GH).

However, a recent theoretical study on the dissociation of protonated glycylglycine (GG) showed that the 'diketopiperazine' pathway is kinetically disfavored with a free energy barrier (ΔG_{298}) of 86.7 kJ mol⁻¹ higher than the N-protonated 'oxazolone' pathway, so that the $b_2(\text{diketopiperazine})$ ion may not be formed even though it is the most stable ion structure. [Balta et al., 2003] This study demonstrates that aside from the stability of the fragment ion

(and the associated neutral lost), knowledge on the energy barriers are essential in evaluating the competition between dissociation pathways in protonated peptides.

Wysocki and co-workers first demonstrated the very selective (preferred) cleavage of the histidine-proline (H-P) amide bond in the angiotensin family of protonated peptides, and provided experimental evidence in support of the formation of b_i (bicyclic) ions (i = location of histidine in the peptide), different from that of b_i (oxazolone-His) ions. The proposed reaction mechanism involves *nucleophilic attack of the side chain imidazole N^π (nitrogen at the 3-position) at a neighboring amide carbon on the C-terminal side*, forming a b_i (bicyclic) ion, as illustrated for the case of protonated GlyHis in **Scheme 8.2**.

Recently, Harrison and co-workers reported that, based on experimental observations and theoretical calculations, the linear penta-peptide YAGFL-NH₂ yields b_5 ions with the classical oxazolone structure initially, then further isomerize to yield the b_5 (diketopiperazine) ion upon collisional activation. [Harrison et al., 2006] By isomerization to an ion having a cyclic structure, the b_5 ion loses its sequence-specific information in the 5th amino acid residue. Hence, the isomerization process is viewed as an undesirable complicating phenomenon which could make peptide sequencing by MS/MS to be more difficult.

Studies in our laboratory also show that, at least under high collisional activation (RF) voltages of the ion trap mass analyzer, the MS/MS spectra of b_2 ions derived from protonated model tripeptides GHG and HGG and cyclo(GH) are very similar. On the other hand, it is still not known that aside from the b_2 (diketo-His) ions, whether the b_2 (oxazolone-His) and b_2 (bicyclic) ions could be competitively formed under different mass spectrometric collisional activation conditions.

Theoretical studies on the dissociation of protonated model dipeptides containing histidine remains not reported in the literature because the computation work is very demanding due to relatively larger size of the histidine-containing dipeptide system involved. However, recent success and theoretical studies presented in Chapter 6 and Chapter 7 suggest that density functional theory calculations could still be manageable for such complicated chemical system if a basis set chosen at a slightly lower level is used in the theoretical study. [Paizs and Suhai, 2005]

Because of the biochemical significance of histidine-containing peptides, and the likely implications of ion structure isomerization to peptide sequencing by MS/MS, we have decided to carry out a combined experimental and theoretical study on the competitive formation of b_2 (oxazolone-His), b_2 (diketo-His) and b_2 (bicyclic) ions from protonated peptides containing histidine. Specifically, high level density functional theory (DFT) calculations will be carried out to establish the theoretical potential energy surfaces (PES) for formation and isomerization of various b_2 ions from two model protonated histidine-containing dipeptides, glycyl-histidine (GlyHis, or GH) and histidyl-glycine (HisGly, or HG). The stable intermediates, transition states (TS), and energy barriers (ΔH_0 , ΔH_{298} and ΔG_{298}) of the dissociation pathways, which are not dealt with in the previous work of O'Hair and co-workers, [Farrugia et al., 2001] will be found. The theoretical study on dissociation pathways will be supplemented by energy-resolved and time-resolved mass spectrometric data obtained by Ms. Toby P. Y. Lau of Prof. Tsang's research group. The theoretical findings will be used to interpret and rationalize the experimental observations.

8.2 Results and Discussion

8.2.1 Collision-induced Dissociation (CID) of Protonated GlyHisGly and HisGlyGly

In this section, the experimental observations on the dissociation of the protonated GlyHisGly (GHG, His at C-terminal side of glycine) and HisGlyGly (HGG, His at N-terminus of the tripeptide) model peptides will first be presented. The low energy collision induced dissociation (CID) MS/MS spectra were obtained by Ms. Toby P. Y. Lau of Prof. Tsang's research group using a Finnigan-Mat LCQ ion trap mass analyzer (San Jose, USA). The ion trap CID MS/MS spectra of GlyHisGly (GHG) and HisGlyGly (HGG) is shown in Figure 8.1. The b_2 ion is the dominant sequence-specific fragment ion found in the mass spectra, while the y_2 ion is of very low intensity, or even absent in the case of HGG. This is a typical MS/MS spectrum of protonated peptides containing histidine; intense b_i ions are found to provide information on the peptide sequence. .

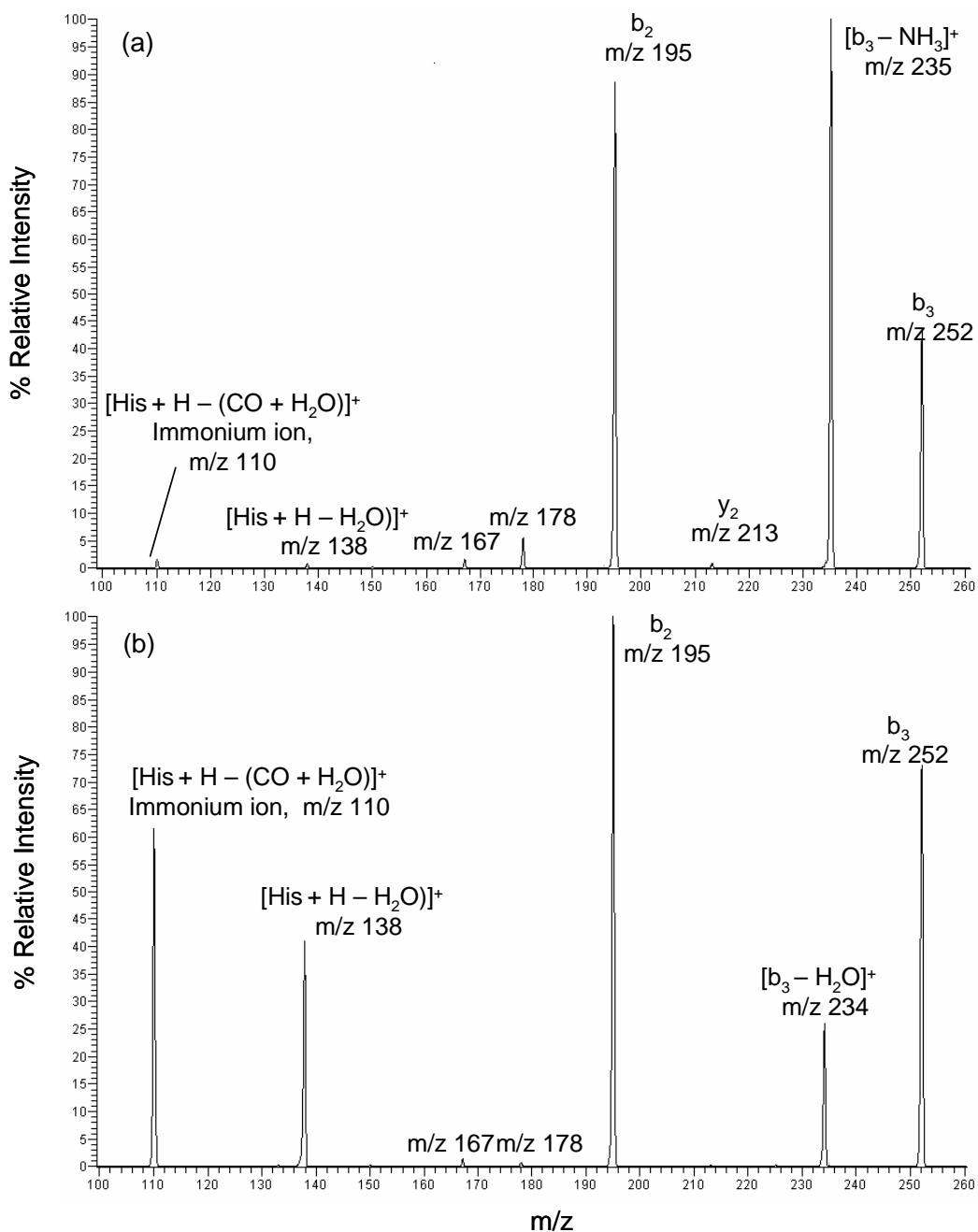


Figure 8.1 Ion trap MS/MS spectra of (a) protonated GlyHisGly, $[\text{GHG} + \text{H}]^+$, (m/z 270), obtained at a RF activation voltage (V_{p-p}) of 0.7 V, and (b) protonated HisGlyGly, $[\text{HGG} + \text{H}]^+$, (m/z 270), obtained at a RF activation voltage (V_{p-p}) of 0.7 V (both: ion trap mass analyzer conditions: normal scan mode, multiplier at -1100 volts; trap offset at -8 volts; isolation width at m/z 2; ion activation time in 10 ms; q_z at 0.25)

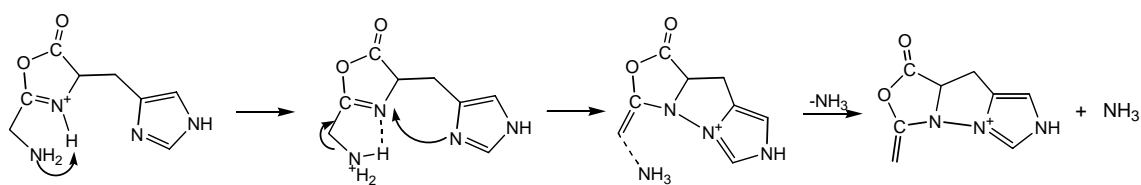
Further dissociation of b₂ ions derived from protonated GlyHisGly

An energy-

resolved MS/MS breakdown graph is comprised of plots of % relative fragment ion abundances as a function of collision energies. The ion trap MS/MS breakdown graph for b₂ ions of [GHG + H]⁺ (m/z 195) and [cyclo(GH) + H]⁺ ions (m/z 195) are shown in Figure 8.2(a) and 8.2(b), respectively. The % relative fragment ion abundances are found to be very similar for the two ions in the high activation (RF) voltage region (0.66 - 1.0 V). However, in the low activation (RF) voltage region (0.38 - 0.64 V), the b₂ ion of [GHG + H]⁺ dissociates to yield very abundant [b₂ - NH₃]⁺ ions (due to loss of NH₃) different from the [cyclo(GH) + H]⁺ ion. This observation indicates that aside from the b₂(diketo-His) ion, other possible structures of b₂ ions, i.e., the b₂(oxazolone-His) and/or b₂(bicyclic) ions, may initially be formed at low collision energies (refer to **Scheme 8.2**).

Low energy CID MS/MS spectra obtained with the ion trap mass analyzer is known to favor formation of fragment ions with low critical energies; i.e., the average internal energy of the dissociating protonated peptide precursor ions (dissociations within a time frame of 5-30 milliseconds) is relatively low compared to that observed in a triple quadrupole or a quadrupole-(time-of-flight) (Q-TOF) tandem mass spectrometers (dissociations within a much shorter time frames of a few tens of microseconds). [Catinella et al., 2000; McLuckey and Goeringer, 1997; Gronowska et al., 1990] In order to confirm the ion trap CID observations, the breakdown graph obtained under the more energetic CID conditions of a Q-TOF tandem mass spectrometer were obtained (Figure 8.3 (a) and (b)), which again confirmed the preferred loss of NH₃ from the b₂ ion of protonated GHG at low collision energies (8-16 eV range, with % abundance of the [b₂ - NH₃]⁺ ion exceeding the 20% ion abundance of [cyclo(GH) + H]⁺). Thus, both the ion trap and Q-TOF breakdown graphs

suggest that the $b_2(\text{oxazolone-His})$ and/or $b_2(\text{bicyclic})$ ions are energetically preferred to be formed, at least at low collisional energies near the appearance threshold region. As the $b_1(\text{bicyclic})$ ions are known to prefer losing CO rather than NH_3 [Tsapralis et al., 2004], the intense loss of NH_3 at low-collision energies is very likely to be originated from the $b_2(\text{oxazolone-His})$ ion. The proposed pathway for the loss of NH_3 from $b_2(\text{oxazolone-His})$ ion is shown in **Scheme 8.3**.



$b_2(\text{oxazolone-His})$ from GH

Scheme 8.3 The proposed pathway of loss of NH_3 from $b_2(\text{oxazolone-His})$ ion of $[\text{GlyHis} + \text{H}]^+$

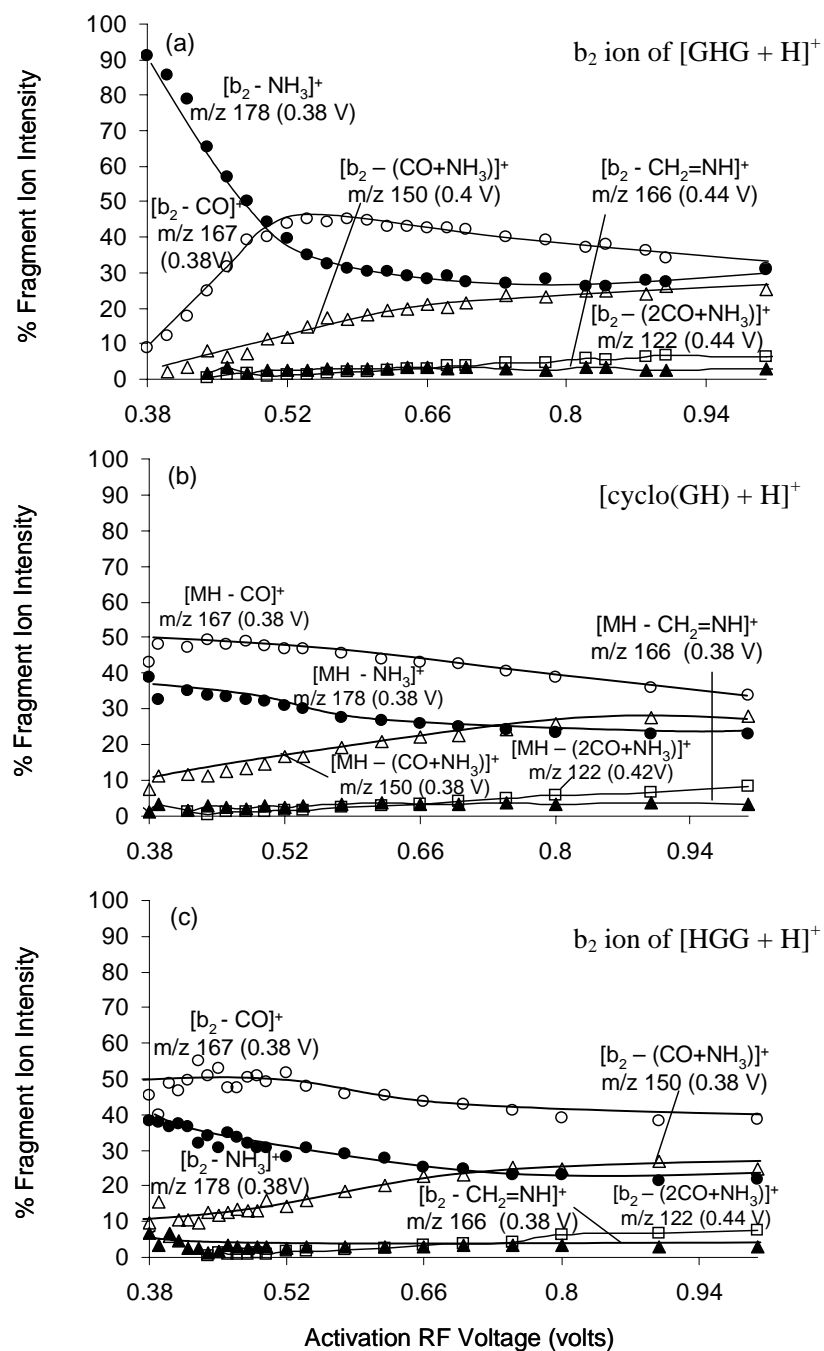


Figure 8.2 Ion trap energy-resolved MS/MS breakdown graphs of (a) b_2 ion of protonated GlyHisGly, $[\text{GHG} + \text{H}]^+$ (m/z 195), (b) protonated cyclo(GH), $[\text{cyclo}(\text{GH}) + \text{H}]^+$ (m/z 195), and (c) b_2 ion of protonated HisGlyGly, $[\text{HGG} + \text{H}]^+$ (m/z 195) ((a) (b) (c) ion trap mass analyzer conditions: normal scan mode, multiplier at -1100 volts; trap offset at -8 volts; isolation width at m/z 2; ion activation time at 10 ms; q_z at 0.25)

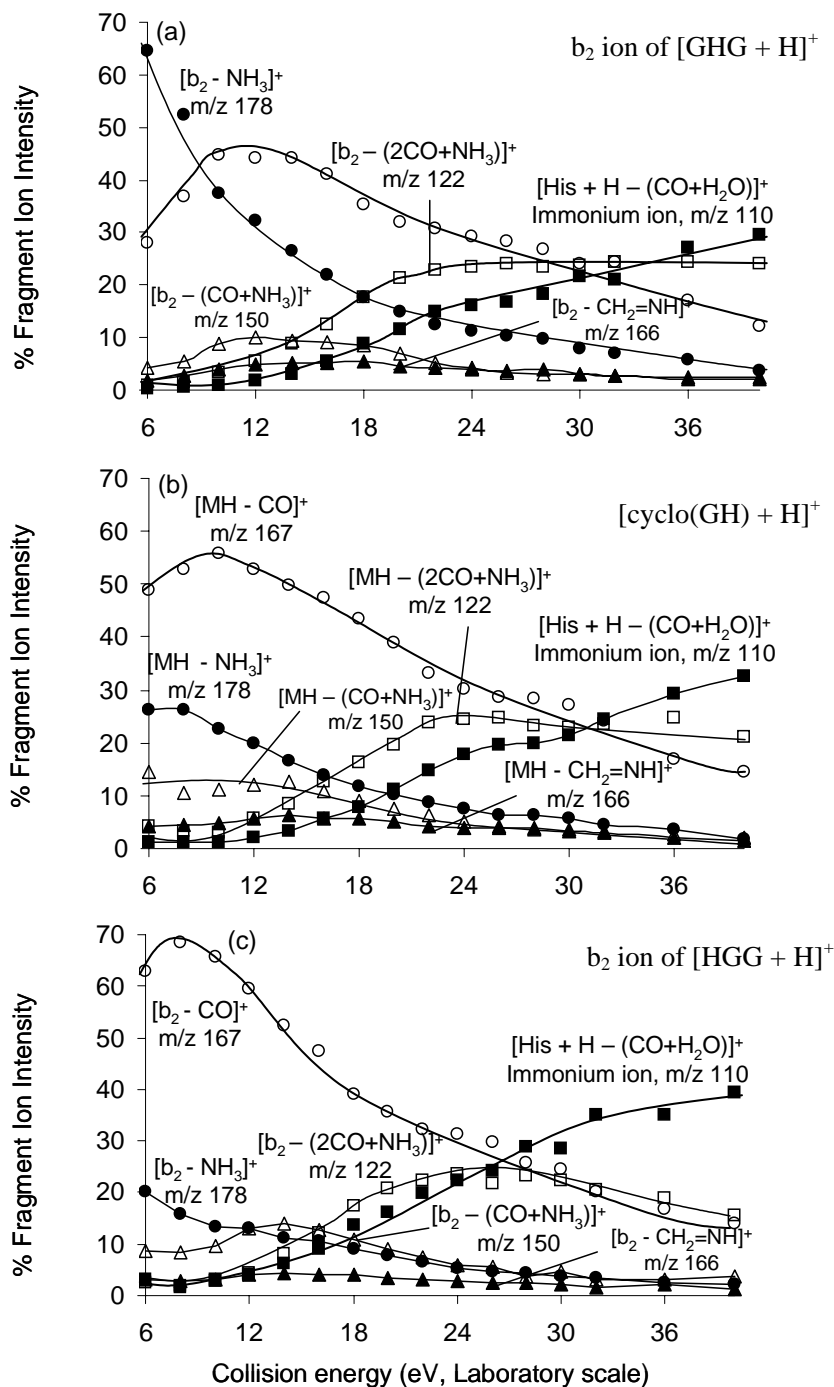


Figure 8.3 Q-TOF energy-resolved MS/MS breakdown graphs of (a) b_2 ion of protonated GlyHisGly, $[GHG + H]^+$ (m/z 195), (b) protonated cyclo(GH), $[cyclo(GH) + H]^+$ (m/z 195), and (c) b_2 ion of protonated HisGlyGly, $[HGG + H]^+$ (m/z 195) ((a)(b)(c) generated by 15 % attenuation at 10 eV of the precursor ion beam intensity)

Experimental evidence indicating isomerization from b_2 (oxazolone-His) ion to b_2 (diketo-His) ion derived from protonated GlyHisGly

The results of the ion trap time-resolved study of the dissociation of b_2 ion of $[\text{GHG} + \text{H}]^+$ (m/z 195) and $[\text{cyclo}(\text{GH}) + \text{H}]^+$ (m/z 195) are shown in Figure 8.4. For the b_2 ion of $[\text{GHG} + \text{H}]^+$, the $[\text{b}_2 - \text{CO}]^+ / [\text{b}_2 - \text{NH}_3]^+$ intensity ratio increases with increasing the collisional activation time, but remains less than that of $\text{cyclo}(\text{GH})$ even at a relatively long activation time of 80 milliseconds. The observed results strongly suggest that more b_2 (oxazolone-His) ions isomerize to the b_2 (diketo-His) ions with increasing collision activation time, so that more loss of CO and NH_3 are derived from the b_2 (diketo-His) ions formed at long activation times. However, even at very long activation times, the $[\text{b}_2 - \text{CO}]^+ / [\text{b}_2 - \text{NH}_3]^+$ intensity ratio is not the same as that of

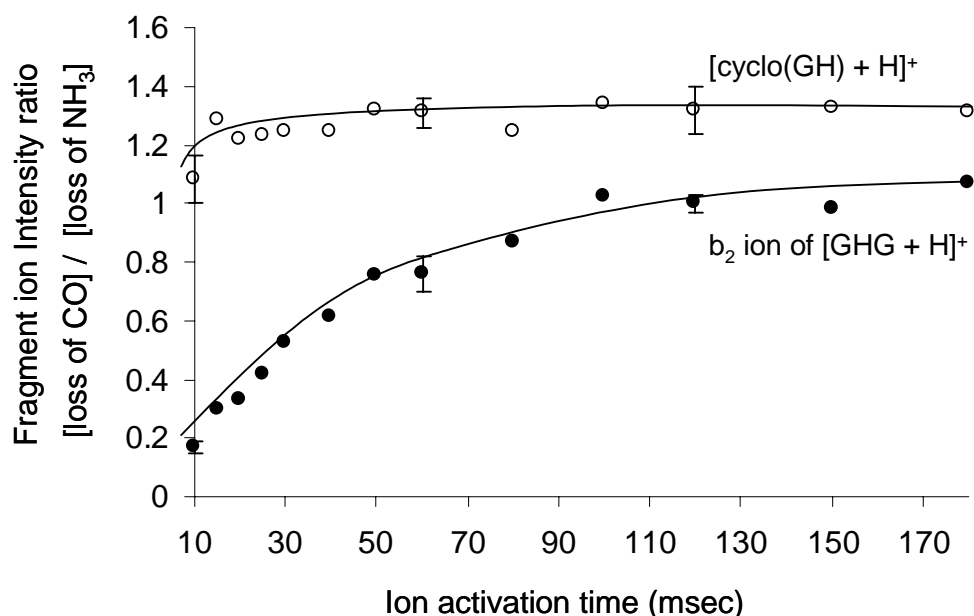


Figure 8.4 Ion trap time-resolved MS/MS study of b_2 of protonated GlyHisGly, $[\text{GHG} + \text{H}]^+$, (m/z 195) versus $[\text{cyclo}(\text{GH}) + \text{H}]^+$ (m/z 195) (both: ion trap mass analyzer conditions: normal scan mode, multiplier at -1100 volts; isolation width at m/z 2; trap offset at -8 volts; q_z at 0.25; activation RF voltage in 0.42 V)

$[\text{cyclo}(\text{GH}) + \text{H}]^+$, suggesting that complete isomerization to the $\text{b}_2(\text{diketo-His})$ structure has not been achieved.

Further dissociation of b_2 ions derived from Protonated HisGlyGly

Similarly,

energy-resolved and time-resolved studies were conducted with b_2 ions derived from protonated HisGlyGly (HGG) where histidine is located at the N-terminus of the model tripeptide. The quadrupole-time-of flight (Q-TOF) energy-resolved MS/MS breakdown graph of b_2 ions derived from $[\text{HGG} + \text{H}]^+$ (m/z 195) and that of $[\text{cyclo}(\text{GH}) + \text{H}]^+$ (m/z 195) are shown in Figure 8.3(c) and 8.3(b), respectively. As in the case of $[\text{GHG} + \text{H}]^+$, both ions dissociate to yield the same fragment ions due to loss of CO, NH_3 , $(\text{CO} + \text{H}_2\text{O})$, $(\text{CO} + \text{NH}_3)$, $\text{CH}_2=\text{NH}$ and $(2\text{CO} + \text{NH}_3)$ neutrals, but the % relative abundance of the fragment ions differ over the entire collision energy range of 8 – 28 eV. In the low collision-energy region ($\sim 12 - 14$ eV), the b_2 ion of $[\text{HGG} + \text{H}]^+$ shows more prominent loss of CO than $[\text{cyclo}(\text{GH}) + \text{H}]^+$. Both the $\text{b}_i(\text{oxazolone})$ and $\text{b}_i(\text{bicyclic})$ ions are known to dissociate further by preferred loss of CO. At higher collisional energies ($\sim 14 - 40$ eV), the % fragment abundances of b_2 ions of $[\text{HGG} + \text{H}]^+$ resemble more to that of $[\text{cyclo}(\text{GH}) + \text{H}]^+$, but still remain different. For example, the % abundance of the $[\text{His} + \text{H} - (\text{CO} + \text{H}_2\text{O})]^+$ fragment ion exceeds the intensity of the $[\text{b}_2 - \text{CO}]^+$ ion at ~ 24 eV collision energy for the b_2 ion, but remains less than that of the $[\text{M} + \text{H} - \text{CO}]^+$ ion for $[\text{cyclo}(\text{GH}) + \text{H}]^+$. This indicates that aside from the $\text{b}_2(\text{diketo-His})$ ion, other possible structure of b_2 ions, i.e., the $\text{b}_2(\text{oxazolone-His})$ ion is likely to be formed initially at low collision energies at the microsecond time scale and more energetic CID conditions of a Q-TOF mass spectrometer, and remain at noticeably significant proportions even at higher collision energies. The $\text{b}_2(\text{bicyclic})$ ion is unlikely to be formed because its

formation is possible only when histidine is located at the C-terminal side of glycine (refer to **Scheme 8.2**)

Experimental evidence indicating isomerization from $b_2(\text{oxazolone-His})$ to $b_2(\text{diketo-His})$ ion derived from protonated HisGlyGly

Contrary to the energy-resolved breakdown graphs obtained under Q-TOF CID conditions (microsecond time scale), and with much longer (millisecond) time scale of the ion trap mass analyzer, the energy-resolved breakdown graph of the b_2 ions derived from $[\text{HGG} + \text{H}]^+$ (Fig. 8.2 (c)) are almost the same as that of $[\text{cyclo}(\text{GH}) + \text{H}]^+$ (Figure 8.2 (b)). One possible explanation is that given sufficient time, the initially formed $b_2(\text{oxazolone-His})$ ions have isomerized to the $b_2(\text{diketo-His})$ structure in the millisecond time frame of the ion trap mass analyzer.

The results of energy-resolved studies are further corroborated by ion trap time-resolved studies. As shown in Figure 8.5, the ion trap $[\text{b}_2 - \text{CO}]^+ / [\text{b}_2 - \text{NH}_3]^+$ intensity ratio as a function of collisional activation time for the b_2 ions of $[\text{HGG} + \text{H}]^+$ is nearly the same as that of $[\text{cyclo}(\text{GH}) + \text{H}]^+$, indicating that isomerization of initially formed $b_2(\text{oxazolone-His})$ (or $b_2(\text{bicyclic})$ ion) to $b_2(\text{diketo-His})$ ion is nearly complete in the millisecond time scale of the ion trap mass analyzer. This is in direct contrast to the Q-TOF CID results, which indicate that the $b_2(\text{oxazolone-His})$ ions (or $b_2(\text{bicyclic})$ ions) initially formed cannot isomerize completely to the $b_2(\text{diketo-His})$ ion in the relatively short time frame (microsecond) of the Q-TOF mass spectrometer.

8.2.2 Dissociation of Protonated GlyHis: Theoretical Potential Energy Surface (PES) for Competitive Formation of b_2 (oxazolone-His), b_2 (diketo-His) and b_2 (bicyclic) ions

The smallest protonated peptide system that could yield the b_2 (oxazolone-His) and b_2 (diketo-His) ions with histidine at the C-terminal side of glycine is the model dipeptide GlyHis. For this reason, we have explored theoretically the energetics of competitive formation of the b_2 (oxazolone-His), b_2 (diketo-His) and b_2 (bicyclic) from protonated GlyHis; the proposed pathways and the corresponding potential energy surface (PES) are shown in Figure 8.6.

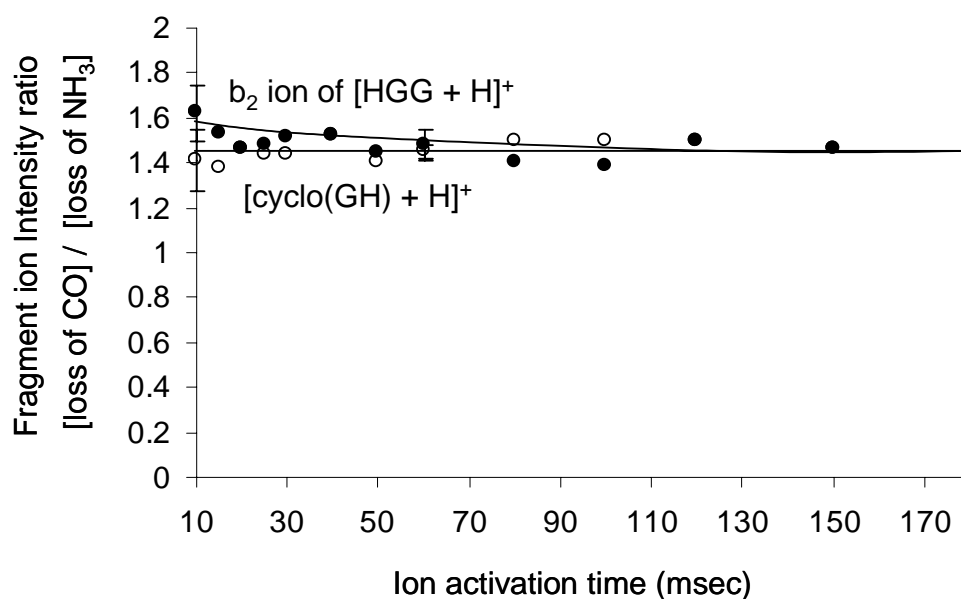


Figure 8.5 Ion trap time-resolved MS/MS study of b_2 ion of protonated HisGlyGly, $[\text{HGG} + \text{H}]^+$, (m/z 195) versus protonated cyclo(GH), $[\text{cyclo}(\text{GH}) + \text{H}]^+$, (m/z 195) (both: ion trap mass analyzer conditions: normal scan mode, multiplier at -1100 volts; isolation width at m/z 2; trap offset at -8 volts; q_z at 0.25; activation RF voltage in 0.46 V)

Following the notations used in the previous chapter, the labels **1**, **3**, etc. denote the various minima (stable intermediates), and the labels **TS2**, **TS4**, etc. denote the various transition structures (TS) between the minima on the PES. All the intermediates and transition structures are fully optimized at the B3-LYP/6-31G(d) level, and the nature of stationary points were confirmed by frequency calculations. Moreover, the transition structures are verified to be connecting the specific minimum by Intrinsic Reaction Coordinate (IRC) calculations. The optimized geometries of the various intermediates and TS are shown in Figure 8.7. With these structures, single point energy calculations were performed at the same level of theory, i.e. B3-LYP/6-31G(d). The electronic energies at 0K of all species were corrected with B3-LYP/6-31G(d) zero-point vibrational energies, scaled by 0.9806 [Scott and Radom, 1996]. All the discussions below are based on energetics at 0K unless otherwise stated.

Proposed Pathway for formation of b_2 (oxazolone-His) ions The proposed mechanism of b_2 (oxazolone-His) formation from protonated GlyHis is shown in the corresponding potential energy surface (PES) (Fig. 8.5(a)). Starting from the most stable conformer of protonated GlyHis (species **1**), species **2** (a less stable conformer of protonated GlyHis) is formed after a simple bond rotation between the carbon of the imidazole ring and the methylene group (-CH₂-) of the main carbon chain. It is formed to facilitate the proton transfer from the N^π-nitrogen of the imidazole ring to the hydroxyl oxygen (O_H) at the C-terminus via the transition species **TS3**. After the proton transfer, a loose ion-molecule complex, species **4**, is formed. Species **4** is actually a loose ion-molecule complex with a water molecule (H₂O) weakly bound to the 2-(aminomethyl)-4-(1H-imidazol-4-ylmethyl)-5-oxo-4,5-dihydro-3H-1,3-oxazol-1-ium ion, which is more commonly known as the

$b_2(\text{oxazolone-His})$ ion [Farrugia et al., 2001]. Before the H_2O is about to be detached, it could rotate freely to form a relatively more stable complex, species **5**, with H_2O hydrogen bonded to the N^π of the imidazole ring ($\text{OH}\cdots\cdots\text{N}^\pi$) and the secondary amino hydrogen of the oxazolone ring ($\text{H}_2\text{O}\cdots\cdots\text{HN}$). After the detachment of H_2O , the $b_2(\text{oxazolone-His})$ is formed (species **6** + H_2O). The energy barrier for the formation of $b_2(\text{oxazolone-His})$ of this process, i.e., the energy difference between species **1** and species (**6** + H_2O), is 129 kJ mol^{-1} .

Formation Pathway of $b_2(\text{diketo-His})$ The formation of $b_2(\text{diketo-His})$ is another competitive dissociation pathway of protonated GlyHis. The proposed formation mechanism of $b_2(\text{diketo-His})$ is also shown in the corresponding potential energy surface (PES) (Fig. 8.5(a)). Starting from the most stable conformer of protonated GlyHis (species **1**), species **7** is formed after the carbonyl group ($-\text{COOH}$) is rotated to the same side of the amino group ($-\text{NH}_2$) at the N-terminus, such that the hydroxyl oxygen (O_H) is near to the amino group. After the proton is transferred from the amino group to O_H via transition species **TS8**, an ion-molecule species **9** is formed. A water molecule (H_2O) is weakly attached to the 5-(3,6-dioxopiperazin-2-yl)-1*H*-imidazol-3-ium, which is also denoted as $b_2(\text{diketo-His})$ in this section. H_2O could freely move around the molecule and attach to other possible binding sites in order to obtain a more stable structure; it is finally attached to the τ -nitrogen (N^τ) of the imidazole ring (species **10**). After the H_2O is detached from the molecule, a stable species, $b_2(\text{diketo-His})$ is formed (species **11** + H_2O). The 0K enthalpy of the formation of $b_2(\text{diketo-His})$ of this process, i.e., the energy difference between species **1** and species (**11** + H_2O), is 38 kJ mol^{-1} , with an energy barrier at **TS8** of 190 kJ mol^{-1} .

Proposed pathway for formation of $b_2(\text{bicyclic})$ ions The proposed dissociation pathway of protonated GlyHis leading to the formation of the $b_2(\text{bicyclic})$ ion is shown in the

corresponding potential energy surface (PES) (Fig. 8.6(b)). Starting from the most stable conformer of protonated GlyHis (species **1**), species **12** is formed after a simple bond rotation between the carbon of the imidazole ring and the methylene group (-CH₂-) of the main carbon chain, so that the N^π-nitrogen of the imidazole ring is near to the hydroxyl oxygen (O_H). Species **14** is formed after the proton is transferred from N^π of the imidazole group to O_H via the transition species **TS13**. Species **14** is an ion-molecule complex which a water molecule (H₂O) weakly bound to a bicyclic molecule, 6-[(aminoacetyl)amino]-5-oxo-2,5,6,7-tetrahydropyrrolo[1,2-*c*]imidazol-4-ium. For simplicity, it is named as the b₂(bicyclic) ion in this study. After the detachment of H₂O, the b₂(bicyclic) ion is formed (species **15** + H₂O). The 0K enthalpy of the formation of b₂(diketo-His) of this process, i.e., the energy difference between species **1** and species (**15** + H₂O), is 163 kJ mol⁻¹, with an energy barrier at **TS13** of 180 kJ mol⁻¹.

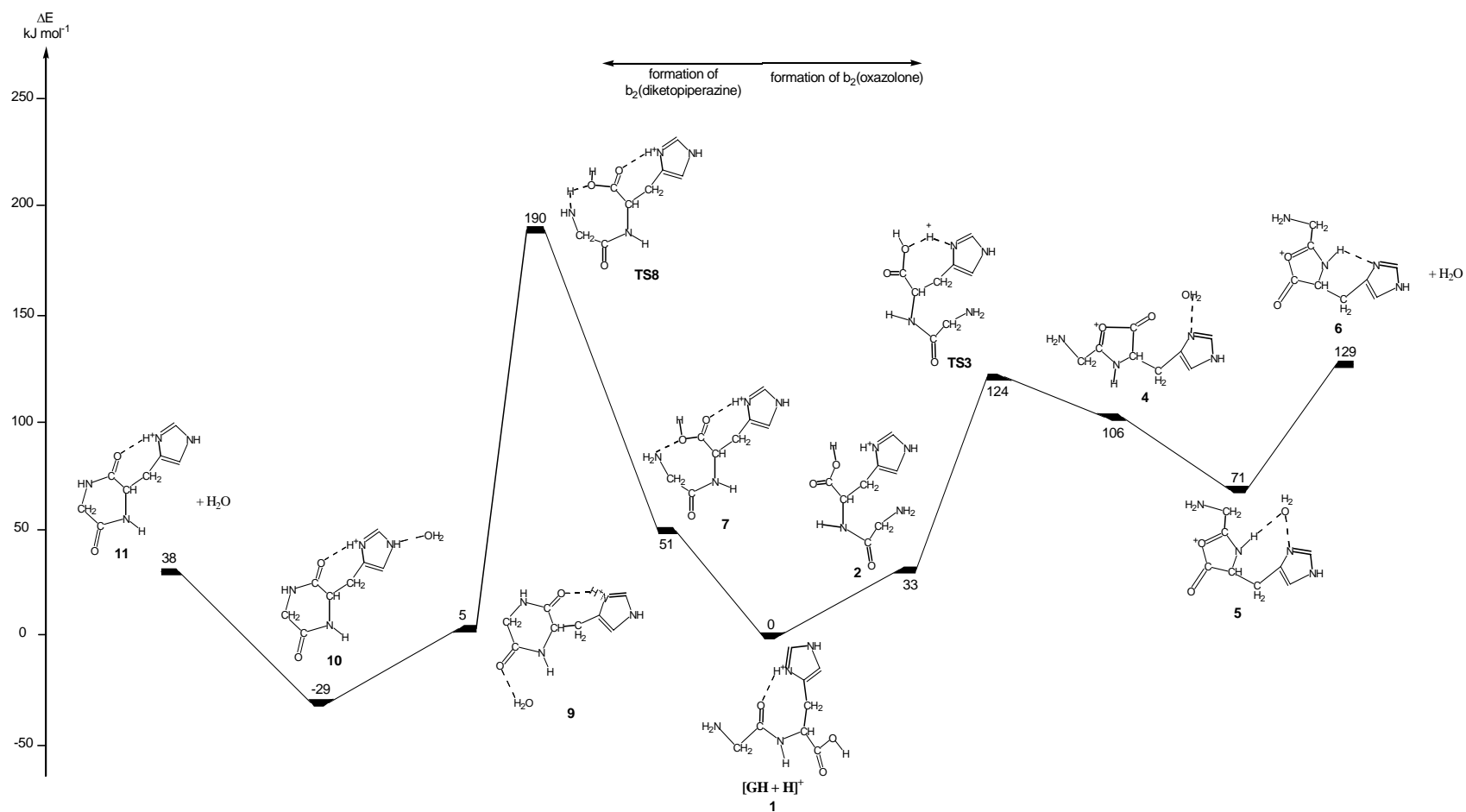


Figure 8.6 (a) Potential energy surface (PES) of the dissociation of $[\text{GlyHis} + \text{H}]^+$, leading to the formation of $b_2(\text{oxazolone})$ and $b_2(\text{diketopiperazine})$ at 0K, calculated at the B3-LYP/6-31G(d)//B3-LYP/6-31G(d) level

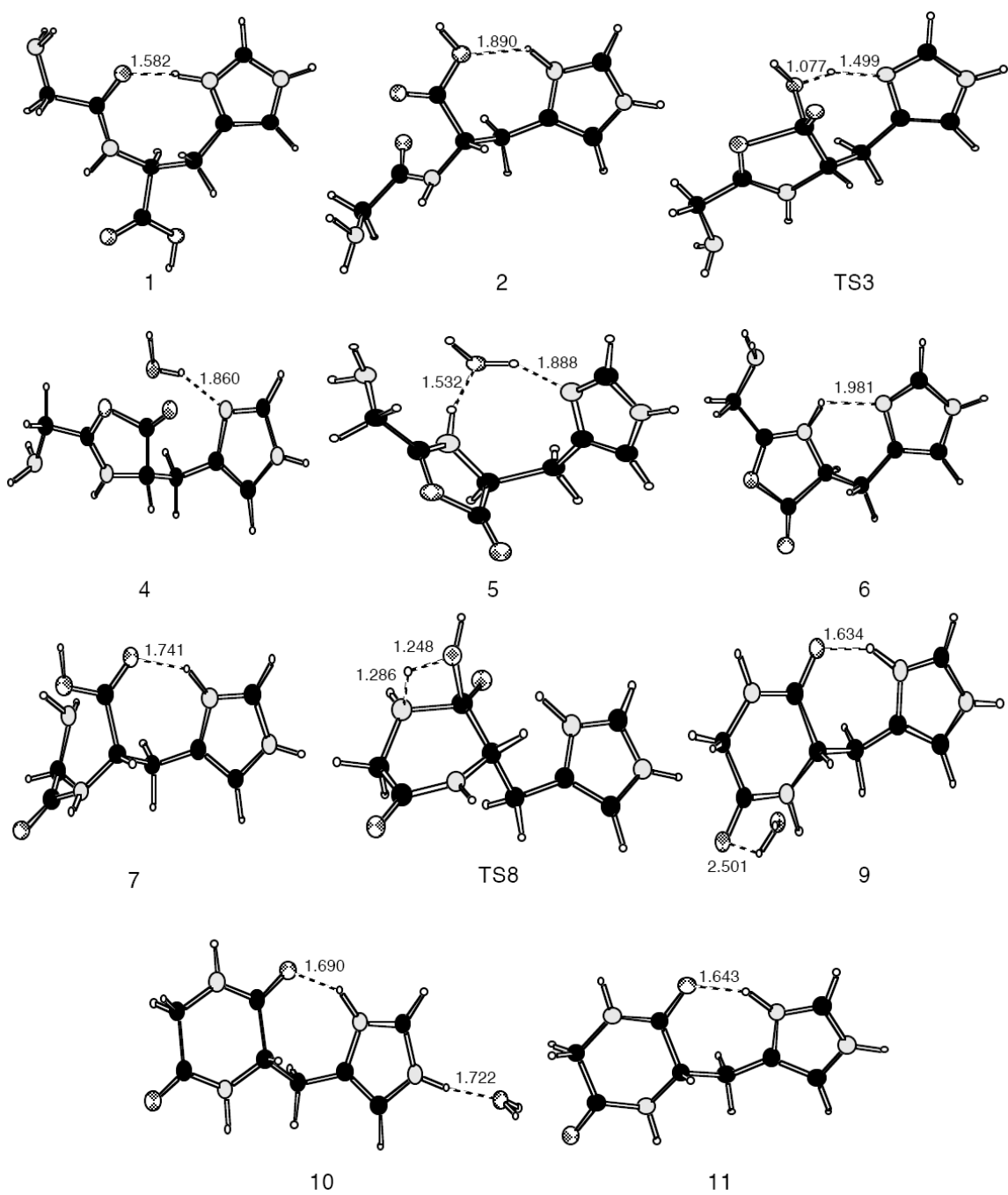


Figure 8.7(a) Optimized geometries (at B3-LYP/6-31G(d) level) of the various intermediates and transition species shown in the potential energy surface (PES) of formation of b_2 (oxazolone) and b_2 (diketopiperazine) from protonated GlyHis

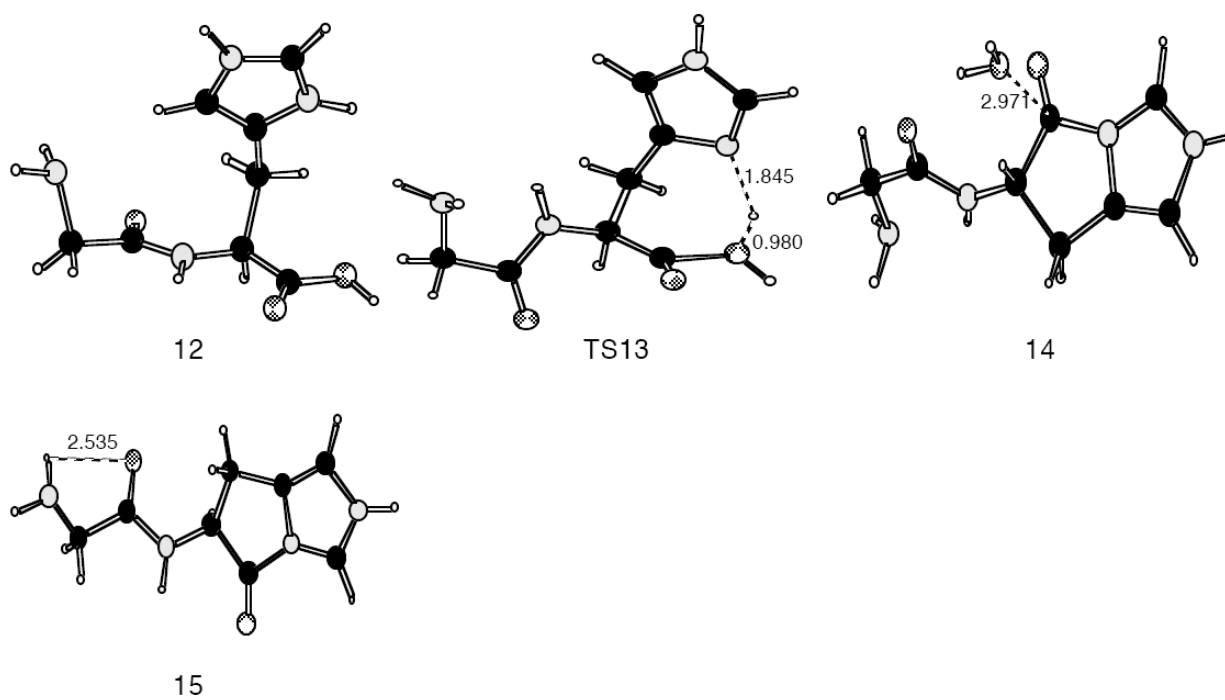


Figure 8.7(b) Optimized geometries (at B3-LYP/6-31G(d) level) of the various intermediates and transition species shown in the potential energy surface (PES) of formation of b_2 (bicyclic) from protonated GlyHis

Table 8.1 Energy barriers for the formation of different b_2 ions and further isomerization on the [GlyHis / HisGly + H]⁺ potential energy surface^a: the relative enthalpies (ΔH_0 , ΔH_{298} at 0K and 298K), Gibbs free energies (ΔG_{298} at 298K, in kJ mol⁻¹) and entropies (ΔS_{298} at 298K, in J mol⁻¹)

	[GlyHis + H] ⁺				[HisGly + H] ⁺			
	ΔH_0	ΔH_{298}	ΔG_{298}	ΔS_{298}	ΔH_0	ΔH_{298}	ΔG_{298}	ΔS_{298}
<i>b₂ formation</i>								
b ₂ (oxazolone)	129 ^b	134	90	148	233 ^f	233	232	3
b ₂ (diketopiperazine)	190 ^c	186	200	-485	234 ^g	230	242	-40
b ₂ (bicyclic)	180 ^d	182	180	7	/	/	/	/
<i>further isomerization</i>								
b ₂ (oxazolone)→ b ₂ (diketopiperazine)	330 ^e	333	305	94	348 ^h	350	325	84

^a Theoretical calculated ΔH_0 , ΔH_{298} , ΔG_{298} and ΔS_{298} values are based on the potential energy surface at 0K calculated at B3-LYP/6-31G(D)//B3-LYP/6-31G(D) level

^b Formation of b₂(oxazolone) from [GlyHis + H]⁺, structure **6** of Figure 8.6(a).

^c Via transition structure **TS8** of Figure 8.6(a).

^d Via transition structure **TS13** of Figure 8.6(b).

^e Via transition structure **TS7i** of Figure 8.8.

^f Via transition structure **TS5** of Figure 8.10.

^g Via transition structure **TS10** of Figure 8.10.

^h Via transition structure **TS12i** of Figure 8.12.

The theoretically estimated energy barriers (ΔH_0 at 0K) for competitive formation of the b_2 (oxazolone-His), b_2 (diketo-His), and b_2 (bicyclic) ions from protonated GlyHis, together with the calculated ΔH_{298} , ΔG_{298} and ΔS_{298} values, are listed in Table 8.1. As shown in Table 8.1, the order of critical energies (dissociation energy barriers of different structures in kJ mol^{-1}) is: b_2 (oxazolone-His) (129) < b_2 (bicyclic) (180) < b_2 (diketo-His) (190). The theoretical order of critical energies is in agreement with experimental observations, indicating that the formation of b_2 ions is competitive, and the product ions might actually be a mixture of b_2 ions with three different structures, if sufficient collisional energy (exceeding the energy barrier of formation of b_2 (diketo) ion at 190 kJ mol^{-1}) is available. On the other hand, as the b_2 (oxazolone-His) pathway has the lowest critical energy among the three pathways, the formation of b_2 (oxazolone-His) ion is energetically preferred over the formation of b_2 (diketo-His) and b_2 (bicyclic) ions at low collisional energies. Furthermore, once the critical energies are exceeded, formation of b_2 (diketo-His) ion is entropically (kinetically) disfavored, as indicated by the relatively large negative ΔS_{298} values of $-485 \text{ J mol}^{-1} \text{ K}^{-1}$ for the energy barriers. Taken together, the b_2 (oxazolone-His) is very likely the dominant b_2 ion formed from the dissociation of protonated GlyHis at low collision energies; the formation of b_2 (oxazolone-His) ion is both energetically and entropically preferred over the formation of b_2 (diketo-His) and b_2 (bicyclic) ions.

8.2.3 Dissociation of Protonated GlyHis: Proposed Pathway for Isomerization of $b_2(\text{oxazolone-His})$ ion to $b_2(\text{diketo-His})$ ion

According to the ion trap time-resolved study of b_2 ion of protonated glycyl-histidyl-glycine ($[\text{GHG} + \text{H}]^+$) in Section 8.2.1 (Fig. 8.4), the proportion of $b_2(\text{diketo-His})$ ions relative to that of the $b_2(\text{oxazolone-His})$ ions increases with the activation time, or with increasing internal energies supplied to the ion via longer activation times. In other words, even though the $b_2(\text{oxazolone-His})$ ion is energetically favored to be formed (as indicated by the lower energy barriers, $\sim 61 \text{ kJ mol}^{-1}$, refer to Fig. 8.6(a)) from the dissociation of protonated GlyHis, it will further isomerize to the $b_2(\text{diketo-His})$ ion through molecular rearrangement if ‘additional’ internal energy is imparted to the ion via collisional activation. Because the $b_2(\text{diketo-His})$ ion is much more stable than the $b_2(\text{oxazolone-His})$ ion ($\sim 91 \text{ kJ mol}^{-1}$), isomerization to the most stable product ion is likely to occur eventually. However, reverse isomerization from $b_2(\text{diketo-His})$ back to $b_2(\text{oxazolone-His})$ is unlikely to process because of the relatively large reverse energy of activation energy required. For this reason, we have explored theoretically the energetics and mechanism of isomerization from $b_2(\text{oxazolone-His})$ ion to $b_2(\text{diketo-His})$ ion of protonated GlyHis; the proposed pathway and the corresponding potential energy surface (PES) is shown in Figure 8.8. The optimized geometries of the various intermediates and transition species are shown in Figure 8.9.

Proposed isomerization pathway of $b_2(\text{oxazolone-His})$ to $b_2(\text{diketo-His})$ for protonated

GlyHis The formation pathway of $b_2(\text{oxazolone-His})$ from GlyHis has been briefly discussed in the previous section. Starting from the $b_2(\text{oxazolone-His})$ ion (species **6**), bond lengthening occurs between the carbonyl group ($\text{C}=\text{O}$) and the oxygen of the oxazolone ring. The amino nitrogen from the amino group (NH_2) tends to form a bond with the carbonyl

group to compensate the positive charge on the carbocation ($^+C=O$) via transition species **TS7i**. After bond formation, species **8i** is formed, where the protonation site is located at the amino nitrogen (N^+H_2) of the diketopiperazine ring. The proton is then transferred from the N^+H_2 of the diketopiperazine ring to the π -nitrogen (N^π) of the imidazole ring via transition species **TS9i** to yield species **10i**. However, species **10i** is not the most stable form of the product in this pathway; it changes to be a more stable conformer (species **11i**) via a simple bond rotation. Species **11i** has the same structure and conformation as the b_2 (diketo-His) ion which has been discussed in the previous Section 8.2.2. The 0K enthalpy of isomerization from b_2 (oxazolone-His) to b_2 (diketo-His), i.e., the energy difference between species **1** and species (**11i** + H_2O), is 38 kJ mol^{-1} , with an energy barrier at **TS7i** of 330 kJ mol^{-1} .

The theoretically estimated energy barriers at 0K for isomerization from b_2 (oxazolone-His) to b_2 (diketo-His) of protonated GlyHis, together with the calculated ΔH_{298} , ΔG_{298} and ΔS_{298} values, are listed in Table 8.1. The energy difference between the barrier of the formation of b_2 (oxazolone-His) and that of further isomerization is about 201 kJ mol^{-1} ; the relatively high energy difference could account for the incomplete isomerization as shown in the ion trap time-resolved study of b_2 ion derived from protonated glycyl-histidyl-glycine ($[GHG + H]^+$) (Fig. 8.4).

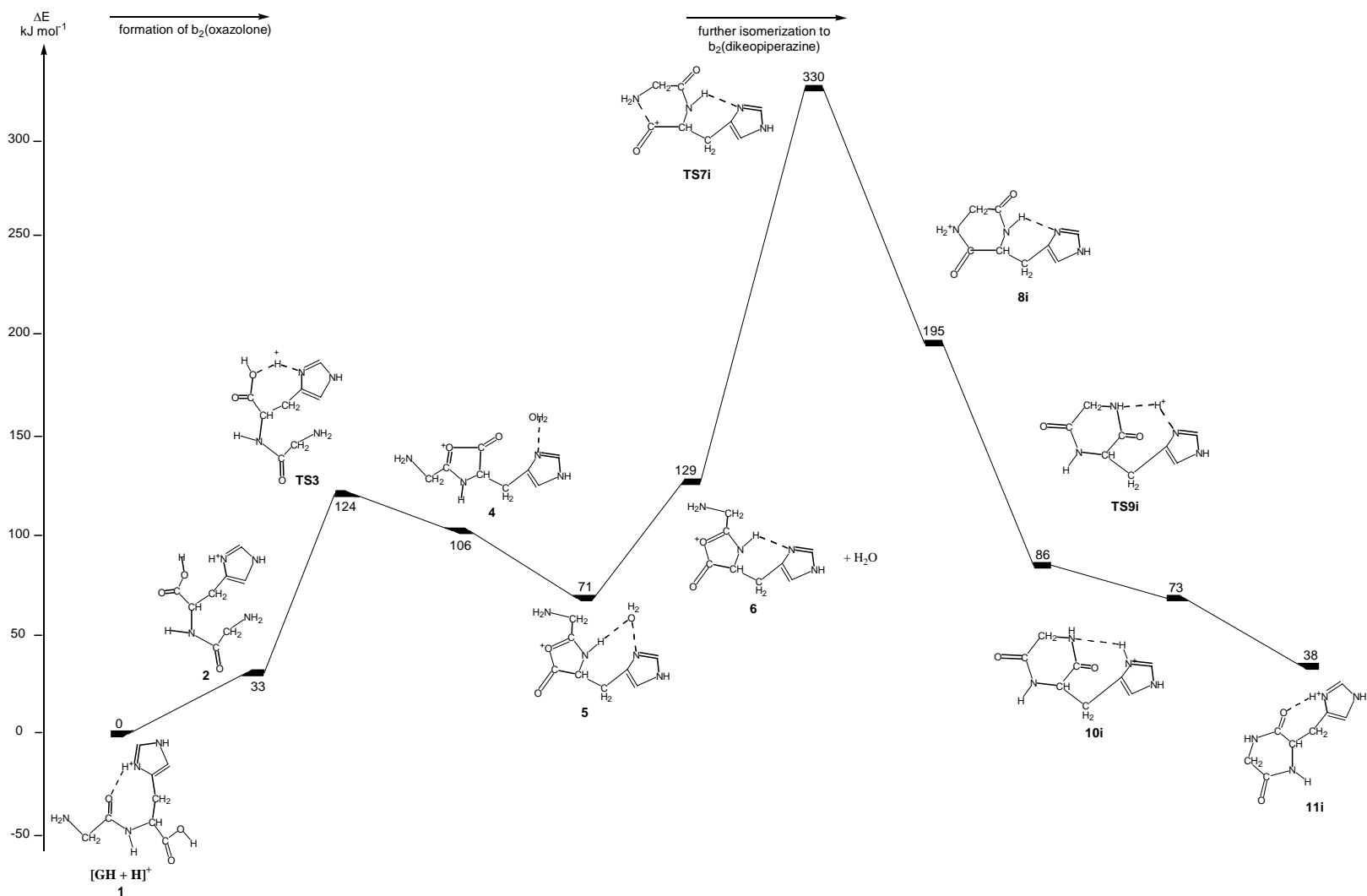


Figure 8.8 Potential energy surface (PES) of the dissociation of $[\text{GlyHis} + \text{H}]^+$, leading to the formation of b_2 (oxazolone) and further isomerization to b_2 (diketopiperazine) at 0K, calculated at the B3-LYP/6-31G(d)//B3-LYP/6-31G(d) level

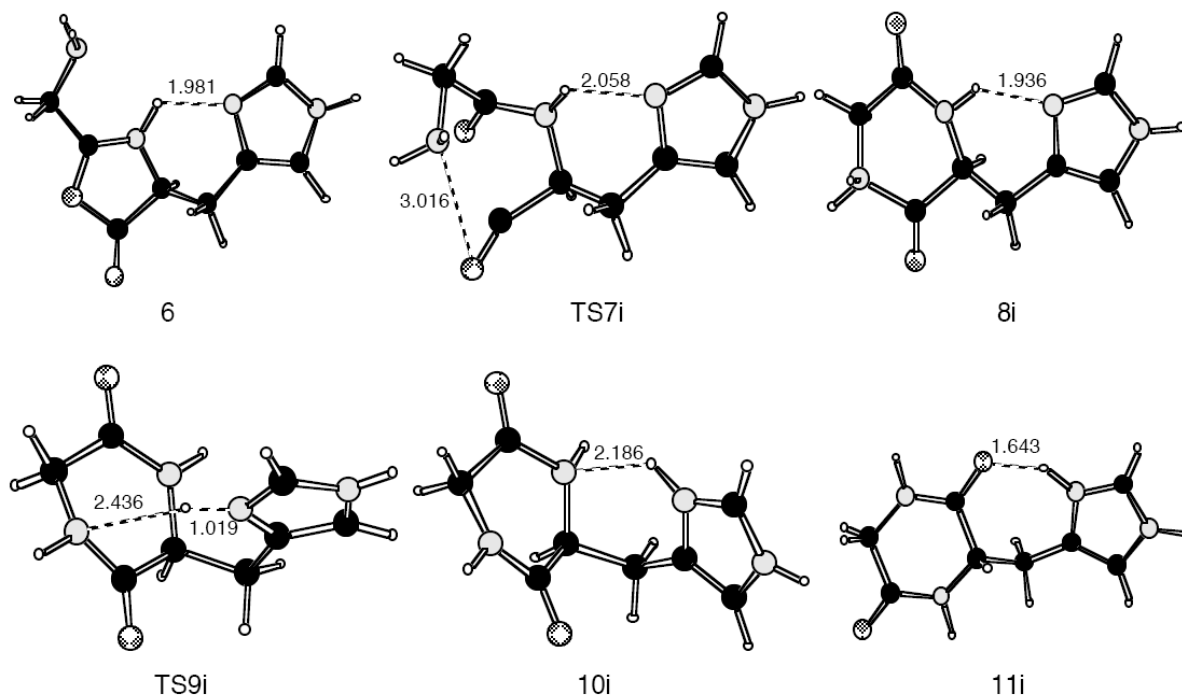


Figure 8.9 Optimized geometries (at B3-LYP/6-31G(d) level) of the various intermediates and transition species shown in the potential energy surface (PES) of further isomerization to b_2 (diketopiperazine) from protonated GlyHis

8.2.4 Dissociation of Protonated HisGly: Theoretical Potential Energy Surface (PES) for Competitive Formation of b_2 (oxazolone-His) and b_2 (diketo-His) ions

In this section, the dissociation pathway of protonated HisGly is theoretically studied. It is likely that the location of histidine (His) residue in dipeptides will affect its dissociation mechanism. As a result, it is of interest to find out the difference in dissociation mechanisms and critical energies due to the positional effect, i.e., when His is located at the C-terminus (Section 8.2.2 and 8.2.3) versus the N-terminus (current Section 8.2.4). For this reason, we have explored theoretically the energetics of competitive formation of the

$b_2(\text{oxazolone-His})$ and $b_2(\text{diketo-His})$ ions from the dissociation of protonated HisGly; the proposed pathways and the corresponding potential energy surface (PES) is shown in Figure 8.10. The optimized geometries of the various intermediates and TS are shown in Figure 8.11. The discussions below are based on energetics at 0K unless otherwise noted.

Formation Pathway of $b_2(\text{oxazolone-His})$ The proposed formation mechanism of $b_2(\text{oxazolone-His})$ ion from protonated HisGly is shown in the corresponding potential energy surface (PES) (Fig. 8.10). Starting from the most stable conformer of protonated HisGly (species **1**), species **2** is formed after a simple bond rotation, which is a less stable conformer of protonated HisGly. It is formed to facilitate proton transfer from the π -nitrogen (N^π) of the imidazole ring to the amide oxygen (CO). Species **3** is formed where the proton is attached to the amide bond oxygen, forming a weak hydrogen bond with the carbonyl oxygen at the C-terminus. After a simple bond rotation, species **4** is formed where the proton is now nearer to the hydroxyl oxygen (O_H) at the C-terminus. The proton is then further transferred to the O_H at the C-terminus via transition species **TS5** to form species **6**. Species **6** is a loose ion-molecule complex where a water molecule (H_2O) is weakly attached to the 2-[1-amino-2-(1*H*-imidazol-4-yl)ethyl]-5-oxo-4,5-dihydro-3*H*-1,3-oxazol-1-ium, which is the $b_2(\text{oxazolone-His})$ ion for protonated HisGly [Farrugia et al., 2001]. Before the H_2O is about to be detached, it could rotate freely to form a relatively more stable ion-molecule complex, species **7** is then formed with the H_2O attached to the τ -nitrogen (N^τ) of the imidazole ring. After the loss of H_2O , $b_2(\text{oxazolone-His})$ is formed (species **8** + H_2O). The 0K enthalpy of the formation of $b_2(\text{oxazolone-His})$ of this process, i.e., the energy difference between species **1** and species (**8** + H_2O), is 143 kJ mol^{-1} , with an energy barrier at **TS5** of 233 kJ mol^{-1} .

Formation Pathway of $b_2(\text{diketo-His})$ The formation of $b_2(\text{diketopiperazine})$ is another competitive dissociation pathway for protonated HisGly. The proposed formation mechanism of $b_2(\text{diketo-His})$ is also shown in the corresponding potential energy surface (PES) (Fig. 8.10). Starting from the most stable conformer of protonated HisGly (species **1**), species **9** is formed after the carbonyl group ($-\text{COOH}$) is rotated to the same side of the amino group ($-\text{NH}_2$) at the N-terminus, such that the hydroxyl oxygen (O_H) is nearer to the amino group. After the proton is transferred from the amino group to O_H via transition species **TS10**, an ion-molecule complex **11** is formed. A water molecule (H_2O) is weakly attached to the 4-[(3,6-dioxopiperazin-2-yl)methyl]-1*H*-imidazol-3-ium, which is the $b_2(\text{diketo-His})$ ion for protonated HisGly. After the H_2O is detached from the molecule, a stable species, the $b_2(\text{diketo-His})$ ion is formed (species **12**). The 0K enthalpy of the formation of $b_2(\text{diketo-His})$ of this process, i.e., the energy difference between species **1** and species (**12** + H_2O), is 60 kJ mol^{-1} , with an energy barrier at **TS10** of 234 kJ mol^{-1} .

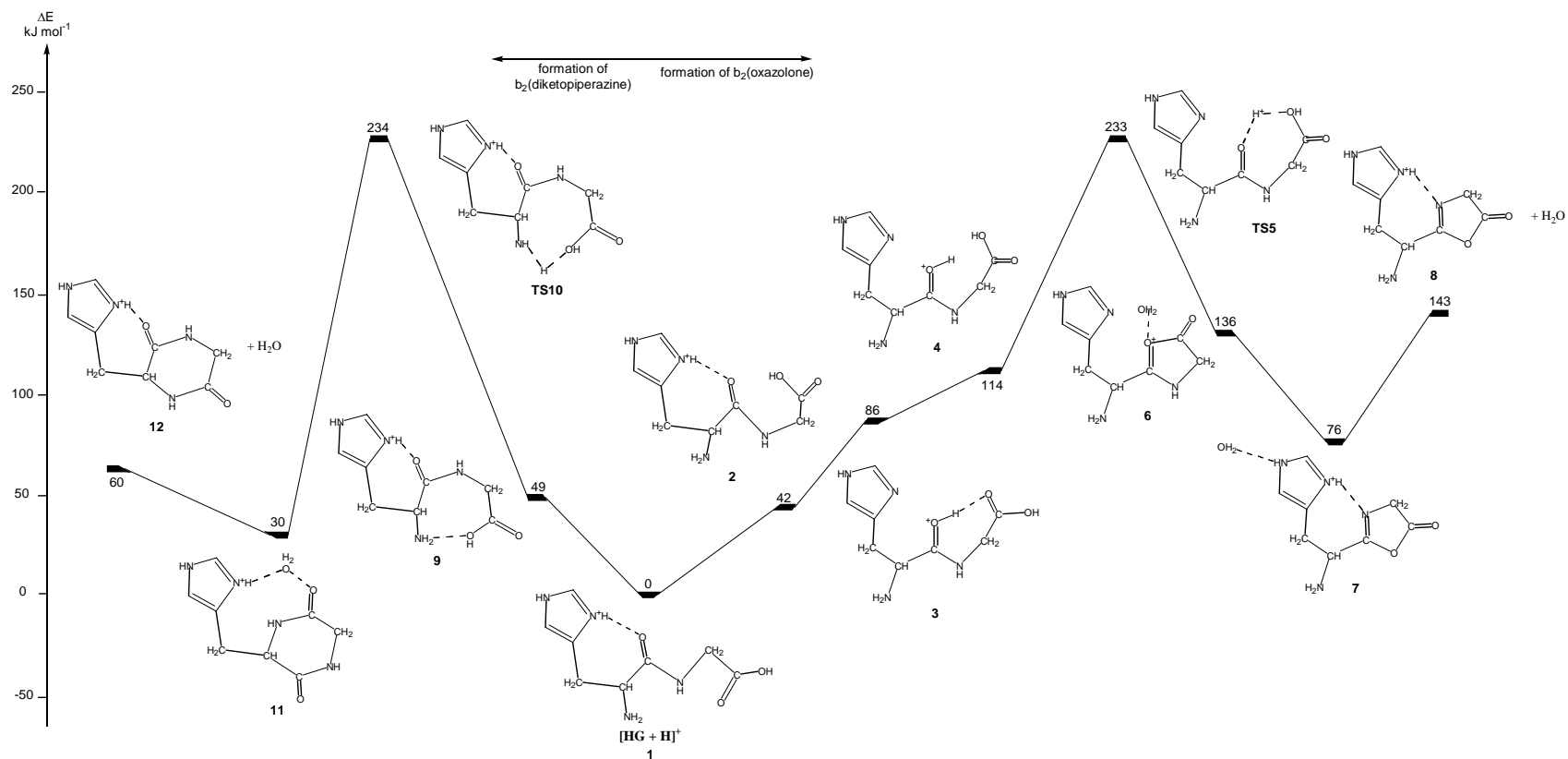


Figure 8.10 Potential energy surface (PES) of the dissociation of $[\text{HisGly} + \text{H}]^+$, leading to the formation of b_2 (oxazolone) and b_2 (diketopiperazine) at 0K, calculated at the B3-LYP/6-31G(d)//B3-LYP/6-31G(d) level.

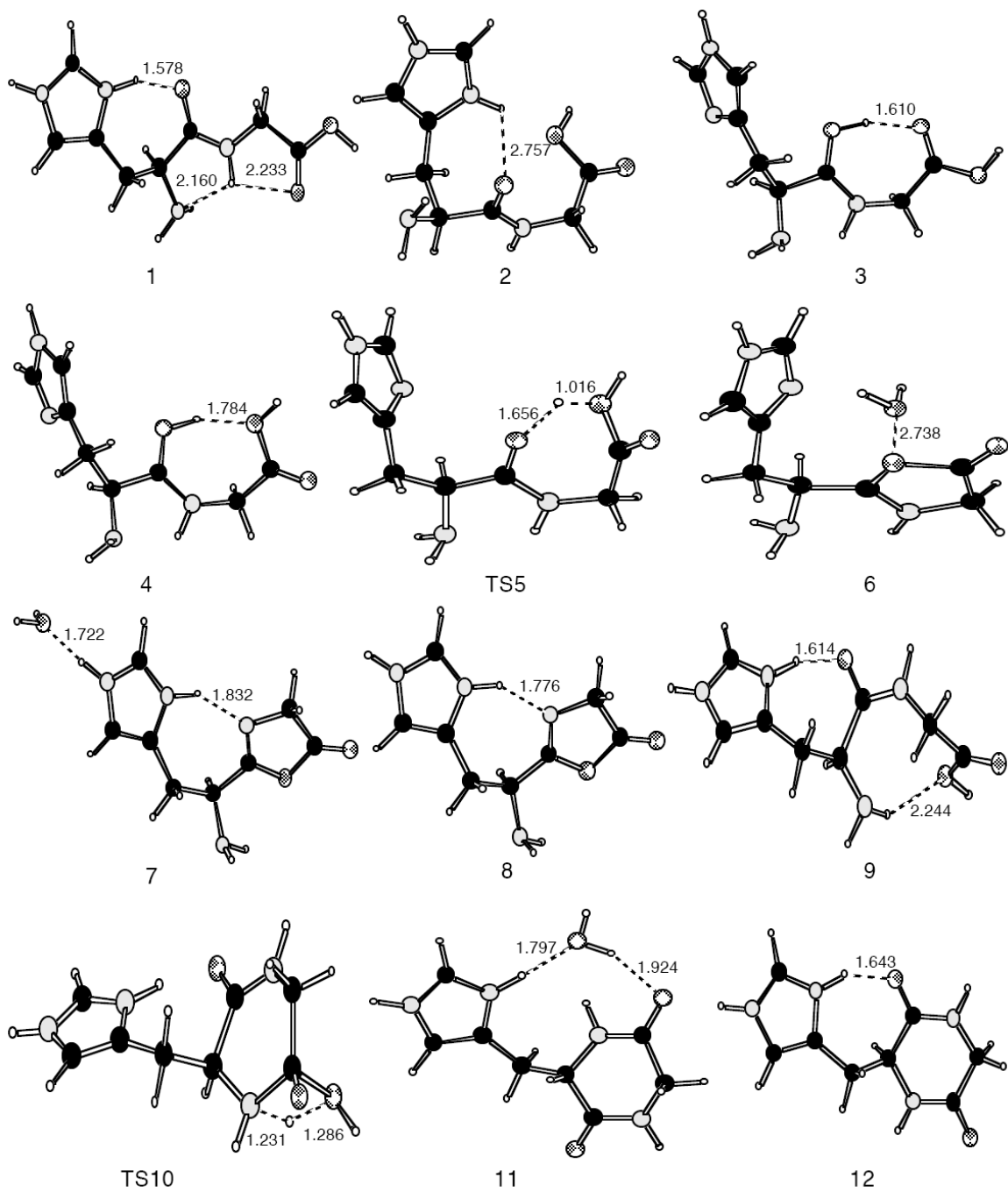


Figure 8.11 Optimized geometries (at B3-LYP/6-31G(d) level) of the various intermediates and transition species shown in the potential energy surface (PES) of formation of b_2 (oxazolone) and b_2 (diketopiperazine) from protonated HisGly

The theoretically estimated energy barriers at 0K for competitive formation of the $b_2(\text{oxazolone-His})$ and $b_2(\text{diketo-His})$ from protonated HisGly, together with the calculated ΔH_{298} , ΔG_{298} and ΔS_{298} value, are listed in Table 8.1. As shown in Table 8.1, the order of critical energies (in kJ mol^{-1}) are: $b_2(\text{oxazolone-His})$ (233) \sim $b_2(\text{diketo-His})$ (234). As the two pathway have very similar critical energies, it is likely that the formation of these two b_2 ions is competitive, and the product ions are actually a mixture of $b_2(\text{oxazolone-His})$ and $b_2(\text{diketo-His})$ ions over the whole range of collisional energies. However, once the critical energies are exceeded, the formation pathway of $b_2(\text{diketo-His})$ are entropically disfavored, as indicated by the relatively large negative ΔS_{298} values of $-40 \text{ J mol}^{-1} \text{ K}^{-1}$ for the energy barriers of formation of $b_2(\text{diketo-His})$ ion. As a result, the $b_2(\text{oxazolone-His})$ ion is both energetically and entropically slightly preferred over that of $b_2(\text{diketo-His})$, and is likely to be formed in larger initially proportions from the dissociation of protonated HisGly.

8.2.5 Dissociation of Protonated HisGly: Proposed Pathway for Isomerization of $b_2(\text{oxazolone-His})$ ion to $b_2(\text{diketo-His})$ ion

According to the ion trap time-resolved study of b_2 ions of protonated histidyl-glycyl-glycine ($[\text{HGG} + \text{H}]^+$) in Section 8.2.1 (Fig. 8.5), the fragmentation behavior (as indicated by the ratio of ion intensities due to the loss of CO versus the loss of NH_3) of b_2 ions of $[\text{HGG} + \text{H}]^+$ relative to that of cyclo-(GH) (with the same structure of $b_2(\text{diketo-His})$) are nearly identical throughout the entire activation time range, indicating that the isomerization rate is fast and nearly complete in the millisecond time frame of the ion trap analyzer. The $b_2(\text{diketo-His})$ ion is much more stable than $b_2(\text{oxazolone-His})$ by $\sim 83 \text{ kJ mol}^{-1}$. Similar to the case of

protonated GlyHis (Section 8.2.3), further isomerization of the $b_2(\text{oxazolone-His})$ ions to $b_2(\text{diketo-His})$ ions could take place when ‘additional’ internal energy is imparted to the ions via collisional activation. For this reason, we have explored theoretically the energetics and mechanism of isomerization from $b_2(\text{oxazolone-His})$ ion to $b_2(\text{diketo-His})$ ion for protonated HisGly, and the proposed pathway and the corresponding potential energy surface (PES) is shown in Figure 8.12. The optimized geometries of the various intermediates and transition species are shown in Figure 8.13.

Proposed isomerization pathway of $b_2(\text{oxazolone-His})$ to $b_2(\text{diketo-His})$ for protonated

HisGly The formation pathway of $b_2(\text{oxazolone-His})$ ion from protonated HisGly has been briefly discussed in the previous section. Starting from the $b_2(\text{oxazolone-His})$ ion, (species **8**), bond rotation along C-C bond linking the oxazolone ring occurs and species **9i** is formed. Via **TS10i**, bond lengthening occurs between the carbonyl group (C=O) and the oxygen of the oxazolone ring. After bond breaking, the amide nitrogen (N) immediately forms a bond with the carbonyl group to compensate the positive charge on the carbocation ($^+\text{C=O}$), leading to the formation of species **11i**. A proton is then transferred from the amino nitrogen (NH₂) at the N-terminus to the nitrogen of the triangular ring via transition species **TS12i** to form species **13i**. Species **13i** has the same structure and conformation as the $b_2(\text{diketo-His})$ ion. The 0K enthalpy of the further isomerization from $b_2(\text{oxazolone-His})$ to $b_2(\text{diketo-His})$ of this process, i.e., the energy difference between species **1** and species (**13i** + H₂O), is 60 kJ mol⁻¹, with an energy barrier at **TS12i** of 348 kJ mol⁻¹.

The theoretically estimated energy barriers at 0K for further isomerization from $b_2(\text{oxazolone-His})$ to $b_2(\text{diketo-His})$ of protonated GlyHis, together with the calculated ΔH_{298} , ΔG_{298} and ΔS_{298} values, are listed in Table 8.1. Unlike the case of protonated GlyHis with His at the

C-terminus, the energy difference between the barrier of the formation of $b_2(\text{oxazolone-His})$ and that of further isomerization for protonated HisGly is lower to about 115 kJ mol^{-1} only, which is much smaller than that of protonated GlyHis ($\sim 201 \text{ kJ mol}^{-1}$). The relatively lower energy difference could explain why nearly complete isomerization of the b_2 ions of protonated histidyl-glycyl-glycine ($[\text{HGG} + \text{H}]^+$) was observed in the ion trap time-resolved study as shown in Section 8.2.1 (Fig. 8.5). Thus the location of histidine in the dipeptide does exert a significant effect on the rate and extent of $b_2(\text{oxazolone-His})$ ion to $b_2(\text{diketo-His})$ ion isomerization.

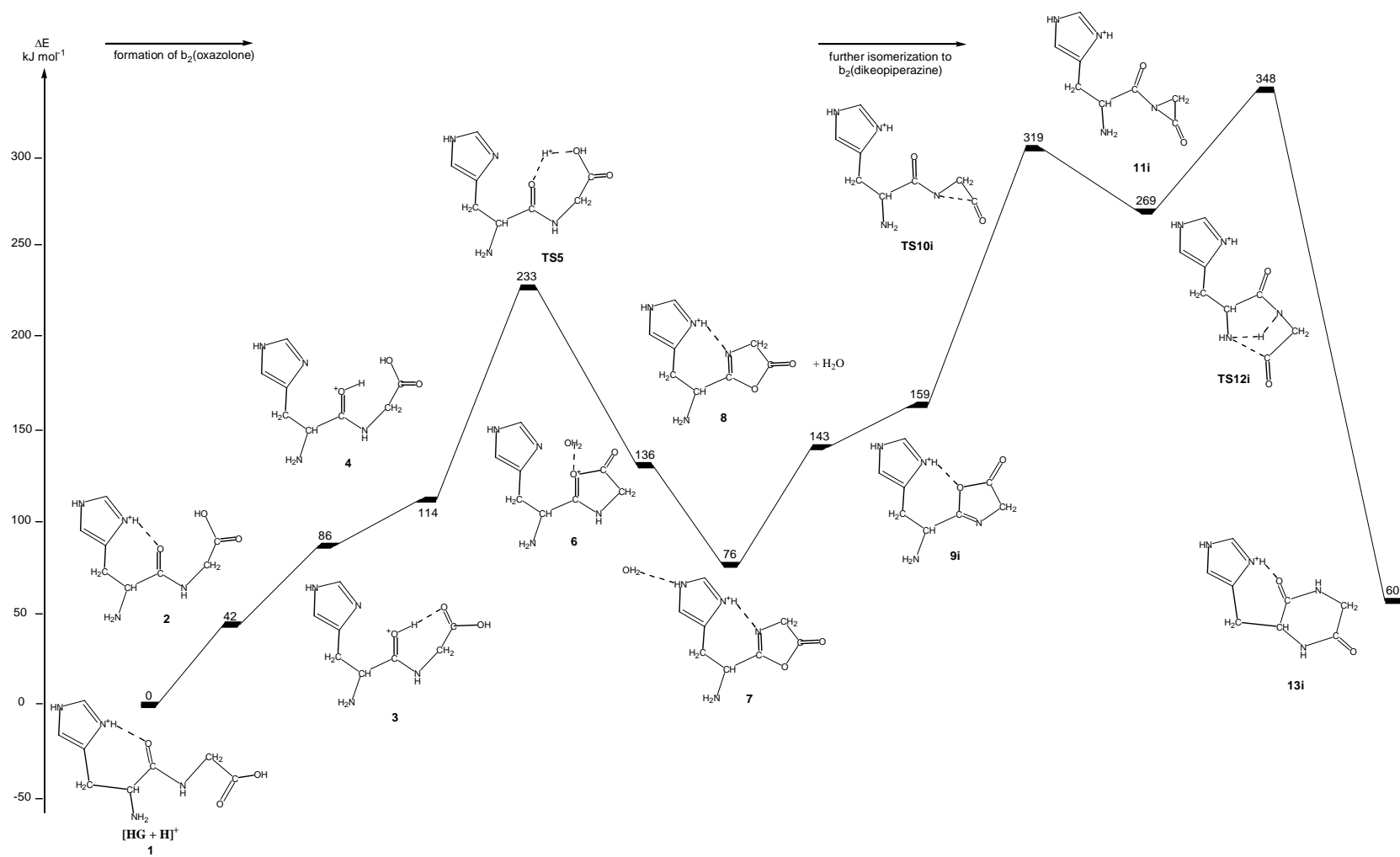


Figure 8.12 Potential energy surface (PES) of the dissociation of $[\text{HisGly} + \text{H}]^+$, leading to the formation of $b_2(\text{oxazolone})$ and further isomerization to $b_2(\text{diketopiperazine})$ at 0K, calculated at the B3-LYP/6-31G(d)//B3-LYP/6-31G(d) level

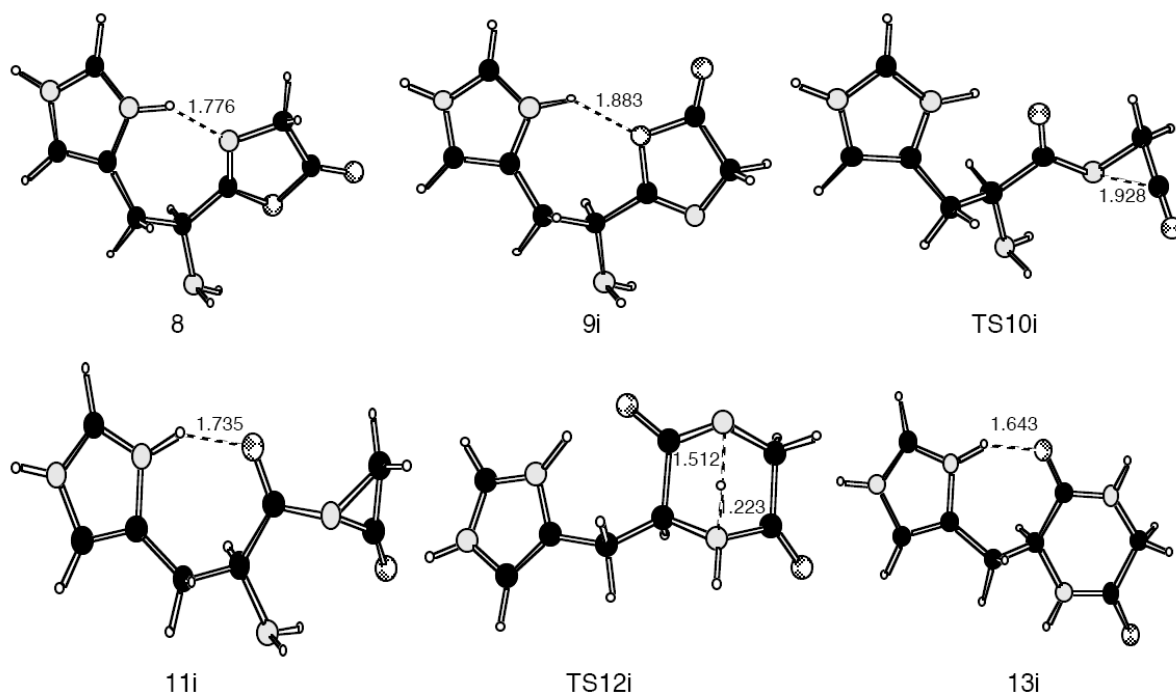


Figure 8.13 Optimized geometries (at B3-LYP/6-31G(d) level) of the various intermediates and transition species shown in the potential energy surface (PES) of further isomerization to b_2 (diketopiperazine) from protonated HisGly

8.3 Conclusion

In this study, by using protonated GlyHis and HisGly as model dipeptides, we have shown theoretically that the formation of b_2 ions having the b_2 (oxazolone-His), b_2 (diketo-His) and/or b_2 (bicyclic) structures are actually competitive, i.e., they have similar energy barriers. Nevertheless, we have found that the b_2 (oxazolone-His) ion is the energetically and entropically favored b_2 ion to be formed, at least initially at low collisional energies. The detailed mechanisms for the formation of these three b_2 ion structures have been elucidated.

As the b_2 (diketo-His) ion structure is much more stable than the b_2 (oxazolone-His) structure, initially formed b_2 (oxazolone-His) ions could further isomerize to b_2 (diketo-His) ions if there is sufficient internal energy imparted to the b_2 ions by collisional activation. The energy barrier for isomerization is found to be dependent on the location of histidine in the dipeptide at 330 and 348 kJ mol^{-1} for protonated GlyHis and HisGly, respectively. The difference in isomerization energy barriers is consistent with experimental observation in ion trap energy-resolved MS/MS studies: isomerization is only partially achieved for b_2 ions derived from protonated GlyHisGly, but complete isomerization is found for b_2 ions derived from protonated HisGlyGly in the millisecond time frame of the ion trap mass analyzer.

The newly found isomerization process for b_2 ions of protonated histidine-containing peptides has implications for peptide sequence identification by MS/MS. To a very large extent, the isomerization process leads to 'masking' of the location of histidine at the N-terminus, and at the second position C-terminal to the N-terminal amino acid residues, with the result that the location of histidine in the two locations cannot be clearly defined through MS/MS sequence analysis. To solve this analytical problem, chemical derivatization, either at the N-terminal amino acid or with histidine, to prevent the cyclization pathway leading to the formation of b_2 (diketo-His) ions need to be carried out prior to the MS/MS analysis.

Chapter 9 Suggestions for Further Works

In this work, very good agreement (within $\pm 11 \text{ kJ mol}^{-1}$, refer to Table 7.2) was obtained between experimental and theoretical *proton affinity* values for molecules as large as the model α -/ β -dipeptides and (β -Ala)His. However, we found the discrepancy between experimental and theoretical *potassium cation affinity* values is relatively large and unacceptable at $\pm 25 \text{ kJ mol}^{-1}$ for arginine. This highlights the limitations of both the mass spectrometric kinetic method and the theoretical density functional theory protocol adopted in the present study to estimate the absolute alkali metal cation binding energies. Arginine is the largest of the α -amino acids investigated with the highest K^+ affinity. Experimentally, a suitable reference (anchoring) compound with known and comparable K^+ affinity to arginine could not be found for the kinetic method measurements. By our own experience, the accuracy of theoretically estimated affinity values also deteriorates with increasing molecular size of the system under investigation. Hence, for future studies in alkali metal cation binding affinities, the experimental and theoretical methodology described in the present work should be limited to molecular systems smaller than arginine.

Our theoretical studies show that the relative stabilities of the charged-solvated **CS1** and zwitterionic **ZW1** K^+ binding modes of β -Phe and β -Glu are different from their α -analogues, with the **CS1** more favored to be formed in β -amino acids. The dissociation of alkali metal cationized dipeptides have been shown to proceed mainly via zwitterionic intermediates and transition structures.[Feng et al., 2003] Given these findings, it is likely that the dissociation of alkali metal cationized ($\text{M}^+=\text{Li}^+, \text{Na}^+$ and K^+) β -amino acids and with functionalized side chains and associated β -peptides may differ from their α -analogues, and provide an alternative

means of differentiating isomeric α -/ β -amino acids and peptides. Hence, it is worthwhile to extend our studies on K^+ affinity of β -amino acids to the collision-induced dissociation of metal cationized β -amino acids with functionalized side chains and β -peptides containing these β -amino acids, with the aim of finding alternative method of distinguishing isomeric α -/ β -analogues.

Preliminary results from our laboratory also revealed that formation of b_n ions (n = no. of amino acid in the peptide), derived by elimination of a water molecule with a peptide backbone (amide) oxygen (not the carboxylic $-OH$ oxygen, and denoted as $b_n(\text{dehydration, } -H_2O)$ here), are also common among model and bioactive histidine-containing peptides. Given the success demonstrated in the present study of using DFT calculations to establish the pathways of dissociation of protonated histidine-containing dipeptides, it is proposed that similar studies can be conducted to establish the mechanisms of $b_n(\text{dehydration, } -H_2O)$ ion formation. These studies will lead to better understanding of the rules governing the formation of sequence-specific fragment ions from protonated histidine-containing peptides, and enhance the success rate of determining the sequence of histidine-containing peptides by tandem mass spectrometry.

As far as we know, the isomerization of the $b_5(\text{oxazolone})$ ion derived from a protonated pentapeptide YAGFL-NH₂ [Harrison et al., 2006] and the $b_2(\text{oxazolone-His})$ ion from protonated histidine-containing peptides are the only two examples reported so far. Sequence information is lost as a b_i (oxazolone) ion isomerizes to a b_i (diketopiperazine) ion with a protonated cyclo-peptide structure, reducing the success rate of peptide sequencing by MS/MS determination. Hence, it is of practical importance to investigate further the

prevalence of b_i (oxazolone) ion isomerization, and the underlying structural and energetic requirements for such process to occur. Experimentally, the occurrence of isomerization is indicated by finding CID-MS/MS spectra of b_i ions similar to that of the corresponding protonated cyclo-peptide. A systematic theoretical study of the relative stabilities of b_i (oxazolone) and b_i (diketopiperazine) ions, and the energy barriers of formation and isomerization of selected protonated model peptides of different sizes (e.g. $i = 2$ to 7 for $n > i$), and in terms of the ring size of the final cyclic b_i (diketopiperazine) ions) and different compositions of amino acids, similar to the study described in Chapter 8 of this thesis, could be conducted. These studies would reveal the scope of b_i (oxazolone) ion to b_i (diketo) ion isomerization and its likely impact, though unwelcome, on peptide sequencing by tandem mass spectrometry.

References

- Abirami, S., Wong, C.C.L., Tsang, C.W. and Ma, N.L. "Dissociation of alkaliated alanine in the gas phase: the role of the metal cation". *Chemistry Europe Journal*, Vol. 11, pp. 5289–5301 (2005)
- Aebersold, R. and Mann, M. "Mass spectrometry-based proteomics". *Nature*, Vol. 422, pp. 198–207 (2003)
- Addario, V., Guo, Y., Chu, I.K., Ling, Y., Ruggerio, G., Rodriquez, C.F., Hopkinson, A.C. and Siu, K.W.M. "Proton affinities of methyl esters of N-acetylated amino acids". *International Journal of Mass Spectrometry*, Vol. 219, pp. 101-114 (2002)
- Alcami, M., Mo, O. and Yanez, M., "Computational chemistry: A useful (sometimes mandatory) tool in mass spectrometry studies". *Mass Spectrometry Reviews*, Vol. 20, pp. 195-245 (2001)
- Armentrout, P.B. "Cation-ether complexes in the gas phase: Thermodynamic insight into molecular recognition", *International Journal of Mass Spectrometry*, Vol. 193, pp. 227-240 (1999)
- Armentrout, P.B. "Entropy measurements and the kinetic method: A statistically meaningful approach". *Journal of the American Society for Mass Spectrometry*, Vol. 11, pp. 371-379 (2000)
- Babizhayev, M.A, Deyev, A.I., Yermakova, V.N., Semiletov, Y.A., Davydova, N. G., Kurysheva, N.I., Zhukotskii, A.V. and Goldman, I. M. "N-acetylcarnosine, a natural histidine-containing dipeptide, as a potent ophthalmic drug in treatment of human cataracts". *Peptides*, Vol. 22, pp. 979–994 (2001)
- Baerends, E.J. and Gritsenko, O.V., "A quantum chemical view of density functional theory". *Journal of Physical Chemistry*, Vol. 101, pp. 5383–5403 (1997)

- Ballard, K.D. and Gaskell, S.J. "Sequential mass-spectrometry applied to the study of the formation of internal fragment ions of protonated peptides". *International Journal of Mass Spectrometry and Ion Processes*, Vol. 111, pp. 173-189 (1991)
- Balta, B, Aviyente, V and Lifshitz, C. "Elimination of water from the carboxyl group of GlyGlyH⁺". *Journal of the American Society for Mass Spectrometry*, Vol. 14, pp. 1192–1203 (2003)
- Bartolotti, L.J. and Flurchick, K. "Review in Computational Chemistry", Vol. 7, pp. 197 (1996)
- Becke, A.D. "Density – functional thermochemistry .3. The role of exact exchange". *Journal of Chemical Physics*, Vol. 98, pp. 5648-5652 (1993)
- Beranova, S.; Cai, J, and Wesdemiotis, C. Unimolecular chemistry of protonated glycine and its neutralized form in the Gas Phase. *Journal of the American Chemistry Society*, Vol. 117, pp. 9492-9501 (1995)
- Biemann, K. "Contributions of mass-spectrometry to peptide and protein structure". *Biomedical and Environmental Mass Spectrometry*, Vol. 16, pp. 99-111 (1988)
- Biemann, K. and Martin, S.A. "Mass-spectrometric determination of the amino-acid-sequence of peptides and proteins". *Mass Spectrometry Reviews*, Vol. 6, pp. 1-75 (1987)
- Bojesen, G, Breindahl, T. and Andersen, U.N. "On the sodium and lithium ion affinities of some α -amino acids". *Organic Mass Spectrometry*, Vol. 28, pp. 1448-1452 (1993)
- Boldyrev, A.A and Severin, S.E. "The histidine-containing and anserine: distribution, properties and biological significance". *Advances in Enzyme Regulation*, Vol. 30, pp.175-194 (1990)
- Bouchoux, G. and Salpin, J.Y. Gas-phase Basicities of glycine, alanine, proline, serine, histidine and some of their peptides by the thermokinetic method, *European Journal of Mass Spectrometry*, Vol. 9, pp. 391-402 (2003)

Bruyneel, C., Pham-Tran, N.N., Nguyen, M.T. and Zeegers-Huyskens, T. “Theoretical and experimental study of the conformation and vibrational frequencies of N-acetyl-L-alanine and N-acetyl-L-alaninate”. *Spectroscopy Letters*, Vol. 36, pp. 537-550 (2003)

Burk, P., Koppel, I.A., Koppel, I., Kurg, R., Gal, J.F., Maria, P.C., Herreros, M., Notario, R., Abboud, J.L.M., Anvia, F. and Taft, R.W. “ Revised and expanded scale of gas-phase lithium cation basicities. An experimental and theoretical study”, *Journal of Physical Chemistry A*, Vol. 104, pp. 2824-2833 (2000).

Burlet, O., Orkiszewski, R.S., Ballard, K. D. and Gaskell, S. J. “Charge promotion of low-energy fragmentations of peptide ions”. *Rapid Communications in Mass Spectrometry*, Vol. 6, pp. 658-662 (1992a)

Burlet, O., Yang, C.Y. and Gaskell, S.J. “Influence of cysteine to cysteic acid oxidation on the collision-activated decomposition of protonated peptides – evidence for intraionic interactions”. *Journal of the American Society for Mass Spectrometry*, Vol. 3, pp. 337 -344 (1992b)

Busch, K. L., Glish, G. L. and McLuckey, S. A. *Mass Spectrometry/Mass Spectrometry: Techniques and Applications of Tandem Mass Spectrometry*, VCH Publishers, New York, pp. 333 (1988)

Cassady, C.J., Carr, S.R, Zhang, K. and Chungphillips, A. “Experimental and Ab initio studies on protonations of alanine and small peptides of alanine and glycine”. *Journal of Organic Chemistry*, Vol. 60, pp. 1704-1712 (1995)

Catinella, S., Pelizzi, N., Barbosa, S., Favretto, D., Seraglia, R. and Traldi, P. “On the detailed mechanisms of collision-induced dissociation experiments performed by electrospray ion trap”. *Rapid Communications in Mass Spectrometry*, Vol. 16, pp. 1897-1902 (2002)

Cerda, B.A, Hoyau, S., Ohanessian, G. and Wesdemiotis, C. “Na⁺ binding to cyclic and linear dipeptides. Bond energies, entropies, of Na⁺ complexation, and attachment sites from the dissociation of Na⁺-bound heterodimers and *ab* calculations”. *Journal of the American Chemical Society*, Vol. 120, pp. 2437-2448 (1998)

Cerda, B.A. and Wesdemiotis, C. "Li⁺, Na⁺ and K⁺ binding to the DNA and RNA nucleobases, bond energies and attachment sites from the dissociation of metal ion-bound heterodimers". *Journal of the American Chemical Society*, Vol. 118, pp. 11884-11892 (1996)

Wong, O.Y. *M.Phil Thesis* on "Mass Spectrometric Studies on Protonated and Alkali Metal Cationized β -Amino Acids and β -Peptides", 2006

Cheng, X., Wu, Z. and Fenselau, C. "Collision energy dependence of proton-bound dimer dissociation: Entropy effects, proton affinities, and intramolecular hydrogen-bonding in protonated peptides". *Journal of the American Chemical Society*, Vol. 115, pp. 4844-4848 (1993)

Coleman, J.E., Van Soest, R. and Andersen, R. J. "New Geodiamolides from the Sponge *Cymbastela* sp. Collected in Papua New Guinea". *Journal of Natural Products*, Vol. 62, pp. 1137-1141 (1999)

Cooks, R.G. and Wong, P.S.H. "Kinetic method of making thermochemical determinations: Advances and applications". *Accounts of Chemical Research*, Vol. 31, pp. 379-386 (1998)

Cooks, R.G., Koskinen, J.T. and Thomas, P.D. "The kinetic method of making thermochemical determinations", *Journal of Mass Spectrometry*, Vol. 34, pp. 85-92 (1999)

Cooks, R.G. and Kruger, T.L. "Intrinsic Basicity Determination using Metastable Ions". *Journal of the American Chemical Society*, Vol. 99, No. 4, pp. 1279-1281 (1977)

Cooks, R.G., Patrick, J.S., Kotiaho, T. and McLuckey, S.A. "Thermochemical determinations by the kinetic method". *Mass Spectrometry Reviews*, Vol. 13, pp. 287-339 (1994)

Cox, K.A., Gaskell, S.J., Morris, M. and Whiting, A. "Role of the site of protonation in the low-energy decompositions of gas-phase peptide ions". *Journal of the American Society for Mass Spectrometry*, Vol. 7, pp. 522-531 (1996)

Csonka, I.P., Paizs, B., Lendvay, G., and Suhai, S., "Proton Mobility in Protonated Peptides: a Joint Molecular Orbital and RRKM study". *Journal of American Chemical Society*, Vol. 127, pp. 8571-8579 (2005)

Davidson, M.W. *Molecular Expressions: The Amino Acids Collection – beta Alanine*, Wiley (2003)

Davidson, W.R. and Kebarle, P. "Binding energies and stabilities of potassium ion complexes from studies of the gas phase ion equilibria". *Journal of the American Chemical Society*, Vol. 98, pp. 6133-6138 (1976).

Davies, S. G., Dupont, J. and Easton, R.J.C. "Assignment of the Absolute Configuration to Winterstein's Acid". *Tetrahedron Letters*, Vol. 34, pp. 1291-1294 (1993).

De Hoffmann, E., Charette, J. and Stroobant, V. "Tandem Mass Spectrometry (MS/MS)". In Masson ed., *Mass spectrometry: Principle and applications*, John Wiley & Sons Ltd., Masson, Paris, pp. 132-133 (1996)

Delbene, J.E., Mettee, H.D., Frisch, M.J., Luke, B.T. and Pople, J.A. "Ab initio computation of the enthalpies of some gas-phase hydration reactions". *Journal of Physical Chemistry*, Vol. 87, pp. 3279-3282 (1983)

De Hoffmann, E. and Stroobant, V. *Mass Spectrometry principles and Applications*, 2nd edition, Wiley, 2001.

Dinadayalane, T.C., Sastry, G.N., Leszczynski, J. "Comprehensive theoretical study towards the accurate proton affinity values of naturally occurring amino acids". *International Journal of Quantum Chemistry*, Vol. 106, pp. 2920-2933 (2006)

Dongre, A.R., Jones, J.L., Somogyi, A. and Wysocki, V.H. "Influence of peptide composition, gas-phase basicity, and chemical modification on fragmentation efficiency: Evidence for the mobile proton model". *Journal of American Chemical Society*, Vol. 118, pp. 8365-8374 (1996a)

Dongre, A.R., Somogyi, A. and Wysocki, V.H. "Surface-induced dissociation: An effective tool to probe structure, energetics and fragmentation mechanisms of protonated peptides". *Journal of Mass Spectrometry*, Vol. 31, pp. 339-350 (1996b)

Dookeran, N. N.; Yalcin, T. and Harrison, A. G. "Fragmentation reactions of protonated α -amino acids". *Journal of Mass Spectrometry*, Vol. 31, pp. 500-508 (1996)

Doyle, D.A., Cabral, J.M., Pfuetzner, R.A., Kuo, A., Gulbis, J.M., Cohen, S.L., Chait, B.T. and Mackinnon, R. "The structure of the potassium channel: Molecular basis of K^+ conduction and selectivity". *Science*, Vol. 280, pp. 69-77 (1998)

Drahos, L. and Vekey, K. "Special feature: Commentary - How closely related are the effective and the real temperature". *Journal of Mass Spectrometry*, Vol. 34, pp. 79-84 (1999)

Dunbar, R.C. "Complexation of Na^+ and K^+ to aromatic amino acids: A density functional computational study of cation- π interactions". *Journal of Physical Chemistry A*, Vol. 104, pp. 8067-8074 (2000)

Feng, W.Y., Gronert, C., Fletcher, K.A., Warres, A. and Lebrilla, C.B. "The mechanism of C-terminal fragmentations in alkali metal ion complexes of peptides". *International Journal of Mass Spectrometry*, Vol. 222, pp. 117-134 (2003)

Freer, I., Pedrocchifantoni, G., Picken, D.J. and Overton, K.H. "Stereochemistry of the leucine 2,3-aminomutase from tissue cultures of *Andrographis Paniculata*". *Journal of the Chemical Society-Chemical Communication*, Vol. 3, pp. 80-82 (1981)

El Aribi, H., Orlova, G., Rodriquez, C.F., Almeida, D.R.P., Hopkinson, A.C. and Siu K.W.M. "Fragmentation mechanisms of product ions from protonated tripeptides". *Journal of Physical Chemistry B*, Vol. 108, pp. 18743-18749 (2004)

El Aribi, H., Rodriquez, C.F., Almeida, D.R.P, Ling, Y., Mak, W.W.N., Hopkinson, A.C. and Siu., K.W.M., "Elucidation of fragmentation mechanisms of protonated peptide ions and their products: a case study on glycylglycylglycine using density functional theory and threshold collision-induced dissociation." *Journal of the American Chemical Society*, Vol. 125(30), pp 9229-9236 (2003)

Ervin, K.M. "Microcanonical analysis of the kinetic method. The meaning of the "apparent entropy" ". *Journal of the American Society for Mass Spectrometry*, Vol. 13, pp. 435-452 (2002).

Ervin K.M. "Microcanonical analysis of the kinetic method: The Meaning of the 'Effective Temperature' ". *International Journal of Mass Spectrometry*, Vol. 195/196, pp. 271–284 (2000)

Ewing, N.P., Zhang, X., Cassady C.J. "Determination of the gas-phase Basicities of praline and its di- and tripeptides with glycine: the enhanced basicity of prolylproline", *Journal of Mass Spectrometry*, Vol. 31, pp. 1345-1350 (1996)

Farrugia, J.M., Taverner, T. and O'Hair, R. J. "Side-chain involvement in the fragmentation reactions of the protonated methyl esters of histidine and its peptides". *International Journal of Mass Spectrometry*, Vol. 209, pp. 99-112 (2001)

Feng, W.Y., Gronet, S. and Lebrilla, C. "The lithium cation binding energies of gaseous amino acids". *Journal of Physical Chemistry A*, Vol. 107, pp. 405-410 (2003).

Ferrario, C.M., Chappell, M.C., Dean, R.H. and Iyer, S.N. "Novel angiotensin peptides regulate blood pressure, endothelial function, and natriuresis". *Journal of the American Society of Nephrology*, Vol. 9, pp. 1716-1722 (1998)

Frisch, M.J., Trucks, G.W., Schlegel, H.B., Scuseria, G.E., Robb, M.A., Cheeseman, J.R., Zakrzewski, V.G., Montgomery, J.A., Jr., Stratmann, R.E., Burant, J.C., Dapprich, S., Millam, J.M., Daniels, A.D., Kudin, K.N., Strain, M.C., Farkas, O., Tomasi, J., Barone, V., Cossi, M., Cammi, R., Mennucci, B., Pomelli, C., Adamo, C., Clifford, S., Ochterski, J., Petersson, G.A., Ayala, P.Y., Cui, Q., Morokuma, K., Malick, D.K., Rabuck, A.D., Raghavachari, K., Foresman, J.B., Cioslowski, J., Ortiz, J.V., Baboul, A.G., Stefanov, B.B., Liu, G., Liashenko, A., Piskorz, P., Komaromi, I., Gomperts, R., Martin, R.L., Fox, D.J., Keith, T., Al-Laham, M.A., Peng, C.Y., Nanayakkara, A., Gonzalez, C., Challacombe, M., Gill, P.M.W., Johnson, B., Chen, W., Wong, M.W., Andres, J.L., Gonzalez, C., Head-Gordon, M., Replogle, E.S. and Pople, J.A., eds., *Gaussian 03*, Revision B.04, Gaussian, Inc., Pittsburgh, PA (2003)

Gapeev, A. and Dunbar, R.C. "Cation- π interactions and the gas-phase thermochemistry of

the Na⁺/phenylalanine complex". *Journal of the American Chemical Society*, Vol. 123, pp. 8360-8365 (2001)

Gokel, G.W., De Wall, S.L. and Meadows, E.S. "Experimental evidence for alkali metal cation- π interactions". *European Journal of Organic Chemistry*, Vol. 17, pp. 2967-2978 (2000)

Gopi, H.N.; Ravindra, G.; Pal, P.P.; Pattanaik, P.; Balaram, H.; Balaram, P. "Proteolytic stability of β -peptide bonds probed using quenched fluorescent substrates incorporating a hemoglobin cleavage site". *FEBS Letters*, Vol. 535(1-3), pp.175-178 (2003)

Grese, R.P., Cerny, R.L., Gross, M.L. "Metal-ion peptide interactions in the gas-phase-A tandem mass-spectrometry study of alkali-metal cationized peptides". *Journal of the American Chemical Society*, Vol. 111, pp. 2835-2842 (1989).

Grewal, R.N., Aribi, H.E., Harrison, A.G., Siu, K.W.M. and Hopkinson, A.C. "Fragmentation of protonated tripeptides: the proline effect revisited". *Journal of Physical Chemistry B*, Vol. 108, pp. 4899-4908 (2004)

Griffith, O. W. "Beta-amino acids: mammalian metabolism and utility as alpha-amino acid analogues". *Annual review of biochemistry*, Vol. 55, pp. 855-878 (1986)

Gronowska, J., Paradisi, C., Traldi, P. and Vettori, U. "A study of relevant parameters in collisional-activation of ions in the ion-trap mass spectrometer". *Rapid Communications in Mass Spectrometry*, Vol. 4, pp. 306-313 (1990)

Guiotto, A., Pozzobon, M., Sanavio, C., Schiavon, O., Orsolini, P. and Veronese, F.M. "An improved procedure for the synthesis of branched polyethylene glycols (PEGs) with the reporter dipeptide Met-b-Ala for protein conjugation". *Bioorganic & Medicinal Chemistry Letters*, Vol. 12, pp. 177-180 (2002)

Hahn, I.S. and Wesdemiotis, C. "Protonation thermochemistry of beta-alanine - An evaluation of proton affinities and entropies determined by the extended kinetic method". *International journal of mass spectrometry*, Vol. 222, pp. 465-479 (2002)

- Harrison, A.G. "Special feature: Perspective - Linear free energy correlations in mass spectrometry". *Journal of Mass Spectrometry*, Vol. 34, pp. 577-589 (1999)
- Harrison, A.G. "The gas-phase basicities and proton affinities of amino acids and peptides". *Mass Spectrometry Reviews*, Vol. 16, pp. 201-217 (1997)
- Harrison, A.G. and Yalcin, T. "Proton mobility in protonated amino acids and peptides". *International Journal of Mass Spectrometry*, Vol. 165, pp. 339-347 (1997)
- Harrison, A.G., Young, A.B., Bleiholder, C., Suhai, S. and Paizs, B. "Scrambling of sequence information in collision-induced dissociation of peptides". *Journal of the American Chemical Society*, Vol. 128, pp. 10364-10365 (2006)
- Hehre, W.J., Radom, L., Scleyer, P.V.R. and Pople, J., eds., *Ab initio Molecular Orbital Theory*, Wiley, New York (1986)
- Herbert, C.G. and Johnstone, R.A.W. In *Mass Spectrometry Basics*, CRC Press LLC, Boca Raton, Florida, Chapters 10 and 25, pp. 65-69 and 183-188 (2003)
- Hille, B. *Ion Channels of Excitable Membranes*, Sinauer, Sunderland, Massachusetts, 3rd. Edition (2001)
- Holbrook, K.A., Pilling, M.J. and Robertson, S.H. *Unimolecular Reactions*, 2nd Edition, John Wiley & Sons Ltd., Chapters 2-4 and 6, pp. 9-114, 145-178 (1996)
- Hook, D.F., Gessier, F., Noti, C., Kast, P. and Seebach, D. "Probing the proteolytic stability of β -peptides containing fluoro- and hydroxy-amino acids", *ChemBioChem*, Vol. 5, pp. 691-706 (2004)
- Hoyau, S., Norrman, K., McMahon, T.B. and Ohanessian, G. "A quantitative basis for a scale of Na^+ affinities of organic and small biological molecules in the gas phase". *Journal of the American Chemical Society*, Vol. 121, pp. 8864-8875 (1999).
- Hoyau, S. and Ohanessian, G. "Interaction of alkali metal cations (Li^+ - Cs^+) with glycine in the gas phase: A theoretical study". *Chemistry-A European Journal*, Vol. 4, pp. 1561-1569

(1998).

Huels, W., Muenster, H., Pesch, R. and Schroeder, E. "Design and performance of a hybrid tandem mass spectrometer with BE/Ion Trap configuration". *Proceedings of the 44th ASMS Conference on Mass Spectrometry and Allied Topics*, Portland, Oregon, May 12-16 (1996)

Huheey, J.E., Keiter, E.A. and Keiter, R.L. *Inorganic Chemistry: Principles of Structure and Reactivity*. In 4th, , Harper College Publishers, pp.187 (1993)

Hunter, E.P.L. and Lias, S. G. "Evaluated gas phase basicities and proton affinities of molecules". *Journal of Physical and Chemical Reference Data*, Vol. 27, pp. 413-656 (1998)

Inagami ,T., Kambayashi, Y., Ichiki, T., Tsuzuki, S., Eguchi, S. and Yamakawa, T. "Angiotensin receptors: Molecular biology and signalling". *Clinical and experimental Pharmacology and Physiology*, Vol. 26, pp. 544-549 (1999)

Jensen, F. *An Introduction to computational Chemistry*, Chichester: New York, N.Y.; Wiley (1999)

Jensen, F. *Introduction to computational Chemistry*, 2nd Edition, John Wiley and Sons, Ltd. (2007)

Jensen, F. "Structure and stability of complexes of glycine and glycine methyl analogous with H⁺, Li⁺, and Na⁺". *Journal of the American Chemical Society*, Vol. 114, pp. 9533-9537 (1992)

Jiang, Y., Lee, A., Chen, J., Ruta, V., Cadene, M., Chalt, B.T. and Mackinnon, R. "X-ray structure of a voltage-dependent K⁺ Channel". *Nature*, Vol. 423, pp. 33-41 (2003)

Jockusch, R.A., Price, W.D. and Williams, E.R. "Structure of cationized arginine (Arg·M⁺, M = H, Li, Na, K, Rb, and Cs) in the gas phase: Further evidence for zwitterionic arginine". *Journal of Physical Chemistry A*, Vol. 103, pp. 9266-9274 (1999).

Jones, J.L., Dongre, A.R., Somogyi, A. and Wysocki, V.H. "Sequence dependence of peptide fragmentation efficiency curves determined by electrospray-ionization surface-induced

dissociation mass-spectrometry". *Journal of American Chemical Society*, Vol. 116, pp. 8368-8368 (1994)

Kaim, W., Schwederski, B., eds., *Bioinorganic Chemistry: Inorganic Elements in the Chemistry of Life: An Introduction and Guide*, John Wiley and Sons, New York, pp. 267-286 (1994)

Kebarle, P. "A brief overview of the present status of the mechanisms involved in electrospray mass spectrometry". *Journal of Mass Spectrometry*, Vol. 35, pp. 804-817 (2000)

Kebarle, P. and Ho, Y.H. *Electrospray Ionization Mass Spectrometry - Fundamentals Instrumentation & Applications*, R. B. Cole edited., John Wiley & Sons, Chichester, pp. 3 (1997)

Kebarle, P. and Tang, P.L. "From ions in solution to ions in the gas phase: The mechanism of electrospray mass spectrometry". *Analytical Chemistry*, Vol. 65, pp. 972A-986A (1993)

Schumacher, K.K, Hauze, D.B., Jiang, J., Szewczyk, J., Reddy, R.E., Davis, F.A. and Joullie, M.M. "First Total Synthesis of Astin G". *Tetrahedron Letters*, Vol. 40, pp. 455-458 (1999)

Kish, M.M., Ohanessian, G. and Wesdemiotis, C. "The Na⁺ affinities of α -amino acids: side-chain substituent effects". *International Journal of Mass Spectrometry*, Vol. 227, pp. 509-524 (2003)

Klassen, J.S., Anderson, S.G., Blades, A.T. and Kebarle, P. "Reaction enthalpies for $M^+L = M^+ + L$, where $M^+ = Na^+$ and K^+ and $L =$ Acetamide, N-Methylacetamide, N,N-Dimethylacetamide, Glycine, and Glycylglycine, from determinations of the collision-induced dissociation thresholds", *Journal of Physical Chemistry*, Vol. 100, pp. 14218-14227 (1996)

Klassen, J.S. and Kebarle, P. "Collision-induced dissociation threshold energies of protonated glycine, glycinamide, and some related small peptides and peptide amino amides". *Journal of American Chemical Society*, Vol. 119, pp. 6552-6563 (1997)

Koch, W. and Holthausen, M.C., eds., *A Chemist's Guide to Density Functional Theory*, Wiley-VCH (2000)

Koopmans, T.A. "The distribution of wave function and characteristic value among the individual electrons of an atom". *Physica (The Hague)*, Vol. 1, pp. 104-113 (1933)

Kulik, W. and Heerma, W. "A study of the positive and negative ion fast atom bombardment mass spectra of α -amino acids". *Biomedical and Environmental Mass Spectrometry*, Vol. 15, pp. 419-427

Kyrikou, I., Grdadolnik, S.G., Tatari, M., Poulos, C. and Mavromoustakos, T. "Structural elucidation and conformational properties of the toxin paralyisin beta-Ala-Tyr". *Journal of Pharmaceutical and Biomedical Analysis*, Vol. 31, pp. 713-721 (2003)

Lau, J.K.-C., Wong, C.H.S., Siu, F.M., Ma, N.L. and Tsang, C.W. "Absolute potassium cation affinities (PCAs) in the gas phase". *Chemistry-A European Journal*, Vol.9, pp. 3383-3396 (2003)

Lee, C., Yang, W. and Parr, R.G. "Development of the Colle-Salvetti correlation-energy formula into a functional of the electron density". *Physical Review*, Vol. 37, pp. 785-789 (1988)

Levsen, K. "The Quasi-Equilibrium Theory". *Fundamental aspects of organic mass spectrometry*, CIP-Kurztitelaufnahme, Weinheim, New York, Verlag Chemie, pp. 25-28 (1978)

Lifshitz, C. "Kinetic Shifts". *European Journal of Mass Spectrometry*, Vol. 8, pp. 85-98 (2002)

Lifshitz, C. "Recent developments in applications of RRKM-QET". *International Journal of Mass Spectrometry and Ion Processes*, Vol. 118, pp. 315-337 (1992)

Lifshitz, C., Gotchiguian, P. and Roller, R. "Time-dependent mass-spectra and breakdown graphs – The kinetic shift in aniline". *Chemical Physics Letters*, Vol. 95, pp. 106-108 (1983)

Lin, T., Payne, A.H. and Glish, G.L. "Dissociation pathways of alkali-cationized peptides: Opportunities for C-terminal peptide sequencing". *Journal of the American Society for Mass Spectrometry*, Vol. 12, pp. 497-504 (2001), and references cited within

Lippard, S.J., Berg, J.M. *Principles of Bioinorganic Chemistry*, University Science Books, Mill Valley, California, (1994)

Loo, J.A. and Muenster, H., "Magnetic sector-ion trap mass spectrometry with electrospray ionization for high sensitivity peptide sequencing". *Rapid Communications in Mass Spectrometry*, Vol. 13, pp. 54-60 (1999)

Lorquet, J. C. "Landmarks in the Theory of Mass Spectra". *International Journal of Mass Spectrometry*, Vol. 200, pp. 43-56 (2000)

Mann, M. and Wilm, M. "Error tolerant identification of peptides in sequence databases by peptide sequence tags". *Analytical Chemistry*, Vol. 66, pp. 4390-4399 (1994)

Marino, T., Russo, N. and Toscano, M. "Interaction of Li^+ , Na^+ , and K^+ with the proline amino acid. Complexation modes, potential energy profiles, and metal ion affinities". *Journal of Physical Chemistry B*, Vol. 107, pp. 2588-2594 (2003).

McCormack, A.L., Somogyi, A., Dongre, A.R. and Wysocki, V.H. "Fragmentation of protonated peptides: surface-induced dissociation in conjunction with a quantum mechanical approach". *Analytical Chemistry*, Vol. 65, pp. 2859-2859 (1993)

McKiernan, J.W., Christina, E.A., Beltrame, Cassady C.J., "Gas-phase Basicities of serine and dipeptides of serine and glycine", *Journal of the American Chemical Society*, Vol. 116, pp. 718-723 (1994)

McLuckey, S.A., Cameron, D. and Cooks, R.G. "Proton Affinities from Dissociations of Proton-Bound Dimers". *Journal of the American Chemical Society*, Vol. 103, No. 6, pp. 1313-1317 (1981)

McLuckey, S.A., Cooks, R.G. and Fulford, J.E. "Gas-phase thermochemical information from triple quadrupole mass spectrometers – Relative proton affinities of amines". *International Journal of Mass Spectrometry and Ion Processes*, Vol. 52, pp. 165-174 (1983)

McLuckey, S.A. and Goeringer, D.E. "Slow heating methods in tandem mass spectrometry". *Journal of Mass Spectrometry*, Vol. 32, pp. 461-474 (1997)

McQuarrie, D. A. and Simon, J. D. *Physical Chemistry: a Molecular Approach*, Sausalito, Calif. : University Science Books (1997)

Midoux, P., LeCam, E., Coulaud, D., Delain, E. and Pichon, C. "Histidine Containing Peptides and Polypeptides as Nucleic Acid Vectors". *Somatic Cell and Molecular Genetics*, Vol. 27, pp. 27-47 (2002)

Miller, C. "Potassium selectivity in proteins-oxygen cage or in the F-ACE". *Science*, Vol. 261, pp. 1692-1693 (1993)

Moision, R. M.; Armentrout, P. B. "Experimental and theoretical dissection of sodium cation/glycine interactions". *Journal of Physical Chemistry A*, Vol. 106, pp. 10350-10362 (2002)

Nagai, K. and Suda, T. "Realization of spontaneous healing function by carnosine". *Methods and findings in experimental and clinical pharmacology*, Vol. 10, pp. 497-507(1988)

Nakamura, R.L., Anderson, J.A. and Gaber, R.F. "Determination of key structural requirements of a K⁺ channel pore". *Journal of Biological Chemistry*, Vol. 272, pp. 1011-1018 (1997).

Needham, J., Kelly, M.T., Ishige, M., Andersen, R.J. "Andrimid and Moiramides A-C, metabolites produced in culture by a marine isolate of the bacterium pseudomonas Fluorescens-structure elucidation and biosynthesis". *Journal of organic Chemistry*, Vol. 59, pp. 2058-2063 (1994).

Nguyen, K.A. and Pachter, R. "Ground state electronic structures and spectra of zinc complexes of porphyrin, tetraazaporphyrin, tetrabenzoporphyrin, and phthalocyanine: A density functional theory study". *Journal of Chemical Physics*, Vol. 114, pp. 10757-10767 (2001)

Nguyen, M. T.; Sengupta, D.; Ha, T. K. Another look at the decomposition of methyl azide and methanimine: How is HCN formed? *Journal of Physical Chemistry*, Vol. 100, pp. 6499-6503 (1996).

- Nold, M.J., Wesdemiotis, C., Yalcin, T. and Harrison, A.G. "Amide bond dissociation in protonated peptides. Structures of the N-terminal ionic and neutral fragments". *International Journal of Mass Spectrometry and Ion Processes*, Vol. 164, pp. 137-153 (1997)
- O'Hair, R. A. J., Broughton, P. S., Styles, M. L., Frink, B. T. and Hadad, C. M. "The fragmentation pathways of protonated glycine: a computational study". *Journal of the American Society for Mass Spectrometry*, Vol. 11, pp. 687-696 (2000)
- Paizs B, Lendvay G, Vekey K, Suhai S. "Formation of b(2)(+) ions from protonated peptides: an ab initio study". *Rapid Communications in Mass Spectrometry*, Vol. 13, pp. 525-533 (1999)
- Paizs, B. and Suhai, S. "Combined quantum chemical and RRKM modeling of the main fragmentation pathways of protonated GGG. II. Formation of b₂, y₁, and y₂ ions". *Rapid Communications in Mass Spectrometry*, Vol. 16, pp. 375-389 (2002)
- Paizs, B. and Suhai, S. "Fragmentation pathways of protonated peptides". *Mass Spectrometry Reviews*, Vol. 24, pp. 508-548 (2005) , and references cited within.
- Paizs, B. and Suhai, S. "Theoretical study of the main fragmentation pathways for protonated glycyglycine". *Rapid Communications in Mass Spectrometry*, Vol. 15, pp. 651-663 (2001)
- Paizs, B. and Suhai, S. "Towards understanding the tandem mass spectra of protonated oligopeptides. 1: Mechanism of amide bond cleavage". *Journal of the American Society for Mass Spectrometry*, Vol. 15, pp. 103-113 (2004)
- Parr, R.G. and Yang, W. *Density Functional Theory*, Oxford University Press (1989)
- Pegova, A., Abe, H. and Boldyrev, A. "Hydrolysis of carnosine and related compounds by mammalian carnosinases". *Comparative Biochemistry and Physiology B-Biochemistry & Molecular Biology*, Vol. 127, pp. 443-446 (2000)
- Pingitore, F., Polce, M. J., Wang, P., and Wesdemiotis, C. Paizs, B. "Intramolecular condensation reactions in protonated dipeptides: carbon monoxide, water, and ammonia losses in competition". *Journal of the American Society for Mass Spectrometry*, Vol. 15, pp. 1205-1238 (2004)

Polce, M.J, Ren, D., Wesdemiotis, C. "Special feature: Commentary - Dissociation of the peptide bond in protonated peptides". *Journal of Mass Spectrometry*, Vol. 35, pp. 1391-1398 (2000)

Polfer, N.C., Paizs, B., Snoek, L.C., Compagnon, I., Suhai, S., Meijer, G., Helden G. v., Oomens, J. "Infrared Fingerprint Spectroscopy and Theoretical Studies of Potassium Ion Tagged Amino Acids and Peptides in the Gas Phase". *Journal of American Chemical Society*, Vol. 127, pp. 8571-8579 (2005)

Rappsilber, J., Moniatte, M., Nielsen, M.L., Podtelejnikov, A.V. and Mann, M. "Experiences and perspectives of MALDI MS and MS/MS in proteomic research". *International journal of mass spectrometry*, Vol. 226, pp. 223-237 (2003)

Reid, G.E., Simpson, R.J. and O'Hair, R.A.J. "A mass spectrometric and ab initio study of the pathways for dehydration of simple glycine and cysteine-containing peptide [M+H](+) ions". *Journal of the American Society for Mass Spectrometry*, Vol. 9, pp. 945-956 (1998)

Robertson D.E., Lesage, S. and Roberts, M.F. "Beta-aminoglutaric acid is a major soluble component of Methanococcus Thermolithotrophicus". *Biochimica Et Biophysica Acta*, Vol. 992, pp. 320-326 (1989)

Rode, J. E., Dobrowolski J. C., Borowiak M. A. and Mazurek, A.P. "A theoretical study on the stability and spectra of cycloaddition products: Methylene- β -lactam isomers". *Physical Chemistry Chemical Physic*, Vol. 4, pp. 3948-3958 (2002)

Rodgers, M.T. and Armentrout, P.B. "Noncovalent interactions of nucleic acid bases (uracil, thymine, and adenine) with alkali metal ions. Threshold collision-induced dissociation and theoretical studies". *Journal of the American Chemical Society*, Vol. 122, pp. 8548-8558 (2000)

Rodriquez, C.F.; Shoeib, T., Chu, I.K., Siu, K.W.M. and Hopkinson, A.C. "Comparison between protonation, lithiations, and argentination of 5-oxazolones: A study of a key intermediate in gas-phase peptide sequencing". *Journal of Physical Chemistry A*, Vol. 104, pp. 5335-5342 (2000)

Roepstorff, P. and Fohlman, J. "Proposal for a common nomenclature for sequence ions in mass-spectra of peptides". *Biomedical Mass Spectrometry*, Vol. 11, pp. 601 (1984)

Rogalewicz, F. and Hoppilliard, Y. "Low energy fragmentation of protonated glycine. An ab initio theoretical study". *International Journal of Mass Spectrometry*, Vol. 199, pp. 235-252 (2000)

Rogalewicz, F., Hoppilliard, Y. and Ohanessain, G. "Fragmentation mechanisms of α -amino acids protonated under electrospray ionization: a collisional activation and ab initio theoretical study". *International Journal of Mass Spectrometry*, Vol. 195/196, pp. 565-590 (2000)

Rossi, F., Lelais, G. and Seebach, D. " Zn^{2+} -complexation by a beta-peptidic helix and hairpin containing beta(3)hCys and beta(3)hHis building blocks: Evidence from CD measurements". *Helvetica Chimica Acta*, Vol. 86, pp. 2653-2661 (2003)

Ruan, C. and Rodgers, M.T. "Cation- π Interactions: Structures and Energetics of Complexation of Na^+ and K^+ with the Aromatic Amino Acids, Phenylalanine, Tyrosine, and Tryptophan". *Journal of the American Chemical Society*, Vol. 126, pp. 14600 -14610 (2004)

Ryzhov, V., Dunbar, R.C., Cerda, B. and Wesdemiotis, C. "Cation- π effects in the complexation of Na^+ and K^+ with Phe, Tyr, and Trp in the gas phase". *Journal of the American Society for Mass Spectrometry*, Vol. 11, pp. 1037-1046 (2000)

Schlosser, A. and Lehmann, W.D. "Five-membered ring formation in unimolecular reactions of peptides: a key structural element controlling low-energy collision-induced dissociation of peptides", *Journal of Mass Spectrometry*, Vol. 35, pp. 1382-1390 (2000)

Schlosser, A. and Lehmann, W.D. "Special feature: Commentary - Five-membered ring formation in unimolecular reactions of peptides: a key structural element controlling low-energy collision-induced dissociation of peptides". *Journal of Mass Spectrometry*, Vol. 35, pp. 1382-1390 (2000)

Schreiber, J.V., Quadroni, M. and Seebach, D. "Sequencing of beta-peptides by mass spectrometry". *Chimia*, Vol. 53, pp. 621-626 (1999)

Scott, A.P. and Radom, L. "Harmonic vibrational frequencies: An evaluation of Hartree-Fock, Moller-Plesset, quadratic configuration interaction, density functional theory, and semiempirical scale factors". *Journal of Physical Chemistry*, Vol. 100, pp. 16502-16513 (1996)

Seebach, D. and Matthews, J.L. "Beta-peptides: a surprise at every turn". *Chemical Communication*, pp. 2015-2022 (1997)

Seebach, D., Schreiber J. V., Arvidsson P. I. and Frackenpohl J. "The Miraculous CD Spectra (and Secondary Structures?) of β -Peptides as They Grow Longer". *Helvetica Chimica Acta*, Vol. 84 pp. 271-279 (2001)

Sewald, N. in *Bioorganic chemistry: Highlights and new aspects*, edited by Diederichsen, U., Lindhorst, T. K., Westermann, B., and Wessjohann, L. A., Weinheim, Wiley (1999)

Silverman, S.K., Lester, H.A. and Dougherty, D.A. "Asymmetrical contributions of subunit pore regions to ion selectivity in an inward rectifier K^+ channel". *Biophysical Journal*, Vol. 75, pp. 1330-1339 (1998)

Siu, F.M., Ma, N.L. and Tsang, C.W. "Alkali metal cation-ligand affinities: Basis set superposition correct for the Gaussian protocols". *Journal of Chemical Physics*, Vol. 114, pp. 7045-7051 (2001a).

Siu, F.M., Ma, N.L. and Tsang, C.W. "Cation- π interactions in sodiated phenylalanine complexes: Is phenylalanine in the charge-solvated or zwitterionic form?". *Journal of the American Chemical Society*, Vol. 123, pp. 3397-3398 (2001b).

Siu, F.M., Ma, N.L. and Tsang, C.W. "The competition between π and non- π cation binding sites in aromatic amino acid: a theoretical study of the alkali metal cation (Li^+ , Na^+ , K^+)-phenylalanine complexes". *Chemistry – A European Journal*, Vol. 10, pp. 1966-1976 (2004).

Schmuck, C. and Wennemers, H. *Highlights in Bioorganic Chemistry*, Wiley-VCH Verlag GmbH & Co. KGaA, Weinheim, 2004; p.63

Steer, D. L.; Lew, R. A.; Perlmutter, P.; Smith, A. I.; Aguilar, M.-I. "Design and synthesis of inhibitors incorporating β -amino acids of metalloendopeptidase EC 3.4.24.15". *Journal of Peptide Science*, Vol. 6, pp.470-477 (2000)

Steer, D. L.; Lew, R. A.; Perlmutter, P.; Smith, A. I.; Aguilar, M.-I. "The use of beta-amino acids in the design of protease and peptidase inhibitors". *Letters in Peptide Science*, Vol. 8, pp. 241-246 (2001)

Struys, E.A., Guerand, W.S., ten Brink, H.J., Jakobs, C. "Combined method for the determination of γ -aminobutyric and α -alanine in cerebrospinal fluid by stable isotope dilution mass spectrometry". *Journal of Chromatography, B: Biomedical Sciences and Applications*, Vol. 732, pp. 245-249 (1999)

Stryer, L., *Biochemistry, 4th ed.*, W.H. Freeman, New York (1995)

Talley, J.M., Cerda, B.A., Ohanessian, G. and Wesdemiotis, C. "Alkali metal ion binding to amino acids versus their methyl esters: Affinity trends and structural changes in the gas phase". *Chemistry-A European Journal*, Vol. 8, pp.1377-1388 (2002)

Tamba, M. and Torreggiani, A. "Hydroxyl radical scavenging by carnosine and Cu(II)-carnosine complexes: a pulse-radiolysis and spectroscopic study". *International Journal of Radiation Biology*, Vol. 75, pp. 1177-1188 (1999)

Teesch, L.M. and Adams, J. "Fragmentations of gas-phase complexes between alkali-metal ions and peptides: Metal-ion binding to carbonyl oxygens and other neutral functional-groups". *Journal of the American Chemical Society*, Vol. 113, pp. 812-820 (1991)

Thorne, G.C., Ballard, K.D. and Gaskell, S.J. "Metastable decomposition of peptide $[M + H]^+$ ions via rearrangement involving loss of the C-terminal amino-acid residue". *Journal of the American Society for Mass Spectrometry*, Vol. 1, pp. 249-257 (1990)

Tomlinson, M.J., Scott, J.R., Wilkins, C.L., Wright, J.B., White, W.E. "Fragmentation of an alkali metal-attached peptide probed by collision-induced dissociation Fourier transform mass spectrometry and computational methodology.". *Journal of Mass Spectrometry*, Vol. 34(9), pp. 958-968 (1999)

Tsang, C. W.; Harrison, A. G. Chemical ionization of amino acids. *Journal of the American Chemical Society*, Vol. 98, pp. 1301-1308 (1976)

Tsang, Y. *Ph.D. Thesis* on “Mass Spectrometric Studies on Alkali Metal Cationized Amino Acids and Peptides”, 2003

Tsang, Y., Siu, F.M., Ho, C.S., and Ma, N.L. and Tsang, C.W. “Experimental validation of theoretical potassium and sodium cation affinities of amides by mass spectrometric kinetic method measurements”. *Rapid Communications in Mass Spectrometry*, Vol. 18, pp. 345-355 (2004).

Tsaprailis, G., Nair, H., Somogyi, A., Wysocki, V.H., Zhong, W., Futrell, J.H., Summerfield, S.G. and Gaskell, S.J. “Influence of secondary structure on the fragmentation of protonated peptides”. *Journal of American Chemical Society*, Vol. 121, pp. 5142-5154 (1999)

Tsaprailis, G., Nair, H., Zhong, W., Kuppanan, K., Futrell, J.H., Wysocki, V.H. “A mechanistic investigation of the enhanced cleavage at histidine in the gas-phase dissociation of protonated peptides”. *Analytical Chemistry*, Vol. 76, pp. 2083-2094 (2004)

Uggerud, E. “The unimolecular chemistry of protonated glycine and the proton affinity of glycine: a computational model”. *Theoretical Chemistry Accounts*, Vol. 97, pp. 313-316 (1997)

Van Dongen, W. D.; Heerma, W.; Haverkamp, J. and de Koster, C. G. “The b₁-fragment ion from protonated glycine is an electrostatically-bound ion/molecule complex of CH₂=NH₂⁺ and CO”. *Rapid Communications in Mass Spectrometry*, Vol. 10, pp. 1237-1239 (1996)

Vekey, K. “Internal Energy Effects in Mass Spectrometry”. *Journal of Mass Spectrometry*, Vol. 31, pp. 445-463 (1996)

Veronese, F. M., Sacca, B., de Laureto, P.P., Sergi, M., Caliceti, P., Schiavon, O. and Orsolini, P. “New PEGs for peptide and protein modification, suitable for identification of the PEGylation site”, *Bioconjugate Chemistry*, Vol. 12, pp. 62-70 (2001)

Wang, Z., Chu, I.K., Rodruquez, C.F., Hopinson, A.C., and Siu, K.W.M. “ α,ω -Diaminoalkanes as models for bases that dicoordinate the proton: an evaluation of the kinetic

method for estimating their proton affinities". *Journal of Physical Chemistry A*, Vol. 103, pp. 8700-8705 (1999)

Talaty, E.R., Cooper, T.J., Osburn, S. and Van Stipdonk, M.J. "Collision-induced dissociation of protonated tetrapeptides containing beta-alanine, gamma-aminobutyric acid, epsilon-aminocaproic acid or 4-aminomethylbenzoic acid residues". *Rapid Communications in Mass Spectrometry*, Vol. 20, pp. 3443-3455 (2006)

Tinto, W.F., Lough, A.J., McLean, S., Reynolds, W.F., Yu, M. and Chan, W.R. "Geodiamolides H and I, Further Cyclodepsipeptides from Marine Sponge *Geodia* sp.". *Tetrahedron*, Vol. 54, pp. 4451-4458 (1998)

Wong, C.H.S. *Ph.D. Thesis* on "Theoretical studies on potassium cation-ligand interaction", 2004

Wong, C.H.S., Siu, F.M., Ma, N.L. and Tsang, C.W. "A theoretical study of potassium cation-glycine (K^+ -Gly) interactions". *Journal of Molecular Structure-TheoChem*, Vol. 588, pp. 9-16 (2002).

Wu, L., Meurer, E.C., Young, B., Yang, P., Eberlin, M.N. and Cooks, R.G. "Isomeric differentiation and quantification of a, b-amino acid-containing tripeptides by the kinetic method: alkali metal-bound dimeric cluster ions". *International Journal of Mass Spectrometry*, Vol. 231, pp. 103-111 (2004)

Wysocki, V.H., Tsaprailis, G., Smith, L.L. and Brechi, L.A. "Mobile and localized protons: a framework for understanding peptide dissociation". *Journal of Mass Spectrometry*, Vol. 35, pp. 1399-1406 (2000)

Wysocki, V.H., Tsaprailis, G., Smith, L.L., Brechi, L.A. "Special feature: Commentary - Mobile and localized protons: a framework for understanding peptide dissociation". *Journal of Mass Spectrometry*, Vol. 35, pp. 1399-1406 (2000)

Wytttenbach, T., Witt, M. and Bowers, M.T. "On the stability of amino acid zwitterions in the gas phase: The influence of derivatization, proton affinity, and alkali ion addition". *Journal of*

the American Chemical Society, Vol. 122, pp. 3458-3464 (2000)

Yalcin, T., Csizmadia, I.G., Peterson, M.R. and Harrison, A.G. "The structure and fragmentation of B_n ($n \geq 3$) ions in peptide spectra?". *Journal of the American Society for Mass Spectrometry*, Vol. 7, pp. 233-242 (1996)

Yalcin, T., Khouw, C., Csizmadia, I.G., Peterson, M.R. and Harrison, A.G. "Why are B ions stable species in peptide spectra?". *Journal of the American Society for Mass Spectrometry*, Vol. 6, pp. 1165-1174 (1995)

Yamashita, M. and Fenn, J.B. "Electrospray ion source. Another variation on the Free-Jet theme". *Journal of Physical Chemistry*, Vol. 88, pp. 4451-4459 (1984a)

Yates, J.R. "Mass spectral analysis in proteomics". *Annual Review of Biophysics and Biomolecular Structure*, Vol. 33, pp. 297-316 (2004)

Yates, J.R., Eng, J.K., Clauser, K.R. and Burlingame, A.L. "Search of sequence databases with uninterpreted high-energy collision-induced dissociation spectra of peptides". *Journal of the American Society for Mass Spectrometry*, Vol. 7, pp. 1089-1098 (1996)

Yates, J.R., Eng, J.K., McCormack, A.L. and Schieltz, D. "Method to correlate tandem mass spectra of modified peptides to amino acid sequence in the protein database". *Analytical Chemistry*, Vol. 67, pp. 1426-1436 (1995)

Zatta, P., Tognon, G. and Carampin P. "Melatonin prevents free radical formation due to the interaction between beta-amyloid peptides and metal ions [Al(III), Zn(II), Cu(II), Mn(II), Fe(II)]". *Journal of Pineal Research*, Vol. 35, pp. 98-103 (2003)

Zheng, Y., Xu, Y. and Xu, Y. "Review on small peptides in protein nutrition". *Siliao Yanjiu*, Vol. 2, pp. 7-9 (2006)

Potassium Cation Binding to α -Amino Acids and Dipeptides : A Combined Theoretical and Experimental Study

Chun-Wai Tsang¹, Yuet Tsang¹, Carrie Hoi-Shan Wong¹, Fung-Ming Siu¹, Jackie Man-Kit Cheng¹, Tracy Ho-Man Lee¹, Seduraman Abirami² and Ida Ngai-Ling Ma^{2*}

¹The Hong Kong Polytechnic University, Hong Kong. ²Institute of High Performance Computing, Science Park Road, Singapore 118261

Introduction

The non-covalent binding between K^+ and proteins structures underlies many fundamental biological processes and enzyme functions. Here we report a combined theoretical and experimental study on the binding of K^+ to model biological ligands (20 common α -amino acids and 6 model dipeptides, GlyGly, AlaAla, GlyPro, ProGly, PheGly, GlyPhe).

Methodology

The K^+ affinities were measured by a combination of standard and extended kinetic method measurements using the validated theoretical G2(MP2, SVP)-ASC K^+ affinities values (in kJ mol^{-1} at 0 K) of acetamide(118.7), N-methylacetamide(125.6) and N,N-dimethylacetamide (129.2) as the 'starting' reference values (Tsang *et al.*, *Rapid Comm. Mass Spectrom.*, 18, 345-355, 2004). Theoretical studies on K^+ binding geometries and energies were carried out at the 3-LYP/6-311+G(3df,2p)/B3-LYP/6-31G(d) level of theory, with ZPE corrections at B3LYP/6-31G(d) level and scaled by 0.9806. Plausible K^+ binding geometries of the six model dipeptides were first found using the Monte Carlo Multiple Minimum (MCM) conformational searching technique, with AMBER* force field implemented in the MacroModel 7.0 package.

Results and Discussion

The experimental K^+ affinities ($\Delta H_{(K^+)}^{\circ}$, kJ mol^{-1}) of 20 α -amino acids are shown in Table 1. The K^+ affinities of the six model dipeptides are : PheGly (155.4) > GlyPhe (151.9) > GlyPro (145.4) > ProGly (142.7) > AlaAla (142.0) > GlyGly (139.0). The experimental K^+ affinities are in very good agreement with theoretical values at 0 K, $\Delta H_{(K^+)}^{\circ}$, to within +9 and $\pm 15 \text{ kJ mol}^{-1}$ for most of the amino acids and dipeptides, respectively. The theoretical studies showed that, with the exception of the zwitterionic (ZW) form of K^+ -Pro/Gln/Glu/His/Arg (Figure 1), K^+ bound complex of α -amino acids are in their most stable bi- or tridentate charge-solvated (CS) forms (Table 1). The most stable CS complexes of GlyGly, AlaAla, ProGly and GlyPhe involve bidentate K^+ binding to the two carbonyl C=O oxygens due to the strong 'local' ion-dipole interactions associated with these two binding sites. Tridentate binding involving the amide C=O, carboxylic C=O, and N-terminal -NH₂ / aromatic- π sites are the most stable CS binding mode for GlyPro and PheGly. The ZW form of K^+ bound dipeptides are generally $\sim 50 \text{ kJ mol}^{-1}$ less stable than the most stable CS forms.

Table 1 Experimental and theoretical K^+ affinities (kJ mol^{-1}) of 20 α -amino acids

Amino Acid	Expt $\Delta H_{\text{expt}}^{\text{a}}$	Potassium Cation Affinity				$\Delta H_{\text{O}(\text{CS})} - \Delta H_{\text{O}(\text{ZW})}^{\text{c}}$	$\Delta H_{\text{O}(\text{expt})} - \Delta H_{\text{O}(\text{theory})}^{\text{d}}$
		Theoretical ΔH_{O} at 0 K		ZW			
		CS1 ^a	CS2 ^b				
Gly	119	117 (O=C, OH)	114 (O=C, NH ₂)	105	12	2	
Ala	123	123 (O=C, OH)	117 (O=C, NH ₂)	116	7	0	
Cys	124	123 (O=C, NH ₂ , OH _(side))	115 (O=C, OH)	117	6	1	
Val	127	128 (O=C, OH)	121 (O=C, NH ₂)	124	4	-1	
Leu	128	128 (O=C, OH)	121 (O=C, NH ₂)	124	4	0	
Ile	129	129 (O=C, OH)	123 (O=C, NH ₂)	126	3	0	
Ser	133	136 (O=C, NH ₂ , OH _(side))	124 (O=C, OH)	122	14	-3	
Met	135	143 (O=C, NH ₂ , S)	127 (O=C, OH)	140	3	-8	
Pro	135	130 (O=C, OH)	119 (O=C, NH)	143	-13	-8	
Thr	136	141 (O=C, NH ₂ , OH _(side))	130 (O=C, OH)	122	19	-5	
Asp	137	148 (O=C, O=C, NH ₂)	132 (O=C, OH)	127	21	-11	
Phe	139	142 (π , O=C, NH ₂)	139 (π , O=C)	127	15	-4	
Tyr	140	144 (π , NH ₂ , OH)	141 (π , O=C)	132	12	-5	
Glu	140	142 (O=C, OH)	142 (O=C, O=C, NH ₂)	148	-6	-8	
Lys	144	153 (O=C, NH ₂ , NH ₂)	135 (O=C, OH)	119	34	-9	
Asn	149	164 (O=C, O=C, NH ₂)	142 (O=C, OH)	146	18	-15	
Trp	151	153 (π , O=C)	152 (π , O=C, NH ₂)	135	18	-2	
Gln	154	164 (O=C, O=C, NH ₂)	151 (O=C, OH)	172	-8	-18	
His	155	163 (C=O, N ⁺)	162 (C=O, NH ₂ , N ⁺)	164	-1	-9	
Arg	163	189 (O=C, NH ₂)	-	199	-10	-36	

^a CS1, the most stable charge-solvated (CS) conformer of K^+ -amino acid complex. ^b CS2, the second most stable charge-solvated (CS) conformer of K^+ -AA complex. ^c The difference between theoretical affinities, ΔH_{O} , for the most stable K^+ charge-solvated (CS) and zwitterionic (ZW) binding mode. ^d The difference between experimental affinities and theoretical affinities of the most stable charge-solvated (CS) or zwitterionic (ZW) binding mode indicated by BOLD font.

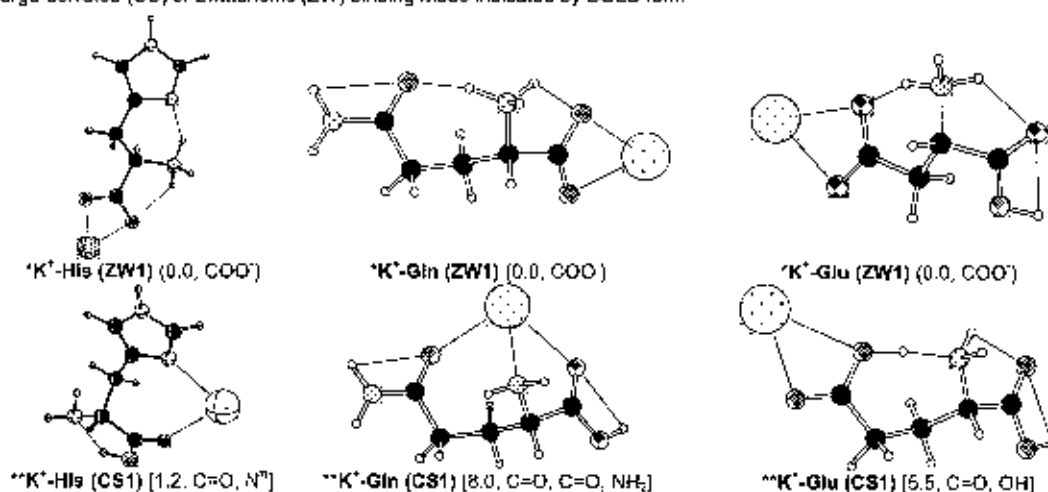


Figure 1 The optimized geometries of K^+ -His/Gln/Glu complexes. The theoretically calculated relative binding energies at 0K (in kJ mol^{-1}) and sites of binding of the most stable (indicated by *) and second most stable binding mode (indicated by **) are shown in parenthesis () and square brackets [], respectively.

Acknowledgement

The financial support of the Research Grants Council of Hong Kong (Area of Excellence Project No. P-10/2001 and CERG Project No. PolyU 5286/02P to C.W.T.) is gratefully acknowledged.

Fragmentation Pathways of Protonated β -Alanine and β -Peptides: An Energy-Resolved Tandem Mass Spectrometric and Theoretical Study

Jackie M. K. Cheng, Onyx O. Y. Chan, P. K. So, and C. W. Tsang*

The Hong Kong Polytechnic University, Hong Kong.

The fragmentation pathways of protonated (H^+) β -Ala and β -peptides were studied and compared with that of α -Ala and their α -analogues. Energy-resolved CID (MS/MS and MS² spectra as a function of collision energies) of protonated β -Ala and β -dipeptides, and $\text{b}_1(\text{oxazolone}) / \text{b}_2(\text{oxazinone})$ ions derived from the β -dipeptides, were monitored with a Finnigan-LCQ ion trap mass analyzer and Micromass Q-TOF II tandem mass spectrometer. The potential energy surfaces for dissociation of $\text{H}^+(\beta\text{-Ala})$ and model β -dipeptides, $\text{H}^+\text{-Gly}(\beta\text{-Ala})$ and $(\beta\text{-Ala})\text{Gly}$, including transition structures, intermediates and final products, were theoretically explored by calculations using density functional theory at the B3-LYP/6-311+G(3df,2p)//B3-LYP/6-31G(d) level.

Unlike $\text{H}^+(\alpha\text{-Ala})$, which shows concerted loss of ($\text{H}_2\text{O} + \text{CO}$) only, $\text{H}^+(\beta\text{-Ala})$ dissociates by preferred loss of water (H_2O) to yield a stable b_1 ion ($m/z=72$, shown by MS/MS studies to be a protonated β -lactam), and loss of ketene (CH_2CO) and ketene + water ($\text{CH}_2\text{CO} + \text{H}_2\text{O}$), while loss of methanimine ($\text{NH}=\text{CH}_2$), ammonia (NH_3) and ammonia + carbon monoxide ($\text{NH}_3 + \text{CO}$) are observed under more energetic CID conditions. (Figure 1) The energetics of the dissociation pathways are found by high level density functional theory calculations, and are consistent with experimental observations. (Table 1) Compared to α -alanine, the difference in structure and stability of the fragment ions, neutrals lost, stable intermediates and transitional structures of the dissociation pathways of β -alanine are directly related to the presence of the 'extra' $-\text{CH}_2-$ unit in the carbonyl backbone. For example, the predominant formation of protonated β -lactam fragment ion at m/z 72 is due to (i) the stability of the 4-membered β -lactam ring, which otherwise could not be possibly formed in the case of α -alanine, and (ii) the reaction is favored by entropy changes. (Figure 2)

For the fragmentation pathways of protonated β -peptides, the formation of β -Ala specific fragment ions is dependent of the location, C-terminus versus N-terminus, of β -Ala in the β -dipeptide. For $\text{Xxx}(\beta\text{-Ala})$ β -dipeptides ($\text{Xxx} = \text{Gly, Leu, Phe and Met}$), formation of the unique $\text{b}_2(\text{oxazinone})$ ions is energetically favored over y_1 ion formation. (Figure 3(a)) For $(\beta\text{-Ala})\text{Xxx}$ β -dipeptides with β -Ala at the C-terminus ($\text{Xxx} = \text{Gly, Phe, Trp and His}$), fragment ions due to loss of NH_3 and/or formation of b_1 (protonated β -lactam) ions which are indicative of the presence and location of β -Ala, are competitive with y_1 ion formation. (Figure 3(b)) The above mentioned characteristic dissociation pathways of protonated model β -dipeptides, $\text{Gly}(\beta\text{-Ala})$ and $(\beta\text{-Ala})\text{Gly}$, were also established by high level density function theory calculations, which are consistent with experimental observations. The presence of the extra backbone $-\text{CH}_2-$ unit in β -Ala does have found to be a structural effect on the fragment of β -dipeptides

Acknowledgement

The funding support of the Hong Kong Polytechnic University and Research Grant Council of the Hong Kong Administrative Region, China (Project no. PolyU 5012/04) are gratefully acknowledged.

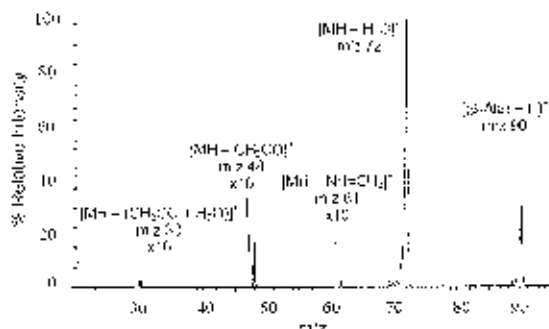


Figure 1 Ion trap MS/MS spectra of protonated β -alanine, $[(\beta\text{-Ala}) + \text{H}]^+$ (m/z 90), obtained at a RF activation voltage (V_p) of 0.66 V.

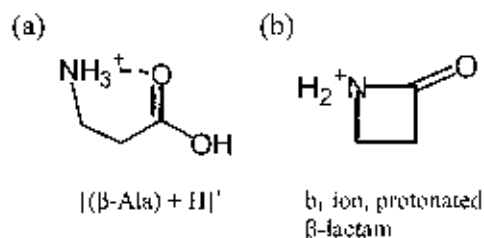


Figure 2 Schematic structures of (a) protonated β -alanine, $[(\beta\text{-Ala}) + \text{H}]^+$ (m/z 90) and (b) b_1 ion, protonated β -lactam (m/z 72)

Table 1 The relative enthalpies (ΔH_0 , ΔH_{298} at 0K and 298K), Gibbs free energies (ΔG_{298} at 298K, in kJ mol⁻¹) and entropies (ΔS_{298} at 298K, in J mol⁻¹) of the highest energy barriers for the loss of small neutrals on the $[(\beta\text{-Ala}) + \text{H}]^+$ potential energy surface.^[a]

neutral loss	$[(\beta\text{-Ala}) + \text{H}]^+$			
	ΔH_0	ΔH_{298}	ΔG_{298}	ΔS_{298}
$\text{H}_2\text{O} / \text{CH}_3\text{OH}$	170 (0.38)	177	129	64
CH_2CO	163 (0.46)	167	158	30
$(\text{CH}_3\text{CO} + \text{H}_2\text{O} / \text{CH}_3\text{OH})$	234 (0.46)	244	144	336
NH_3	264 (- ^[b])	271	253	60
$(\text{CO} + \text{NH}_3)$	485 (- ^[b])	496	466	101

^[a] Theoretical calculated ΔH_0 , ΔH_{298} , ΔG_{298} and ΔS_{298} values are based on the potential energy surface at 0K. The appearance threshold energy (in V) for observation of the corresponding fragment ions under ion trap CID conditions is shown in italics in parenthesis.

^[b] Not observed under ion trap CID conditions, but observed under triple quadrupole CID conditions.

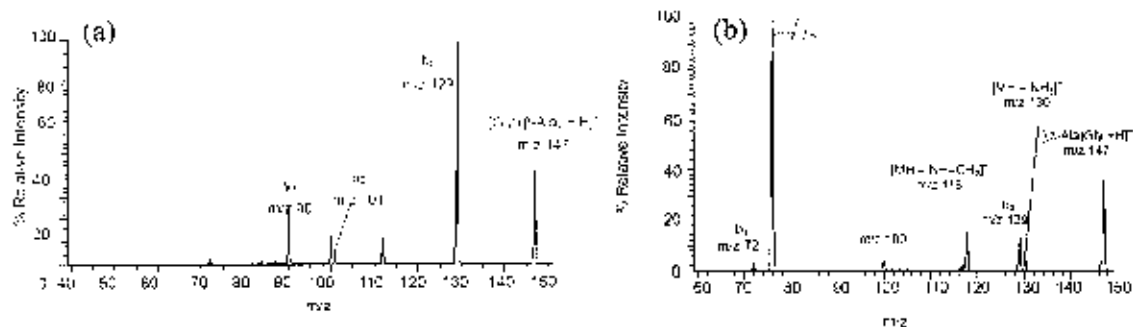


Figure 3 Ion trap MS/MS spectra of protonated (a) Gly(β -Ala) (m/z 147) obtained at a RF activation voltage (V_p) of 0.68 V, and (b) (β -Ala)Gly (m/z 147) obtained at a RF activation voltage (V_p) of 0.66 V.